

MAX-PLANCK-INSTITUT FÜR PHYSIK  
(WERNER-HEISENBERG-INSTITUT)

## Report to the Fachbeirat

2007 – 2010

### Part II: Scientific Achievements

*Cover Photo:*

The cover photo shows two crystals to be used for the CRESST (Cryogenic Rare Event Search with Superconducting Thermometers) experiment located at the Laboratori Nazionali del Gran Sasso (LNGS) in Italy. The CRESST experiment is designed for direct detection of weakly interacting massive particles, accounting for the dark matter observed in the universe. The Max-Planck-Institut für Physik is substantially contributing to all essential aspects of the experiment.

# Contents

<b>1</b>	<b>The ATLAS Experiment at the Large Hadron Collider LHC</b>	<b>3</b>
1.1	Detector Commissioning and Computing . . . . .	6
1.1.1	The Semiconductor Tracker SCT . . . . .	6
1.1.2	The Hadronic End-cap Calorimeter HEC . . . . .	11
1.1.3	The Muon Drift Tube Chambers MDT . . . . .	17
1.1.4	Computing . . . . .	23
1.2	ATLAS Physics Analysis . . . . .	26
1.2.1	Standard Model Processes . . . . .	26
1.2.2	Top-Quark Physics . . . . .	29
1.2.3	Searches for the Higgs Boson . . . . .	33
1.2.4	Search for Physics Beyond the Standard Model . . . . .	37
1.2.5	Analyses Summary . . . . .	40
1.3	Detector Upgrade . . . . .	41
1.3.1	R&D towards a novel Pixel Detector for the SLHC . . . . .	41
1.3.2	Upgrade of the HEC: Motivation and Options . . . . .	46
1.3.3	Upgrade of the Muon system for High Luminosities . . . . .	49
<b>2</b>	<b>Publications</b>	<b>62</b>



# Chapter 1

## The ATLAS Experiment at the Large Hadron Collider LHC

(L. Andricek, A. Barajas-Velez, A. Bangert, T. Barillari, M. Beimforde, N.Ch. Benekos, S. Bethke, B. Bittner, J. Bronner, D. Capriotti, G. Cortiana, D. Dannheim, A. D’Orazio, V. Danielyan, G. Dedes, J. Dubbert, Th. Ehrich, J. Erdmann, A. Fischer, M. Fras, C. Delle Fratte, N. Ghodbane, P. Giovannini, T. Göttfert, M. Groh, W. Haberer, J. Habring, P. Haefner, M. Härtig, R. Härtel, A. Hambarzumjan, Th. Haubold, S. Horvat, J. Huber, A. Jantsch, St. Kaiser, M. Kilgenstein, A. Kiryunin, S. Kluth, O. Kortner, S. Kotov, H. Kroha, S. Leber, F. Legger, M. Lippert, J. v. Loeben, A. Macchiolo, S. Menke, S. Mohr dieck-Möck, P. Mooshofer, H.-G. Moser, R. Nisius, H. Oberlack, S. Patarraia, G. Pospelov, I. Potrap, E. Rauter, D. Rebutzi, O. Reimann, R. Richter, R.H. Richter, A. Rudert, D. Salihagic, P. Schacht, J. Schieck, J. Schmaler, S. Schmidl, H. von der Schmitt, Ph. Schwegler, P. Seidler, R. Sedlmeyer, R. Seuster, M. Stadler, S. Stern, S. Stonjek, I. Thiel, G. Tratzl, Ch. Valderanis, M. Vanadia, P. Vanoni, B. Weber, P. Weigell, H. Wetteskind, A. Wimmer, G. Winkl Müller, J. Yuan, X. Zhuang, V. Zhuravlov, J. Zimmer)

The LHC experiments started to take data for high-energy proton-proton collisions in March 2010. The accelerator provides substantial luminosity at 7 TeV proton-proton centre-of-mass energy since, and event data corresponding to  $0.3 \text{ pb}^{-1}$  have been recorded by ATLAS so far. The luminosity of LHC will continue to improve rapidly in the 2nd half of the 2010 running period, with the aim to collect  $1 \text{ fb}^{-1}$  by the end of 2011, when a shutdown is planned to go towards the design c.m.s. energy of 14 TeV.

Since the last report to the Fachbeirat [1] (p.74-112), the ATLAS group at MPP has made extensive use of cosmic and single-beam data to have detector, soft-

ware and computing facilities well-commissioned before collisions data arrived. Thanks to these efforts, performance in tracking and calorimetry was close to the design values very early on. For instance, the mass peaks of known particles accessible with initial luminosity are as expected. See section 1.1 for the final phases of detector installation, and for commissioning.

Physics analyses with the luminosity collected by Mid 2010 have resulted in a first set of ATLAS physics papers. Analyses of processes which require higher luminosity, as expected before end of 2010 and beyond, are well prepared. Fig. 1.1 gives an overview of signal and background cross sections at LHC. See section 1.2 for those parts of physics analyses in which MPP is firmly involved.

The LHC future planning foresees a substantial increase of luminosity beyond the design of the present machine, to further extend its physics reach. MPP participates in detector and electronics development with the aim of exploiting higher event rates with ATLAS. See section 1.3 for the detector upgrade activities at MPP.

The detector is described in detail in the ATLAS Detector paper [2]. In the remainder of this introduction we briefly recall the ATLAS components with MPP involvement. Along the path of particles starting at the interaction point, these are: inner detector (semiconductor tracker, pixel detector upgrade); calorimeter (hadronic endcap and its upgrade); muon spectrometer (precision drift tubes and upgrade).

### The Inner Detector

Tracking detectors at the LHC have to face three major challenges: high occupancy, severe radiation damage and a short bunch crossing interval. A typical hard interaction like  $t\bar{t}$  production creates several hundred

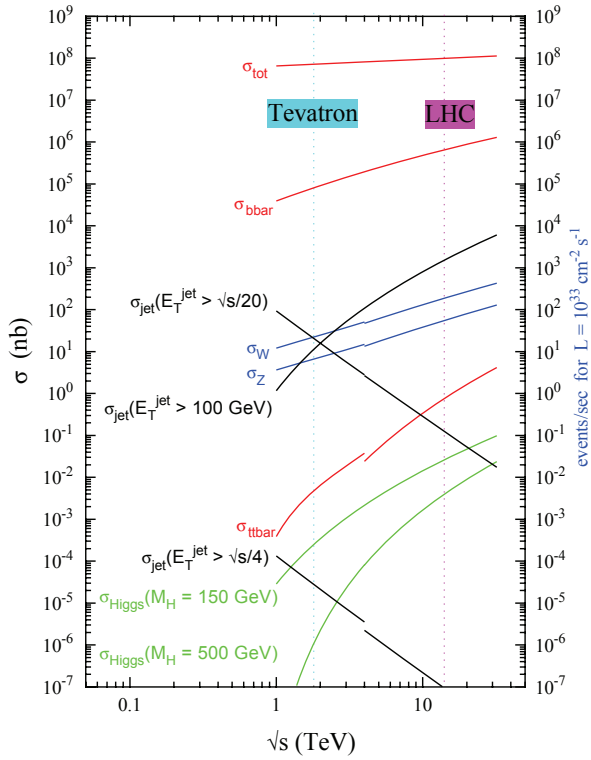


Figure 1.1: Particle production cross-sections in proton-proton collisions as a function of the centre-of-mass energy  $\sqrt{s}$  and the corresponding number of events produced per second at a luminosity of  $\mathcal{L} = 10^{34} \text{ cm}^{-2} \text{ s}^{-1}$  planned for the LHC. The red dotted line marks the collision energy of the LHC. The increase of cross-section is several orders of magnitude compared to the Tevatron at Fermilab.

charged particles within a rapidity range of  $|\eta| \leq 2.5$ . In ten years of operation a flux of up to  $5 \cdot 10^{14} \text{ n}_{\text{eq}}/\text{cm}^2$  (1 MeV neutron equivalent) particles cause substantial radiation damage to the SemiConductor Tracker (SCT). Furthermore the short bunch crossing interval of 25 ns demands fast sensors with fast readout electronics. The layout for the silicon part of the ATLAS Inner Detector (ID) is described in [3]. A sketch of the ID, Fig. 1.2, shows the separation of the ID into a central (barrel) part and two endcaps.

The complete ID is operated in a 2 T axial field. Detailed descriptions and specifications of the ID, its components and the expected performance can be found in [2, 4]. It is designed to provide a resolution in transverse momentum, in the plane perpendicular to the beam axis, of  $\sigma_{p_T}/p_T = 0.0005 p_T/\text{GeV} \oplus 0.01$  and a transverse impact parameter resolution of  $10 \mu\text{m}$  for high momentum particles in the central detector region [2].

Occupancy and radiation damage vary strongly

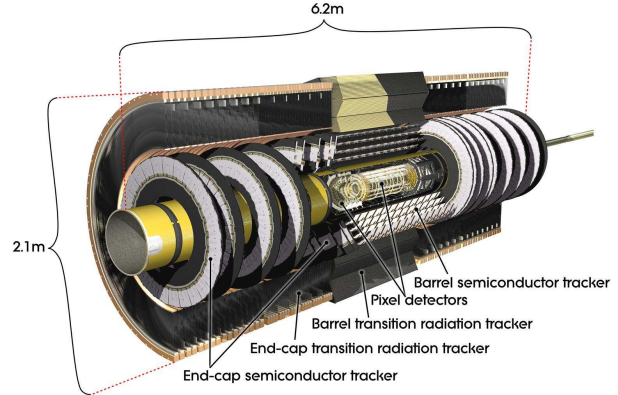


Figure 1.2: Sketch of the ATLAS Inner Detector.

within the ID volume. To cope with this, depending on the distance to the beam line,  $R$ , the ID is segmented into three parts, each using a different detector technology:

- In the innermost region,  $5 \text{ cm} \leq R \leq 12 \text{ cm}$  a high granularity silicon pixel detector with about 80 M readout channels is used. It offers an excellent space point resolution and low occupancy. The high resolution of this detector is essential for secondary vertex reconstruction, needed e.g. for  $\tau$ -lepton and b-quark identification.
- In the intermediate region,  $30 \text{ cm} \leq R \leq 51 \text{ cm}$ , a silicon micro-strip detector, the SCT, is used. The strips are oriented to measure with high precision the track coordinates transverse to the beam. A small stereo angle between two faces of a detector module allows measuring the orthogonal coordinate, albeit with less precision. The detector measures up to four space points per track. For the SCT the total area of silicon is about  $61 \text{ m}^2$ .
- Finally, for  $56 \text{ cm} \leq R \leq 107 \text{ cm}$ , the transition radiation tracker (TRT) uses straw tubes. The large number of straws allows continuous tracking with on average 36 hits per track, which, despite the moderate space resolution of single hits, results in a high precision measurement at large radii. In addition, the ability to detect transition radiation improves the electron/pion separation. The challenge for this detector is to cope with the high occupancy.

The MPP made major contributions to the design of the pixel- and micro-strip silicon detectors, and at

MPP we have built about 30% of all SCT endcap modules. The actual performance of the ID after the final installation including the cosmic ray data analysis from the year 2008 is discussed in [5]. At the LHC, the ID already served to measure the multiplicities and spectra of charged particles in minimum bias interactions at a proton-proton center of mass energy of 900 GeV [6], presenting the first ATLAS LHC physics result.

### The Hadronic End-cap Calorimeter

The ATLAS calorimeters consist of two different technologies – liquid argon sampling calorimeters for the electromagnetic, hadronic endcap and forward calorimeters with lead, copper and copper/tungsten as respective absorber materials and a scintillator - iron tile sampling calorimeter for the hadronic barrel system. They are designed to measure and identify electrons and photons with high precision  $\Delta E/E \approx 10\%/\sqrt{E}$  up to pseudo-rapidities of  $|\eta| < 2.5$  and to reconstruct jets with  $\Delta E/E \approx 50\%/\sqrt{E}$  for  $|\eta| < 3$  and with  $\Delta E/E \approx 100\%/\sqrt{E}$  in the forward region  $3 < |\eta| < 5$ . High granularity and calorimetric coverage up to  $|\eta| \approx 5$  are also needed for the reconstruction of missing transverse energy.

There are two end-caps in the ATLAS calorimeter system. The Hadronic Endcap Calorimeter (HEC), which covers the pseudo-rapidity range  $1.5 < |\eta| < 3.2$ , consists of two independent mechanical units ('wheels') per end-cap: the front and the rear wheel. Each wheel has a diameter of  $\approx 4$  m. The absorber structure of the two wheels consists of parallel copper plates of 25 mm (50 mm) for the front (rear) wheels. There is a gap of 8.5 mm of LAr between adjacent absorber plates. Three electrodes divide this gap into four separate LAr drift zones of 1.8 mm width each. Each calorimeter wheel is divided into 32 individual modules. A front (rear) module collects the signal in 24 (16) LAr gaps. The signals of two adjacent gaps are collected and transmitted to an amplifier channel in the 'active pad' electronics, which is located in the cold LAr volume. Finally the signals corresponding to a tower pointing to the interaction point are summed. There are four such longitudinal segmentations for each end-cap tower. The signal processing of the HEC employs the notion of 'active pads' which keeps the detector capacities at the input of the amplifiers small and thereby achieves a fast rise time of the signal [138]. Short coaxial cables are used to send the signals from the pads to preamplifier and summing

boards (PSB) located at the perimeter of the wheels inside the liquid argon. These PSB's carry highly integrated amplifier and summing chips in Gallium-Arsenide (GaAs) technology.

### The Muon Spectrometer

The muon spectrometer [2, 45] of the ATLAS experiment is equipped with three layers of muon detectors in a toroidal magnetic field of 3 – 6 Tm bending power generated by a superconducting air-core magnet system. The spectrometer is designed to provide muon momentum resolution of better than 10% for transverse momenta up to 1 TeV over a pseudo-rapidity range of  $|\eta| \leq 2.7$ . This requires a very accurate track sagitta measurement with three layers of muon detectors which have to be aligned relative to each other with an accuracy of up to  $30 \mu\text{m}$  in the bending direction in the magnetic field. Drift chambers with very high spatial resolution of  $40 \mu\text{m}$ , the Monitored Drift Tube (MDT) chambers, have been developed to cover the active area of the spectrometer of  $5500 \text{ m}^2$  with only 5% gaps mainly in the region of the detector feet.

The cylindrical central part of the spectrometer (barrel) contains eight race-track shaped magnet coils of 25 m length and 5 m radial width. The layout of the muon chambers follows the eightfold symmetry of the magnet around the proton beam axis in eight small and eight large azimuthal sectors (see Figure 1.3). The barrel part of the spectrometer is complemented by two endcaps each consisting of eight superconducting coils housed in a common cryostat fitting into the inner bore of the barrel toroid magnet and three wheel-shaped layers of muon detectors.

The MDT chambers built in Munich consist of two triple layers of 30 mm diameter aluminium drift tubes of 3.8 m length equipped with a central gold-plated tungsten-rhenium sense wire which are separated by an aluminium space frame. The drift tubes are operated with Ar:CO<sub>2</sub> (93:7) gas mixture at a pressure of 3 bar and a gas amplification of 20,000 (corresponding to a operating voltage between tube wall and wire of 3080 V) and provide a position resolution of about  $80 \mu\text{m}$ . The sense wires are positioned within a chamber with an accuracy of better than  $20 \mu\text{m}$  in order to achieve the required spatial resolution of the chambers [46].

In the years 2001 to 2006, 88 MDT chambers were constructed at the MPP [47] containing about 36000 drift tubes. They cover about 15% of the active area of the spectrometer.

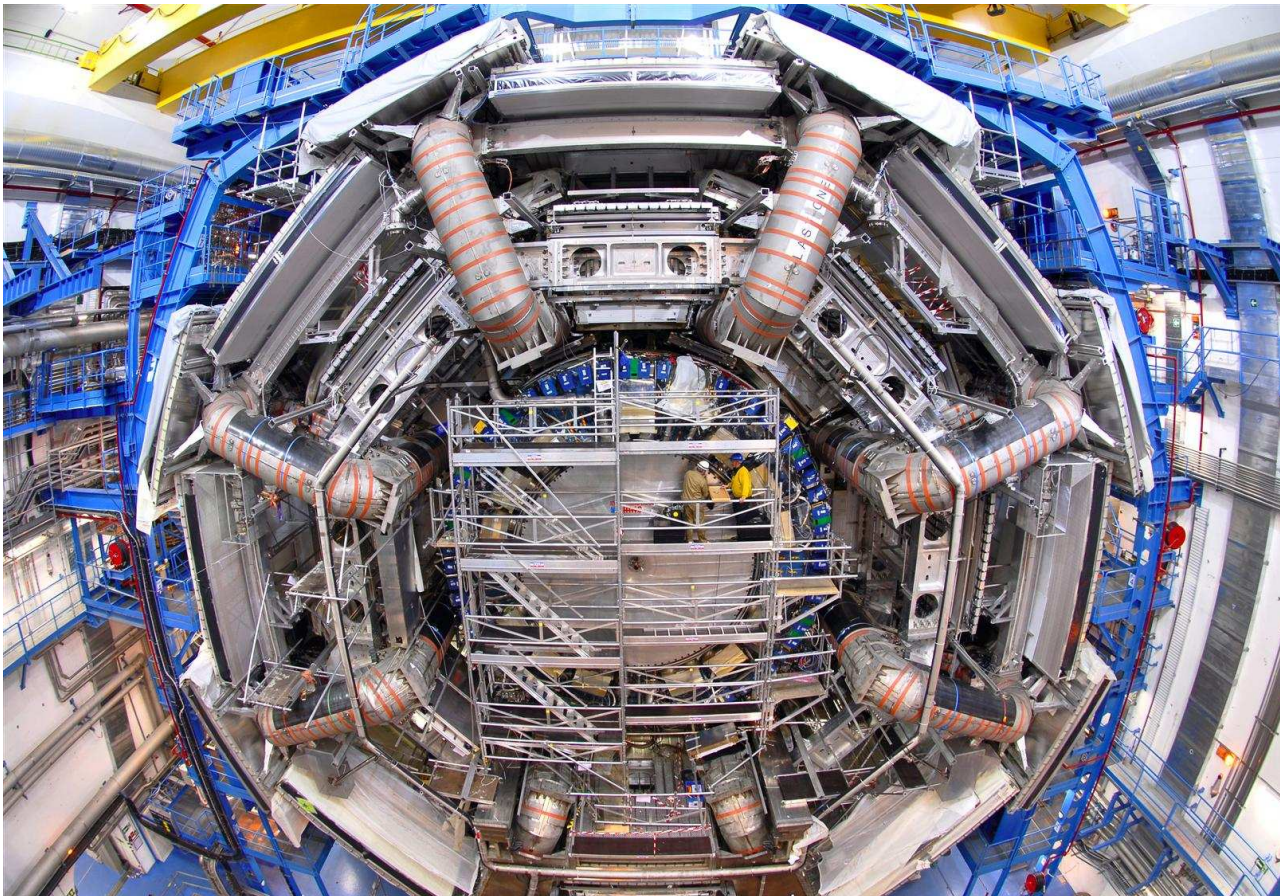


Figure 1.3: The barrel part of the ATLAS muon spectrometer viewed from the LHC tunnel after completion of the muon chamber installation in November 2006. The MDT chambers built in Munich are mounted on rails on the outside of the eight superconducting magnet coils.

## ATLAS Computing

The construction and operation of the computing system for the ATLAS experiment is a major undertaking carried out by the ATLAS collaboration with support from the Worldwide LHC Computing Grid (WLCG) collaboration. The MPP contributes its share to this task with a large Linux cluster located at the Rechenzentrum Garching (RZG) of the MPG. This cluster serves as a part of the Munich ATLAS Tier-2 centre, hosts the Munich calibration and alignment centre for the ATLAS Muon system and provides our institute's users with large computing and storage resources. In addition the MPP ATLAS group has several members working on central computing tasks for ATLAS.

## 1.1 Detector Commissioning and Computing

### 1.1.1 The Semiconductor Tracker SCT

Because of the MPP experience with silicon microstrip sensors and the unique possibilities offered by the associated semiconductor laboratory (HLL = HalbleiterLabor), MPP participated in the design and construction of the SCT.

Mechanically the SCT consists of three main units, namely the barrel and two identical endcaps. The barrel covers the region of central rapidity,  $|\eta| \leq 1$ , and the detector modules, i.e. the smallest mechanically sensitive units of the SCT, are arranged on four cylinders around the beam axis. The endcaps extend the acceptance up to  $|\eta| \leq 2.5$ . Here the modules are arranged on nine disks per endcap, and are oriented perpendicular to the beam axis.

Due to the radial arrangement the endcap modules use wedge shaped sensors glued back to back in pairs.

The sensor dimensions are about  $6.4\text{ cm} \times 6.4\text{ cm}$  and the strip pitch of the 768 strips per sensor is varying in the range  $(64\text{--}90)\mu\text{m}$ . Electrically, the two sensors of either pair are chained in series. One pair has a radial strip orientation, while the second pair is rotated by  $40\text{ mrad}$  in order to yield stereo information. The binary readout electronics is located on a double sided hybrid attached to the end of the module. In the binary mode the only information retained per channel is whether the observed signal was above or below a discriminating threshold. To equalize the efficiency of all channels for detecting a passing particle, the discriminating thresholds can be set individually for each channel by means of calibration capacitors. On a fully populated disk, three different types of endcap modules, inner, middle and outer modules, are arranged in three rings.

A major challenge for the ATLAS SCT is the large radiation level which leads to severe radiation damage of the sensors and the readout electronics, calling for cold operation ( $-10^\circ\text{C}$ ) of the silicon sensors. The cold operation and the dissipation of the heat generated by the electronics and the sensor leakage currents leads to mechanical stress. To ensure stable positions of the modules during operation needed for high quality tracking, the system requires a very high geometrical stability,

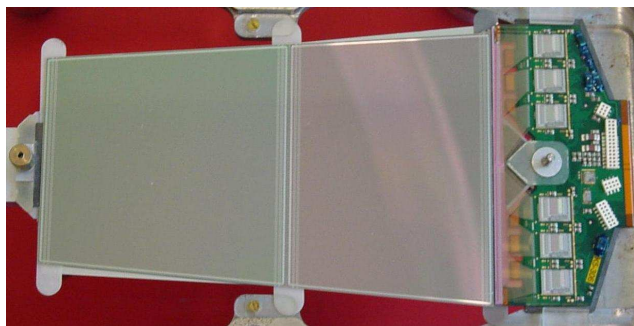


Figure 1.4: View of a middle module constructed by MPP technicians.

### MPP Engagements in the ID

In the years 1997–2006 the MPP engagement mainly concentrated on 1) the development of a cost-effective design for radiation-tolerant silicon strip sensors, 2) the design work for the endcap modules concentrating on the mechanical and thermal performance, 3) the construction of 424 SCT endcap modules of the middle type, Fig. 1.4, which amount to about 30% of all

endcap modules, 4) the integration, as well as performance measurements with cosmic ray muons, of the combined SCT and TRT detectors at the surface before their installation into the ATLAS cavern, and 5) the alignment of the silicon part of the ID with particle tracks. Detailed reports of the work performed by

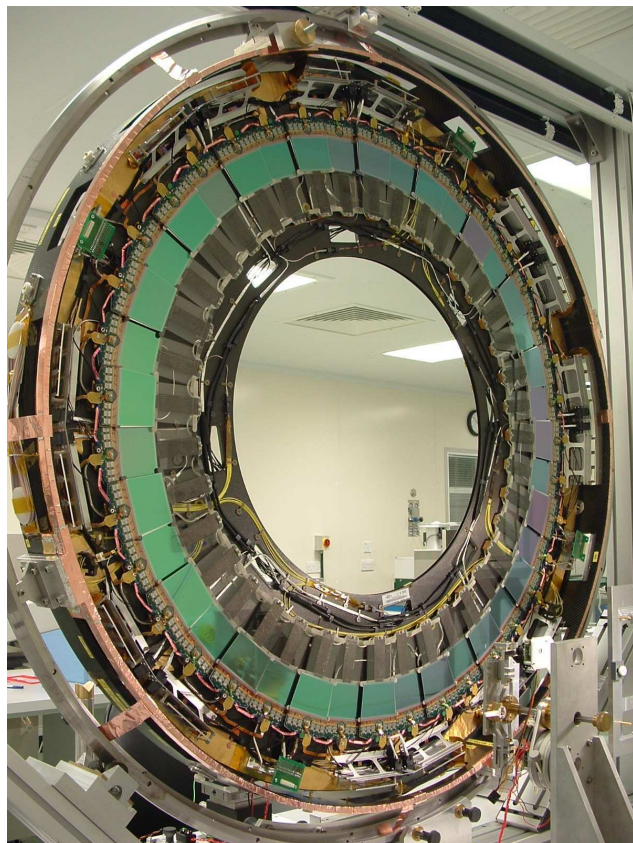


Figure 1.5: First disc equipped with MPP short middle modules.

the MPP group in the years 1997–2006 can be found in [7] (p.63-67), [1] (p.77-85). The properties of the sensors are described in [8], details of the endcap modules and their production process are given in [9]. The first 40 short middle modules<sup>1</sup>, produced by MPP, and mounted onto one endcap disc at Liverpool, are shown in Fig. 1.5.

In the years 2007–2010 for the present ATLAS detector the MPP group mainly worked on the SCT commissioning with emphasis on detector monitoring, and the alignment of the silicon part of the ID with particle tracks.

<sup>1</sup>The only difference between middle- and short middle modules is that the latter only carry one sensor per module side, i.e. the second sensor is replaced by a glass plate that is insensitive to passing particles, but retains the mechanical stability of the module. Short middle modules are used at the largest rapidities.

## SCT Commissioning

The MPP is contributing to the SCT detector commissioning in the area of online monitoring.

The SCT read-out-system (ROS) is structured in various layers. The ROS monitoring is used to continuously control the detector operation, and thereby also gives valuable information on the LHC beam condition that ATLAS is facing. It comprises error searches at chip-, link-, or read-out-driver level, but also information on the actual illumination of the SCT by means of strip occupancies. The ROS monitoring is mostly independent of the ATLAS trigger system, and can give even faster feedback on much more data, than what is eventually written to tape. The MPP group provides a ROS monitoring expert, whose task is to constantly maintain and extend the ROS monitoring software and its interface to the online monitoring of the ATLAS SCT as a whole. The fast feedback achieved is a valuable input to the detector operation, and has already led to a detailed understanding of some LHC conditions that otherwise would have been difficult to get.

## Detector Alignment with Particle Tracks

Since 2004 the MPP group develops software for the alignment of the SCT and pixel detector parts of the ATLAS ID based on particle tracks. To achieve the best possible reconstruction of tracks the exact location of all read-out channels needs to be known. In a first step this is achieved by a geometrical survey of the detector, however, for the ultimate precision the use of particle tracks is mandatory.

A crude estimate of the alignment precision aimed at can be obtained from the requirement that the detector misalignment should lead to a degradation of any track parameter of at most 20% [3](p. 215). Using this requirement, the misalignment for SCT modules in the direction perpendicular to the strip orientation should not exceed  $12\ \mu\text{m}$ . Final physics aims of ATLAS are even more demanding. For improving on the determination of the mass of the W-Boson, i.e. for an accuracy of better than 25 MeV, an alignment accuracy of about  $1\ \mu\text{m}$  transverse to the beam direction is needed [10].

As an example, for the SCT optical surveys are performed for the location of the silicon sensors within the modules (see above), and for the mounting points of the modules on the discs and barrel cylinders. The accuracy obtained with the external methods is better than  $5\ \mu\text{m}$  for the positions of the sensors within

a module. For the module locations one expects larger uncertainties. For the SCT endcap modules the expected precision from external measurements is about  $50\ (100)\ \mu\text{m}$  transverse (parallel) to the beam direction, which is not precise enough to achieve the physics goals of ATLAS.

From the above it is clear that in any case the ultimate precision has to be obtained using the trajectories of charged particles observed in real data. Using the external measurements as starting points, the knowledge of the module locations is improved by the alignment procedure based on particle tracks. The MPP strategy uses an iterative procedure to constrain the six degrees of freedom for individual modules by means of a  $\chi^2$  minimization of the sum of unbiased track residuals (see below) with respect to the alignment parameters per module. This method is called the local  $\chi^2$  algorithm. Figure 1.6 shows the local co-

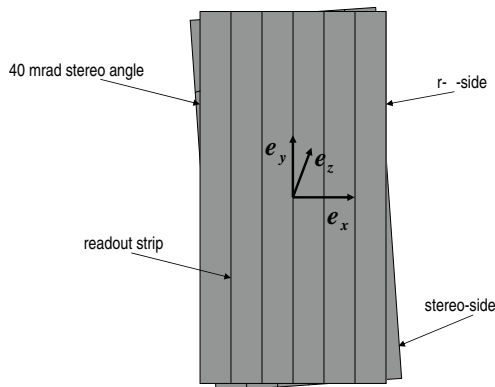


Figure 1.6: Local coordinate system of an SCT module.

ordinate system of an SCT module. The six degrees of freedom are the three coordinates along three axes running perpendicular to the strip, along the strip and perpendicular to the module plane ( $x, y, z$ ), and the three angles of rotation around these axes, namely  $\alpha$ ,  $\beta$  and  $\gamma$ . For a given single strip that gave a signal above threshold and is associated to a fitted track, the unbiased residual is defined as the smallest distance in space between the actual location of the strip and the fitted trajectory obtained when excluding that hit from the track fit. By means of iterations, this method incorporates the correlation of the locations of the modules traversed by a particle.

The algorithm has initially been implemented into the ATLAS reconstruction software for the SCT detector [11]. It was extended to also incorporate the pixel detector [12] by treating the two precise pixel measurements along the two dimensions of the pixel

as two independent measurements in analogy to the two hits recorded on the two sensors of an SCT module. Thereby the basic mathematical framework could be kept the same, facilitating the simultaneous alignment of pixel and SCT detectors.

In the conventional alignment procedures the detector geometry is only updated after a large number of particle tracks has been analyzed, and the  $\chi^2$  has been minimized with respect to the alignment parameters. As an alternative a KALMAN filter approach has been implemented and studied [13]. Here the knowledge gained by analyzing the tracks from one event is immediately fed back resulting in a geometry update after each event. The basic functionality of the KALMAN approach has been achieved. However, no striking advantage in convergence speed has been observed. In addition, in contrast to e.g. the local  $\chi^2$  algorithm, the KALMAN filter algorithm cannot be parallelized. Therefore, this possible advantage could always be compensated by parallel computing, and consequently this approach is no longer followed in ATLAS.

The local  $\chi^2$  algorithm has been used in very different environments like Monte Carlo simulated proton-proton interaction events [14], data from an ID combined test beam (CTB) run [15, 16], simulated interactions of protons with the rest gas in the beam pipe, data recorded from cosmic ray muons taken at the surface [17] as well as after completion of the ATLAS detector at its final position [15, 18], and finally with proton-proton collision data from the LHC.

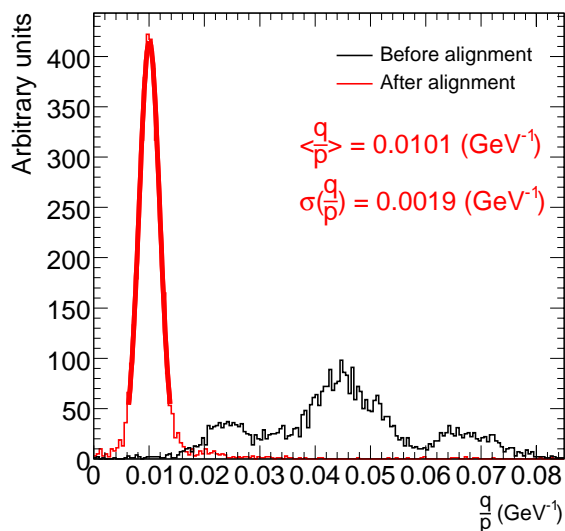


Figure 1.7: Improvement of the momentum resolution by the CTB alignment

In these studies it became evident that for each of

the data sets, due to their specific limitations, additional features had to be implemented into the algorithm to either make it properly converge, or to improve on its performance. The separation of the alignment into three subsequent levels, L1 to L3, (L1  $\equiv$  global structures, i.e. barrel and endcaps, L2  $\equiv$  superstructures, i.e. barrel layers and endcap discs, L3  $\equiv$  individual modules) has been performed and an enrichment of overlap hits (pairs of neighboring modules on superstructures slightly overlap, see Fig. 1.5) was implemented into the algorithm for better convergence [15].

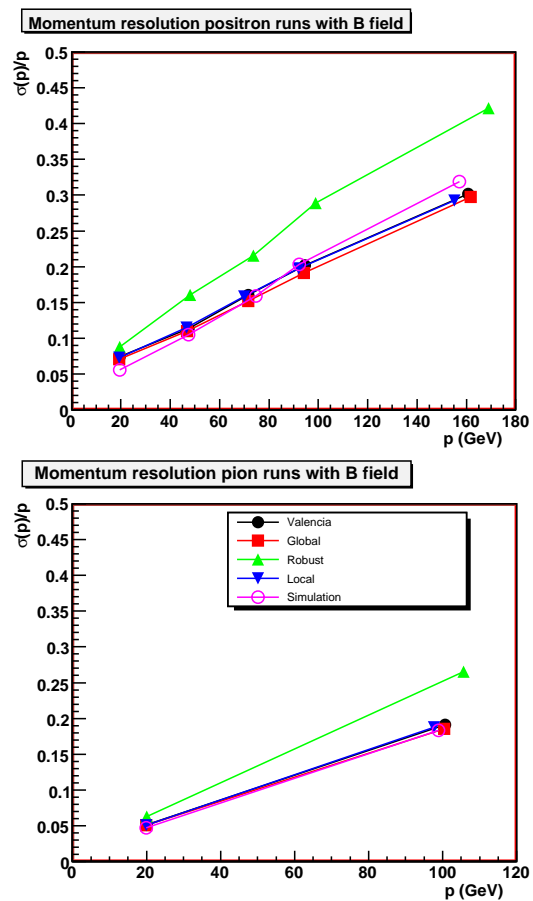


Figure 1.8: Momentum resolution for different momenta and for positrons (top) and pions (bottom) for the CTB setup when using different alignment algorithms.

For the CTB setup the improvement of the momentum resolution is seen in Fig. 1.7 [16], where the  $1/\text{momentum resolution}$  before and after performing the alignment is shown for pions with 100 GeV momentum. The initially wide distribution is greatly improved, and after the alignment the narrow distribution peaks at the correct value. In Fig. 1.8 [16] the performance of the MPP algorithm is compared to other al-

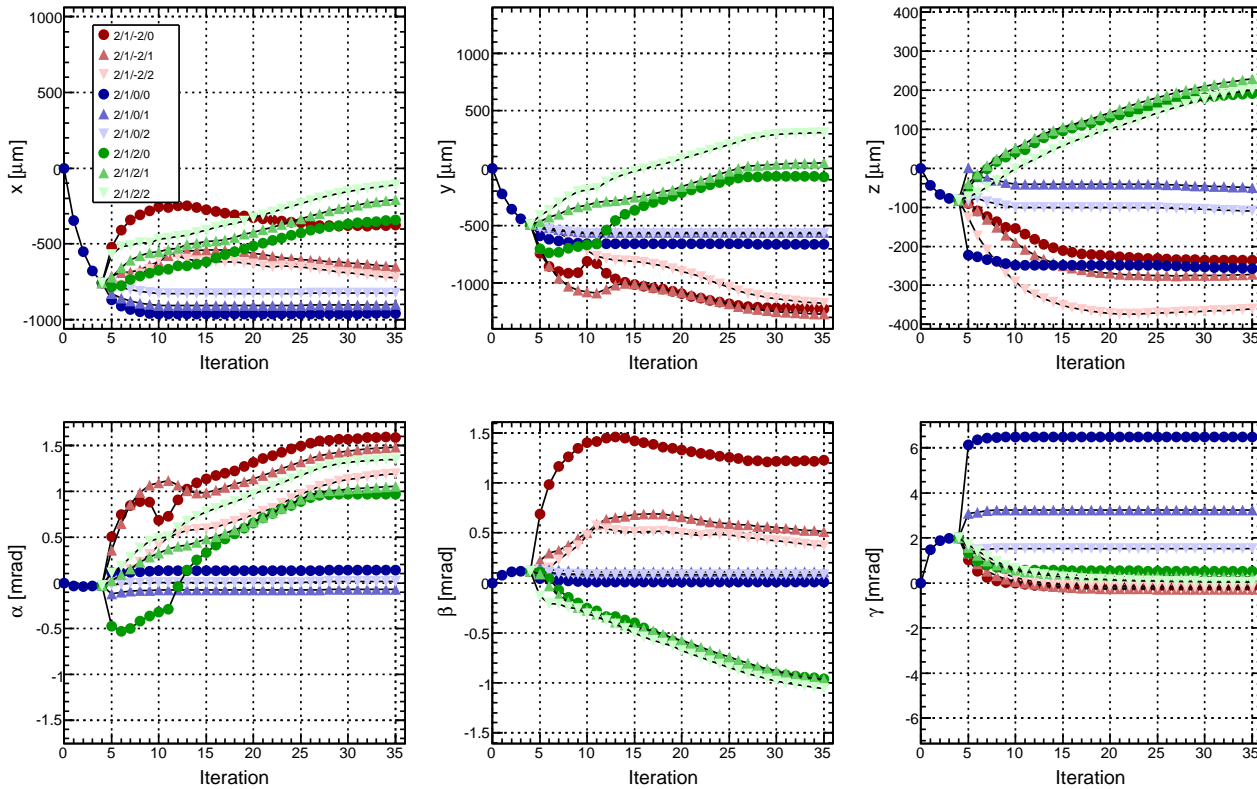


Figure 1.9: Flow of alignment parameters of the pixel layers and discs during alignment iterations for cosmic ray data.

gorithms used in ATLAS, and also to the expectation of the ATLAS Monte Carlo simulation based on the perfect knowledge of the geometry. Here, the figure of merit is the momentum resolution as a function of the known momentum. The algorithms perform similar, with the exception of the robust algorithm that, due to its simplistic but robust implementation, is slightly worse. The other algorithms also closely match the expected resolution.

For the cosmic ray muon analysis the limited illumination of the detector in the ATLAS cavern poses a challenge. Due to the geometry, cosmic rays pass barrel modules mostly perpendicular to the sensors, but endcap modules almost parallel. This renders some degrees of freedom only loosely constrained, most notably for the SCT endcaps. To accommodate this, further improved mixed levels of alignment were constructed, i.e. the level L32 (barrel L3 SCT alignment, but endcaps only L2 SCT alignment) has been implemented, supplemented by additional soft constraints to limit the parameter movements of badly constrained degrees of freedom by means of pseudo hits with appropriate uncertainties [18].

For the cosmic ray alignment Fig. 1.9 shows the

flow of the six alignment parameters of the pixel layers (blue) and discs (green, red) with consecutive iterations, using five iterations at L1 followed by thirty iterations at L2. A perfect convergence would manifest itself in horizontal lines, which is clearly better fulfilled for the barrel layers than for the discs that, due to the inclination angle of the cosmic ray muons, are less well constrained. Nevertheless, as displayed in Fig. 1.10, the residual distributions for pixel and SCT modules in barrel and endcaps are greatly improved after L2 (blue) and the final (red) alignment. Again, when comparing to the expectation for perfect knowledge of the geometry (yellow), all distributions move the right way, with the SCT barrel modules (lower left) getting the closest. The alignment based on cosmic ray data will constitute the basis for the alignment to follow with tracks coming from the interaction vertex in proton-proton collisions at the LHC.

The influence on the alignment caused by constraining the tracks to a common vertex, as well as the impact of systematic detector mis-alignments on the performance of the ATLAS b-tagging algorithms, have also been studied [14].

Finally, the recovery of so called weak deformation

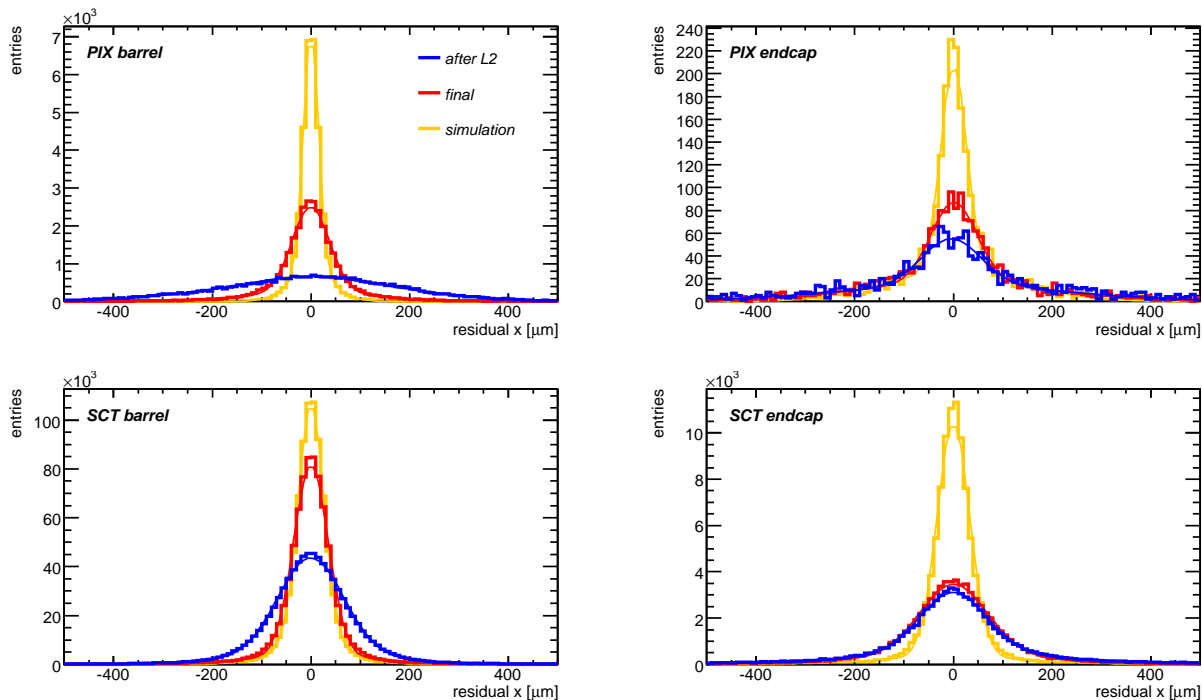


Figure 1.10: Improvements in the residual distributions for the alignment using cosmic ray data.

modes of the detector, i.e. systematic deformations that either leave track parameters virtually unchanged, or lead to changed, but consistent parameters, was thoroughly studied. The deformations were implemented into the simulation [18], and their impact on the track parameters, as well as on the measured invariant mass of the Z-Boson reconstructed from  $Z \rightarrow \mu\mu$  events, was investigated [19].

The progress of the ATLAS ID alignment has been constantly reported outside of ATLAS [20–22] by members of the MPP group. At present the alignment based on proton-proton collision data from the LHC is underway. It turned out that the SCT end-cap alignment obtained from the cosmic ray analysis is easily improved by inclusion of this data. However, the SCT barrel alignment is already so precise that significant improvements need further adaptations of the software like inclusion of constraints provided by invariant masses from known resonances.

### 1.1.2 The Hadronic End-cap Calorimeter HEC

The ATLAS MPP calorimeter group has contributed to the construction, assembly, installation and commissioning of the hadronic end-cap calorimeter (HEC) system [25,42], to the cold electronics of the HEC em-

ploying the novel concept of ‘active pads’ [138], to the read-out system of the calorimeter, and to the trigger summation for the HEC. The group has also taken over the responsibility for the hadronic calibration of the ATLAS calorimeter [35] and its application to  $t\bar{t}$  [39] and jet analyses [36, 37]. The large  $t\bar{t}$  cross section provides even in the LHC start-up phase a reasonable statistic of  $t\bar{t}$  events. In the very first stage they will yield a powerful in-situ test of the hadronic calibration in ATLAS.

**Present HEC Cold Electronics.** The signal processing of the HEC employs the notion of ‘active pads’ which keeps the detector capacities at the input of the amplifiers small and thereby achieves a fast rise time of the signal [138]. Short coaxial cables are used to send the signals from the read-out pads to preamplifier and summing boards (PSB) located at the perimeter of the wheels inside the liquid argon. Figure 1.11 shows a fully assembled HEC wheel in the horizontal position on the assembly table with the PSB boards (see Fig. 1.12) at the outer circumference.

The lateral segmentation is  $\Delta\eta \times \Delta\phi = 0.1 \times 0.1$  up to  $\eta = 2.5$  and  $\Delta\eta \times \Delta\phi = 0.2 \times 0.2$  for higher  $\eta$ , and the longitudinal granularity is a fourfold read-out segmentation. The detector capacitance varies from 40 to 400 pF giving a rise time variation from 5 to 25 ns.

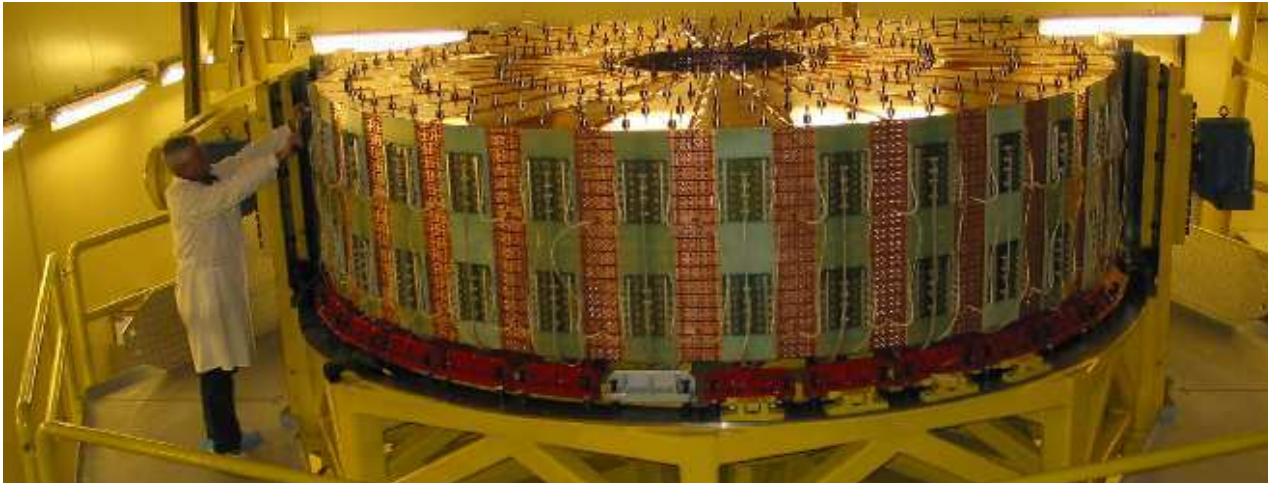


Figure 1.11: A HEC wheel fully assembled on the assembly table showing the ‘active pad’ electronics. The PSB boards with the GaAs IC’s are mounted at the periphery of the wheel.

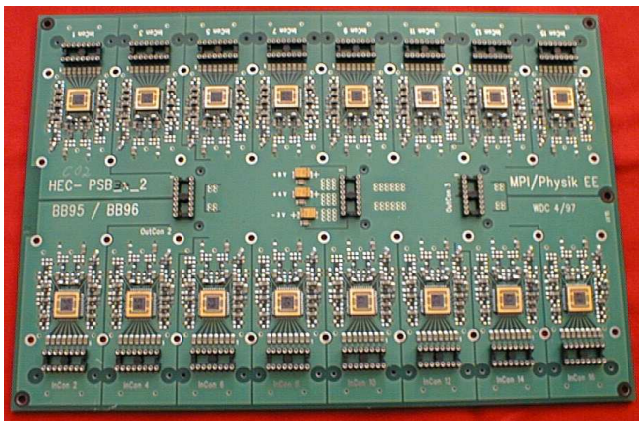


Figure 1.12: Picture of a Preamplifier and Summing Board PSB showing the 16 GaAs IC’s with the related input connectors. The output connectors are in the center of the board.

These PSB’s carry highly integrated amplifier and summing chips in Gallium-Arsenide (GaAs) technology. The signals from a set of preamplifiers from longitudinally aligned pads (2, 4, 8, or 16 for different regions of the calorimeter) are then actively summed forming one output signal, which is transmitted to the cryostat feed-through.

The GaAs TriQuint QED-A  $1\ \mu\text{m}$  technology has been selected for the front-end ASIC because it offers excellent high frequency performance, stable operation at cryogenic temperatures and radiation hardness [138]. The front-end chip consists of 8 identical preamplifiers and two drivers. The summing scheme is implemented with external components and intercon-

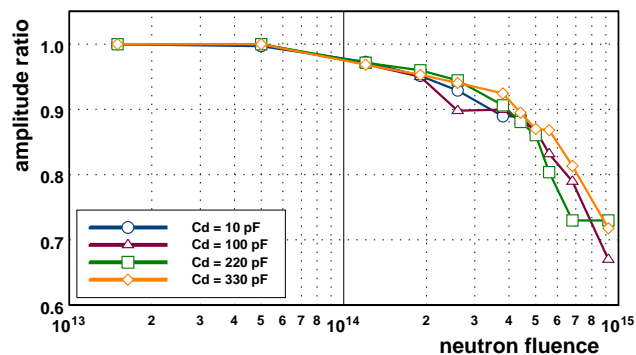


Figure 1.13: The signal amplitude measured after values of neutron fluence from  $1.5 \times 10^{13}$  to  $9 \times 10^{14} n/cm^2$  for 4 different detector capacities. Shown is the ratio to the signal amplitude before the irradiation.

nections made on the PSB (see Fig. 1.12) at the outer circumference.

In the hadronic endcap calorimeter a neutron fluence of  $0.2 \times 10^{14} n/cm^2$  is expected after 10 years of LHC operation at high luminosity. It is known that GaAs is a radiation resistant semiconductor. The radiation hardness has been studied at the *IBR - 2* reactor in Dubna, Russia, with a set of pre-production chips. Various types of tests have been performed. Seven chips were exposed to a total fluence of fast neutrons of  $(1.11 \pm 0.15) \times 10^{15} n/cm^2$  and an integrated  $\gamma$  dose of  $(3.5 \pm 0.3) \text{ kGy}$ . A second set of 8 chips was irradiated with  $\gamma$ 's up to a total dose of  $(55 \pm 8) \text{ kGy}$  accompanied by a fast neutron fluence of  $(1.1 \pm 0.2) \times 10^{14} n/cm^2$ . In these tests the ASICs

were kept in a cryostat filled with liquid nitrogen. The standard set of characteristics like transfer function, rise time, linearity and equivalent noise current of the preamplifiers was measured. The measurements show that the preamplifier characteristics start to degrade when the neutron fluence exceeds approximately  $3 \times 10^{14}$  n/cm<sup>2</sup>. Fig. 1.13 shows the degradation of the amplitude with neutron irradiation for four different values of input (detector) capacitance. Such a degradation will result in a non-uniform response, which is critical since between 2 and 16 read-out pads are summed, and will ultimately impact the resolution required for physics measurements.

Similar measurements with  $\gamma$ -irradiation show that the characteristics stay unchanged up to a dose of at least 50 kGy. Both boundary values are well above the radiation levels expected in the final ATLAS environment at LHC.

Another important practical aspect of the cold electronics is the heating of the chips that can finally result in bubbling of the liquid argon. The bubbles propagating to a LAr detector gap can cause high voltage discharges. Therefore the power consumption has to be kept low.

### Data Analyses from Beam Tests

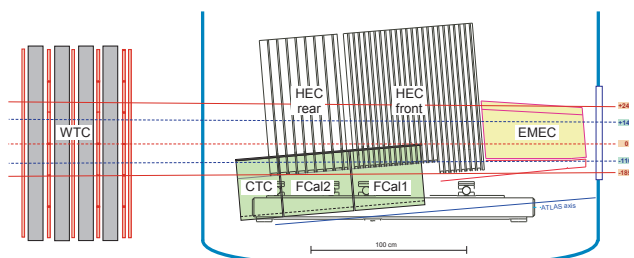


Figure 1.14: Schematic view of the calorimeter set-up of the 2004 combined beam test. Shown are the inner EMEC (front), the HEC, the FCal1 and FCal2 modules (below the HEC modules). In addition, the cold tail catcher (CTC, behind FCal2) and the warm tail catcher (WTC, outside of cryostat) are shown as well.

The analysis of data from HEC only [26] and combined beam tests of the calorimeters, which were pursued in 2002 and 2004, [27–30] (see description of these beam tests in our previous report [1] (p.85-94)), is continued and still provides valuable insights into the calibration of the detector response and the simulation of hadronic showers.

In the latest beam test the modules have been exposed to beams of electrons, pions and muons with energies up to 200 GeV covering the transition region  $2.5 < |\eta| < 4.0$  [31]. This is a particularly complex region of overlap of the three end-cap calorimeters. The electromagnetic endcap calorimeter (EMEC), the HEC and the forward calorimeter (FCal) modules are positioned as in ATLAS, including all details of cryostat walls and supports (dead material). One quarter of the front and rear HEC wheels have been assembled, but with small modules which cover in size only the forward  $\eta$  region. Similarly, one EMEC inner wheel module (1/8 of the EMEC wheel) and 1/4 of the FCal1 and FCal2 have been assembled. Fig. 1.14 shows a schematic of the set-up of the different calorimeter modules. The beam enters through the cryostat window from the right at a nominal position of  $y = 0$  cm.

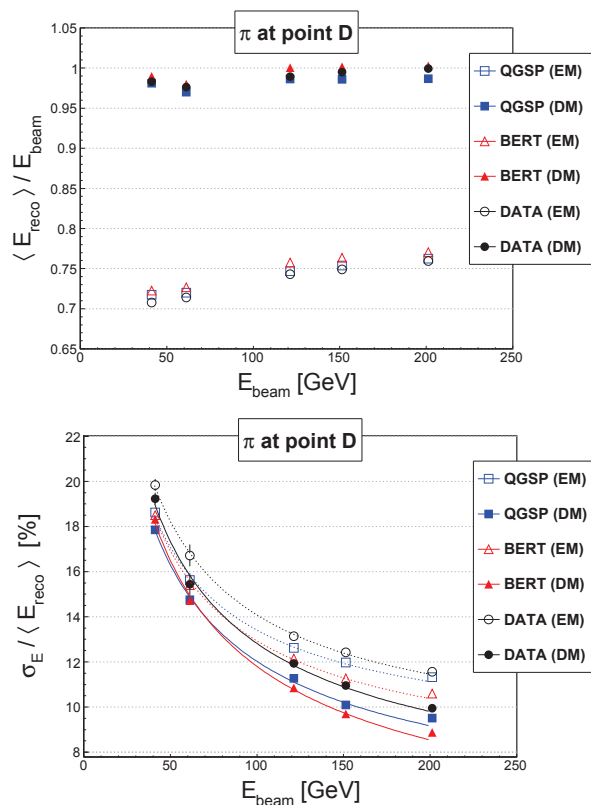


Figure 1.15: Linearity (upper plot) and resolution (lower plot) for charged pions in the EMEC/HEC region (point D) of the 2004 combined test beam. Open symbols are for uncalibrated (EM), filled symbols for local hadron calibrated clusters (DM). The data is compared to Geant4 simulations with the Quark-Gluon String Precompound (QGSP) model and a variant of it adding Bertini intra-nuclear cascades (BERT).

The validity of the local hadron calibration ap-

proach (described in more detail further below) was tested for the first time on real data in a diploma thesis [43] in 2008 utilizing as a first step the calibration constants derived for ATLAS. The results for linearity and resolution for charged pions in the EMEC/HEC region before and after calibration are depicted in figure 1.15 in comparison to the expectations for two different hadronic showering models (so called hadronic physics lists in Geant4 [41]).

The linearity is found to be restored within 1% beyond 60 GeV and within 3% below that energy. Both shower models are in good agreement with the data for the linearity before and after the calibration. The resolution is improved by the calibration although the constants are not optimized for the test beam setup. Here both shower models predict better resolutions compared to data but the same relative improvement due to calibration is found for both simulations and the data. The test beam results are used to further tune the shower models in Geant4.

The currently ongoing analysis of the test beam data focuses on the performance with dedicated constants.

### Commissioning of the HEC

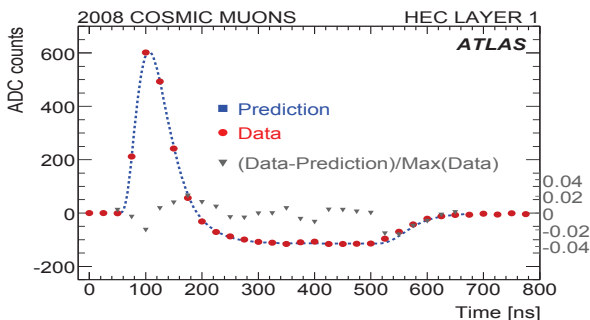


Figure 1.16: Typical pulse shapes, recorded during the cosmic ray campaign, for the first layer of the HEC. The relative difference between data and prediction is indicated by triangles on the right scale.

**Cosmic Muons.** First tests reconstructing the real particle response in ATLAS have been done using muons from cosmic rays in the years 2007 and 2008 [42, 44]. For the HEC the incoming cosmic ray flux is mostly parallel to the orientation of the absorber plates and the LAr gaps. Nevertheless, using inclined tracks and reconstructing the effective track length in individual read-out cells, a cross check of the calibration can be done. Alternatively the energy in the calorimeter cells alone can be used to select data sam-

ples independent of the muon tracks. This approach has been adopted for the pulses in figure 1.16. Only small deviations (3 – 5%) of the prediction from the data in the peak region and the end of the negative undershoot are observed.

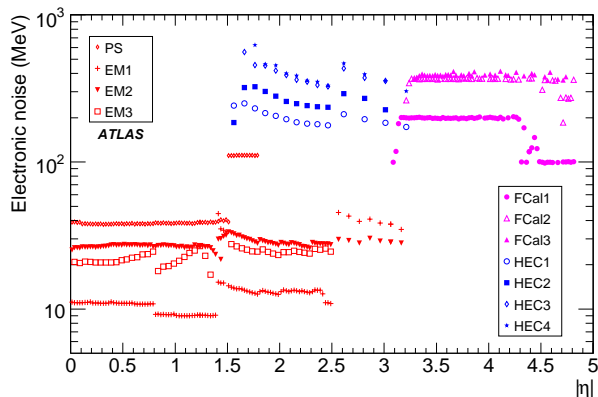


Figure 1.17: Electronic noise ( $\sigma_{\text{noise}}$ ) in randomly triggered events at the EM scale in individual cells for each layer of the LAr calorimeter as a function of  $|\eta|$ . Results are averaged over  $\phi$ .

Random triggers in the cosmic data are taken to measure the electronics noise, and the stability of pedestal with time. Figure 1.17 shows the measured noise on cell level for each layer of the LAr calorimeter as a function of  $|\eta|$ . Here the noise is defined as the measured width of the distribution of the reconstructed energy per cell in events without any expected ionization signal. Good agreement with predicted values from simulations [2] is observed and the uniformity in  $\phi$  and the symmetry in  $\eta$  is within a few percent. The stability of the pedestals in the HEC was monitored over 6 months and showed variations of 2 MeV only – well below the numerical precision of the energy computation which is 8 MeV.

The transverse missing energy in random triggers is sensitive to correlated noise in the calorimeter and has been used together with noise suppression methods to search for unaccounted effects in the noise description. Figure 1.18 shows  $E_T^{\text{miss}}$  computed for all cells above  $2\sigma_{\text{noise}}$  and for cells inside topological clusters [34] which are seeded by cells above  $4\sigma_{\text{noise}}$ . Both are consistent with the Gaussian model of electronics noise although the agreement in the stricter suppressing case using topological clusters is a bit worse due to the enhanced sensitivity to details in the noise description. The absence of large tails shows that the electronics noise is well under control and not perturbed by large

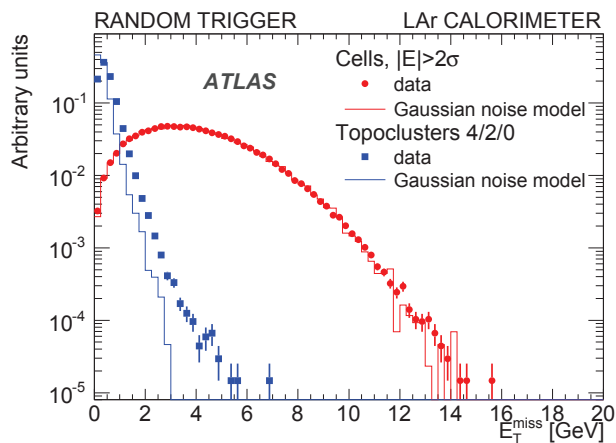


Figure 1.18:  $E_T^{\text{miss}}$  distribution with LAr calorimeter cells for 135,000 randomly triggered events in June 2009. The dots (squares) show the cell-based (cluster-based) methods in the data, and the histograms show the equivalent distributions for the Gaussian noise model.

correlated effects.

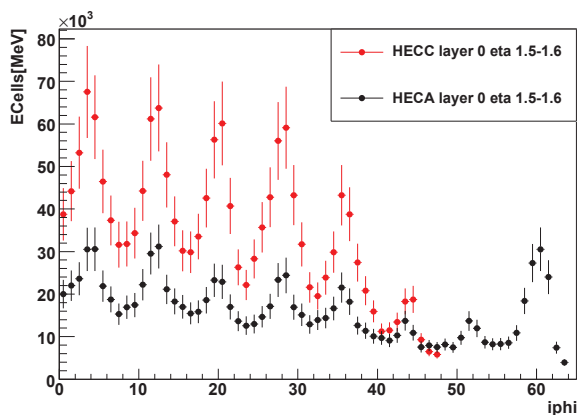


Figure 1.19: The average cell energy vs. the phi index on side A (C) the HEC in black (red) for 85 beam splash events from 2008. The periodic structure is due to the material in the endcap toroid magnets.

**Beam Splash Events.** The turn on of the LHC in 2008 and again in 2009 provided with so-called beam-splash-events another set of commissioning data. In beam splash events circulating single beams at 450 GeV are dumped on collimators some 140 m upstream of the detector and cause a large particle spray to pass the detector from one end-cap to the other leaving huge amounts of energy (typical are 1000 TeV and more) in the calorimeters. The comparison for each endcap of the average cell energy as function of  $\eta$  and

$\phi$  for the 85 beam splash events observed in 2008 allowed to identify all channels with reduced high voltage, where the decrease in signal is larger than 20% [44]. Figure 1.19 shows the average cell energies on both sides for a given bin in  $|\eta|$  as a function of  $\phi$ . The missing quadrant on the C-side (missing dots at high  $\phi$  indices) was caused by a malfunctioning power supply which is meanwhile operational again. Currently about 1% of all channels in the LAr calorimeters are not operational and a few percent require a correction for reduced high voltage.

The relative timing for the readout of the calorimeter systems was also tuned with the splash events. Since at these large energies the time resolution is well below 1 ns the expected time differences due to time-of-flight and the trigger could be confirmed within  $\pm 2$  ns [42].

**Collisions.** Finally late in 2009 the first collisions at center-of-mass energies of  $\sqrt{s} = 900$  GeV have been recorded with the ATLAS detector. Comparisons to simulations of QCD processes (minimum bias events) allowed a first validation of the clustering and calibration scheme described in the next paragraph.

Examples for these early validations with physics events are shown in figures 1.20 and 1.21.

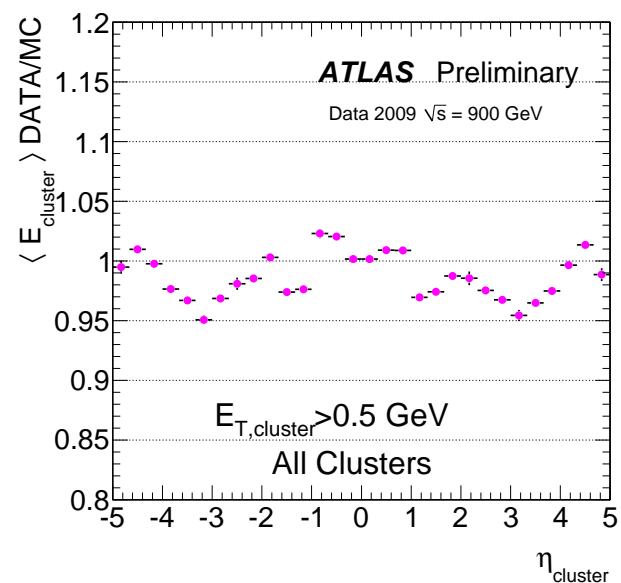


Figure 1.20: Ratio of average uncalibrated cluster energies to expectations from simulations for collisions at  $\sqrt{s} = 900$  GeV.

Both figures demonstrate that the systematic error for the clustering and the calibration are well under

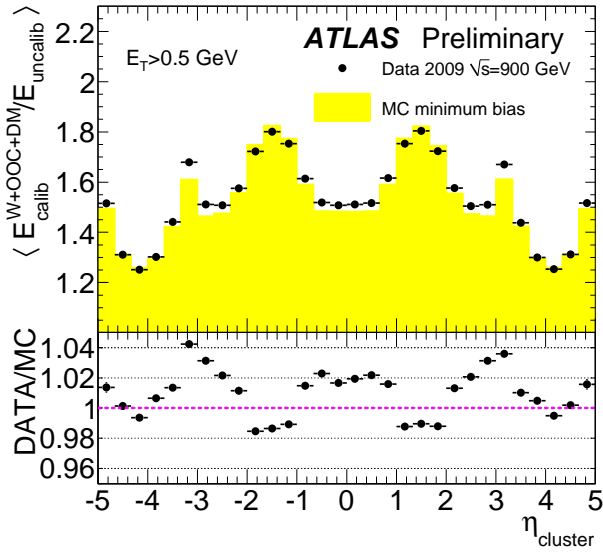


Figure 1.21: Average calibrated cluster energies normalized to uncalibrated energies (upper plot) and the ratio data to simulation (lower plot) for collisions at  $\sqrt{s} = 900$  GeV. The simulation is shown in yellow in the upper plot.

control and currently are on the level of  $< 5\%$ .

### Local Hadron Calibration

The local hadronic calibration [35], which is developed in large parts in our group has been further refined in the reporting period and validation efforts started with collisions data and with simulated  $t\bar{t}$ -events [39, 44].

The aim of the method is to provide the energy on the hadron level for each individual cluster in the calorimeter which in turn serve as input to the reconstruction of higher level objects like jets [36, 37] and missing transverse energy [38]. The most important steps in this procedure are:

1. **Topological Clustering.** Clusters [34] are reconstructed in the calorimeters around seed cells with very significant energy ( $|E| > 4\sigma_{\text{noise}}$ ). Neighboring cells in the same and in neighboring layers are added to the cluster regardless of their energy and expand the cluster further by their respective neighbors in case they're found to have  $|E| > 2\sigma_{\text{noise}}$ . Clusters are merged in this step if they share a cell with  $|E| > 2\sigma_{\text{noise}}$ . The so-found clusters are split and regrouped again around local energy maxima ( $E > 500$  MeV). In

this step merging of clusters is not allowed and border cells are shared among the clusters. The resulting clusters have a close correspondence to individual particles hitting the detector and thus motivate the local hadron calibration approach.

2. **Classification.** Each cluster is compared by means of cluster shape variables like depth and energy density with a-priori probabilities for such shapes derived from simulations of charged and neutral pions. If the resulting probability of the cluster to stem from a charged pion is above 50% the cluster is classified as hadronic, those with values below as electromagnetic. The probability  $p_{\text{had}}$  to be hadronic is stored as well for each cluster.
3. **Cell Weighting.** Invisible hadronic energy deposits are recovered in this step by applying cell weights  $w_{\text{cell}}$  derived from charged pion simulations to the cells in all clusters. The weights are functions of cell position, cell energy density and cluster energy as inspired by the H1 weighting scheme [32, 33]. Since electromagnetic showers do not lead to invisible energies (i.e. their weight ought to be 1) the final weight per cell is given by  $p_{\text{had}} \times w_{\text{cell}} + (1 - p_{\text{had}}) \times 1$ .
4. **Out-Of-Cluster Corrections.** Both, electromagnetic and hadronic showers lose energies on the edge of the shower due to the applied noise cuts. Averaged corrections depending on  $\eta$ , shower depth and energy are derived for both and applied with the same probabilities as in the weighting step.
5. **Dead-Material Corrections.** Energy deposits in non-instrumented material upstream of, in between, and beyond the calorimeter is recovered in this step. The correlation of the losses with energy deposits in calorimeter layers close to the dead-material (like the pre-sampler for any material upstream) is used here and parameterized corrections are applied again with the probability weighted sum of hadronic and electromagnetic corrections.
6. **Jet-Level Corrections.** Finally some corrections need to be applied to the jets made out of the calibrated clusters mainly due to particles not leaving any signal in the calorimeter and thus not accounted for in the correction steps above. The

main reasons for missing signals are the noise threshold for seeding clusters, the magnetic field bending charged particles with low  $p_T$  outside the jet acceptance and absorbed particles in the dead material upstream of the calorimeters.

Figure 1.22 shows the comparison of the average cluster energies normalized to the uncalibrated energy as a function of  $\eta$  after the individual cluster calibration steps outlined above in the first collisions data. For this inclusive plot low energetic clusters dominate and the largest corrections are applied in the out-of-cluster and dead-material correction steps. As already shown in figure 1.21 the agreement with simulations is better than 4% for all  $\eta$  regions.

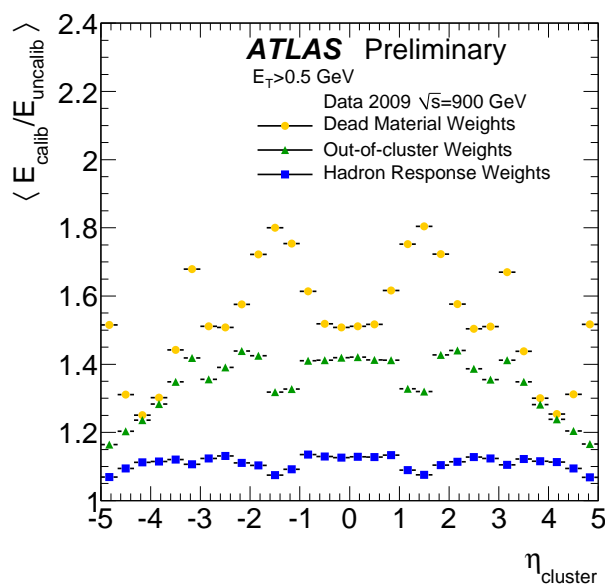


Figure 1.22: Average cluster energies normalized to the uncalibrated energy after various calibration steps for collisions at  $\sqrt{s} = 900$  GeV.

Current developments focus on the jet-level corrections, where the energy distribution of the constituent clusters in a jet is used to estimate the lost energy fraction, and the validation of the local hadron calibration with isolated hadrons in collision data at  $\sqrt{s} = 7$  TeV and inclusive cluster samples extending the studies shown here for  $\sqrt{s} = 900$  GeV.

Another focus concerns the work on refined simulations for jets in ATLAS with the ability to tag each energy deposit with the originating hadron produced by the generator. This technique allows to use the jet simulations directly instead of single particle simulations to derive the local hadron calibration constants.

First simulations with this new labeling scheme are already available and refined calibration constants are expected within the next few months.

### 1.1.3 The Muon Drift Tube Chambers MDT

The 88 Monitored Drift Tube chambers built at the Max-Planck-Institut für Physik were installed in the ATLAS experiment from February to June 2006, after being integrated with their respective trigger chambers and tested at CERN in 2005 [48–51] (see Figure 1.3). The chambers were the first to be mounted on the rail system in the barrel part of the spectrometer and were positioned with an accuracy of about 1 mm [50], well within the specifications. The barrel part and the middle wheels of endcaps of the muon spectrometer were installed in 2006, the missing inner and outer endcap wheels followed in 2008, completing the muon spectrometer. 10 of 62 additional chambers improving the acceptance in the barrel-endcap transition region have been installed in 2009, the rest will follow in 2012.

The Max-Planck-Institut für Physik has taken a leading role in the commissioning of the ATLAS muon spectrometer and, via a representative in the ATLAS Muon Steering Group, is responsible for the overall coordination of the operation and maintenance of all MDT chambers since beginning of 2008. In addition, our MDT group provides on-call gas system and detector experts, as well as the data quality expert, who is responsible for the final sign-off of the MDT data. The MPP team is also involved in providing training and documentation for the shifters operating the detector in the ATLAS control room.

The commissioning of the MDT chambers should have followed their installation closely, but it was delayed due to the late installation of the final services in the experiment—the routing of the low and high voltage cables, readout fibres, and gas pipes and valves—and the availability of the commercially manufactured power supply boards. Thus, the commissioning phase of the muon spectrometer spanned from the end of 2006—with only 13 MDT chambers operational on temporary services—to September 2008, when the first beam was circulated in the Large Hadron Collider (LHC), and 98.8% of the 350000 channels of the 1088 MDT chambers of the muon spectrometer were operational.

A notable exception to the general commissioning strategy were the MPP MDT chambers: immediately after their installation and in regular intervals afterwards their gas tightness, HV stability and the sta-

bility of the chamber geometry has been tested [50]. As a result, these chambers exhibited less problems than other types when finally put into operation. The chambers were connected to the ATLAS gas system in 2007 and to the power supplies and read-out chain in 2008 by a team of 3 technicians and 4 physicists from MPP. Due to their exposed position at the outside of the ATLAS detector and the hostile environment with cooling and cryogenic stations and electronics racks on the surrounding structures nearby, the MPP chambers showed an increased noise pickup compared to the inner chambers. The situation was remedied by designing additional low-pass filters for the high voltage lines which were mounted on all MPP chambers in 2008 [52]. These filters are now also used on other chambers in the muon spectrometer which suffer from high noise rates.

The commissioning of the ATLAS muon spectrometer encompasses the connection of services to the chambers and the electronic racks in the experimental cavern. The MPP team supported this global work with 1–2 technicians and 2–4 physicists during 2007 and 2008. About 50% of all barrel MDT chambers were connected by the team and subsequently integrated in the read-out and debugged. Faulty front-end electronics cards were exchanged and high voltage failures due to a few broken anode wires in the drift tubes or dirt in the Faraday cages—caused by the ongoing installation of other subdetectors—were fixed. The channel mapping of the optical fibres for the read-out and the high and low voltage cabling of the whole spectrometer was verified and corrected. After the chambers had been integrated in the read-out of the experiment, data taken with cosmic ray muons is used to verify their proper operation and test their performance [53, 54]. An event display of one of the first recorded cosmic muons traversing the entire muon spectrometer is shown in Figure 1.23; see Figure 1.3 for a comparison with the installed detector.

A major part of the commissioning phase consisted of taking into operation the recirculating MDT gas system—the largest gas system of any LHC experiment. This effort was coordinated and to a large part executed by the MPP team. The system consists of 15 distribution racks serving 226 individual gas manifolds, each connected to 4 to 32 MDT chambers. The total gas volume of  $2.2 \times 10^6$  bar L is exchanged once every 24 hours, and about 10% of the gas is replaced. In addition to the 2.8 million O-ring seals of the on-chamber gas distributions. The systems has 4500 man-

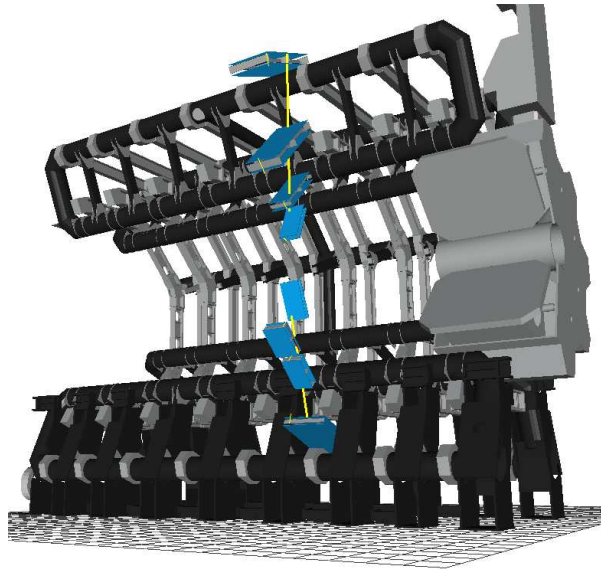


Figure 1.23: A cosmic muon traversing the ATLAS muon spectrometer, recorded in 2008. Only the MDT chambers with hits close to the reconstructed track and part of the toroid magnet system is shown. The topmost MDT chamber was built at MPP.

ual valves and 18000 connections. Stringent requirements exist for the allowed leak rate which should not exceed  $2 \cdot 10^{-7}$  bar L/s per drift tube to avoid back diffusion of air into the system which would change the space to drift relation and degrade the drift tube efficiency. The vast majority of all chambers and connections fulfils the tightness requirements after several hundreds of leaks were repaired. At the moment, the total leak rate of the system is about 30% higher than the allowed limit, caused by several larger leaks which will be repaired during the next LHC shutdown when access is possible. No adverse effect of the larger leaks has been observed so far. The purging of all MDT chambers, the leak search and repair, and the adjustment of the distribution system took an estimated manpower of 1.5 man years during 2007 and 2008. Periodic leak tests are still performed to spot new leaks in the system.

As all other subdetectors of the ATLAS experiment, the MDT system has entered routine operation in 2009 and 2010. Annual failure rates of the active and passive front-end electronics on the chambers, the high voltage distribution, and the detector control system are all well below 1%, but the more than 50000 different components nevertheless requires a continuous maintenance of the system to which the Max-Planck-Institut für Physik contributes a major share of manpower and expertise. The MDT system has been oper-

ational with 99.7% of all channels taking high quality data for the past two years.

### **Muon Detector Commissioning with Cosmic Rays**

The MPP group is contributing to all aspects of the software development for the analysis of the ATLAS muon detector data, including the calibration of the space drift-time relationship of the MDT chambers [55–61], the alignment of the muon spectrometer with muon tracks [50, 52, 62–66], the evaluation and monitoring of the data quality of the muon detector [67, 68], optimisation of the muon reconstruction for the high background rates expected at the LHC [64, 69], and the Monte Carlo simulation programs for the muon spectrometer [70, 71]. The first two projects which are of central importance for the operation and performance of the ATLAS muon spectrometer and in which the MPP group plays a leading role are discussed in more detail in the following.

**Drift Tube Calibration.** The pressurised drift-tube technology has been chosen for the ATLAS muon tracking chambers because of the high spatial resolution of better than  $80\ \mu\text{m}$  which can be achieved for individual drift tubes by measuring the drift time of the ionisation electrons to the sense wires. In order to reach the required spatial resolution of the chambers of  $40\ \mu\text{m}$  not only the the sense wires have to be positioned in a chamber with an accuracy of  $20\ \mu\text{m}$  but also the space drift-time relationship of the approximately 400,000 drift tubes in ATLAS has to be known with the same precision. The drift properties of the electrons depend on the temperature and pressure of the drift gas as well as on the magnetic field and the rate of background hits from neutrons and photons which can be very high at the Large Hadron Collider (LHC). For the regular calibration of the space drift-time relationship, correlations between the positions measurements of the drift tubes hit by a traversing muon can be used.

We have developed fast and efficient algorithms for the determination of the space drift-time relationship [49, 55] and of the spatial resolution [56] of the MDT chambers which are now part of the ATLAS data reconstruction software. The algorithms have been extensively tested with simulated data, cosmic ray commissioning data [54, 55], in a muon beam at CERN [57, 58] and under LHC operating conditions, in magnetic fields and at high background rates, using test beam data taken by our group at the Gamma

Irradiation Facility at CERN [59]. A model for magnetic field corrections to the space drift-time relationship has been derived from the measurements [60].

The large sample of cosmic ray muons recorded by the ATLAS detector in 2008 and 2009 allowed detailed studies of the robustness of the calibration algorithms. The  $r$ - $t$  calibration algorithm showed robust operation for all the chambers apart from the chambers with muons at  $30^\circ$  incidence angles where all drift radii are equal. The  $r$ - $t$  calibration method originally applied to straight track segments in triplelayers of the muon chambers had to be extended to curved track segments in the muon chambers to achieve the same level of robustness for all muon chambers [72]. Figure 1.24 shows the accuracy of the space drift-time relationship provided by the improved calibration algorithm as a function of the number of collected muon track segments in a chamber for simulation and cosmic ray data. The required accuracy of  $20\ \mu\text{m}$  is reliably achieved with 3000 muons per chamber for all chambers of the muon spectrometer. The predicted accuracy is confirmed by the studies with muons from cosmic rays.

The dependence of the drift time on the magnetic field strength measured with cosmic rays in the ATLAS detector agrees well with the model based on the test beam measurements (see Figure 1.25).

The MPP group is operating one of the three computing centres dedicated to the calibration and the alignment of the ATLAS muon spectrometer [61] using a special data stream of muon tracks reconstructed by the ATLAS second level trigger algorithms. The commitment of the MPP group to calibrate roughly one third of the MDT chambers and to align the muon detectors with muon trajectories includes the development of fully automated calibration and alignment procedures and monitoring tools [73].

**Muon Chamber Alignment with Tracks.** To achieve the required momentum resolution of the ATLAS muon spectrometer up to the highest muon energies, the relative positions of the chambers have to be continuously monitored and misalignment corrections have to be applied to the measured track sagitta with an accuracy of  $30\ \mu\text{m}$ . The MPP group contributed significantly to the development and test of the high-precision optical alignment monitoring system for the muon spectrometer [45]. The group also developed algorithms for the alignment of the ATLAS muon spectrometer with muon tracks [62–66].

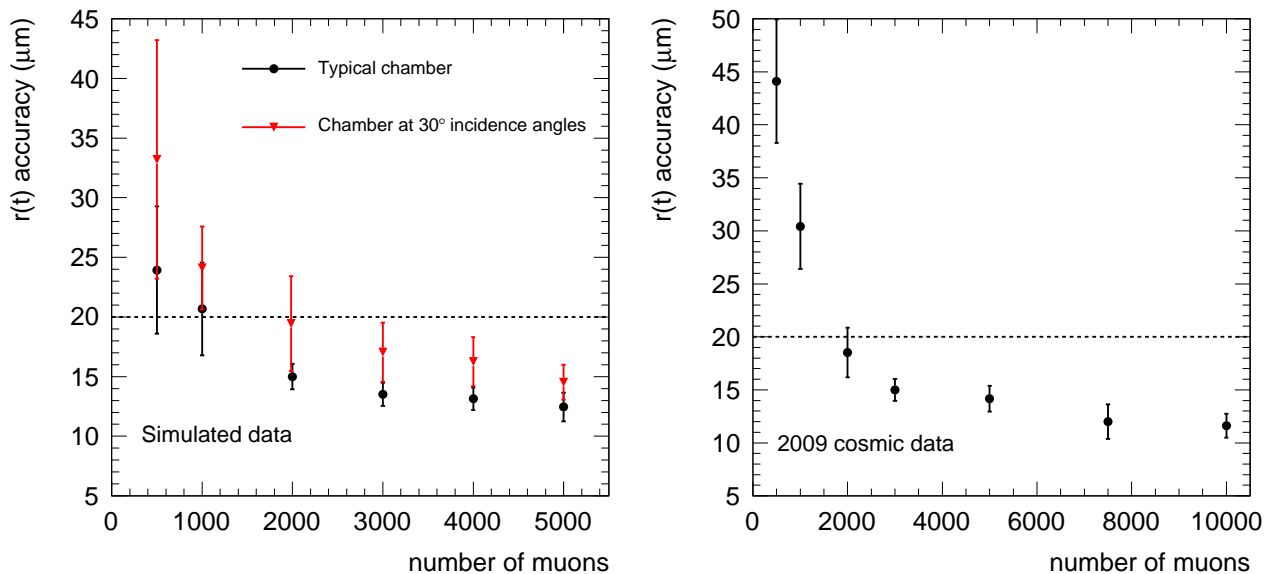


Figure 1.24: Accuracy of the calibration of the space drift-time relationship of the drift tubes of the ATLAS MDT chambers as a function of the number of cosmic muon tracks used per chamber. Left: Simulated data. Right: Cosmic ray data confirming the predicted  $r$ - $t$  accuracies.

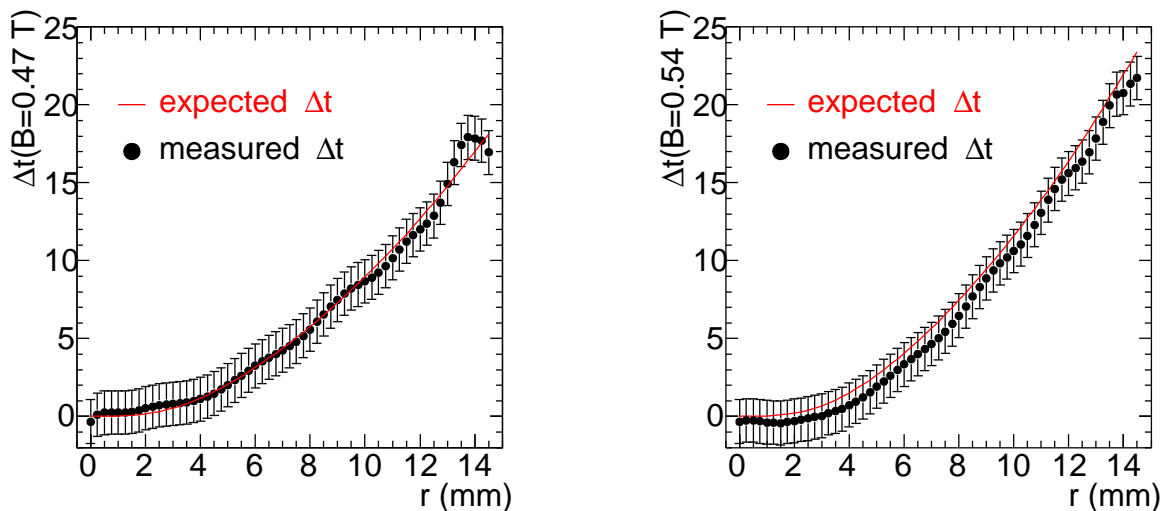


Figure 1.25: Magnetic field corrections to the drift time  $t$  in different regions of magnetic-field strength (0.47 T on the left, 0.54 T on the right) in MDT chambers in the middle layer of the large sectors of the barrel muon spectrometer as a function of the drift distance  $r$ . The measured difference in the drift times with and without magnetic field  $B$  agrees well with the model expectation in red derived from test beam measurements. The error bars of data points correspond to the estimated  $r$ - $t$  accuracy of  $20 \mu\text{m}$ . The drift time correction increases with the distance to the wire because of the deflection of the drifting electrons in the magnetic field oriented in the direction of the tube axis.

In the barrel part of the spectrometer, only the large chamber sectors mounted in between the magnet coils can be fully aligned with optical sensor measurements. The small chamber sectors mounted on the coils (see Figure 1.3) have to be aligned with respect to the large sectors with muon tracks passing through the overlap regions between the the small and large sectors. The

MPP group is providing these alignment corrections using the muon calibration data at the Munich calibration and alignment computing centre [61, 62].

Straight muon tracks measured while the toroid magnets are turned off are needed for the precise determination the initial chamber positions after installation as a starting point for the monitoring of further cham-

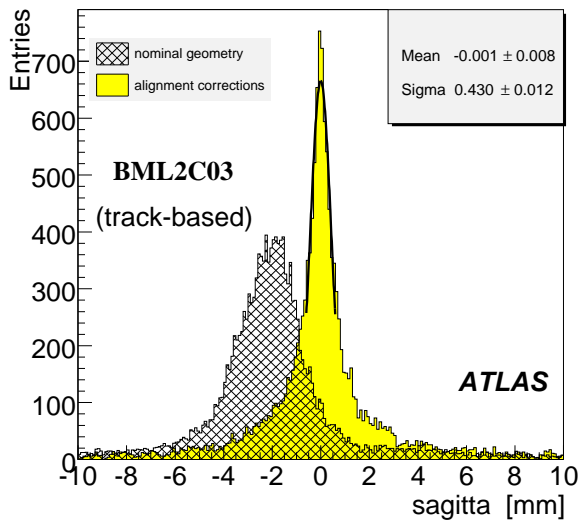


Figure 1.26: Sagitta distributions of straight cosmic ray muon tracks before and after the alignment with tracks. The mean value is on the order of a mm before the alignment procedure consistently with the mechanical installation accuracy. The mean value of the distribution is shifted towards 0 and its width is reduced by the track alignment procedure.

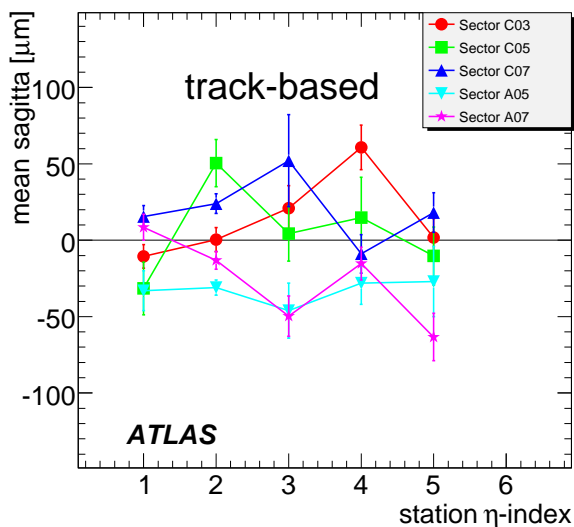


Figure 1.27: Mean value of the apparent track sagitta distributions obtained using a track-based alignment (large sectors). The station index describes the position of the MDT chamber along the z-direction (parallel to the beam pipe). The achieved accuracy of the alignment is independent of the sector and station index.

ber movements by the optical sensors mounted on the chambers. An efficient algorithm has been developed and successfully applied to cosmic ray commissioning data [63]. Figure 1.26 shows the mean value of the apparent sagitta of straight cosmic muon tracks after the initial alignment with straight cosmic muon tracks. In Figure 1.27 the mean value of the apparent

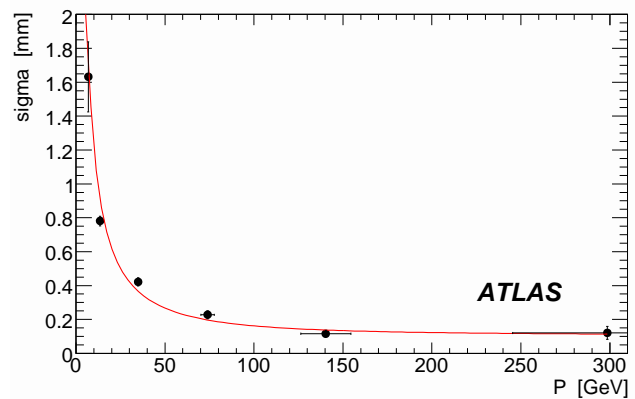


Figure 1.28: Resolution of the sagitta measurement as a function of the muon momentum as measured in ATLAS cosmic ray data. The red line illustrated the fitted resolution which is the quadratic sum of a term proportional to the inverse momentum taking into account multiple scattering and a constant term (of  $100 \mu\text{m}$ ) reflecting the limitation of the resolution by the spatial resolution and the alignment of the muon chambers.

sagitta distributions of the large sectors are shown as a function of the position of the MDT chamber along the z-direction (parallel to the beam pipe). The accuracy of the initial alignment is of the order of  $50 \mu\text{m}$  or better and close to the desired ultimate accuracy of  $30 \mu\text{m}$ . Improvements of the alignment accuracy are expected when chamber deformations will be taken into account in the track reconstruction. The measurement of the sagitta resolution of straight tracks in the muon spectrometer as a function of the muon momentum measured by the inner detector is presented in Figure 1.28. It improves with increasing momentum as multiple scattering decreases with increasing momentum and reaches a plateau value of about  $100 \mu\text{m}$  at high momenta reflecting the limited spatial resolution and the residual misalignment of the muon chambers. The achieved resolution is about a factor 2 larger than the target value of  $50 \mu\text{m}$  because the chambers are only aligned with  $50 \mu\text{m}$  instead of  $30 \mu\text{m}$  precision.

The method is being extended to the alignment of the muon chambers with curved muon tracks in the magnetic field during normal operation of the experiment in order to verify the optical alignment corrections. This requires an independent measurement of the muon momentum which is insensitive to misalignment of the MDT chambers along the muon track. The MDT chambers with their two triple or quadruple layers of precisely positioned drift tubes measure not only track coordinates with high accuracy but also the local track direction. This feature can be utilised for inde-

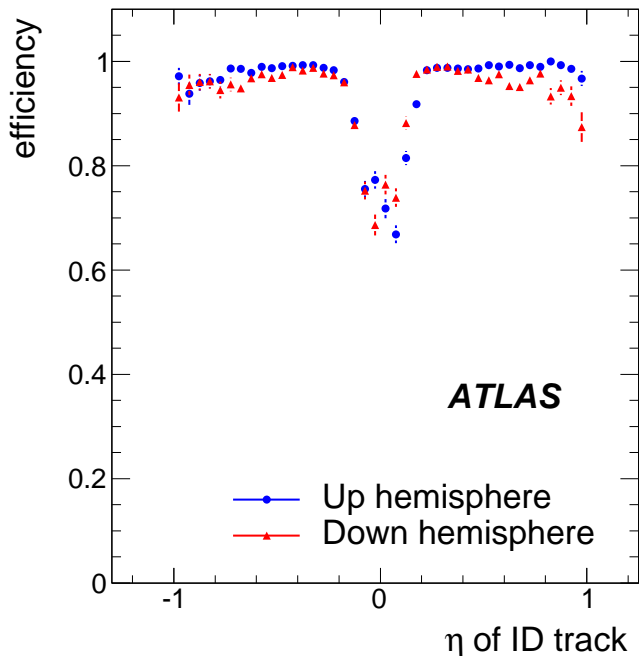


Figure 1.29: Track reconstruction efficiency in the muon spectrometer as a function of the pseudorapidity of the cosmic ray muon reconstructed by the inner detector. The muon momentum in the inner detector was requested to be greater than 5 GeV for the top part and greater than 9 GeV for the bottom part. The loss of efficiency in the region near  $|\eta| = 0$  is due to acceptance holes of the muon spectrometer needed for services of the inner detector and the calorimeters.

pendent momentum determination from measurement of the track deflection angles between the inner and the outer chamber layer and between the two multilayers of the chambers in the middle layer located inside the magnetic field. Studies with simulated data showed that the required alignment accuracy can be achieved within two days of data taking at the nominal LHC luminosity of  $10^{33} \text{ cm}^{-2} \text{ s}^{-1}$  [64, 66].

### Muon Identification Performance

The huge sample of cosmic ray muons made it possible to study the performance of the muon identification in great detail up to muon momenta of 300 GeV [74, 75]. Figure 1.29 shows the track reconstruction efficiency in the ATLAS muon spectrometer for cosmic ray muons reconstructed in the inner detector. The efficiency is close to 100% in the instrumented regions of the muon spectrometer. The drop of the efficiency at  $|\eta| = 0$  is caused by the acceptance gap of the muon spectrometer which is needed for the services of the inner detector and the calorimeters.

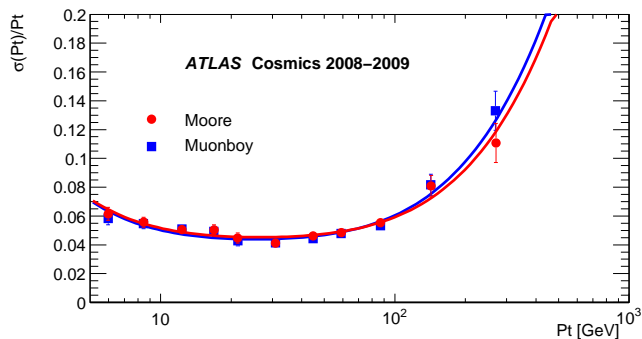


Figure 1.30: Transverse momentum resolution of the muon spectrometer evaluated by comparing the momentum of cosmic ray muons measured in the top part of the spectrometer with the momentum in the bottom part of the spectrometer in the barrel region of the muon spectrometer. The results of two complementary track reconstruction algorithms show similar performance.

The momentum of cosmic ray muons traversing the entire ATLAS detector are measured twice, first in the top part of the muon spectrometer, then in the bottom part of the muon spectrometer. The comparison of the two momentum measurements allowed us to measure the fractional momentum resolution of the muon spectrometer up to muon with  $p_T = 300$  GeV (see Figure 1.30). The measured momentum resolution is in agreement with the expected momentum resolution for  $p_T \lesssim 100$  GeV, but is a factor 2-3 worse than expected above 300 GeV due to the residual misalignment of the muon spectrometer.

The muon reconstruction efficiency and the momentum scale and resolution will be measured for low  $p_T$  with  $J/\Psi \rightarrow \mu^+\mu^-$  decays and for high  $p_T$  with  $Z \rightarrow \mu^+\mu^-$  decays in  $pp$  collision data at the LHC [76, 77]. First  $J/\Psi \rightarrow \mu^+\mu^-$  events have been observed by the ATLAS experiment. The invariant mass distribution of the  $J/\Psi \rightarrow \mu^+\mu^-$  events is shown in Figure 1.31

The position of the  $Z$  resonance peak is a measure for the momentum scale, its width a measure for the momentum resolution. The muon reconstruction efficiency will be measured by the so-called "tag-and-probe method". In the tag-and-probe method events with an isolated muon and an inner detector track giving an invariant mass compatible with the  $Z$  boson mass are selected. The fact that one of the two tracks is identified as muon ensure that the second track is also a muon and one can count how often the second track is reconstructed as a muon. The method has been studied on Monte-Carlo data and is able to reproduce the muon reconstruction efficiency with a systematic

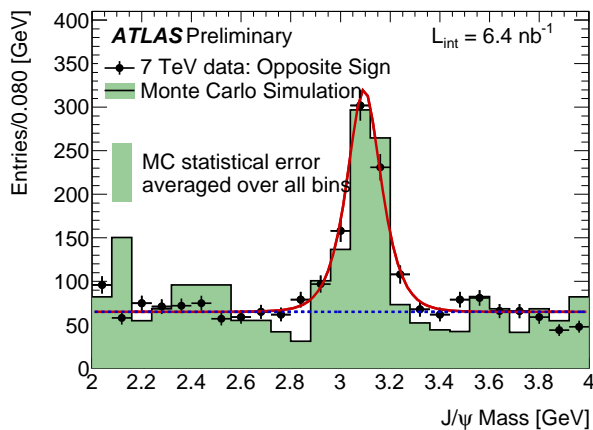


Figure 1.31: Invariant mass distribution of reconstructed  $J/\Psi \rightarrow \mu^+\mu^-$  candidates. The points with error bars are data. The solid line is the result of maximum likelihood unbinned fit to all dimuon pairs in the mass window 2-4 GeV and the dashed line is the result for the background of the same fit. MC from both prompt  $J/\Psi$  and minimum bias simulation are superimposed.

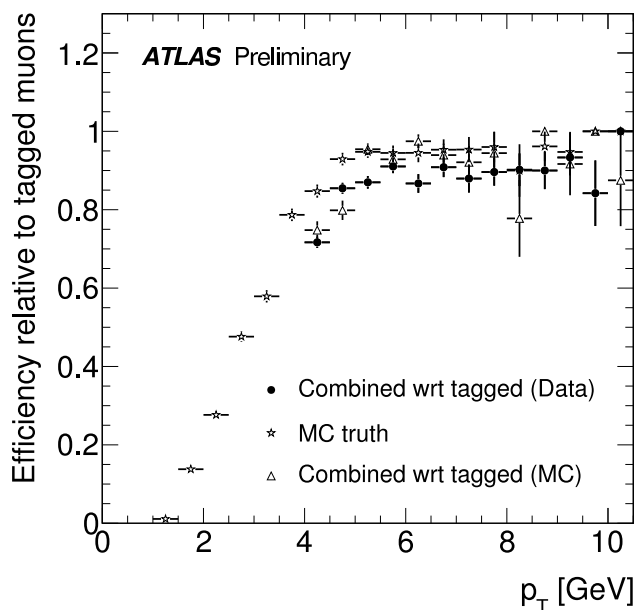


Figure 1.32: Comparison of the relative efficiency of the standard muon reconstruction algorithm with respect to reference muons as defined in the text with the Monte-Carlo prediction for  $p_T > 4$  GeV. The star-shaped symbols labelled as MC truth show the standard muon reconstruction efficiency for muons identified as true muons in the simulation.

uncertainty of 0.2%.

First  $Z \rightarrow \mu^+\mu^-$  candidate events have been observed in the ATLAS detector. One such event is shown in Figure 1.33. In the early phase of the LHC

operation the rate of dimuon decays of  $Z$  bosons is too low for the tag-and-probe method and alternative methods have to be used to get a handle on the muon spectrometer reconstruction efficiency. The efficiency of the standard muon reconstruction is measured with respect to an alternative muon identification approach. In the alternative approach an inner detector track which deposits only little energy in the calorimeters and which can be matched with a track segment in the muon spectrometer is identified as muon. The relative efficiency of the standard muon reconstruction with respect to the alternative selection is shown as a function of the transverse muon momentum in Figure 1.32 [78]. The relative efficiency agrees with the Monte-Carlo prediction within errors. It is lower than the true efficiency as the alternative muon selection has a lower rejection power against muons from pion and kaon decays in flight than the standard reconstruction.

At transverse momenta below 20 GeV the momentum resolution in the momentum resolution is significantly larger than in the inner detector and can be measured by comparing the momentum measured in the muon spectrometer with the momentum measured in the inner detector. The resolution measured this way is in agreement with the Monte-Carlo prediction and the measurement with cosmic ray muons within the measurement uncertainties (see Figure 1.34) [79].

The analysis of cosmic ray data and the first results of the analysis of  $pp$  collision data confirm the expected performance of the muon spectrometer.

### 1.1.4 Computing

The rate of triggered and filtered data from the experiment data acquisition system (DAQ) will be about 200 beam-crossing events per second. This rate translates to more than 300 MB/s given an expected event size of ca. 1.6 MB. When the additional data generated by event reconstruction is taken into account, several PB of physics data per year will have to be handled by the ATLAS computing system [80, 81]. The large volume of the data and the enormous computing resources needed to perform data reduction and extract physics results necessitated the adoption of the Grid computing paradigm by ATLAS and the other LHC experiments. The LHC Computing Review [82] provides a good overview of the worldwide LHC computing.

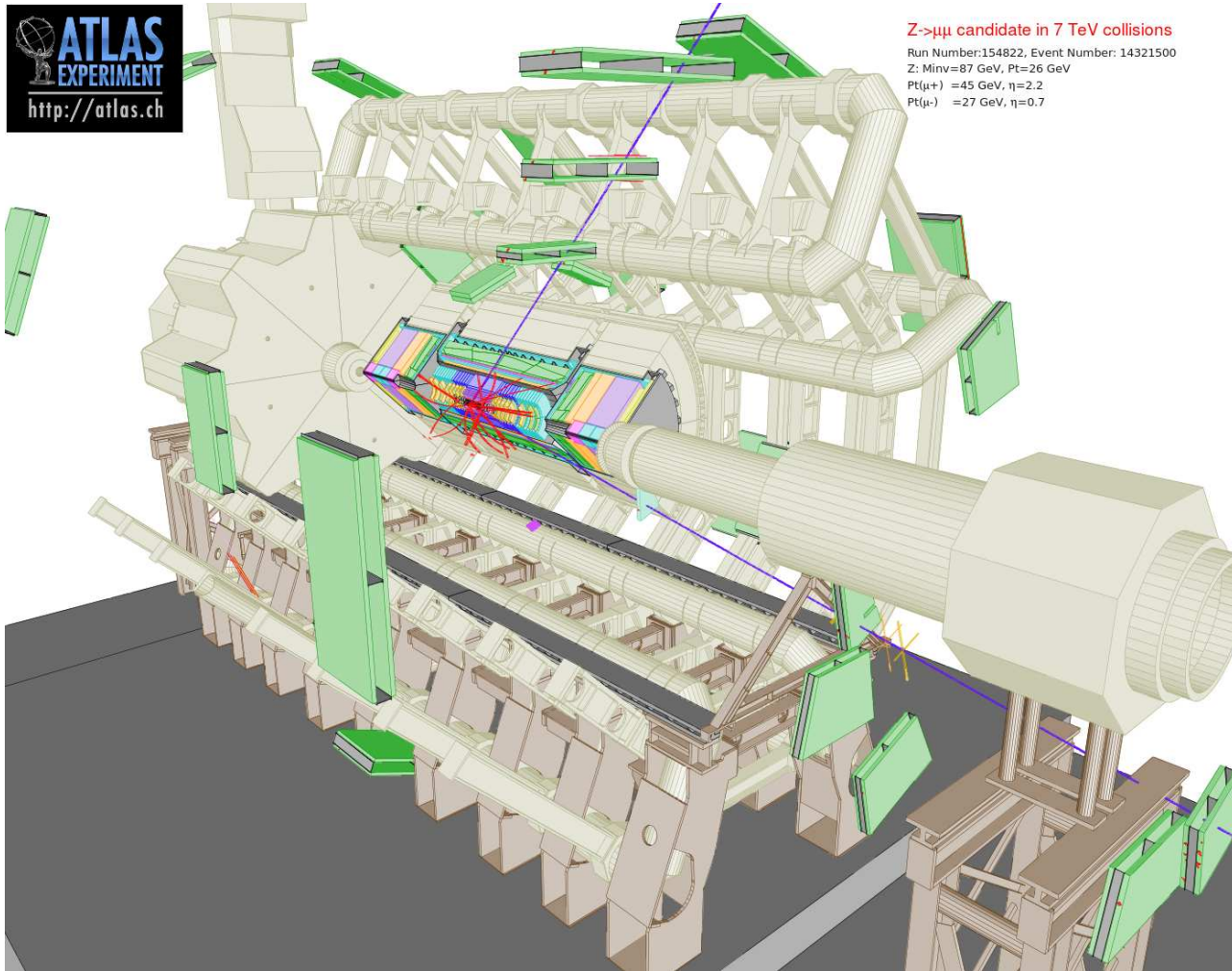


Figure 1.33: Event display of a  $Z \rightarrow \mu^+\mu^-$  candidate event recorded at a centre-of-mass energy of  $\sqrt{s} = 7$  TeV

### ATLAS Computing Model

The ATLAS computing model [80] is based on the established procedure of performing several successive steps of data reduction. The data coming from the DAQ is termed RAW data and will be passed through the event reconstruction immediately after recording (prompt reconstruction). The next step of data reduction leads to event summary data (ESD, about 500 kB/event) consisting of reconstructed particle tracks and calorimeter clusters and the corresponding hits after noise suppression. The last step of central data reduction results is the analysis object data (AOD, about 100-200 kB/event) where essentially only the reconstructed particle momenta and identity information is kept. The working groups in ATLAS can define their own derived physics data (DPD), which are typically 10 kB/event.

The ATLAS computing system [81] is organised in a hierarchical manner with three levels (or tiers)

of distributed and interconnected computing centres mapped approximately to the different levels of reduced data. The single Tier-0 centre at CERN serves the four LHC experiments and provides mass storage of raw data and processing capacity for the prompt reconstruction. The reduced data (ESD and AOD) are distributed to the Tier-1 centres along with the RAW data.

ATLAS has ten Tier-1 centres; one of them is operated by the FZ Karlsruhe in Germany (GridKa). The responsibility of the Tier-1 centres is to store between them a copy of the RAW data, provide processing capacity for deriving ESD/AOD data from RAW data (reprocessing) and to make ESD and AOD data sets available for organised physics analyses.

Each of the Tier-2 centres in turn are connected to one of the Tier-1 centres. There are about 30 Tier-2 centres serving ATLAS and their responsibility is to provide processing capacity to run the ATLAS simu-

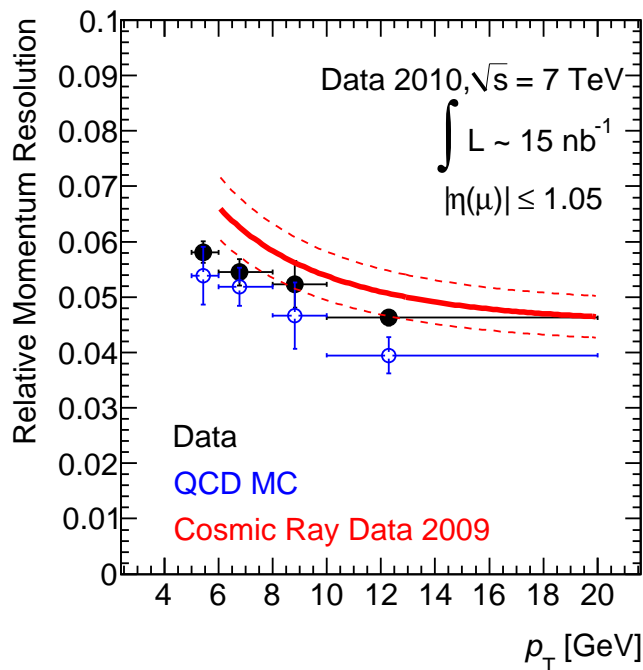


Figure 1.34: Comparison of the momentum resolution in the barrel part of the muon spectrometer measured with muons from  $pp$  collisions in comparison with the expected resolution from Monte-Carlo data and the analysis of cosmic ray data. The measured resolution agrees with the prediction within the measurement uncertainties.

lation and to run scheduled and unscheduled physics analyses by working groups or individual users with AOD data. In addition the derivation of calibration constants may be performed at Tier-2 centres. The Tier-2 centres will each hold approximately 1/3 of the total AOD data such that the usually three Tier-2 centres connected to a regional Tier-1 centre together hold the entire AOD data set.

Tier-3 centres correspond to local computing facilities operated at institutes and dedicated to the local ATLAS groups, while Tier-4 corresponds to individual user's workstations.

### Worldwide LHC Computing Grid

The WLCG collaboration lead by CERN with all major institutes participating in the LHC as partners provides the computing resources needed for timely and successful analysis of the LHC experiments data [83]. One of the most important goals of the WLCG is to deliver the necessary software to manage the distributed data storage and computing tasks as well as to give transparent access to the data to all collaborators of an LHC experiment.

The Institute is an official member of the WLCG

collaboration. It is the responsibility of the ATLAS group at MPP to contribute a large fraction of the resources needed to build and operate a Tier-2 centre in Munich for use by the ATLAS collaboration.

### Munich Tier-2/Tier-3 Computing Centre

The two ATLAS groups in Munich at the MPP and the Ludwig-Maximilians-University Munich (LMU) (Prof. D. Schaile) have agreed to build and operate a Tier-2 centre for ATLAS of the average size as specified in [80]. The centre is hosted by the RZG and the Leibniz Rechenzentrum (LRZ) in Garching. The four parties MPP, LMU, RZG, and LRZ have signed a memorandum of understanding (MOU) outlining the details of the project.

The contributions of MPP/RZG and LMU/LRZ are expected to be about equal in size. It is foreseen to add 100% of the CPU resources and 50% of the storage resources needed for the Tier-2 centre in order to support local computing requirements for the Munich calibration and alignment centre and at the Tier-3 level. The hardware is one homogeneous setup and the sharing of resources between Tier-2, Munich calibration and alignment centre and Tier-3 can be adjusted during operation according to the needs of the experiment or the local working groups.

The hardware is located on the sites of the two computing centres RZG and LRZ in Garching. Such a federation of computing centres is explicitly foreseen in the WLCG to operate a common Tier-2 service.

The total resource requirements for the Munich Tier-2/Tier-3 computing centre for 2010 are estimated as 11.8 kHS06<sup>1</sup> for data processing and 650 TB for data storage on disk. This corresponds to approximately 1700 CPU cores and about 33 file servers with 20 TB RAID storage each. A wide area network (WAN) connection with a sustained bandwidth of 30 MB/s is supplied by RZG for import and export of data.

### MPP Computing Facility at RZG

The computing facility serves the whole institute and the main users are currently the ATLAS and MAGIC groups.

The system consists now of 8 IBM BladeCenter H equipped each with 14 single-board computers. Common services such as power supply and LAN are pro-

<sup>1</sup>7 HS06 correspond roughly to one core of a AMD or Intel multicore CPU from 2009

vided by the BladeCenter. The single-board computers have two CPUs (Intel Xeon 3.2 GHz or Xeon 54xx quad-core), 2 GB RAM/core and a bandwidth of 1 Gb/s to the LAN. Data are stored on integrated file-servers, which connect 12, 16 or 28 large SATA hard-disks (currently 300, 500 or 750 GB) each to RAID arrays via dedicated PCI expansion cards. The total useable disk space is more than 300 TB.

The RZG maintains the operating system (OS), currently Suse Linux Enterprise Server (SLES) 10, batch queue system (Sun grid engine SGE), and other system services. The mass data storage system dCache developed by DESY and FNAL has also been installed and is used by ATLAS. The MPP user groups, e.g. ATLAS, have to install and maintain their own experiment software on this platform.

The RZG operates several servers running the LCG software needed to connect the MPP computing facility to the WLCG. One person from MPP seconded to RZG runs together with staff from RZG the WLCG services, responds to problem reports, installs upgrades, and interacts with our users. Some of the WLCG services run as virtual machines [84], since this makes it more convenient to use the required Scientific Linux OS instead of SLES10 as is standard at RZG.

Our Tier-2 site is monitored on a regular basis by the WLCG. Performance is quantified by availability, defined as the fraction of time a site is available, and reliability, defined as the fraction of time a site is available corrected for known and announced downtimes. Our site has with few exceptions reached values above 90 %, accepted as good by WLCG, for both measures.

## 1.2 ATLAS Physics Analysis

For a long time the MPP ATLAS group has been continuously working on the preparation of physics analysis of hadron collision data at the LHC. The results obtained in the years 1997-2007, including preparatory work based on Tevatron data, are described in the previous reports [7] (p.82-84), [1] (p.106-112), [85], and references therein.

The present physics studies for the ATLAS experiment cover a broad physics range. Already at the early stage of data taking, a number of Standard Model (SM) processes occur in abundance. These processes allow for detailed studies of the detector performance, as well as for the precision measurements of QCD and electroweak observables. The few hundred  $\text{nb}^{-1}$  of

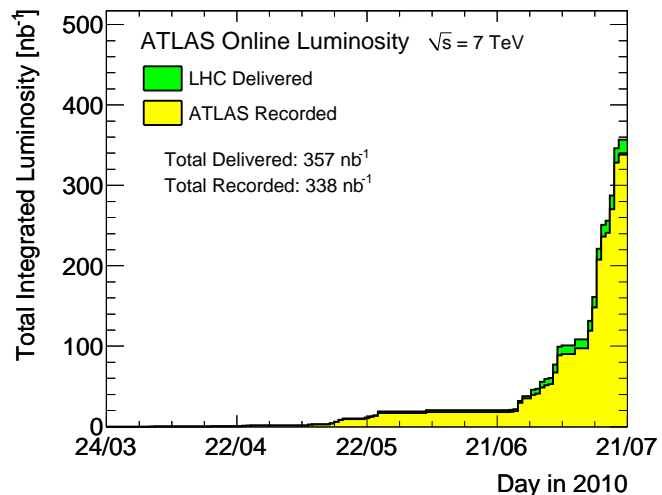


Figure 1.35: Time evolution of the cumulative luminosity since the start of the LHC operation at  $\sqrt{s} = 7$  TeV.

data collected so far (see Figure 1.35) yielded the first measurements of inclusive lepton distributions, as well as the initial measurements of cross-sections for electroweak gauge boson production. Also the properties of top-quark production will very soon become measurable as the integrated luminosity increases. The methods to determine the mass of the top-quark explained below will show their full potential when applied to the data of the ongoing 2010-2011 run of LHC with an expected luminosity of about  $1 \text{ fb}^{-1}$ .

A good understanding of SM processes is essential also for new discoveries. The ATLAS discovery potential is explored in searches for the Higgs boson both in the Standard Model and in supersymmetric extensions, as well as in a generic search for supersymmetric particles and other phenomena like the lepton flavour violation. The sensitivity to many of these processes is expected to exceed the current limits from experiments at other colliders by the end of 2010, once an integrated luminosity of about  $200 \text{ pb}^{-1}$  is reached. The ongoing investigations are described in more detail below.

### 1.2.1 Standard Model Processes

#### Inclusive Lepton Cross Sections

At the LHC  $pp$  collision events with highly energetic electrons and muons in the final state provide clean signatures for many physics processes of interest. A good understanding of the inclusive electron

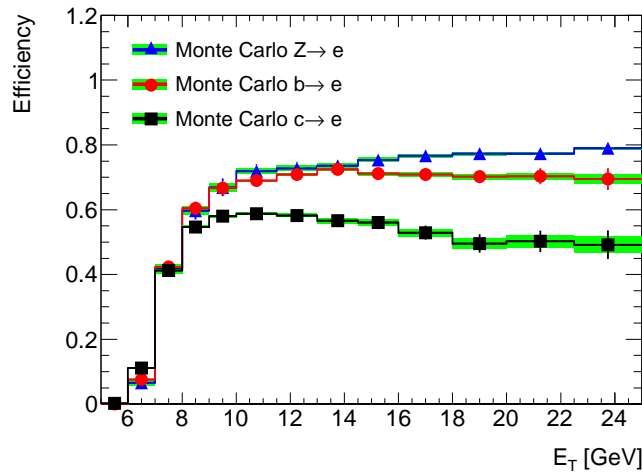


Figure 1.36: Monte-Carlo prediction of the electron reconstruction efficiency for electrons from heavy quark and Z boson decays. [88]

and muon cross sections is therefore of great importance. The MPP group contributes to these measurements [86–88].

At the LHC electrons are produced predominantly in decays of heavy quarks with transverse energies below about 30 GeV and in decays of  $W$  and  $Z$  bosons at higher transverse energies. The MPP group significantly contributed to the optimisation of the electron selection criteria to arrive at an electron selection efficiency which is flat in the transverse electron energy (see Fig. 1.36). The first measured inclusive electrons spectrum at a centre of mass energy of 7 TeV at the LHC is shown in Fig. 1.37 in comparison with the prediction of the Pythia minimum bias Monte-Carlo. The MPP group contributes to the study of the observed 20% discrepancy between data and Monte-Carlo prediction, using the increasing statistics of the inclusive electron sample.

The MPP group is also involved in the measurement of the inclusive muon cross section contributing with its experience in muon performance studies. The measured inclusive muon  $p_T$  spectrum is presented in Fig. 1.38 where it is compared to the Pythia 6.4 minimum bias Monte-Carlo prediction. The measured spectrum is well reproduced by the Monte-Carlo simulation. The discrepancy observed for  $p_T > 20$  GeV is due to muons originating from  $W$  and  $Z$  boson decays. According to the Monte-Carlo simulation, the main sources of muons at transverse momenta below 20 GeV are in-flight decays of charged pions and kaons and the decays of heavy-flavour hadrons. Methods to separate the contribution of pion and kaon de-

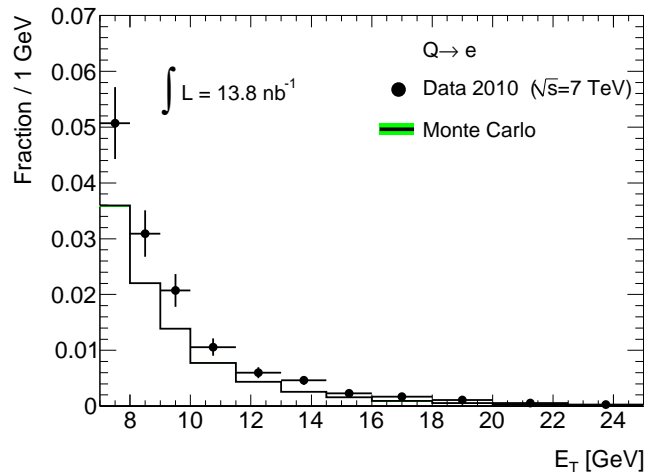


Figure 1.37: Comparison of the measured distribution of the transverse energies of prompt electrons from  $c$  and  $b$  decays with the Pythia 6.4 minimum bias Monte-Carlo predictions. [88]

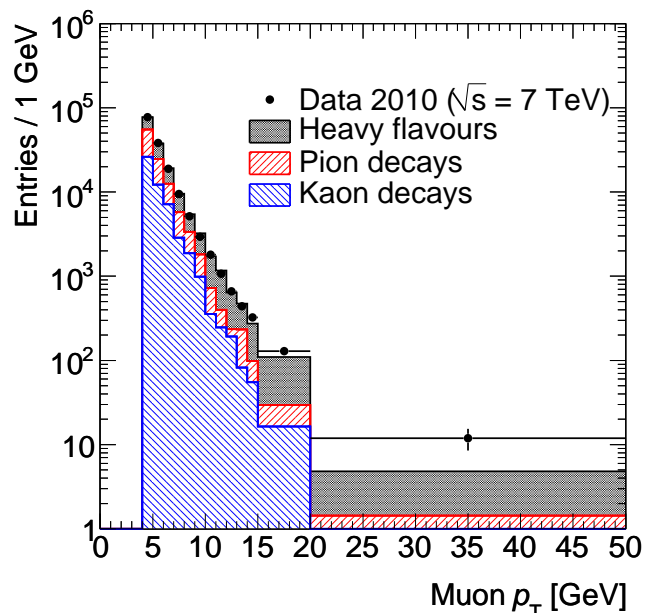


Figure 1.38: Comparison of the measured inclusive muon transverse momentum spectrum with the Pythia 6.4 minimum bias Monte-Carlo prediction. The Monte-Carlo data is decomposed into three sources of muons, namely in-flight decays of charged pions and kaons and the decays of heavy-flavour hadrons. [87]

cays from the other sources are under development.

### Electroweak Gauge Boson Production

The measurement of the  $W$  and  $Z$  boson production is a first essential step in understanding hard electroweak processes in the high-energy regime of the LHC. With a sufficient amount of collected data, precise inclu-

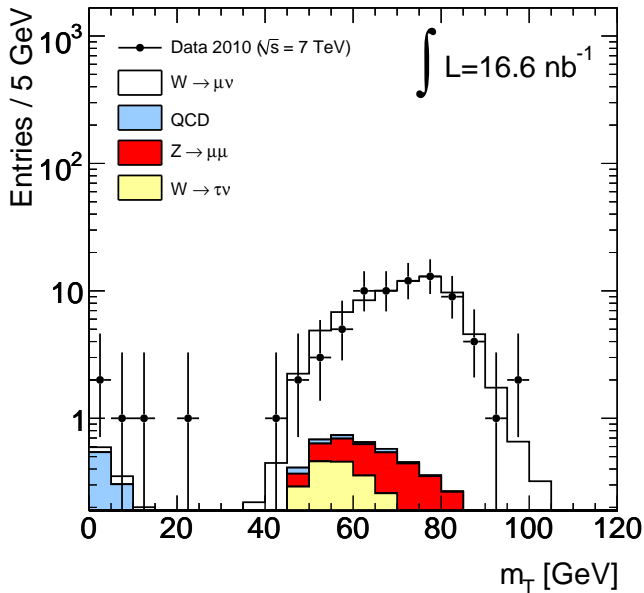


Figure 1.39: Transverse mass distribution of  $W \rightarrow \mu\nu_\mu$  candidates found in  $16.6 \text{ nb}^{-1}$  of  $pp$  collision data collected by ATLAS. [89]

sive and differential cross section measurements can be performed to probe the parton density functions. In addition, these processes are studied with the motivation of estimating the backgrounds to the searches for Higgs bosons and supersymmetric particles. Of particular interest here is the electroweak gauge bosons production in association with jets, where the bosons are decaying into electrons, muons or  $\tau$  leptons.

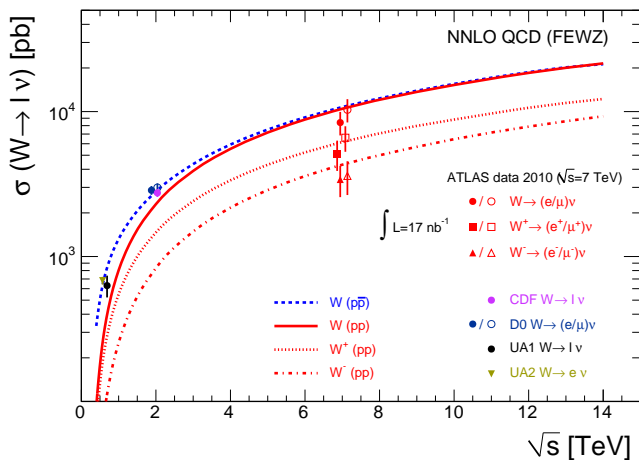


Figure 1.40: Comparison of the measured  $W$  cross section with the NNLO prediction. The expected asymmetry in the production cross sections of  $W^+$  and the  $W^-$  boson is confirmed by the cross section measurements. [89]

$W$  bosons have been observed in  $16.6 \text{ nb}^{-1}$  of  $pp$  collision data collected with ATLAS: 43  $W$  bosons in the  $e\nu_e$  final state and 67  $W$  boson in the  $\mu\nu_\mu$  fi-

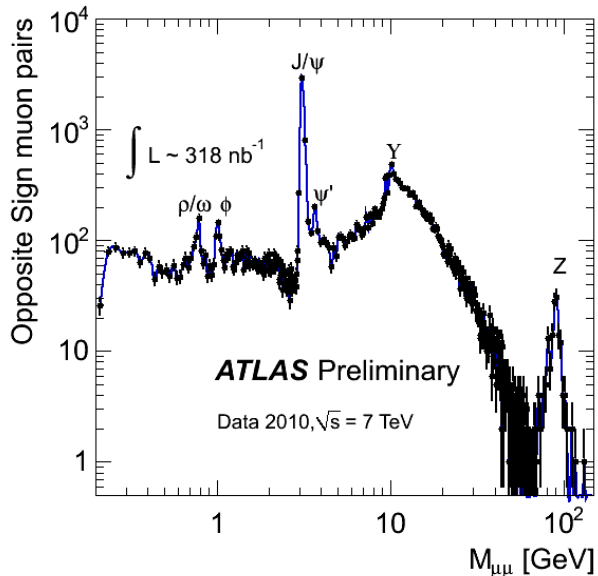


Figure 1.41: Invariant mass spectrum of oppositely charged muons in  $318 \text{ nb}^{-1}$  of  $pp$  collision data. [89]

nal state. As expected for  $pp$  collisions, more  $W^+$  than  $W^-$  bosons have been detected, 70  $W^+$  and 40  $W^-$  bosons. Fig. 1.39 shows the transverse mass distribution of the  $W \rightarrow \mu\nu_\mu$  candidates confirming the observation of  $W$  bosons. The Monte-Carlo prediction is consistent with the measured distribution and has a negligible background contamination. The total inclusive  $W$ -boson production cross section times the leptonic branching ratio is measured to be

$$\sigma = [8.5 \pm 1.3(\text{stat}) \pm 0.7(\text{syst}) \pm 0.9(\text{lumi})] \text{ nb}$$

for the  $W \rightarrow e\nu_e$  channel and

$$\sigma = [10.3 \pm 1.3(\text{stat}) \pm 0.8(\text{syst}) \pm 1.1(\text{lumi})] \text{ nb}$$

for the  $\mu\nu_\mu$  channel. The experimental errors of the cross sections are dominated by the statistical errors of the numbers of observed  $W$  candidates and the 11% uncertainty of the luminosity measurement. The measured  $W$  production cross section agrees well with the NNLO calculations as shown in Fig. 1.40. The measurement of the  $W$  production cross section required a good understanding of the lepton identification efficiencies besides the reliable measurement of the luminosity. As reported in 1.1.3 the MPP group has significantly contributed to the understanding of the performance of the muon identification in  $pp$  collision data. The measurement of the muon identification efficiency reduced the systematic cross section uncertainty caused by the uncertainty of the Monte-Carlo efficiency predictions to less than 3%.

Also candidates for  $Z \rightarrow \ell^+\ell^-$  decays with isolated charged leptons have been found by ATLAS.

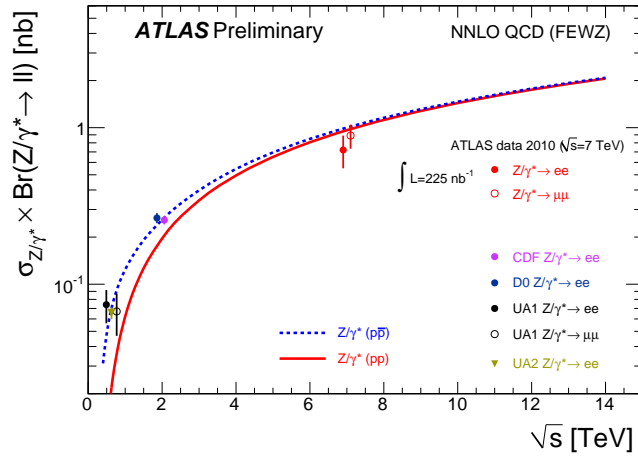


Figure 1.42: Comparison of the measured values of  $\sigma_Z \cdot BR(Z \rightarrow \ell\ell)$  for  $\ell = e, \mu$  with the theoretical predictions based on NNLO QCD calculations. [90]

Figure 1.41 shows the dimuon invariant mass spectrum for oppositely charged muons collected with the ATLAS detector. In addition to resonance peaks at the masses of  $\rho/\omega$ ,  $J/\psi$ ,  $\psi'$ , and  $Y$  mesons a resonance peak at 91 GeV, the mass of the  $Z$  boson, is clearly visible with very small background. In the  $229 \text{ nb}^{-1}$  of  $pp$  collision data 46  $Z \rightarrow e^+e^-$  and 79  $Z \rightarrow \mu^+\mu^-$  events were observed in the mass window of  $66 \text{ GeV} < m_{\ell^+\ell^-} < 116 \text{ GeV}$ . The measured cross sections of  $\sigma = [0.72 \pm 0.11(\text{stat}) \pm 0.10(\text{syst}) \pm 0.08(\text{lumi})] \text{ nb}$  for  $Z \rightarrow e^+e^-$  and

$\sigma = [0.89 \pm 0.10(\text{stat}) \pm 0.07(\text{syst}) \pm 0.10(\text{lumi})] \text{ nb}$  for  $Z \rightarrow \mu^+\mu^-$  are in agreement with the theoretical prediction (see Figure 1.42).

The increase in statistics of  $W$  and  $Z$  bosons expected in the next months will allow us to improve the precision of the cross section measurements, to investigate the  $W^+W^-$  production asymmetry, and to measure the cross sections of the production of the weak gauge bosons for 0, 1, and more than 1 accompanying jet. The measurement of the differential  $Z$  production cross section will be used to probe parton density functions.

## 1.2.2 Top-Quark Physics

### Overview

The top-quark is by far the heaviest known elementary building block of matter. The precise knowledge of the quantum numbers of the top-quark helps to further constrain the parameters of the Standard Model, and is a mandatory prerequisite for any study of new physics that will almost inevitably suffer from top-

quark reactions as background processes. In addition, the top-quark should have the strongest couplings to any mechanism that generates mass, which makes it a very interesting object for an unbiased search for this mechanism.

The present main interest of the top-quark physics analysis work of the MPP group is the investigation of the  $t\bar{t}$  production process, and particularly the determination of the mass of the top-quark ( $m_{\text{top}}$ ) and the production cross-section ( $\sigma_{t\bar{t}}$ ) in the reaction  $t\bar{t} \rightarrow b\bar{b}W^+W^-$ .

The analyses use two decay channels of the  $W$ -boson pair, the lepton+jets channel, where the  $W$ -boson pair decays into  $\ell\nu qq'$  with  $\ell = e, \mu$  (branching ratio,  $BR = 30\%$ ) and the all-jets channel, where both  $W$ -bosons decay into a  $qq'$  pair ( $BR = 44\%$ ). In both channels  $m_{\text{top}}$  is obtained from hadronically decaying  $W$ -bosons and the corresponding b-jet.

The main background reactions to  $t\bar{t}$  production, as determined from Monte Carlo simulations, are the  $W$ +n-jets production, QCD multijet production, single top-quark production, and that fraction of the  $t\bar{t}$  production where the  $W$ -boson pair decays via the other decay channels. The QCD multijet production process is special due to the huge cross-section before any cut, such that event samples fully covering the signal phase space cannot be simulated with sufficient statistics, especially for the lepton+jets channel, where the selected lepton mostly results from a wrongly reconstructed jet. Eventually this background contribution has to be obtained from data. So far, initial studies of this background based on Monte Carlo samples have been performed and methods to evaluate it from the data, like the matrix-method, have been implemented. The matrix-method was successfully applied to estimate the background fraction from Monte Carlo samples with a deliberately unknown composition of signal and background events [91]. In the MPP investigations, for the first time the  $k_t$ -jet algorithm has been used in top physics analyses at ATLAS [15, 92] Because of a better stability against divergences, this algorithm is theoretically preferred over the traditionally applied cone-jet algorithm. By now also the experimental advantages became apparent, such that since recently a variant of it, namely the anti- $k_t$  jet algorithm is the ATLAS standard.

At present the analyses are optimised on Monte Carlo samples and are ready to be applied to the data to be taken still this year. The results presented below do not yet contain ATLAS collision data. The analyses

are mostly performed assuming the initially envisaged proton-proton centre of mass energy of  $\sqrt{s} = 10$  TeV and for integrated luminosities  $\mathcal{L}_{\text{int}}$  of several 100  $\text{pb}^{-1}$ . An overview of the recent activities is given below, the initial investigations were reported in [1] (p.106-112), [85].

### Lepton + Jets Channel

The lepton+jets channel is the best compromise of branching fraction and signal-to-background ratio (S/B), defined as the ratio of  $t\bar{t}$  signal events to physics background events. Therefore most of the effort is invested in this channel. At MPP a number of analyses have been performed to arrive at the most sensitive observable and analysis strategy for obtaining  $m_{\text{top}}$  from the invariant mass of the three jets assigned to the decay products of the hadronically decaying top-quark. Different event- and jet selection algorithms, observables, jet calibration schemes (see Sec. 1.1.2), and fitting methods have been exploited for this.

In the lepton + jets channel the charged lepton with a high transverse momentum<sup>1</sup> ( $p_{\text{T}}$ ) from the decay of one W-boson is utilised to trigger and identify the event, and to efficiently suppress background without genuine charged leptons, i.e. from the QCD multijet production. In general, the event selection for the lepton + jets channel requires an isolated electron or muon within the good acceptance of the detectors, which has a transverse momentum of more than 20 GeV and lies within the rapidity range of  $|\eta| < 2.5$ . Since the initial state is balanced in  $p_{\text{T}}$ , to account for the neutrino a missing transverse energy of more than 20 GeV is required. In addition, at least four jets are required within the same range of rapidity, and having transverse momenta of more than 40 GeV for the three highest  $p_{\text{T}}$  jets, and more than 20 GeV for the fourth jet. All jets should be well separated from the identified lepton. Given the different emphasis of the analyses, these requirements are slightly modified or additional requirements like the presence of identified b-jets, or restrictions to the reconstructed invariant mass of the W-boson are imposed. With these selections,

<sup>1</sup>In the ATLAS right-handed coordinate system the  $x$ -axis points towards the centre of the LHC ring, the  $y$ -axis points upwards and the  $z$ -axis points in the direction of the counter-clockwise running proton beam. The polar angle  $\theta$  and the azimuthal angle  $\phi$  are defined with respect to the  $z$ -axis and  $x$ -axis, respectively. The pseudo-rapidity is defined as  $\eta = -\ln(\tan(\theta/2))$  and the radial distance in  $(\eta, \phi)$  space is  $\Delta R = \sqrt{\Delta\eta^2 + \Delta\phi^2}$ .

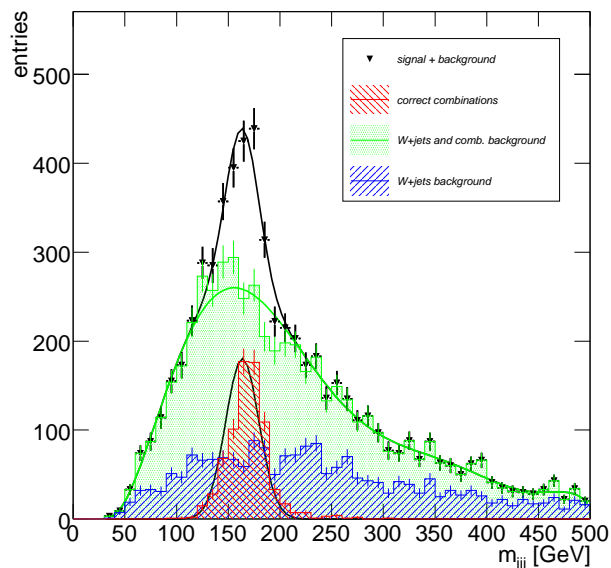


Figure 1.43: The reconstructed top-quark mass together with a fit.

for each lepton sample an average signal efficiency of about 10% is reached, and the S/B is about 1.5.

The standard assignment of jets to the top-quark and the W-Boson are as follows. For each event, from all jets with  $p_{\text{T}} > 20$  GeV the three jet combination which maximises the transverse momentum is chosen to form the hadronically decaying top-quark. This algorithm is named the  $p_{\text{T}}$ -max method. Out of this, the two jet pair with the smallest  $\Delta R$  is taken to represent the W-boson. A typical top-quark mass spectrum observed with these requirements [18], and only using signal events and W + n-jets events, is shown in Fig. 1.43. In this example, the spectrum is fitted with a Gaussian function to parametrise the correct combinations leading to the top-quark mass and width, and a sum of Chebyshev polynomials used to describe the events stemming from the sum of the physics background events and wrong jet combinations in selected signal events. The Gaussian part of the fit is also shown separately and compared to the red histogram made from the correct jet triplet. In this case correct jet triplets are defined as those combinations of jets where the reconstructed four-vector of the jet triplet coincides with that of the top-quark to within  $\Delta R = 0.1$ .

From this figure it is clear that firstly the correct jet triplets constitute only a small part of the events in the peak region around the generated top-quark mass of 172.5 GeV, secondly that the shape of the combinatorial background can well influence the fitted peak value, and thirdly that the shown W + n-jets contribu-

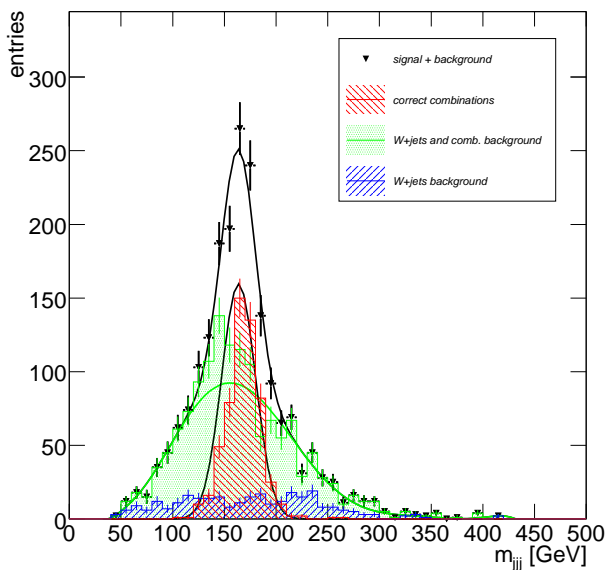


Figure 1.44: Same as Fig. 1.43 but with an additional likelihood selection.

tion is still sizeable and not entirely flat.

These issues are addressed, e.g. by using other algorithms to select the jet triplet, or by exploiting additional variables or a constrained fit that both help to separate signal from background. Additional algorithms studied include the so-called  $\Delta R$  method that exploits the angular correlations between the two b-jets that should have a large  $\Delta R$ , and the two light-jets that should have a small  $\Delta R$ . This algorithm works without explicitly using b-jet identification, instead from a  $p_T$  ordered jet list the first two jets are assumed to be the b-jets and the next two jets to stem from the W-Boson decay. On these jets the angular requirements are applied. Whether the decrease in statistical precision compared to the  $p_T$ -max method is compensated by superior features like an improved resolution, or a smaller bias in the reconstructed mass, is under investigation.

Due to the presence of the decay of the top-quarks that correlate the W-Bosons and their corresponding b-quarks, the signal events should exhibit a different correlation of the observed jet structure than the background processes without top-quarks. The separation of the jets can be monitored when running the  $k_r$ -jet algorithm by studying the  $d_{\text{merge}}(M \rightarrow M - 1)$  values at which an  $M$ -jet configuration is reduced to an  $(M - 1)$ -jet configuration. In a multivariate analysis it was found that the  $d_{\text{merge}}$  values in signal and background events are not sufficiently different to be used as discriminating variables [18]. In contrast, a likeli-

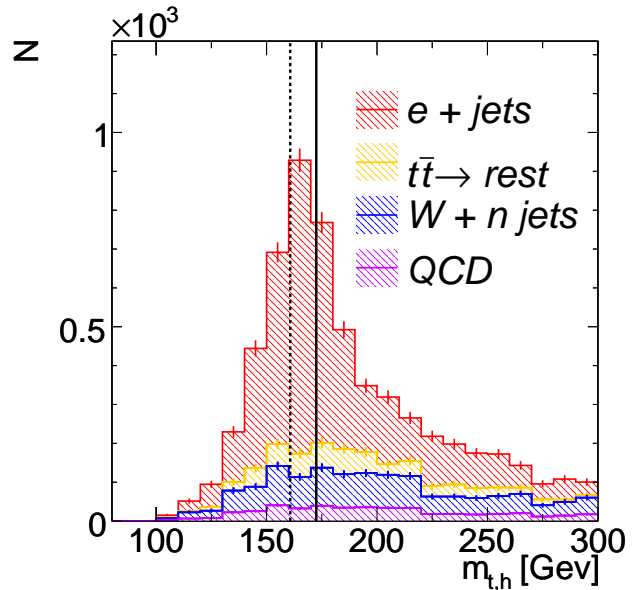


Figure 1.45: The top-quark mass distribution when applying a constrained fit selection. The vertical lines indicate the generated top-quark mass (full) and reconstructed value from the jet four-vectors before applying the kinematical fit (dashed).

hood function build from seven event variables, like e.g. the invariant mass of the charged lepton and its assigned b-jet, or the  $\Delta R$  between the W-Boson and the b-jet from the hadronically decaying top-quark candidate, is clearly able to significantly improve the S/B, while retaining most of the events where the correct jet triplet was selected. This is demonstrated in Fig. 1.44.

A kinematic fit exploiting as constraints the known W-Boson mass both for the leptonic and the hadronic W-Boson decays, and in addition the equality of the two corresponding reconstructed top-quark masses mainly serves three purposes. Firstly, it increases the efficiency for selecting the correct jet triplet by making more detailed use of the entire event. Secondly, it provides a quality measure, namely the probability  $P(\chi^2)$  of the fit, to better suppress background events. Finally, it improves on the resolution of the top-quark mass provided the uncertainties of the measured quantities and their correlations are properly understood, something that is only expected after a larger data set has been analysed. Compared to the  $p_T$ -max method the efficiency for selecting the correct jet triplet is increased by about 15% absolute, and about 25% of the background events can be removed [93] by requiring  $P(\chi^2) > 0.15$ . An example of such a selection for events with four reconstructed jets and requiring  $P(\chi^2) > 0.15$  is shown in Fig. 1.45. The better sup-

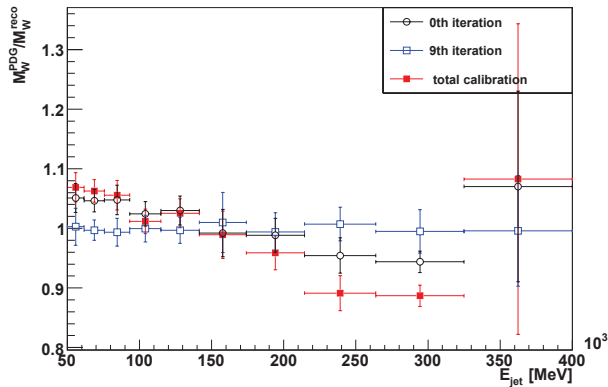


Figure 1.46: In-situ calibration of the W-Boson mass as function of the light-jet energy.

pression of the W + n-jets events compared to Fig. 1.43 is apparent. It has been verified that this improvement, is very stable against variations of the assumed object resolutions. Since at the moment only initial approximations are made for the resolution of the objects, the possible improvement in the mass resolution is not yet exploited.

The largest systematic uncertainty in any determination of  $m_{\text{top}}$  stems from the imperfect knowledge of the jet energy scale (JES), which depends on kinematic properties like  $p_{\text{T}}$  and  $\eta$  of the jets, and is different for light-jets and b-jets. Therefore, one of the most important features of any  $m_{\text{top}}$  estimator is the stability against the variation of the JES. To minimise the JES uncertainty on the measured  $m_{\text{top}}$  two paths are followed: one is a calibration by means of the known W-boson mass ( $M_{\text{W}}^{\text{PDG}}$ ) to obtain the JES for light-jets, the other is exploring the stabilised top-quark mass ( $m_{\text{top}}^{\text{stab}}$ , see below) to be as independent as possible of the actual JES value, without actually determining it.

In the lepton + jets channel an iterative in-situ calibration of the JES for the selected events has been performed [44]. Jets are treated in the massless limit with unchanged reconstructed angles, such that any change in the invariant two-jet mass ( $M_{\text{W}}^{\text{reco}}$ ) can be expressed in energy dependent JES factors. The jet calibration then makes use of the fact that  $M_{\text{W}}^{\text{reco}}$  calculated from the jets assigned to the W-boson decay has to match  $M_{\text{W}}^{\text{PDG}}$ . The energy bins are chosen logarithmically from 50 GeV to 400 GeV and the resulting calibration factors, which are consecutively applied per iteration, are shown in Fig. 1.46 for the initial situation, the 9<sup>th</sup> iteration and the final result. The flatness of the calibration factors of the 9<sup>th</sup> iteration with values close to unity clearly shows that the fit has converged. Com-

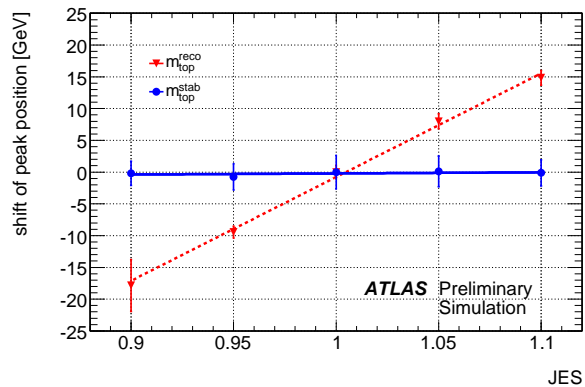


Figure 1.47: Stability of  $m_{\text{top}}^{\text{reco}}$  and  $m_{\text{top}}^{\text{stab}}$  against JES changes.

paring the initial and final situation reveals that the iterations slightly change the simple picture one would have obtained by once adjusting the peak of the initial distribution to  $M_{\text{W}}^{\text{PDG}}$ . When applying this global scaling method the uncertainty on  $m_{\text{top}}$  from the JES uncertainty is considerably reduced [44].

The variable  $m_{\text{top}}^{\text{stab}}$  is calculated as the ratio of the reconstructed masses of the top-quark and the W-Boson candidates from the selected jet triplet. For convenience this ratio is multiplied by  $M_{\text{W}}^{\text{PDG}}$ . The main consequence of using  $m_{\text{top}}^{\text{stab}}$  is a strong event-by-event cancellation of the JES dependence of the three-jet and two-jet masses in the mass ratio, while retaining the sensitivity to  $m_{\text{top}}$ . The quantitative gain in stability when using  $m_{\text{top}}^{\text{stab}}$  instead of the jet triplet invariant mass  $m_{\text{top}}^{\text{reco}}$  is apparent from Fig. 1.47 taken from [94]. Using this variable a template analysis has been developed [91, 94, 95]. In this analysis Probability Density Functions (PDFs) are constructed from templates of the signal events at various assumed  $m_{\text{top}}$  values and from a template of the combined physics background events. The signal PDF linearly depends on  $m_{\text{top}}$ , whereas the background PDF does not. Using pseudo-experiments for a given luminosity the sensitivity of the method, together with the systematic uncertainties from various sources, has been estimated. An example of a pseudo experiment is shown in Fig. 1.48 for the muon channel and for  $\sqrt{s} = 10 \text{ TeV}$  and  $\mathcal{L}_{\text{int}} = 100 \text{ pb}^{-1}$ . For this situation the statistical uncertainty for the combined electron and muon channel is about 2 GeV. The total systematic uncertainty is estimated to be about 3.8 GeV for each channel, still dominated by the systematic uncertainty from the JES for light jets and b-jets [94].

The determination of the combinatorial- and

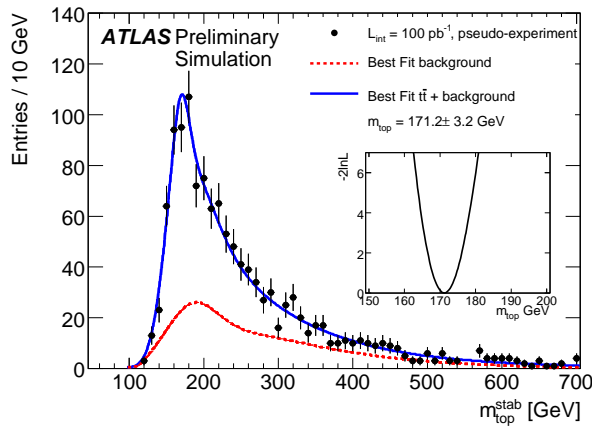


Figure 1.48: Pseudo-experiment mimicking early ATLAS data in the muon channel.

physics background from data rather than from Monte Carlo samples likely results in a reduced systematic uncertainty. For this purpose a data driven method was developed that explores the  $m_{\text{top}}^{\text{reco}}$  and  $R_{\text{top}} = m_{\text{top}}^{\text{reco}}/M_W^{\text{reco}}$  distributions at the same time. The idea is to use e.g. the events from the sideband region of the  $m_{\text{top}}^{\text{reco}}$  distribution to predict the shape of the background contribution to the  $R_{\text{top}}$  distribution. An initial investigation ignoring possible shape differences of the combinatorial- and physics background, and using a simple four-vector smearing approach, yields promising results, and will be extended to fully simulated Monte Carlo events and eventually data.

A direct fit to the  $m_{\text{top}}^{\text{reco}}$  distribution and the template method lead to different systematic uncertainties. An analysis is underway to systematically compare the two approaches. This is done for the  $p_T$ -max and for a selection method that defines the top-quark as the jet triplet with the minimum sum of the three  $\Delta R$  values.

Concerning the cross-section measurement an initial investigation of a cut and count analyses with and without using b-jet identification has been performed [14]. It exploits the lepton+jets channel at  $\sqrt{s} = 10 \text{ TeV}$  and for  $\mathcal{L}_{\text{int}} = 200 \text{ pb}^{-1}$ . For the sources of systematic uncertainties investigated the total systematic uncertainty on the cross-section is estimated to be about 30%.

### All-Jets Channel

In the all-jets channel only jet requirements and jet topologies can be used to separate the signal from the background reactions. Consequently, this channel suffers from a much higher background from the QCD

multijet production. Here, events with isolated leptons are vetoed, and the missing transverse energy is required to be consistent with zero. In addition, at least six jets, not consistent with being purely electromagnetic, and two of which are identified b-jets, are required within  $|\eta| < 2.5$ . By exploring the transverse energies of the jets and the angular correlation of the two b-jets, the S/B is improved by several orders of magnitude to about  $10^{-1}$ , while retaining a signal efficiency of about 10%. In this procedure the use of b-jet identification is absolutely essential. In addition, the availability of a multi-jet trigger with appropriate thresholds is imperative to not lose the signal events already at the trigger stage. This involves a delicate optimisation to retain a sufficiently high efficiency for the signal events, while not saturating the ATLAS readout system with the QCD multijet events. The trigger conditions have been carefully studied, and the use of some trigger signals are suggested to ATLAS. Under the assumption that these will be available, and when exploiting the above event selection, a mass distribution has been isolated, where the signal starts to be visible on a still large background. For this analysis the next steps are the optimisation of the background description and a fit to the distribution to access the sensitivity to  $m_{\text{top}}$ .

### 1.2.3 Searches for the Higgs Boson

The origin of particle masses is one of the most important open questions in particle physics. In the Standard Model, the answer to this question is connected with the prediction of a new elementary neutral particle, the Higgs boson  $H$ . The mass  $m_H$  of the Higgs boson is a free parameter of the theory. The theoretical upper limit of about 800 GeV leaves a wide mass range to be explored. The experimental lower bound of 115 GeV has been set at a 95% confidence level by the direct searches with LEP experiments, while the upper bound of 185 GeV is derived from the electroweak precision measurements. The recent searches at the Tevatron have also excluded a SM Higgs boson in the mass range of  $162 \text{ GeV} < m_H < 166 \text{ GeV}$ .

In the minimal supersymmetric extension of the Standard Model (MSSM), the Higgs mechanism predicts the existence of five Higgs bosons, three neutral ( $h/H/A$ ) and two charged ones  $H^\pm$ . Their production cross sections and decays are determined by two independent parameters, e.g. the ratio  $\tan \beta$  of the vacuum expectation values of the two Higgs doublets in this model and the mass  $m_A$  of the pseudoscalar Higgs bo-

son. Current experimental searches at LEP and Tevatron exclude at a 95% confidence level the  $A$  boson mass values below 93 GeV, as well as the  $\tan\beta$  values below 2. For an  $A$  boson mass of up to 200 GeV, also the high  $\tan\beta$  values above 40 are excluded.

The search for the Higgs boson is one of the main motivations for the LHC and the ATLAS experiment. The high cross sections of the background processes exceeding the signal by many orders of magnitude call for selective triggers, efficient background suppression and reliable prediction of the background contributions. Until recently, the MPP group has been devoted to the preparation for an early Higgs boson discovery during the first years of LHC running at the nominal centre of mass energy of 14 TeV. The results obtained in these studies can be found in the newly published review of the ATLAS physics potential [98]. As of lately, the searches are being optimised for the initial LHC operation at a centre of mass energy of 7 TeV. With a relatively low expected total integrated luminosity of  $1 \text{ fb}^{-1}$ , the Higgs boson discovery is rather unlikely under these operating conditions. However, the allowed Higgs boson mass range can be constrained beyond the present experimental limits, as summarised in [99, 100].

### The Standard Model Higgs Boson

The expected potential for the Standard Model Higgs boson discovery is shown in Fig. 1.49. In the mass range above 180 GeV, the key discovery channel is the Higgs boson decay into four charged leptons via two intermediate  $Z$  bosons. The lower mass range can only be covered by the combination of searches in several Higgs boson decay modes.

The clearest signature is found in the four-lepton decay channel  $pp \rightarrow H \rightarrow ZZ^{(*)} \rightarrow 4\ell$  which also allows for a precise Higgs boson mass measurement. The reconstruction of this channel strongly relies on the high lepton identification efficiency and good momentum resolution of the ATLAS detector. The reducible  $Zb\bar{b}$  and  $t\bar{t}$  background processes can be suppressed by means of the  $Z$  boson mass reconstruction and the requirement of a low jet activity in the vicinity of each lepton. The remaining reducible background is small compared to the irreducible  $pp \rightarrow ZZ^{(*)}$  background. In addition to the optimisation of the analysis selection criteria, our studies include the detailed evaluation of the theoretical and experimental systematic uncertainties for both signal and background processes [101]. We also evaluate the potential to ex-

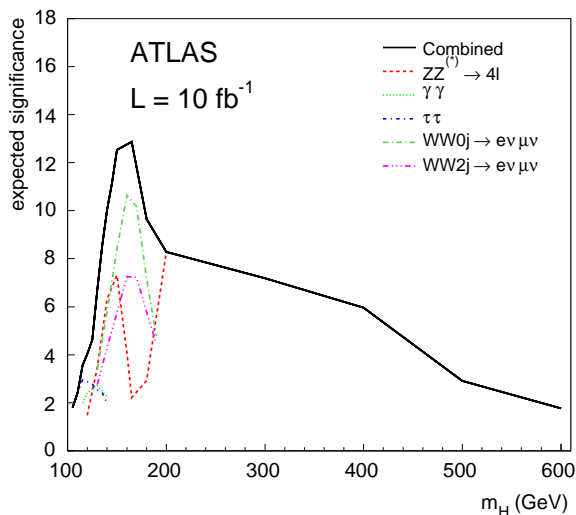


Figure 1.49: Discovery potential of the ATLAS experiment for the Standard Model Higgs boson. The statistical significance expected for an integrated luminosity of  $10 \text{ fb}^{-1}$  at a centre of mass energy of 14 TeV is shown for the different Higgs boson decay modes and their combination as a function of the Higgs boson mass  $m_H$ . [98]

clude a part of the allowed Higgs boson mass range in the initial phase of LHC operation [102], including the development of the methods for the precise determination of the background contributions from data. The expected exclusion limits are shown in Fig. 1.50 (top picture). The best upper limit on the Higgs boson production, obtained for the Higgs boson mass around 200 GeV, is still about a factor of two above the Standard Model prediction. The exclusion reach is especially low in the mass region around 160 GeV, where the  $H \rightarrow ZZ^*$  decays are strongly suppressed by the Higgs boson decays into two on-shell  $W$  bosons.

Due to the high branching ratio for the decay  $H \rightarrow W^+W^- \rightarrow (\ell^+\nu)(\ell^-\bar{\nu})$ , the Higgs boson with a mass between 140 GeV and 180 GeV can be excluded in this channel during the initial phase of LHC operation. In combination with the four-lepton and the two-photon decay channels, the exclusion reach is slightly improved to cover the mass range from 135 GeV to 190 GeV, as shown in Fig. 1.50 (bottom picture). Due to the two neutrinos in the final state of the Higgs boson decays into  $W$  bosons, no precise measurement of the Higgs boson mass is possible. Precise determination of the background contributions is therefore required to exclude the presence of signal events. For this purpose, we are measuring the Standard Model background processes with present LHC data. The

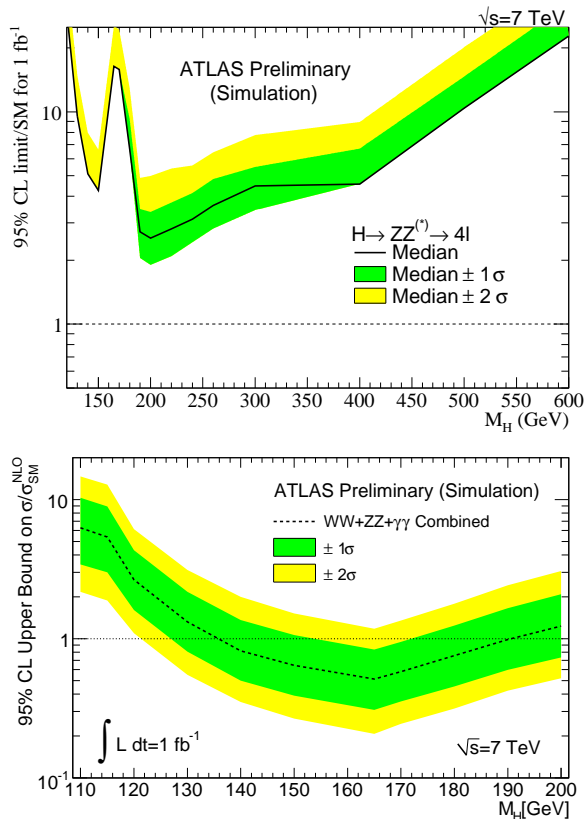


Figure 1.50: Expected upper limits (95% confidence level) on the Standard Model Higgs boson production rate in the  $H \rightarrow ZZ^{(*)} \rightarrow 4l$  channel alone (top picture) and after the combination with the  $H \rightarrow WW \rightarrow \ell\nu\ell\nu$  and  $H \rightarrow \gamma\gamma$  channels (bottom picture). Both figures are shown as a function of the Higgs boson mass at an integrated luminosity of  $1 \text{ fb}^{-1}$  and a centre of mass energy of 7 TeV, normalised to the Standard Model prediction. The bands indicate the 68% and 95% probability regions in which the limit is expected to fluctuate in the absence of signal. [100]

$H \rightarrow WW$  decay channel also allows for an early Higgs boson discovery during the LHC operation at 14 TeV. Parallel to the optimisation of the event selection criteria in this context [103], we have developed a new algorithm for the jet reconstruction [66, 104], which is used for the suppression of the  $t\bar{t}$  and  $W + jets$  backgrounds to the Higgs boson production via the  $W$  or  $Z$  gauge boson fusion. The algorithm reconstructs the jets using particle tracks in the inner detector instead of energy depositions in the calorimeters. The inner detector tracks can be associated to common vertices leading to a jet reconstruction probability which is insensitive to the presence of multiple proton-proton interactions per beam collision (pile-up events).

In the mass range below 140 GeV, the Higgs boson predominantly decays into  $b\bar{b}$  pairs. Due to the large

contribution of QCD background in the gluon-fusion production mode, this decay can only be triggered and discriminated from the background in the production mode of the Higgs boson in association with a  $t\bar{t}$  pair. Our studies have shown that the discovery potential in the  $H \rightarrow b\bar{b}$  decay channel is very much limited by the large experimental systematic uncertainties [105, 106].

The second most frequent mode which can be observed in the mass range below 140 GeV is the decay into a  $\tau^+\tau^-$  pair. This decay can only be discriminated against the background processes in the Higgs boson production mode via the  $W$  or  $Z$  gauge boson fusion where two additional forward jets in the final state provide a signature for background rejection. The decay modes with both  $\tau$  leptons decaying leptonically ( $\ell\ell$  mode) as well as with one hadronic and one leptonic  $\tau$ -decay ( $lh$  mode) have been studied [51, 107]. The event selection criteria have been optimised using multivariate analysis techniques. With a neural network based background rejection method, the signal significance is improved compared to the standard analysis with sequential cuts on the discriminating variables, as shown in Fig. 1.51.

### Higgs Bosons Beyond the Standard Model (MSSM)

The searches for the three neutral Higgs bosons predicted by the MSSM differ to some extent from the searches for the SM Higgs particle. Compared to the Standard Model, the neutral Higgs boson decay modes into two intermediate gauge bosons are suppressed in the MSSM, while the  $A$  and  $H$  boson decays into charged lepton pairs,  $\mu^+\mu^-$  and  $\tau^+\tau^-$  are enhanced. The latter decay channel has an about three hundred times higher branching ratio compared to the first one but is more difficult to reconstruct and provides a less precise determination of the Higgs boson mass.

Our studies of MSSM Higgs boson decays into two  $\tau$  leptons are summarised in [108]. The dominant background contribution originates from the  $Z \rightarrow \tau^+\tau^-$  and  $t\bar{t}$  processes and can be suppressed by the requirements on the presence of  $b$  jets in the final state and large angular separation between the two decaying leptons. This channel provides the highest sensitivity reach for the neutral MSSM Higgs bosons.

Motivated by the excellent muon reconstruction in the ATLAS detector, we also study the prospects for the search in the channel with MSSM Higgs boson decays into two oppositely charged muons. The event selection criteria are optimised for the best discovery potential taking into account the theoretical and

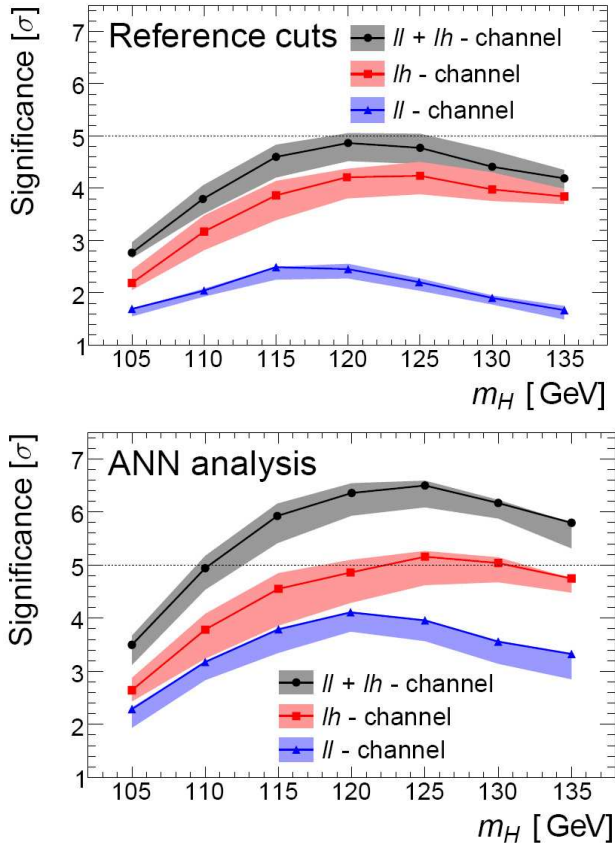


Figure 1.51: Discovery potential for the Higgs boson search in the  $H \rightarrow \tau^+\tau^-$  decay channel, shown separately for the  $ll$  and  $lh$  decay modes and their combination at an integrated luminosity of  $30 \text{ fb}^{-1}$  and a centre of mass energy of 14 TeV. The results are obtained using the standard analysis with sequential cuts on the discriminating variables (top picture), as well as for neural network based analysis (bottom picture). The shaded bands indicate the effect of the experimental systematic uncertainties. [51]

experimental systematic uncertainties [109]. The invariant dimuon mass distribution after all analysis selection criteria is shown for the signal and dominant background processes in Fig. 1.52. The dominant  $Z \rightarrow \mu^+\mu^-$  and  $t\bar{t}$  background contributions are rather large compared to the signal and are subject to sizeable experimental systematic uncertainties, particularly with regard to the jet energy scale. It is therefore important to measure this background contribution with data. This can be done by combining the information from the side-bands of the invariant dimuon mass distribution with the measurements on the  $e^+e^-$  control sample. The latter is motivated by an almost vanishing Higgs boson decay probability into two electrons, while the background contributions are similar for the dimuon and the dielectron final states.

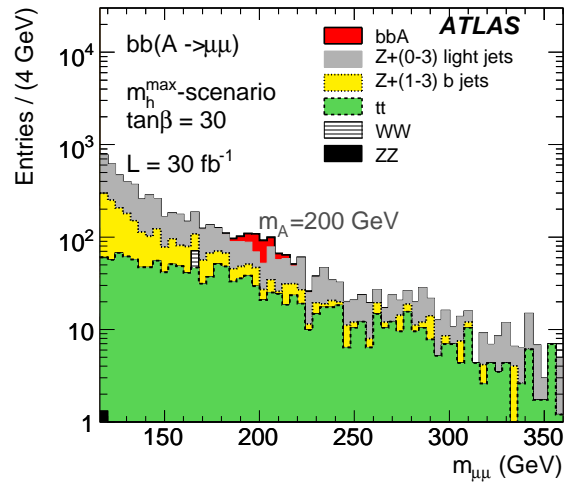


Figure 1.52: Invariant dimuon mass distributions of the main backgrounds and the  $A$  boson signal at mass  $m_A = 200 \text{ GeV}$  and  $\tan\beta = 30$ , obtained for the integrated luminosity of  $30 \text{ fb}^{-1}$  at a centre of mass energy of 14 TeV. Only events with at least one reconstructed  $b$  jet in the final state are selected. [109]

The expected ratio of invariant dielectron and dimuon mass distributions is shown in Fig. 1.53 after all analysis selection criteria and after correcting for the different electron and muon reconstruction and identification efficiency. We perform a detailed study of the

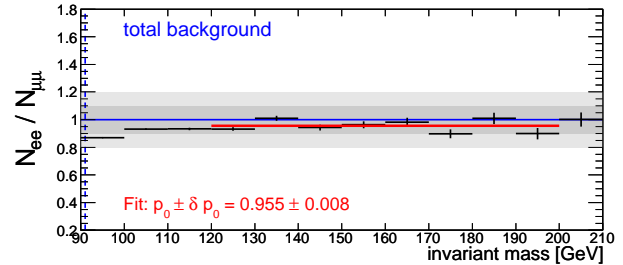


Figure 1.53: Ratio of the dilepton invariant mass distributions for the  $e^+e^-$  control sample and the total  $\mu^+\mu^-$  background for the Higgs boson search in the  $h/A/H \rightarrow \mu^+\mu^-$  channel, shown for an integrated luminosity of  $4 \text{ fb}^{-1}$ . [110]

background estimation from data in [110, 111]. The presented method allows for a significant decrease of systematic uncertainties and thus in an improved sensitivity reach for the MSSM Higgs boson search in the  $\mu^+\mu^-$  decay channel. Especially during the initial phase of LHC running with the limited amount of data, the introduced control data samples are essential for obtaining reliable exclusion limits. The exclu-

sion reach with early data at a centre of mass energy of 7 TeV has been evaluated for the  $h/H/A \rightarrow \mu^+\mu^-$  channel in [112], see Fig. 1.54. At an integrated luminosity of  $1 \text{ fb}^{-1}$  one cannot improve the current limits reached by the Tevatron experiments using this channel alone. However, its combination with searches in a more sensitive  $h/H/A \rightarrow \tau^+\tau^-$  decay channel allows for an improved coverage of the  $(m_A, \tan\beta)$  parameter space.

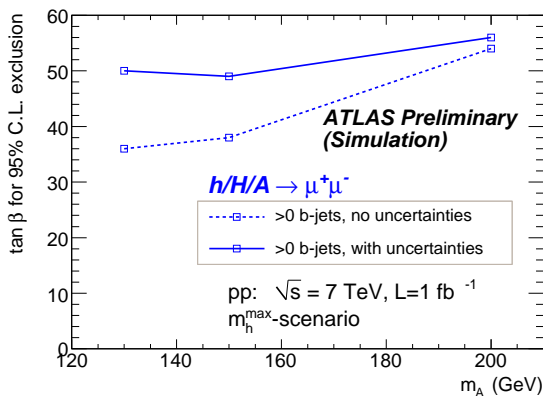


Figure 1.54: The  $\tan\beta$  values needed for an exclusion of the neutral MSSM Higgs bosons shown as a function of the Higgs boson mass  $m_A$  for the analysis mode with at least one b-jet in the final state. An integrated luminosity of  $1 \text{ fb}^{-1}$  and a centre of mass energy of 7 TeV are assumed. Dashed lines represent the results assuming zero uncertainty on the signal and background, while the full lines correspond to the results with both signal and background uncertainty taken into account. [100]

The light neutral MSSM Higgs boson is difficult to distinguish from the Standard Model Higgs boson. Clear evidence for physics beyond the Standard Model would be provided by the discovery of charged scalar Higgs bosons. We have studied the prospects for the search for the charged MSSM Higgs bosons in the decay channel  $H^\pm \rightarrow \tau^\pm\nu_\tau$  which dominates for relatively small Higgs boson masses below 200 GeV [113, 114]. The charged Higgs bosons are produced in top quark decays in  $pp \rightarrow t\bar{t} \rightarrow (bH^\pm)(bW^\mp)$  events. The  $\tau$  leptons from  $H^\pm$  decays are reconstructed in their hadronic decay modes while the  $W$  bosons from top quark decays are required to decay leptonically. Since  $H^\pm$  mass cannot be reconstructed because of the undetected neutrinos in the final state, these events can only be distinguished as an excess of events with reconstructed  $\tau$  leptons and large missing transverse energy above the high background of standard model decays of top quark pairs. In

Fig. 1.55, the discovery region in the  $(m_{H^\pm}, \tan\beta)$  plane is shown for a charged Higgs boson in the above production and decay mode assuming different amounts of integrated luminosity. The theoretical and experi-

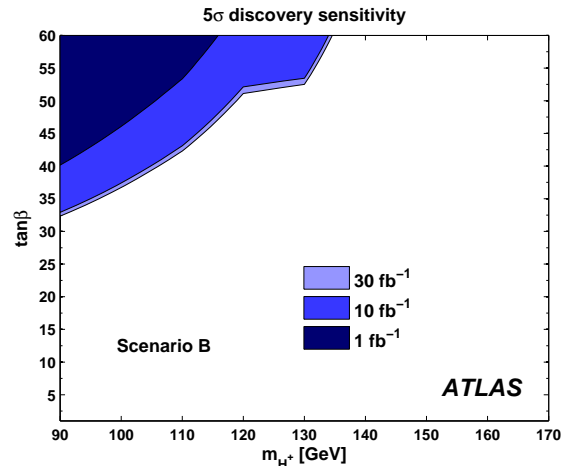


Figure 1.55: The  $\tan\beta$  values needed for a discovery of the charged MSSM Higgs bosons shown as a function of the Higgs boson mass  $m_{H^\pm}$  for different levels of integrated luminosity. A centre of mass energy of 14 TeV is assumed. The decays  $H^\pm \rightarrow \tau^\pm\nu_\tau$  can be discovered with at least  $5\sigma$  significance in all shaded regions of the parameter space. [113]

mental systematic uncertainties have been taken into account. We have developed the methods to decrease the original instrumental background uncertainty of 50% down to 10% by means of the control measurements on data [114, 115].

## 1.2.4 Search for Physics Beyond the Standard Model

### Supersymmetric Particles

Supersymmetry (SUSY) is the theoretically favoured model for physics beyond the Standard Model. The new symmetry unifying fermions and bosons predicts for each Standard Model particle a new supersymmetric partner with the spin quantum number differing by  $1/2$ . Supersymmetry provides a natural explanation for Higgs boson masses near the electroweak scale. In addition, the lightest stable supersymmetric particle is a good candidate for the dark matter. The SUSY models can also provide solutions to the problem of the unification of the fundamental forces. In order to suppress the SUSY-induced processes violating the baryonic and leptonic quantum numbers, the so-called R-parity has been introduced as a conserved quantum

number. Each SM particle has an R-parity equal to 1, while the supersymmetric partners carry an opposite sign, i.e. an R-parity of -1.

If the mass scale of the SUSY particles is accessible at the LHC, the squarks and gluinos (the superpartners of quarks and gluons with spin 0 and 1/2, respectively) will be copiously produced in  $pp$  collisions. Assuming that the R-parity is conserved in these processes, all supersymmetric particles must be produced in pairs and each will decay to the weakly interacting lightest supersymmetric particle via decay chains involving the production of quarks and leptons. Therefore, the SUSY events at the LHC are characterised by the large missing transverse energy, highly energetic jets and leptons.

If the supersymmetry would be a conserved symmetry, each particle and its superpartner are expected to have an equal mass. However, since the supersymmetric partners of the Standard Model particles are not observed so far, SUSY must be a broken symmetry. A model with the SUSY breaking mechanism mediated by the gravitational interaction is called mSUGRA and is described by the common mass terms  $m_0$  and  $m_{1/2}$  for all boson and fermion masses, respectively, at an energy scale above  $10^{15}$  GeV, where the electroweak and strong interactions are unified (GUT scale).

The searches for SUSY signatures with conserved R-parity are performed in ATLAS by searching for an excess of events in various channels. These channels explore a large variety of possible signatures in the detector, divided according to different jet and lepton multiplicities. Fig. 1.56 shows the  $5\sigma$  discovery reach for the mSUGRA model in the final states with 4 jets and 0 leptons, the states with 4 jets and 1 lepton or in the final states with 2 jets and 2 leptons.

The Standard Model processes with similar signatures as the signal are the top-quark pair ( $t\bar{t}$ ) and the gauge bosons ( $W$  and  $Z$ ) production. These processes are characterised by a large missing transverse energy originating from weakly interacting neutrinos and therefore constitute the main background to SUSY searches at the LHC. Additional important source of the background is the QCD jet production in which the mis-measured jet energy can lead to the high-energy tails in the distribution of the missing transverse energy. It is expected that at the LHC the Monte Carlo prediction will not be sufficient to achieve the good understanding and the control of the background for the SUSY searches. Our studies are concentrating on the data-driven estimation of these, which is essential for

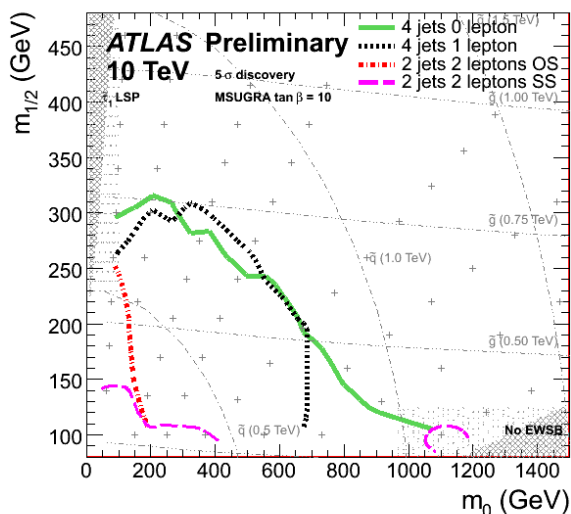


Figure 1.56: The  $5\sigma$  discovery reach of the ATLAS experiment in the search for the mSUGRA signal using channels with various jet and lepton multiplicities in the  $(m_0, m_{1/2})$  parameter space of the mSUGRA model. The discovery reach is evaluated for the centre of mass energy of 10 TeV and an integrated luminosity of  $200 \text{ pb}^{-1}$ .

an early discovery of SUSY with the ATLAS detector.

We have developed the methods for the determination of the  $t\bar{t}$  background contribution from data [119]. The background contribution is measured by means of the control data samples which are free of the SUSY signal contribution. The contribution from the  $t\bar{t}$  production with top quark decays involving the  $\tau$  leptons and non-reconstructed electrons or muons is estimated from similar events with identified muons and electrons. The control data sample is composed mainly of  $t\bar{t}$  events in which both top quarks decay into a b-quark, neutrino and a lepton (electron or muon). Additional kinematic constraints are applied on these events similarly to the criteria used for the signal selection. The number of b-jet pairs passing the kinematic constraints is used to divide the measured data sample into the SUSY-dominated and the  $t\bar{t}$ -dominated region (see Fig. 1.57).

A similar strategy is used to define the control sample with semi-leptonic  $t\bar{t} \rightarrow (\ell\nu b)(qqb)$  decays [120]. In this case the discriminating variable distinguishing between the signal and the background region is the invariant mass of the three nearby jets. In case of the  $t\bar{t}$  events, the value of this variable will be close to the top quark mass (see Fig. 1.58).

The contribution of the  $t\bar{t}$  background with tau leptons produced in top-quark decays can be estimated

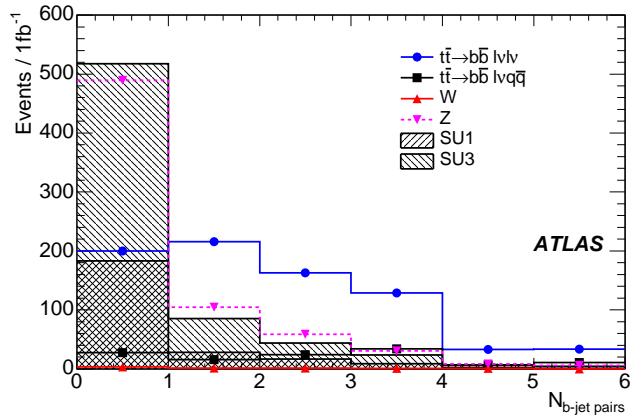


Figure 1.57: Number of b-jet pairs  $N_{b-jet\ pairs}$  selected after the kinematic constraints on the  $t\bar{t} \rightarrow (\ell\nu b)(\ell\nu b)$  process. The  $N_{b-jet\ pairs} > 0$  region is mainly populated by the  $t\bar{t}$  events. This region is used as a control data sample for the estimations of the  $t\bar{t}$  background to the searches for SUSY signatures with one lepton in the final state. The events with  $N_{b-jet\ pairs} = 0$  originate predominantly from the gauge boson production processes and by the SUSY signal. The two typical SUSY models labeled SU1 and SU3 are shown for the signal. [119]

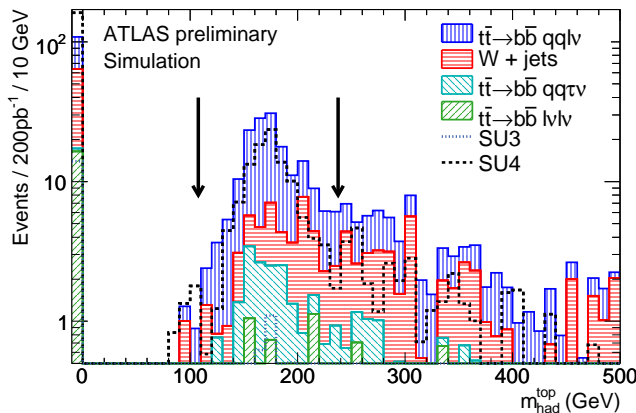


Figure 1.58: Invariant mass of the tree nearby jets in each event. This variable is used for the selection of the control data sample of  $t\bar{t} \rightarrow (\ell\nu b)(qqb)$  events, needed for an estimation of the  $t\bar{t}$  background in SUSY searches with no-lepton signatures. The arrows indicate the selected window for this variable. The contributions of the Standard Model processes are shown by the stacked hatched histograms. The SUSY contribution for two typical SUSY mSUGRA models (SU3 and SU4) are overlaid. [120]

from the control data sample by replacing the reconstructed electron or muon with a simulated tau lepton decay (see Fig. 1.59). Similarly, one can also estimate the contribution of  $t\bar{t}$  with a non-identified electron or muon by removing the reconstructed leptons from

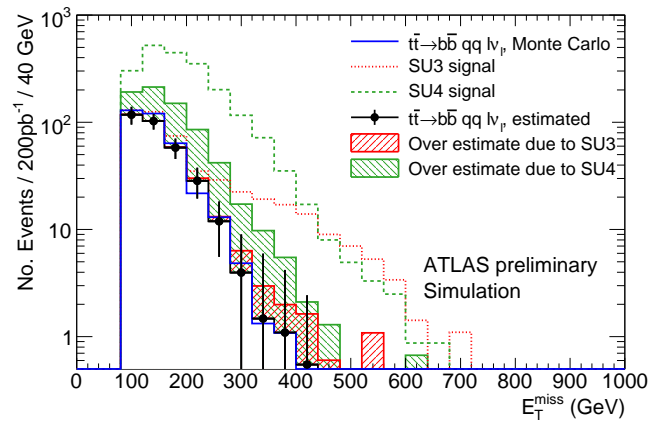


Figure 1.59: Missing transverse energy distribution in the one-lepton final state. The solid line shows the Monte Carlo estimate, circles are the result of data-driven estimation. The shaded histograms show the increase of the data-driven estimates due to the contaminating SUSY signal (represented by SU3 and SU4 models) in the control data sample and the dashed lines show the SUSY signals stacked on the top of the  $t\bar{t}$  background. [120]

each event in the control data sample.

We analysed a set of the most important kinematic variables for the  $70\text{ nb}^{-1}$  of data collected by the ATLAS experiment [121]. We find a good agreement between data and Monte Carlo predictions, indicating that the Standard Model backgrounds for the SUSY searches are well under control (see Fig. 1.60).

### Other Extensions of the Standard Model

The discovery of the neutrino flavour oscillations has shown that the lepton flavour is not a conserved quantity within the Standard Model. Beyond the SM, the lepton flavour violation can occur in many SUSY extensions. One of the lepton flavour violating process accessible at the LHC is a neutrinoless decay of a tau lepton  $\tau \rightarrow \mu\mu\mu$ . Although the Standard Model predicts a very small branching ratio for this decay,  $\mathcal{BR}(\tau \rightarrow \mu\mu\mu) \leq 10^{-14}$ , some extensions of the Standard Model, such as SUSY and models with doubly charged Higgs boson, predict the values which are several orders of magnitude higher. Therefore, the measurement of the branching ratio for the  $\tau \rightarrow \mu\mu\mu$  decay will put stringent limits on the parameters of such models beyond SM.

During one year of data-taking at the low luminosity of  $10^{33}\text{ cm}^{-2}\text{ s}^{-1}$ , ATLAS will collect  $10^{12}$   $\tau$  lepton decays. Due to the very large background contribution only a fraction of these decays can be observed

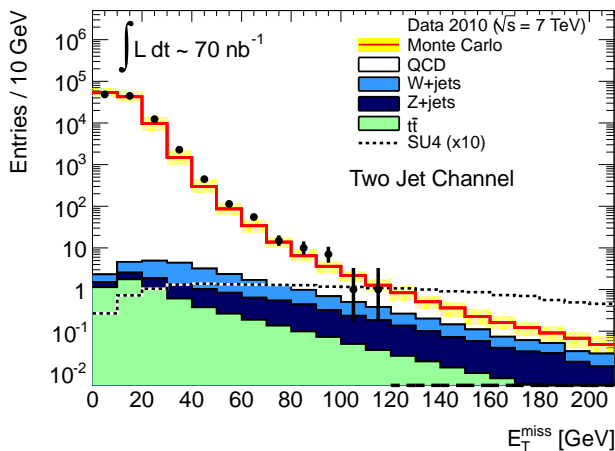


Figure 1.60: Distribution of missing transverse energy in the two-jets final state. Black points show the measurement results with  $70 \text{ nb}^{-1}$  of data collected by the ATLAS experiment. Shaded histograms show the contribution from the gauge boson and top-quark production processes. The open red histogram is the QCD di-jet production process. The prediction of the low-mass mSUGRA model SU4 (enhanced by a factor of 10) is shown by a black dashed line. [121]

in ATLAS, namely the decays of  $\tau$  leptons originating from the  $W$  and  $Z$  boson decays. We studied the sensitivity of the ATLAS detector to the  $\tau \rightarrow \mu\mu\mu$  decay, where the tau lepton is produced in the decay of  $W$  boson [72]. This process is characterised by a large missing transverse energy from the non-detectable neutrino and by the three nearby muon tracks. The main background processes are the production of charmed and beauty mesons, with their subsequent decays into muons (see Fig. 1.61).

The study with the simulated data shows that the upper limit of  $\mathcal{BR}(\tau \rightarrow \mu\mu\mu) \leq 5.9 \cdot 10^{-7}$  can be achieved with  $10 \text{ fb}^{-1}$  of collected data. Extrapolating this expected sensitivity to higher integrated luminosities, an integrated luminosity of  $100 \text{ fb}^{-1}$  has to be collected by the ATLAS experiment to reach the current best upper limit of  $\mathcal{BR}(\tau \rightarrow \mu\mu\mu) \leq 3.2 \cdot 10^{-8}$  (90% CL) by the BELLE experiment.

In addition to the described study of the lepton flavour violation, we pursue the searches for non-Standard Model heavy neutral gauge boson  $Z'$ . This particle is predicted by some extensions of the Standard Model which address the problems of the mass hierarchy and the number of generations of lepton and quarks.

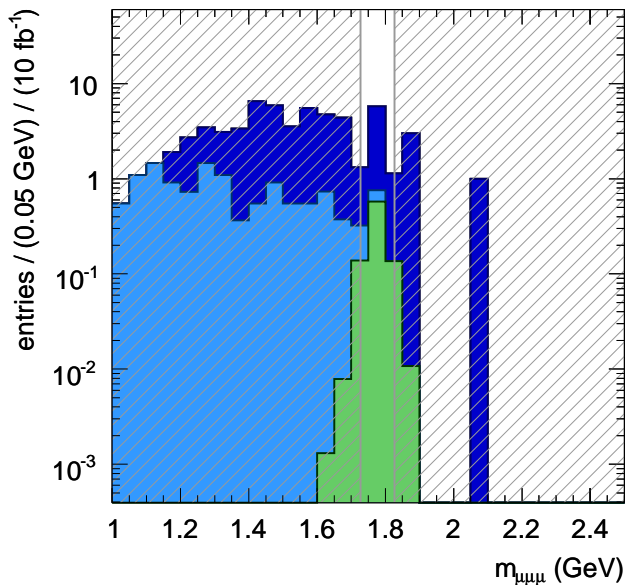


Figure 1.61: Invariant mass distribution of the tree nearby muons, shown for the signal and background processes after applying all analysis selection criteria. The signal consists of the  $\tau \rightarrow \mu\mu\mu$  decays with tau leptons originating from the  $W$  bosons (green), while the background processes include the decays of charmed and beauty mesons. Histograms are normalised to an integrated luminosity of  $10 \text{ fb}^{-1}$  at a centre of mass energy of 14 TeV. Non-shaded area represents the selected mass window for the evaluation of the limits on the branching ratio. [72]

### 1.2.5 Analyses Summary

In summary the MPP physics analyses are well advanced. The MPP group has significantly contributed to the first physics measurements of ATLAS, the measurement of the inclusive lepton transverse momentum spectra and the measurement of the  $W$  and  $Z$  boson production cross sections. A variety of paths are explored in the search for the most appropriate variable and analysis strategy to determine the top-quark mass, a measurement that will soon be dominated by the systematic uncertainty. In the context of the searches for new physics phenomena, many new methods have been developed to understand the background contribution originating from the above SM processes. Strategies for the Higgs boson and supersymmetry searches are optimised for the highest possible sensitivity during the early data taking phase. Members of the group are actively participating in the ATLAS efforts and have presented their own and the ATLAS collaboration results at international conferences [96, 97, 116–118, 122–125].

## 1.3 Detector Upgrade

The design luminosity of the LHC of  $10^{34} \text{ cm}^{-2}\text{s}^{-1}$  is expected to be reached after a few years of data taking at lower luminosity. The *integrated* luminosity after 10 years of operation will be about  $300 \text{ fb}^{-1}$ .

For the study of even lower-cross section phenomena at the LHC, a substantial increase of the LHC luminosity is needed. With a series of upgrades of the CERN accelerator complex an order of magnitude could be achieved, which may yield an integrated luminosity of up to  $3000 \text{ fb}^{-1}$  after 10 years of additional running (Super-LHC or SLHC). To help the LHC detectors to cope with this luminosity increase, a new operation mode of the machine is foreseen ("luminosity levelling"), reducing the decay rate of luminosity during a proton fill in such a way that the peak luminosity at the beginning of the fill will be limited to about  $4 \times 10^{34} \text{ cm}^{-2}\text{s}^{-1}$ , yet yielding a 10 times higher integrated luminosity for the fill.

While this reduction of the *peak* relative to the *integrated* luminosity by a factor of 2.5 represents a substantial alleviation for the operation of the ATLAS detector, the increase of luminosity by a factor of 4 relative to the original design value of  $10^{34} \text{ cm}^{-2}\text{s}^{-1}$  still calls for a major upgrade effort for most subsystems of the ATLAS detector. Tracking detectors, for example, may need higher granularity to cope with the high particle rates while e.g. the overall radiation dose corresponding to  $3000 \text{ fb}^{-1}$  will require new radiation hard readout electronics in all subsystems of the ATLAS detector.

The present planning foresees the installation of the Insertable B-Layer of the Pixel detector (see next section) in the year 2016, with the other upgrade steps to follow by 2020.

### 1.3.1 R&D towards a novel Pixel Detector for the SLHC

#### Overview

The present ATLAS Inner Detector consists of a pixel detector, the Semiconductor Tracker (SCT), and the Transition Radiation Tracker (TRT), which are located at increasing radii from the beam line as described above.

After about five years of operation it is planned to extend the present pixel detector by an additional innermost layer, which will be directly mounted onto a new beam pipe. This upgrade is named the Insertable B-Layer (IBL). After ten years of operation at the LHC

with the design luminosity profile the complete silicon part of the ATLAS Inner Detector most likely has to be replaced due to radiation damage. In addition, an upgrade of the LHC accelerator, named Super-LHC (SLHC), is planned to reach a ten-fold increase in luminosity. Consequently, for a given radius the expected radiation dose and hit occupancy at the SLHC are a factor 5–10 higher than at the LHC. The Inner Detector upgrade, mandatory for running at the SLHC, demands a completely new design for the Inner Detector, rather than upgrading the existing detector. For example, the high hit occupancy leads to an unacceptable occupancy for the TRT detector, which needs to be replaced by a new device with a different detector technology. The choice has been made for a patterned solid state detector with decreasing granularity for increasing radius. Although the general strategy is clear, the details of the layout and also the detector concepts to be used at various radii are still under study.

The geometrical design is developed by the Inner Detector Layout Group, where the MPP is participating. The initial design, the strawman, has been defined in [126]. From this the final design will be obtained by iteration, depending on the results from detector R&D as well as simulation of the expected performance. In any case, the expected increase in radiation dose means that a new generation of radiation tolerant silicon sensors has to be developed for the innermost part of the Inner Detector.

#### MPP Module Design

Utilizing the knowledge and capabilities of the semiconductor laboratory, HLL, who designed both the present pixel and the SCT sensors, the MPP has set out to investigate the feasibility of a novel detector concept for the pixel detector. The R&D [127] is embedded in the ATLAS upgrade activities, and has three main ingredients, 1) the production of  $(75\text{--}150)\mu\text{m}$  thin sensors to increase the radiation tolerance, 2) the use of a novel interconnection technology (SLID, see below) for attaching the readout electronics to the pixel sensors that may lead to a cost effective solution to replace the presently used bump bonding technology, and 3) the vertical integration of analog and digital electronics with inter chip via (ICV), which will allow for individual optimization of the electronic chips. A sketch of a pixel module using this concept, while obeying the restrictions placed by the presently available ATLAS FEI3 read-out electronics, is shown in Fig. 1.62.

For the production of thin sensors the process [128]

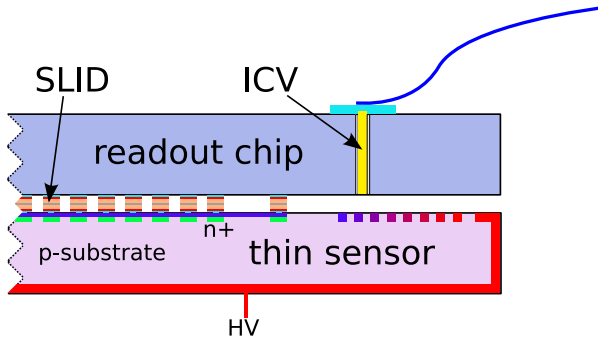


Figure 1.62: Sketch of the MPP module concept.

developed at the HLL is used. These sensors offer beneficial features [129] like a low depletion voltage, low leakage current and high charge collection efficiency (CCE).

The novel Solid-Liquid InterDiffusion (SLID) interconnection technology [130] has been developed by the Fraunhofer IZM Institut in Munich [131], but was not yet applied to sensors made for high energy experiments. The high density interconnection technology allows for smaller pixel sizes than in the current ATLAS hybrid pixel detector, which may be hard to achieve by the presently used bump bonding technique. Besides the interconnection of chips and sensors this technology allows for vertical integration of several layers of thinned chips with ICVs, by using the combined ICV-SLID process. When exploiting this, e.g. the chips performing the analog and digital parts of the read-out can be arranged on top of each other rather than side by side, which makes the design more compact and the signal paths shorter. In addition, the chips can be made using different technologies and optimized individually in terms of speed, power consumption and radiation hardness, allowing for a better overall performance. The first investigations, like the initial design studies and the compatibility investigations of thin sensors with the SLID metalization system and processing steps [132], were already reported in [1] (p.77-85). The results obtained in the years 2007-2010 are described below, starting with the sensor design supported by device simulation, followed by the wafer production and device evaluation, and finally the SLID and ICV investigations.

### Thin Sensors

The design and production of four thin sensor wafers in  $n^+$ -in- $n$  and eight in  $n^+$ -in- $p$  technology, containing a variety of different structures, has been performed.

For the  $n^+$ -in- $n$  technology all four wafers have  $75\ \mu\text{m}$  thin active sensors, whereas for the  $n^+$ -in- $p$  technology four wafers each have  $150\ \mu\text{m}$  and  $75\ \mu\text{m}$  thin active sensors. These wafers were partly processed at the HLL and partly at industrial companies.

The most important structures are firstly strip sensors for CCE measurements, and secondly pixel devices with the ATLAS pixel sensor geometry used to either be connected to the present ATLAS pixel chips, and read-out by the existing data acquisition system to study system issues, or to investigate the ICV-SLID technologies. To determine the implant parameters, and to better understand the behavior of the pixels before and after irradiation as functions of the parameters of the p-spray isolation, a simulation of a restricted part of the pixel array has been set up [133] using the DIOS/TeSCA silicon device simulation software.

The wafer production was very successful in terms of device yield and properties of the diodes, strips and pixel structures before and after irradiation with 26 MeV protons at the Karlsruhe Cyclotron up to fluences of  $10^{16}\ \text{n}_{\text{eq}}/\text{cm}^2$  (1 MeV neutron equivalent) expected at the SLHC. Some results of the wafers

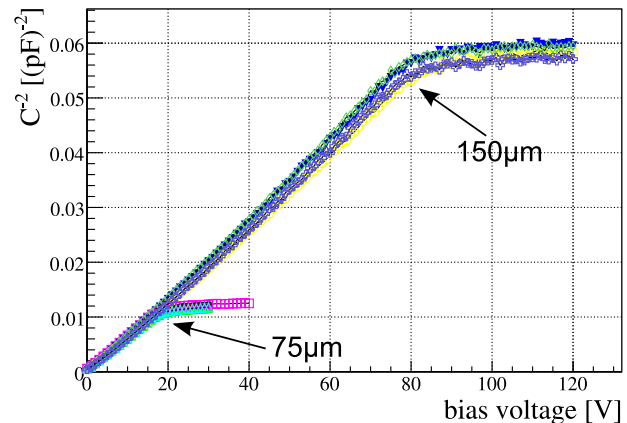


Figure 1.63: Capacitance-voltage characteristics of  $n^+$ -in- $p$  diodes before irradiation.

made using the favored  $n^+$ -in- $p$  option are reported below. The depletion voltage, which is indicated by the kink in the inverse capacitance squared versus voltage behavior shown in Fig. 1.63 for the non-irradiated diodes, is according to the expectation from the resistivity of the silicon material used. The measured values of about 20 V and 80 V also nicely exhibit the predicted quadratic scaling with the sensor thickness. The device yield for the FEI3 compatible pixel structures is 79 working structures out of 80 produced. This yield is defined by the current voltage characteristics

and requiring that the sensor can be biased well above its depletion voltage. This is shown for a subset of 16 sensors in Fig. 1.64, and the one structure marked as failing is displayed with red circles drawing much more current than all the others with a steeply rising behavior at around 150 V. The overall level of leakage current in the plateau of about  $5 \text{ nA/cm}^2$  is very low signaling a very high quality and low impurity processing of the wafers. After irradiation with protons

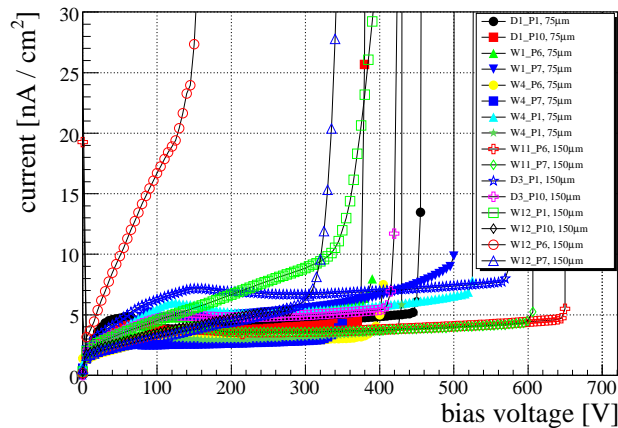


Figure 1.64: Current-voltage characteristics of  $n^+$ -in-p FEI3 pixel sensors before irradiation.

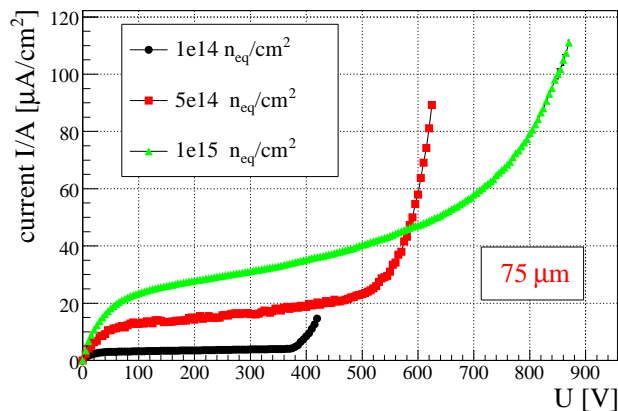


Figure 1.65: Current-voltage characteristics of  $n^+$ -in-p FEI3 pixel sensors after irradiation to three fluences.

up to various fluences the devices show the expected behavior, namely an increased current accompanied by a higher depletion voltage but also a much increased breakdown voltage. This is demonstrated in Fig. 1.65 for pixel sensors with  $75 \mu\text{m}$  active thickness.

A very important, and at present also much debated, property of the sensors is the CCE, which is defined as the collected charge after irradiation normalized to the one obtained before irradiation. The conventional

description of the radiation damage of silicon predicts very low CCE after large fluences. This leads to small signals at increasing noise rendering operation of the device more and more challenging due to a decreasing signal-to-noise (S/N) ratio. The decrease of the collected charge is caused mainly by radiation-induced bulk defects acting as traps for the electrons and holes, produced by the primary particle, on their drift path to the electrodes. As a result it is predicted that only charges from the close vicinity of the electrodes can arrive in time and lead to a detectable signal. Experimental observations from various groups are in clear contradiction to the prediction of a strongly reduced CCE, and rather show that for short collection distances, i.e. thin sensors or 3D sensors<sup>1</sup>, the CCE after strong irradiation reaches unity or even surpasses it. One model to account for this is charge multiplication, which occurs in very high electric fields, and naturally is more likely for thin sensors, since here the bias voltage drops over a shorter distance.

The MPP group investigated this effect experimentally on  $n^+$ -in-p strip sensors, and also by a Monte Carlo simulation propagating the electrons through the detailed electric field of the devices while simulating charge trapping, but also the charge multiplication process, both according to existing models.

The measured CCE as a function of the bias voltage for various sensors and fluences is shown in Fig. 1.66. Clearly sensors of both thicknesses largely surpass the prediction from conventional trapping models (see below), and for the  $75 \mu\text{m}$  thin devices the full charge can be recovered within uncertainties, albeit at increasing voltages for increasing fluences. This is a very important result since it means that the requirements on the minimum signal charge for the newly designed FE-I4 readout chip, to be used for the IBL and for outer layers of the pixel detector for the SLHC, is less demanding than initially thought. However, only the experimental investigation of the module assemblies to be performed later this year will tell whether the S/N value will be high enough after strong irradiation.

The strip sensors used for the CCE measurements shown in Fig. 1.66 are DC coupled to the readout electronics. After irradiation this causes high currents to flow through the readout channels that prevent apply-

<sup>1</sup>In 3D sensors the electrodes are not implanted on the surface as for planar sensors, but as columns through the bulk of the sensor. This enables to achieve short collection distances independent of the bulk thickness, at the expense of the need to use a non-standard expensive production process, which at present has only low yield.

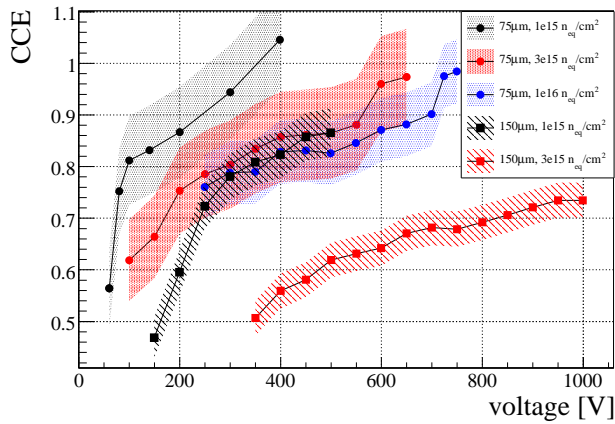


Figure 1.66: Charge collection efficiency of  $n^+$ -in-p strip sensors after irradiation.

ing higher bias voltages than the ones shown to not damage the electronics. In future this limitation will be avoided by an AC coupling of the strips. At present for some of the sensors the use of decoupling pitch adapters between the sensor and the chip effectively leads to an AC coupling. With these measures higher bias voltages can be applied to investigate, whether also for the  $150\mu\text{m}$  thin sensors after irradiation, the full charge can be recovered at even higher voltages.

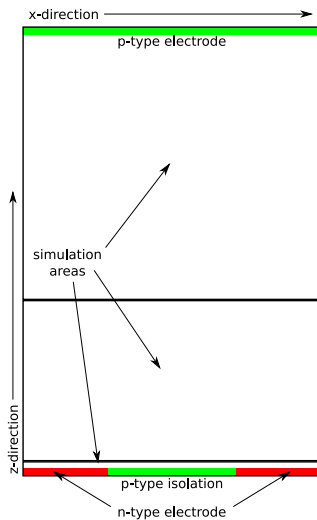


Figure 1.67: Sketch of the 2-dimensional area used for the device simulation.

The simulation of the predicted CCE is done two-dimensional, as shown in Fig. 1.67. In the MC simulation the electrons produced by an incident particle are individually followed through the sensor, and at each step charge trapping and charge multiplication are simulated based on the models available from the literature, and according to the electric field as cal-

culated by the preceding DIOS/Tesca simulation described above [133]. Indeed, at high bias voltage and after large fluences, the electric field exceeds the value needed for charge multiplication, especially so at the boundaries of the p-type and n-type doping in the close vicinity of the collecting electrodes, i.e. the boundaries between the red and green regions close to  $z = 0$  in Fig. 1.67. The predicted CCE for  $75\mu\text{m}$  thin diodes

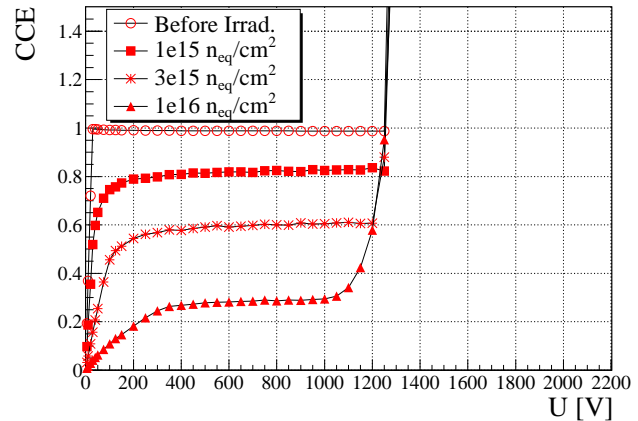


Figure 1.68: Predicted CCE for  $75\mu\text{m}$  thin  $n^+$ -in-p diodes after irradiation.

presented in Fig. 1.68 reveals a strong rise in CCE for fluences from  $3 \cdot 10^{15} \text{ n}_{\text{eq}}/\text{cm}^2$ , however at very high bias voltages well in excess of 1 kV. When comparing this prediction to the experimental result two facts are evident. The measured CCE in the plateau region is much higher than the prediction, e.g. for the  $75\mu\text{m}$  thin diodes at  $1 \cdot 10^{16} \text{ n}_{\text{eq}}/\text{cm}^2$  and at 500 V the measurement is about 0.8 with a prediction of slightly below 0.3. The observed increase of the CCE with the bias voltage is roughly linear, and the predicted step increase due to charge multiplication is not observed. Further investigations are clearly needed before proper predictions for the experimental observations can be made.

For the IBL upgrade a reduction of the inactive region around the active pixel region from the present width of about  $1000\mu\text{m}$  to about  $450\mu\text{m}$  is required. To achieve this, sensors with a so called slim-edge design with 11 instead of 21 guard rings around the active region have been produced. The high voltage behavior of the bare sensors with the slim edge design before and after irradiation is not significantly worse than that of the ones with the present guard ring design, proving that this requirement can be met.

In parallel to the MPP&HLL wafer production,  $n^+$ -in-p pixel sensors of the very same design have been produced at CiS and bump bonded to FEI3 electronics.

Initial tests of these single chip modules are promising, showing adequate noise and sufficient high voltage stability. After irradiation to large fluences they will serve to verify that the passivation layer on top of the sensor is sufficiently insulating. This is needed to avoid sparking between the chip and the sensor which, in the  $n^+$ -in-p sensor technology, are only a few  $\mu\text{m}$  apart, but are kept at a potential difference of several hundred Volt.

### Interconnection and vertical Integration

The SLID interconnection and ICV have been investigated in collaboration with the IZM Munich. A number of wafers containing inactive structures consisting of many long chains of aluminum traces, so called daisy-chains, to be individually connected via SLID have been designed and produced at MPP&HLL. The wafer layout is divided into two halves, one serving the sensor structures, the other half mimicking the chips to be connected to the sensors. These wafers were connected partly in a wafer-to-wafer approach, i.e. one wafer was rotated by 180 degrees and SLID connected to another wafer, and partly in a chip-to-wafer approach, i.e. the chips of one wafer were singularized, individually attached to a handle wafer, and this handle wafer was SLID connected to the sensor wafer. The results shown below are from the wafer-to-wafer connection. The chip-to-wafer approach yielded worse results due to technical problems that have led to an insufficient alignment of the chips on the handle wafer, and consequently a large number of non successful connections. The likely cause of this has been understood, and will be addressed for the next SLID connection run which is underway. The daisy-chains feature different sizes and pitches of SLID connections. Resistance measurements on these chains indicate if at least one connection of a chain is missing. By assuming a binomial probability distribution the SLID inefficiency is calculated from those resistance measurements. It is found to be of the order of one per mill for types where at least one connection was failing, and to be below three per mill for those where all chains were fully intact. Small deliberate vertical steps in the SLID connection, produced by omitting some layers in the structure design, and amounting to at most  $1\ \mu\text{m}$ , did not deteriorate these results. From the fully working chains the resistance per connection was determined to be below  $1.5\ \Omega$  and likely dominated by the contact resistance. These values are small enough for SLID to be used for connecting individual

pixel cells.

In addition to the chains, these wafers contain geometrical structures that allow for the measurement of the positioning accuracy again by performing resistance measurements. The positioning accuracy of the SLID connections can also be deduced from infrared images of connected packages, see Fig. 1.69. The silicon bulk (grey area) is transparent to the infrared light, but the SLID metal layers (dark structures) are not. Consequently, these structures are visible both on the

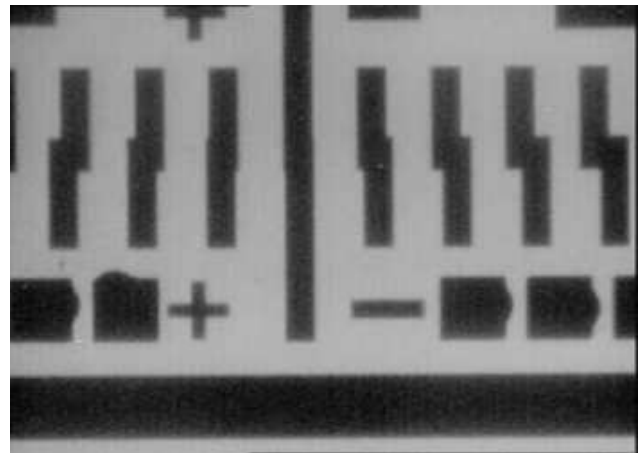


Figure 1.69: Infrared image of SLID connections.

sensor and on the chip surface. Comparing their position and overlap with the wafer design reveals the positioning accuracy. In this way the positioning accuracy for the wafer-to-wafer connection was estimated to be better than  $(5-10)\ \mu\text{m}$ , again precise enough for SLID to be used for connecting individual pixel cells.

The ICVs are needed if vertical integration is attempted. This can be done at two levels, either by connecting individual pixels by ICV, or by only routing the signals from the wire bond pads via ICV to reduce, or even avoid, the presently used balcony for the wire bond pads. However, this needs a special design of the read-out electronics that reserves inactive regions in the chip layout, to allow etching the vias. In the present design of the FEI3 chip such regions are not available for individual pixels. To still show the feasibility of ICV and to develop the processing steps, the present R&D concentrates on etching vias only at the read-out wire bond pads, that by design do not have active parts below them, see Fig. 1.62 for a schematic view. The location and layout of the vias have already been defined, and the first test etching on FEI3 wafers have been performed.

The progress of this R&D has been reported

by members of the group at international conferences [132, 134, 135], including overview presentations of the entire ATLAS R&D on planar silicon sensors [136].

### Summary and Outlook

The future steps of the pixel R&D consists of the production of thin  $n^+$ -in-p sensors for the IBL sensor qualification. Here the MPP design competes with the planar  $n^+$ -in-n design, as well as with 3D- and diamond sensors. The MPP&HLL thin  $n^+$ -in-p wafer production is partly done, and interconnection to the newly developed FEI4 chip with the conventional bump bonding process (the choice of interconnection made for the IBL) at IZM Berlin [137] is planned later this year. The SLID connection to FEI3 chips without ICVs is underway. The preparation of the chip- and sensor wafers has been done, the dicing and singularizing of the chips is presently ongoing, and SLID connections are planned later this summer. For the SLID connection to FEI3 chips with ICVs the design work is finished and first test etchings for the ICVs are underway.

### 1.3.2 Upgrade of the HEC: Motivation and Options

The LAr system consists of a barrel region and two endcap and forward regions. As seen from Fig. 1.70 the radiation levels increase in the forward direction with proximity to the beam. From the barrel to the endcap and from the endcap to the forward calorimeters the flux and average energy of the particles from minimum bias events increases with the consequent growth of multiplicity and density of shower particles. This results in a power density, and hence radiation flux, deposited in the calorimeters reaching levels not seen in previous collider detectors. The ATLAS calorimeters are designed to cope with a peak luminosity of  $10^{34} \text{ cm}^{-2} \text{ s}^{-1}$  and an integrated luminosity of about  $700 \text{ fb}^{-1}$  – sufficient for the currently foreseen  $300 \text{ fb}^{-1}$  for LHC.

Under SLHC conditions both the maximum instantaneous luminosity of  $10^{35} \text{ cm}^{-2} \text{ s}^{-1}$  and the integrated luminosity of about  $3000 \text{ fb}^{-1}$  luminosity collected over an anticipated SLHC lifetime of 10 years will typically increase by an order of magnitude. It is safe to assume that the functioning of the LAr barrel EM calorimeter will suffer neither at highest peak

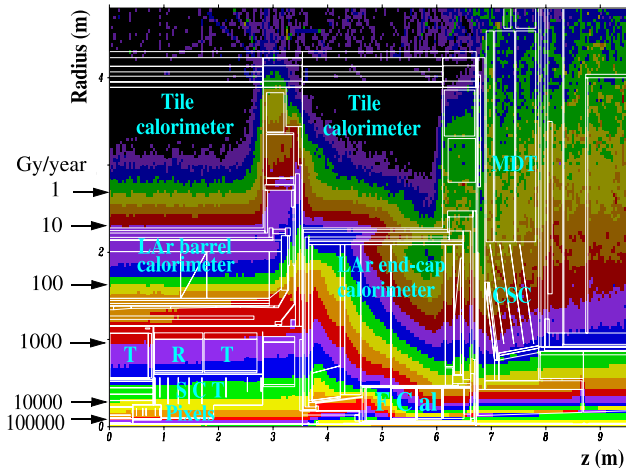


Figure 1.70: The total ionising dose per year calculated by the GCALOR software package in one quarter of the central part of the detector. The locations of the inner detector sub-systems, of the different calorimeters and of the inner endcap muon stations are indicated. The scale on the left gives the integrated dose per year corresponding to the various iso-lines.

luminosities nor from the integrated luminosity collected. Depending on the running conditions and the actual level of radiation, the performance of the forward calorimeter may be degraded due to the increased peak luminosity. On the other hand, it is unclear how much the endcap calorimeters (EMEC and HEC) will be affected. To understand the effects of luminosity on the endcap and forward regions, the so-called HiLum experiment has been launched.

One element which might be affected by the integrated luminosity is the front-end electronics of the HEC which is installed at the perimeter of the HEC in relatively high radiation fields.

In the vicinity of the HEC cold electronics a neutron fluence of  $0.2 \times 10^{14} \text{ n/cm}^2$ , a  $\gamma$  dose of  $330 \text{ Gy}$  and a hadronic fluence of  $3.1 \times 10^{11} \text{ h/cm}^2$  are expected after 10 years of LHC operation at high luminosity. The radiation hardness against all three types of radiation has been studied with both preproduction and production versions of the HEC cold electronics chips both at room temperature and submerged in liquid nitrogen [138]. It was found that neutron irradiation is by far the most dangerous yielding the smallest safety margin. Measurements in these tests showed that the amplifiers start to degrade when the neutron fluence exceeds  $\sim 3 \times 10^{14} \text{ n/cm}^2$ . Compared to ATLAS requirements this amounts to a safety margin of about 15 for 10 years of LHC operation.

Assuming a ten times higher SLHC luminosity the safety margin is essentially eliminated, i.e. the present HEC cold electronics would be operated at its limit. It is therefore planned to develop a new ASIC that will be ten times more radiation hard. It would be available to replace the present GaAs chips at the SLHC.

### The HiLum experiment

In order to establish the operating limits of the LAr endcap and forward calorimeters in conditions as close as possible to those that will occur at the SLHC, test modules of the EMEC, HEC, and FCal calorimeters were exposed to a proton high intensity beam at the IHEP 70 GeV synchrotron in Protvino, Russia [139, 140]. The beam intensities reached up to  $10^{13}$  protons/spill. The performance of the ATLAS liquid-argon endcap calorimeters has been studied over a wide range of ionisation rates including those corresponding to SLHC luminosities and above. The EMEC, HEC, and FCal test modules are each installed in their own cryostats to help isolate potential poisoning of the liquid argon. They were installed one behind the other in the proton beam with interspersed shielding to spread the hadronic showers and to adjust the ionisation rates to be in approximately the same proportions as in ATLAS. The beam is extracted via the bent crystal technique, offering the unique opportunity to cover intensities ranging from  $10^6$  protons per spill (pps) up to  $10^{12}$  pps. In addition, the machine has been operated with the 6 MHz RF bunch structure preserved and with 5 empty bunches between each filled bunch. This operation mode enables us to study the high flux response of the calorimeter modules unaffected by pile-up from previous bunches and thus reconstruct a clean signal of the response over the full drift time of electrons in the liquid argon gaps.

The beam intensity was not constant within a spill but varied from filled bunch to filled bunch. In order to correlate the calorimeter signal with the actual bunch intensity, a Cherenkov counter has been installed to measure the beam intensity in each single bunch, filled or not. The intensity ranges typically from 1 to  $10^6$  protons/bunch. The Cherenkov counter has been operated with air at atmospheric pressure, varying the PMT voltage to match the ADC dynamic range. The read-out was VME based and allowed to measure up to  $6 \times 10^6$  bunch intensities per second.

A low pressure ionization chamber was used to monitor the proton flux per spill up to intensities of

about  $1 \times 10^{11}$  pps. At higher intensities a secondary emission chamber with segmented electrodes monitored the flux and measured the beam profile in x and y.

Refs. [139, 140] describe the measurements on the degradation of the signal amplitude and shape as function of the beam intensity. Figure 1.71 shows the intact pulse shape at low intensities and figure 1.72 the degraded shape at high intensities. The ionisation history over several positive Ar ion drift times preceding the trigger is also recorded to determine the space charge buildup with the required accuracy. These data allow an accurate determination of the positive ion mobility and the bulk ion/electron recombination rate. Addi-

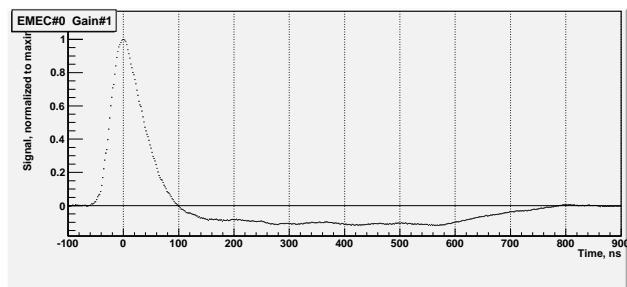


Figure 1.71: Pulse shape at an intensity of  $6 \times 10^7$  protons per spill.

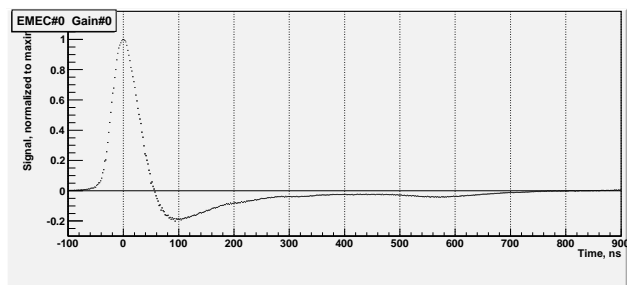


Figure 1.72: Pulse shape at an intensity of  $2 \times 10^{11}$  protons per spill.

tional tests include the measurements of the temperature rise due to beam heating, radiation damage studies, and performance studies of FCal electrodes with smaller LAr gaps.

### Hadronic endcap electronics

**Requirements of the HEC cold electronics for the SLHC upgrade.** For an upgrade, the PSB boards at the circumference of the HEC wheel would be replaced by new, pin-compatible PSB boards with more

radiation hard IC's. This operation can be done without disassembling the HEC wheels but does require that the wheels be removed from the cryostat.

The requirements for the new IC's are:

- Radiation hardness for neutrons up to a factor of 10 better, i.e. up to a fluence of  $\sim 2 \times 10^{15} \text{n/cm}^2$ .
- Low power consumption to stay safely away from the LAr boiling point at the operational pressure and temperature of the liquid argon. This means that the power consumption of the entire chip should not exceed the present level of  $< 0.2 \text{ W}$ .
- As most of the quality control (QC) tests have to be done at room temperature, the gain of the preamplifiers and summing amplifiers should not vary by more than a factor of two from room to LAr temperature.
- The noise has to stay low, i.e. it should not exceed the present level of 50 nA with 0 pF input load or 100 nA with 200 pF load at each preamplifier input; the maximum signal for one preamplifier input is 250  $\mu\text{A}$ , the dynamic range of the preamplifier has to be  $\sim 5 \times 10^3$ , that of the summing amplifier  $\sim 10^4$ .
- As only the summed signal from the full read-out channel can be electronically calibrated, the gain variation of the individual preamplifiers within the IC has to be below 1 %.
- The IC has to be safe against HV discharges in the gaps of the HEC modules.
- The input impedance has to be  $(50 \pm 2) \Omega$  to cope with the existing cabling scheme.

Table 1.1: Characteristics of the SiGe technologies (transistors) studied for radiation hardness using neutron irradiation.

Material	SiGe	SiGe	SiGe
Transistor	Bipolar HBT	Bipolar HBT	Bipolar HBT
Foundry	IHP	IBM	AMS
Process	SGB25V 250 nm	8WLBiCMOS 130 nm MB and HB	BiCMOS 350 nm
Type	npn	npn	npn

**Technologies studied.** The radiation hardness against neutron irradiation has been studied for

Table 1.2: Characteristics of the Si and GaAs technologies (transistors) studied for radiation hardness using neutron irradiation.

Material	Tran- sistor	Foundry	Process	Type
Si	CMOS FET	IHP	SGB25V 250 nm	nmos
Si	CMOS FET	IHP	SGB25V 250 nm	pmos
Si	CMOS FET	AMS	BiCMOS 350 nm	nmos
GaAs	FET	Triquint	CFH800 250 nm	pHEMT
GaAs	FET	Sirenta	250 nm	pHEMT

transistors of SiGe (Table 1.1), Si and GaAs (Table 1.2) technologies.

Typically four structures have been bonded in one ceramic package, which was mounted on a small test board. Up to 8 boards have been aligned in the neutron beam of the cyclotron at Rez/Prague. 37 MeV protons impinge on a D<sub>2</sub>O target to generate a neutron flux up to  $10^{11} \text{n/cm}^2 \text{s}^{-1}$ . The energy spectrum peaks at low energies (1 MeV) with a steep decline towards higher energies. The flux falls off steeply with the distance from the target. The typical integrated flux obtained was of the order of  $2 \times 10^{16} \text{n/cm}^2$  for the closest position relative to the D<sub>2</sub>O target. The performance of the transistors was continuously monitored with a network analyzer recording the full set of S-parameters. In addition, DC parameters (voltages and currents) were also recorded. Fig. 1.73 shows the dependence of the gain on the neutron flux for four IHP bipolar transistors. The two transistors which are in slot one (black and red lines), i.e. closest to the D<sub>2</sub>O target, were exposed to a neutron fluence of  $2.2 \times 10^{16} \text{n/cm}^2$ . They show some degradation above a fluence of  $\sim 2 \times 10^{15} \text{n/cm}^2$ . The corresponding neutron fluence for the equivalent transistors located in slot seven (green and blue lines) is  $\sim 6 \times 10^{14} \text{n/cm}^2$ . They don't show any degradation. In the region of overlap all four transistors show a similar dependence of the gain on the fluence within the systematic error. The results show that the gain is rather stable in the range required for SLHC (including the safety factor of 10), i.e. up to  $2 \times 10^{15} \text{n/cm}^2$ .

Table 1.3 shows the loss of gain for the transistors for two different frequencies, studied at a neutron fluence of  $2 \times 10^{15} \text{n/cm}^2$ . The errors are dominated by systematic effects and are at the few percent level. All technologies investigated show only a small degrada-

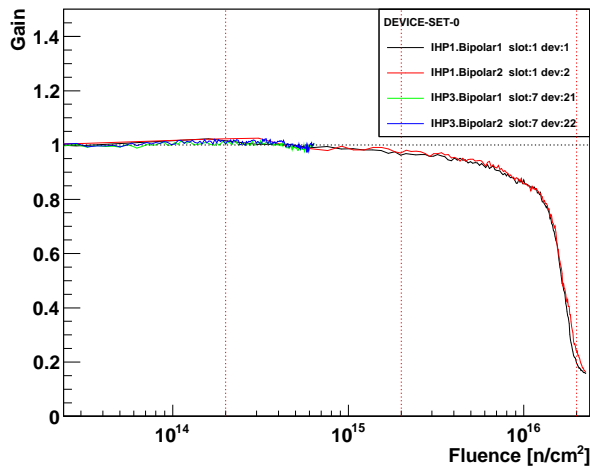


Figure 1.73: Dependence of the gain of four bipolar IHP transistors on the neutron fluence in units of  $\text{n}/\text{cm}^2$ . The vertical dotted lines indicate the expected SLHC irradiation level, the requirements for the HEC cold electronics including the safety factor of 10 and the upper limit of the fluence reached in the irradiation runs.

Table 1.3: Loss of gain of the transistors studied for a neutron fluence of  $2 \times 10^{15} \text{n}/\text{cm}^2$  at two different frequencies.

Material	Transistor	Foundry	Type	10 MHz	40 MHz
SiGe	Bipolar	IHP	npn	5%	3%
SiGe	Bipolar	IBM	npn	5%	2%
SiGe	Bipolar	AMS	npn	5%	5%
Si	CMOS FET	IHP	nmos	4%	2%
Si	CMOS FET	IHP	pmos	4%	3%
Si	CMOS FET	AMS	nmos	3%	3%
GaAs	FET	Triquint	pHEMT	0%	2%
GaAs	FET	Sirena	pHEMT	4%	2%

tion of the gain up to the irradiation level expected for SLHC.

Another important aspect is the variation of the gain with temperature. This dependence has been studied for all technologies in the required range down to liquid  $\text{N}_2$  temperatures. All bipolar technologies show a strong dependence of the operation point with temperature, therefore, to be used at the SLHC, they would require a voltage adjustment when going from room to liquid  $\text{N}_2$  temperatures. This is different for the FET's where the gain variation is rather small within the tem-

perature range studied.

Based on these studies both options, bipolar SiGe as well as CMOS FET technologies, are sufficiently stable under neutron irradiation and are being investigated further. Presently preamplifiers in both technologies are being developed. Studies of the dynamic range and noise performance are ongoing. We plan to irradiate these prototype preamplifiers in cold in the near future.

From the present studies a feasible concept for the design of the future HEC cold electronics IC is evolving, preferentially based on CMOS technology.

### 1.3.3 Upgrade of the Muon system for High Luminosities

The muon system will face two main challenges with luminosities beyond the design value:

- (a) maintenance of excellent tracking efficiency of the MDT drift tube chambers in the presence of high background hit rates, due to converted neutrons and gammas and
- (b) limitation of trigger rates for high- $p_T$  muons at a level of about 20–30% of the overall ATLAS trigger rate, which is planned to remain at the present level of 100 kHz.

In the following chapters we present (a) a R&D project for the upgrade of drift tube chambers to cope with high background rates at the SLHC and (b) a method to upgrade the muon trigger by combining the high position accuracy of the MDT chambers with the high time resolution of the existing muon trigger chambers, decisively improving the selectivity of the muon trigger for high- $p_T$  tracks.

#### Drift tube chambers for tracking in a high-background environment

The outer region of the ATLAS detector, where the muon chambers are located, receives high rates of low-energy neutrons, mainly due to shower leakage from calorimeters and shielding structures in the high- $\eta$  region. At the nominal luminosity gammas from neutron capture and related conversion electrons are expected to generate hit rates in the range 50–300 kHz in each MDT tube. A conversion electron may mask a muon hit if the signal arrives *before* the muon signal, which leads to a muon detection efficiency of  $\exp(-\tau \times f) \approx 1$

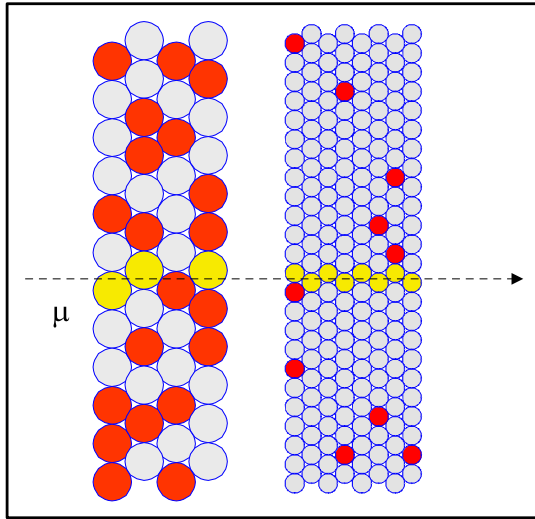


Figure 1.74: Illustration of the tracking quality in 30 mm and 15 mm drift tubes in a region of high  $n/\gamma$  background, as expected at the SLHC. The occupancies from background hits (red dots) are 50 % in the 30 mm tubes but only 7 % in the 15 mm tubes due to shorter drift time and smaller area.

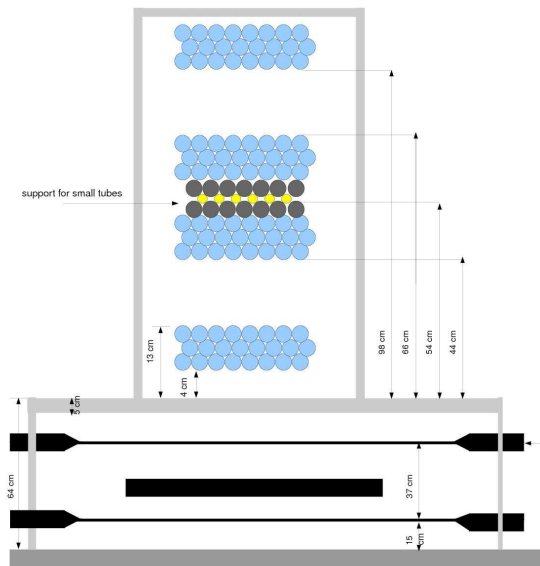


Figure 1.75: In this test setup the coordinates of a cosmic track are measured in 12 layers of 30 mm tubes (blue). The efficiency of the 15 mm tubes (yellow) is defined with respect to the fitted track, as explained in the text. Two scintillators below the setup are used for triggering.

-  $\tau \times f$ , where  $\tau$  is the average drift time in the MDT tubes and  $f$  the rate of hits due to gamma conversions.

At high rates of  $n/\gamma$  background, the efficiency may be further reduced by a decrease of the gas amplification due to space charge from slowly drifting positive ions in the tubes, while the *fluctuations* of the space charge tend to degrade the spatial resolution by up to

about 20 % at the highest rates.

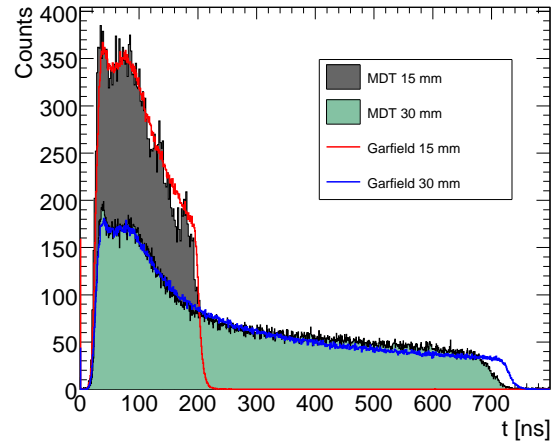


Figure 1.76: Comparison of the drift-time spectra of 30 mm and 15 mm diameter drift tubes at standard gas mixture, gas pressure and gas amplification. The maximum drift times are 700 and 200 ns, respectively, well reproduced by GARFIELD simulation.

The effects of gamma conversions in the MDT tubes have been studied in detail using a muon beam in the presence of intense  $\gamma$ -irradiation of up to  $500 \text{ Hz/cm}^2$  (i.e.  $\sim 300 \text{ kHz/tube}$ ), as delivered by the Gamma Irradiation Facility at CERN (GIF) [59]. While the  $\gamma$ -rates at the GIF correspond to only about 30% of the background levels expected for the hottest regions at the SLHC, the results of these measurements already allow to define the baseline of a chamber design with much improved tracking capability: MDT drift tube with only half the tube diameter offer a reduction of the drift time by a factor 3,5, due to the non-linear relation between track distance from the central wire and drift time ( $r$ - $t$  relation) and in addition by a factor 2 from the exposed area, thus yielding a factor of 7 in the reduction of the hit rate due to  $n/\gamma$  background. Moreover, up to two times more tube layers can be accommodated in the available space, leading to improved track finding efficiency and position resolution (see Fig. 1.74).

The reduction of the tube diameter of the MDT tubes allows to maintain the main advantages of the drift tube concept:

- independence of the position resolution from the angle of incidence onto the chamber plane (contrary to drift chambers with rectangular drift geometry)
- operational independence of each tube, where

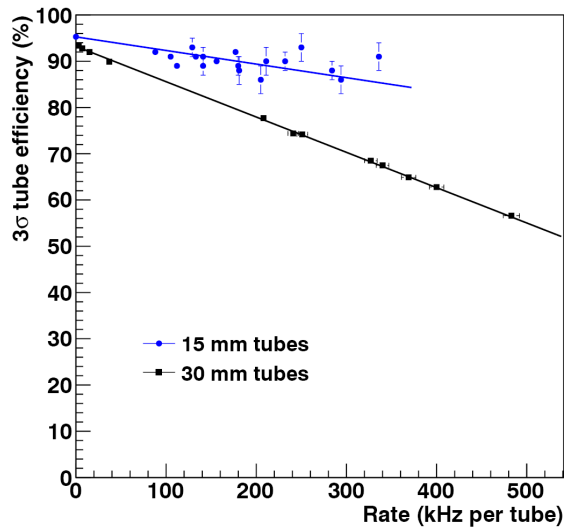


Figure 1.77: Efficiency vs. hit rate per tube for 30 mm and 15 mm drift tubes. For this measurement cosmic muon tracks were detected in the presence of gamma irradiation with adjustable intensity at the GIF facility at CERN.

any malfunction of a tube can only generate a negligible inefficiency

- modularity of chamber construction

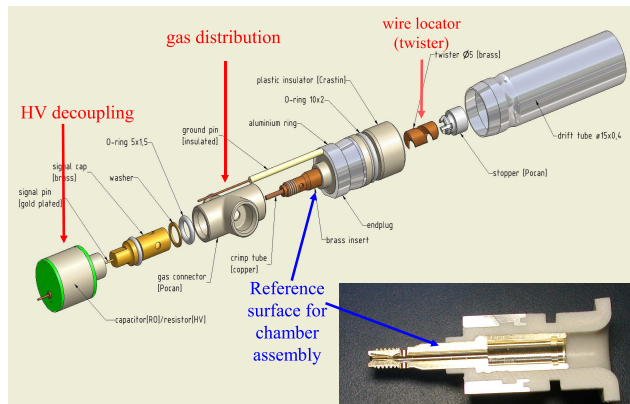


Figure 1.78: Structure of a small drift tube with gas connection and decoupling capacitor in the longitudinal direction (green cylinder). The plastic parts are injection moulded.

Another advantage of maintaining the drift tube concept is that it allows to use the extensive experience with design and operation of the present MDT chambers with 30 mm tube diameter.

To verify the performance of 15 mm ("small") tubes a number of tests was executed, using cosmic muon tracks. A pair of 30 mm ("large") drift tube chambers was used as reference, defining the position of the

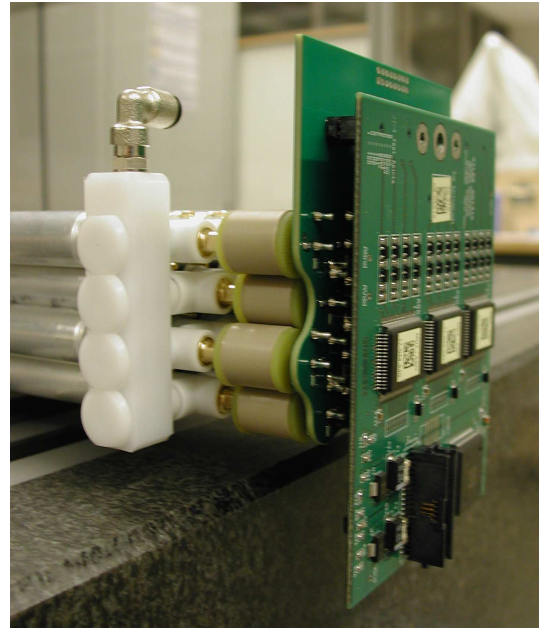


Figure 1.79: Integration of gas distribution system and readout electronics with the small tubes.

muon track, while a layer of small tubes was the device under test (see Fig. 1.75). Tubes along the track are called 'efficient' when the hit is detected inside a  $3\sigma$  road, as defined by the reference tubes.

This measurement was done in the presence of various levels of gamma background due to a close-by, adjustable source (GIF test area at CERN). First tests [145] confirmed the expectation that by reducing the drift tube diameter by a factor of two whilst leaving all operational parameters unchanged, the maximum drift time is reduced by a factor of 3.5 (Fig. 1.76). Fig. 1.77 shows the efficiency of small and large tubes vs. hit rate from conversions, small tubes providing a much better performance, as expected. The efficiency at rate zero deviates from 100 % due to tracks passing across or close to the tube walls and due to  $\delta$ -electrons shifting the position of the hit outside the  $3\sigma$  acceptance road.

Going from large to small tubes as construction elements for MDT chambers poses a number of technical challenges, as the higher tube density requires more refined electrical and gas connections on the same available service area. This is a particular problem for the supply of the tubes with the operating voltage of 2750 V, requiring isolation distances which cannot be realised on the area available for the readout boards. The integration of the HV decoupling condensers into the end-plugs of the tubes was therefore a central requirement for the tube design. In a similar way, gas sup-

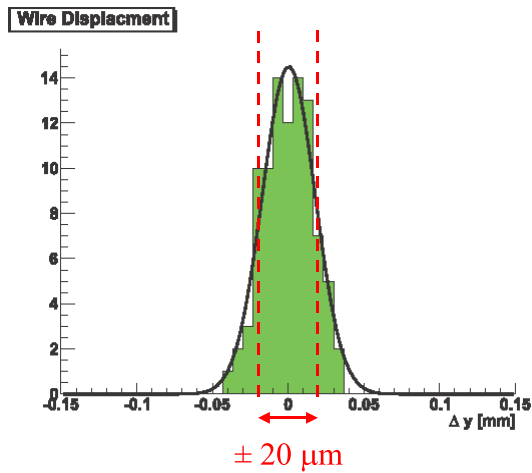


Figure 1.80: Distribution of the wire displacement from the nominal position, the decisive parameter for the measuring accuracy of the MDT chambers.

ply of each MDT tube by individual tubules, as implemented for the 30 mm tube MDTs, did not seem feasible for the production of chambers with four times higher tube density.

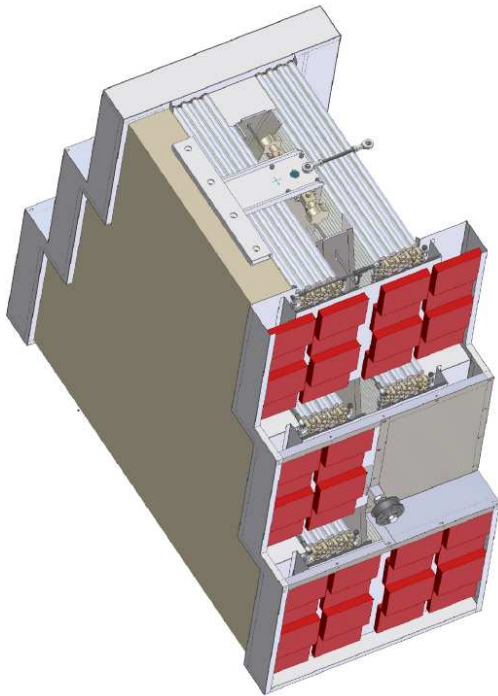


Figure 1.81: Design of a full prototype for a chamber to be implemented into the forward region of the ATLAS detector ("Small wheel").

Development work for small tube chambers started early in 2008 with an innovative tube design, where

HV decoupling and gas distribution are integrated into the design of the end-plug (Fig. 1.78). Fig. 1.79 shows the integrated gas distribution scheme plus readout electronics for a 4-layer module of small tubes.



Figure 1.82: Precision placement of the small MDT tubes in high accuracy 'combs' before gluing with epoxy.

The integration of tubes into chambers is achieved by bonding tubes layer by layer with epoxy glue. This requires a high level of positioning accuracy and fixation during the curing. In production tests the target accuracy of  $20\ \mu\text{m}$  (Fig. 1.80) was obtained by placing the tubes into special supports ("combs"), see Fig. 1.82. All 8 tube layers were glued in a time span of a few hours, curing was overnight, such that the assembly of a tube package took only one day.

Presently, a full prototype of a MDT chamber in small tube technology is under construction (Fig. 1.81). It consists of  $2 \times 8$  tube layers and is designed to fit into the inner part of the muon detector in the very forward direction, where rates are highest. This prototype will be available for tests at the GIF facility by fall 2010. The readout will be achieved with available electronics for the large tube chambers, specially adapted for use with the new chamber geometry.

#### Development of new electronics for small drift tube readout

The readout architecture of the present MDT system is described in [141]. While this proven concept is also applicable to the small tube system, the four times higher channel density is dictating a higher level of integration, more on-board data storage capacity and higher band width for data transfer to the counting room.

In addition, due to the ten times higher target for the integrated luminosity of the SLHC, electronics components have to survive correspondingly higher irradiation doses. Together with the Electronics Division



Figure 1.83: The small tube prototype chamber after assembly, consisting of two packages of 8 tube layers, with 72 tubes per layer and 1152 tubes in total.

of the MPP we are currently developing a new 16-channel Amplifier-Shaper-Discriminator (ASD) chip in IBM 130 nm technology, known to be radiation hard beyond what is expected for the Muon detector at SLHC.

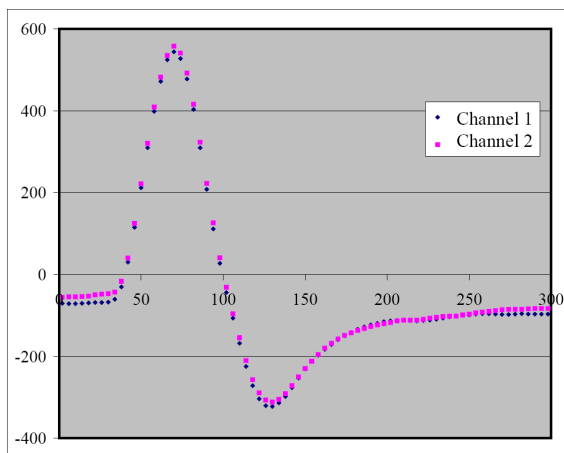


Figure 1.84: Performance of two channels in an ASD chip to be used in the frontend electronics of the MDT drift tubes. Gain and pulse shape of both channels correspond closely to the design parameters and to predictions from simulation.

To study the analog performance of the 130 nm

technology in our application a prototype chip for the ASD with four channels was produced in 2009, showing excellent matching with the design parameters as well as of the gains among the four channels. Fig. 1.84 shows the response of two channels to the injection of a delta-charge.

For the TDC, measuring the drift times in the MDT tubes, a faster, radiation hard technology is introduced, based on developments of the CERN Micro Electronics Group.

For the on-chamber FPGAs, responsible for data formatting and transmission to the counting room, a new firmware is developed by MPP's Electronics Division. The aim is to reduce the sensitivity of the configuration code to single event upsets from ionising particles by the implementation of a high level of code redundancy (Triple Modular Redundancy). Finally, optical data transmission to the counting room will be based on the Gigabit Optical Link (GOL) chipset, developed by CERN. In this transmission scheme 5 Gbit/s will be available, about three times more than in the present SLINK scheme. A schematic diagram of the readout architecture of large and small tube chambers is given in Fig. 1.85.

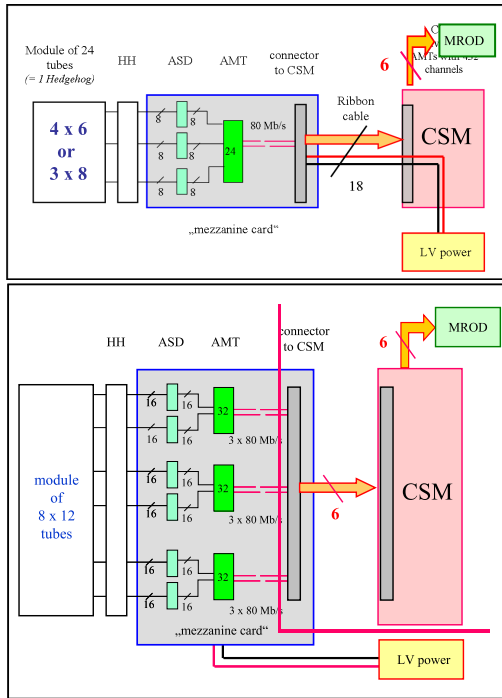


Figure 1.85: Present readout scheme for large MDT tubes, 24 tubes being served by one TDC ('AMT') on a readout card (top). In the future architecture 96 small tubes will be served by a card of comparable size, requiring a higher level of integration (bottom).

### Sharpening of the trigger threshold for high- $p_T$ tracks

The capability to trigger on muon tracks with a transverse momentum ( $p_T$ ) above a certain threshold was one of the principal requirements for the design of the muon spectrometer. MDT chambers with their long drift time of up to 750 ns, spanning 30 beam crossings, are not suited for this task and had to be complemented by specialised trigger chambers, capable of identifying tracks belonging to a given beam crossing.

In the barrel region of the muon detector, the Resistive Plate Chamber (RPC) technology was selected for this purpose. This detector type uses pick-up strips perpendicular to the  $z$ -direction to sense the avalanches generated by traversing particles in the chamber gas, delivering the coordinates of the tracks along the bending direction of the magnetic field [45]. The time resolution of about 20 ns of the RPC chambers is sufficient to tag the beam crossing with about 95% confidence. Fig. 1.86 shows the schematics of the muon Level-1 triggering system in the barrel region. RPC trigger chambers (marked in green) are positioned at three radial positions of the barrel, one in the outer detector layer (BO) and two in the mid-

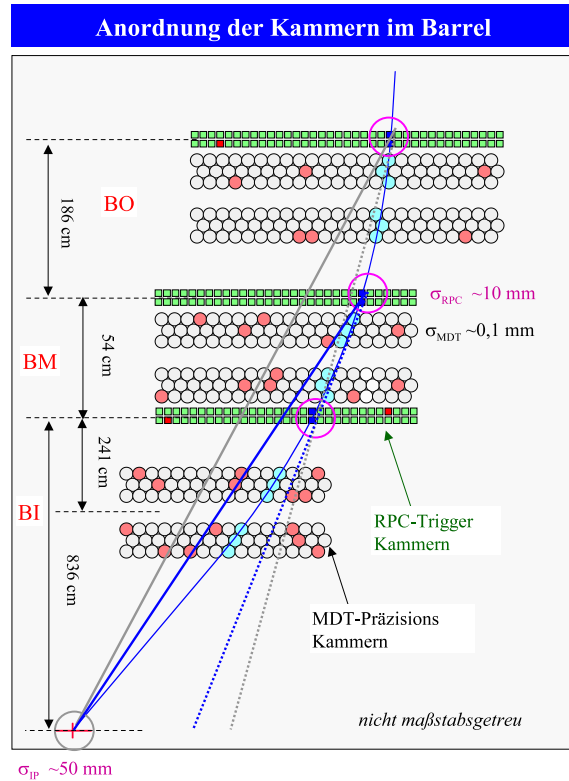


Figure 1.86: Implementation of the Level-1 trigger in the muon barrel region.

dle layer (BM), below and above the middle MDT. This way, three coordinate measurements are obtained along the track, defining the sagitta and thus  $p_T$ .

The implementation of the Level-1 trigger in the muon barrel uses a system of fast coincidences between the pick-up strips of the three RPC layers, estimating  $p_T$  from the bending of the track in the toroidal magnetic field. Due to the width of the RPC strips of 30 mm the  $p_T$  resolution for tracks above 15–20 GeV is not very sharp, the sagitta of a 20 GeV track being only 24 mm. Fig. 1.87 depicts the situation in a quantitative way. With a threshold setting of 20 GeV (red curve) the trigger is still accepting about 60% of the 15 GeV and 15% of the 10 GeV tracks. The corresponding, unwanted extra trigger rates from muons below threshold are by far not negligible, as the cross sections for most muon channels are strongly decreasing with  $p_T$ , while those of the more interesting physics channels (e.g. from W/Z decays) are roughly constant or even increasing, see Fig. 1.88.

For practical and cost reasons the maximum Level-1 trigger rate for ATLAS at the SLHC is planned to remain at the present value of 100 kHz, and therefore the efficient rejection of triggers from low- $p_T$  muon tracks is a prime requirement for the upgrade towards

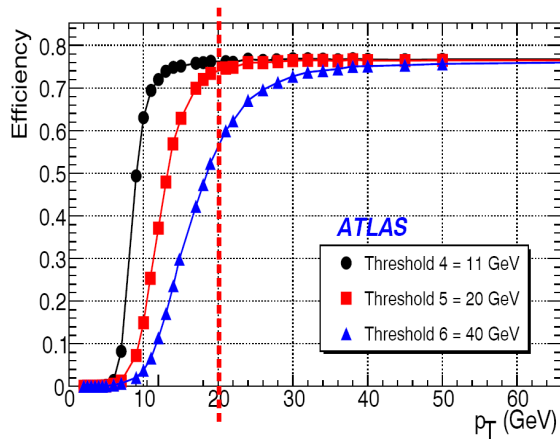


Figure 1.87: Acceptance of the Level-1 trigger vs.  $p_T$  for three typical trigger thresholds. For the 20 and 40 GeV thresholds the transitions from 90–10% efficiency cover a wide  $p_T$ -range, leading to high rates of unwanted triggers.

### SLHC.

Improving the  $p_T$ -selectivity of the muon trigger means improving the precision of the track coordinates available for the Level-1 trigger decision. In the present ATLAS trigger hierarchy tracking information of the MDT is only used at the Level-2 trigger stage, where muon tracks are reconstructed using the precise MDT coordinates, leading to the rejection of more than 90% of the Level-1 muon triggers. Due to considerable computing and data transfer overheads, however, this result is only available after a latency of about 10 ms, three orders of magnitude beyond what is acceptable for the latency of the Level-1 trigger. If a Level-1 trigger arrives later than the maximum allowed latency, information in the front-end buffers of the ATLAS subdetectors may be lost.

The challenge for an improvement of the Level-1 trigger is to design a MDT readout scheme, able to deliver a refined  $p_T$ -value inside a latency of a few microseconds. The present latency budget of  $2,5 \mu\text{s}$  was adapted to the situation at the original LHC and is insufficient for any refinement of the trigger decision.

For SLHC, however, an increase of the latency to  $6,4 \mu\text{s}$  or even  $10 \mu\text{s}$  will be implemented for the front-end data storage of all subdetectors, providing considerable design freedom for Level-1 trigger improvements.

The implementation of an improved muon barrel trigger requires an additional readout path of the MDT, in parallel and independent of the existing non-synchronous, 'standard' readout path (Fig. 1.89).

For this fast MDT readout path the following design

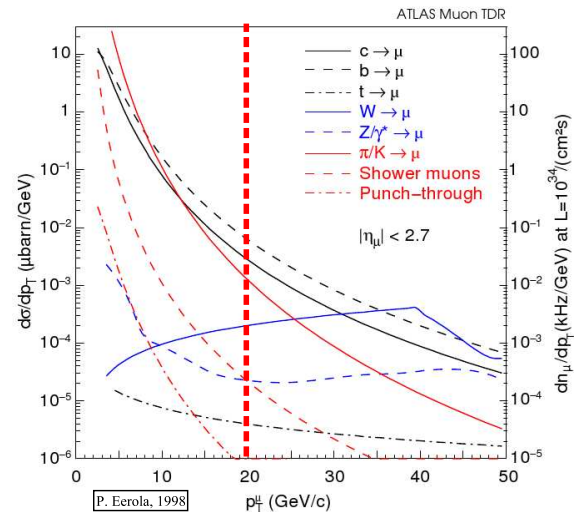


Figure 1.88: Transverse momentum distribution of muons in the ATLAS muon spectrometer for various production channels.

concept is pursued:

- Readout is only activated when a high- $p_T$  candidate is flagged by the RPC trigger logic, saving occupancy and readout bandwidth.
- All MDT tubes but those close to the trajectory of the high- $p_T$  muon candidate, as supplied by the RPC, will be ignored in the fast readout, saving data transfer and processing time.
- The resolution of the MDT drift time will be reduced from 12 to 7 bit. The corresponding position resolution of the MDT of about 1 mm (RMS) being still about a factor 10 better than the one of the RPC, sufficient for a decisive sharpening of the Level-1 trigger threshold. This way data volumes and transmission delays are reduced. For the same reason, data redundancy and format overheads will be reduced to the strict minimum.
- Separate fast communication lines will be installed to reduce transmission delays, while fast local processors will be used for the sagitta and  $p_T$  estimates.

An analysis of the time behaviour of such a readout model shows that a latency of  $4,5\text{--}5,5 \mu\text{s}$  could be achieved and thus would be a realistic option for the upgrade of the muon Level-1 trigger at the LHC. A significant advantage of this scheme would be that the existing RPC trigger chambers would not need any modifications (except electronics).

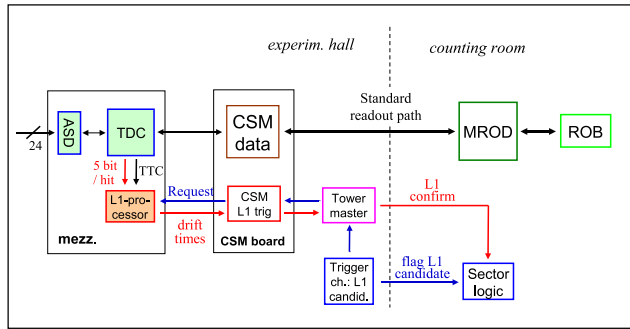


Figure 1.89: Readout architecture to combine the precision track coordinates determined in the MDT chambers with the 'fast' trigger flag supplied by the RPC's.

A similar upgrade scheme could also be applied to the Level-1 trigger in the end-cap region where trigger chambers of the TGC type are used [45]. Because of the different geometry of the toroidal magnetic field and the different location of trigger and MDT chambers, however, a modified architecture and specialised algorithms will have to be used.

In the context of this research program we have submitted four proposals to the ATLAS upgrade coordinator: (a) development of improved muon drift tube detectors [142] (b) development of radiation tolerant readout electronics [143] and (c) development of methods to reduce the data volume [144] or, alternatively, increase the bandwidth of the data acquisition system of the MDT chambers [143] for operation at very high luminosities.

## References

- [1] The MPP ATLAS group, *The ATLAS Experiment at the Large Hadron Collider LHC*, in Report to the Fachbeirat 2004–2006 Part II (2007).
- [2] ATLAS Collaboration, *The ATLAS Experiment at the CERN Large Hadron Collider*, JINST **3** S08003 (2008).
- [3] The ATLAS Collaboration, *Inner Detector Technical Design Report*, CERN/LHCC/97-16 and 97-17 (1997).
- [4] G. Aad *et al.*, The ATLAS Collaboration, *Expected Performance of the ATLAS Experiment - Detector, Trigger and Physics*, CERN-OPEN-2008-020 (2008) arxiv:0901.0512.
- [5] G. Aad *et al.*, The ATLAS Collaboration, *The ATLAS Inner Detector commissioning and calibration*, accepted by Eur. Phys. J. C (2010), arxiv:1004.5293.
- [6] G. Aad *et al.*, The ATLAS Collaboration, *Charged-particle multiplicities in pp interactions at  $\sqrt{s} = 900$  GeV measured with the ATLAS detector at the LHC*, Phys. Lett. B688 (2010) 21–42.
- [7] The MPP SCT group, *The ATLAS Semiconductor Tracker*, in Report to the Fachbeirat 1997–2003 Part II (2004).
- [8] A. Ahmad *et al.*, The ATLAS SCT Collaboration, *The Silicon microstrip sensors of the ATLAS semiconductor tracker*, Nucl. Instr. and Meth. A578 (2007) 98–118.
- [9] A. Abdesselam *et al.*, The ATLAS SCT Collaboration, *The ATLAS semiconductor tracker end-cap module*, Nucl. Instr. and Meth. A575 (2007) 353–389.
- [10] S. Haywood *et al.*, *Offline alignment & calibration of the Inner Detector*, ATLAS-INDET-2000-005, (2000).
- [11] R. Härtel, *Iterative local  $\chi^2$  alignment approach for the ATLAS SCT detector*, diploma thesis, MPP and Technical University München (2005) MPP-2005-174.
- [12] T. Göttfert, *Iterative local  $\chi^2$  alignment algorithm for the ATLAS pixel detector*, diploma thesis, MPP and Würzburg University (2006) MPP-2006-118.
- [13] M. Kayl, *Kalman style alignment approach for the ATLAS SCT and pixel detectors*, diploma thesis, MPP and Technical University München (2007) MPP-2007-18.
- [14] S. Pataraiia, *Studies on top quark-pair production in pp collisions at the Large Hadron Collider with the ATLAS experiment*, PhD thesis, MPP and Technical University München (2009) MPP-2009-181.
- [15] R. Härtel, *Studies on an initial top quark mass measurement at ATLAS in the lepton+jets  $t\bar{t}$  channel and alignment of the Pixel and SCT subdetectors*, Ph.D. thesis, Technische Universität München, MPP-2009-134, Mar 2009.
- [16] A. Ahmad *et al.*, *Alignment of the Pixel and SCT Modules for the 2004 ATLAS Combined Test Beam JINST 3* (2008) P09004.
- [17] E. Abat *et al.*, The ATLAS Collaboration, *Combined performance tests before installation of the ATLAS Semiconductor and Transition Radiation Tracking Detectors*, JINST **3** (2008) P08003.
- [18] T. Göttfert, *Background suppression for a top quark mass measurement in the lepton+jets  $t\bar{t}$  decay channel and Alignment of the ATLAS silicon detectors with cosmic rays*, Ph.D. thesis, Technische Universität München, MPP-2010-4, Dec 2009.
- [19] J. Alison, B. Cooper and T. Göttfert, *Production of Systematically Misaligned Geometries for the ATLAS Inner Detector* ATL-INDET-INT-2009-003.
- [20] R. Härtel, *Alignment of the ATLAS Inner Detector*, ACAT 2007 Conference, Amsterdam April 2007, PoS (ACAT) 049 (2007) MPP-2007-255.
- [21] T. Göttfert, *ATLAS Inner Detector alignment*, HEP 2007 Conference, Manchester July 2007, J. of Physics: Conf. Series 110 (2008) 092012, MPP-2008-216.
- [22] G. Cortiana, *Alignment of the ATLAS Inner Detector Tracking System*, IEEE 2009, Nuclear Science Symposium, Orlando Florida USA 2009, ATL-INDET-PROC-2009-020, MPP-2009-292.

- [23] The ATLAS Collaboration, ATLAS Calorimeter Performance, CERN/LHCC/96-40, ATLAS TDR 1 (1996).
- [24] The ATLAS Collaboration, ATLAS Liquid Argon Calorimeter Technical Design Report, CERN/LHCC/96-41, ATLAS TDR 2 (1996).
- [25] D. M. Gingrich *et al.*, Construction, assembly and testing of the ATLAS hadronic end-cap calorimeter, JINST **2** P05005 (2007).
- [26] The ATLAS Liquid Argon HEC Collaboration, Performance of the ATLAS Hadronic End-Cap Calorimeter in Beam Tests, Nucl.Instr.& Meth. **A482**,94-124 (2002).
- [27] A.E. Kiryunin *et al.*, GEANT 4 Physics Evaluation with Testbeam Data of the ATLAS Hadronic End-cap Calorimeter, Nucl. Instr.& Meth. **A560**,278-290 (2006).
- [28] H. Bartko, Performance of the Combined ATLAS Liquid Argon End-Cap Calorimeter in Beam Tests at the CERN SPS, MPP-2003-186, Diploma Thesis, Technical University Munich (2003).
- [29] The ATLAS Liquid Argon EMEC/HEC Collaboration, Hadronic Calibration of the ATLAS Liquid Argon End-Cap Calorimeter in the Region  $1.6 < |\eta| < 1.8$  in Beamtests, Nucl.Instr.& Meth. **A531**,481-514 (2004).
- [30] The ATLAS Liquid Argon EMEC/HEC Collaboration, Muon Results from the EMEC/HEC Combined Run corresponding to the ATLAS Pseudorapidity Region  $1.6 < |\eta| < 1.8$ , ATL-LARG-2004-006 (2004).
- [31] J. Pinfold *et al.*, Performance of the ATLAS Liquid Argon End-Cap Calorimeter in the Pseudorapidity region  $2.5 < |\eta| < 4.0$  in Beam Tests, Nucl.Instr.& Meth. **A593**,324-342 (2008).
- [32] B. Andrieu *et al.*, Results for pion calibration runs for the H1 liquid argon calorimeter and comparisons with simulations, Nucl. Instrum. Meth. **A336**,499 (1993).
- [33] I. Abt *et al.*, The tracking, calorimeter and muon detectors of the H1 experiment at HERA, Nucl. Instr.& Meth. **A386**,348 (1997).
- [34] W. Lampl, S. Laplace, D. Lelas, P. Loch, H. Ma, S. Menke, S. Rajagopalan, D. Rousseau, S. Snyder, G. Unal, Calorimeter Clustering Algorithms: Description and Performance, ATL-LARG-PUB-2008-002 (2008).
- [35] The ATLAS Collaboration, Local hadronic calibration, ATL-LARG-PUB-2009-001 (2009).
- [36] The ATLAS Collaboration, Jet Reconstruction Performance, ATL-PHYS-PUB-2009-012 (2009).
- [37] The ATLAS Collaboration, Detector Level Jet Corrections, ATL-PHYS-PUB-2009-013 (2009).
- [38] The ATLAS Collaboration, Measurement of missing transverse energy, ATL-PHYS-PUB-2009-016 (2009).
- [39] The ATLAS Collaboration, Light jets in  $t\bar{t}$  events, ATL-PHYS-PUB-2008-CSC-T2 (2008).
- [40] G. Aad *et al.* [The ATLAS Collaboration], Expected Performance of the ATLAS Experiment - Detector, Trigger and Physics, arXiv:0901.0512 [hep-ex] (2009).
- [41] John Paul Archambault *et al.*, The simulation of the ATLAS liquid argon calorimetry, ATL-LARG-PUB-2009-001 (2009).
- [42] The ATLAS Collaboration, G. Aad *et al.*, Readiness of the ATLAS Liquid Argon Calorimeter for LHC Collisions, arXiv:0912.2642 [physics.ins-det] (2009).
- [43] J. Erdmann, Analysis of the Hadronic Calibration of the ATLAS End-Cap Calorimeters using Test Beam Data, MPP-2008-162, Diploma Thesis, LMU Munich (2008).
- [44] E. Rauter, Top Quark Mass Measurement: Prospects of Commissioning Studies for Early LHC Data in the ATLAS Detector, MPP-2009-132, PhD Thesis, TU Munich (2009).
- [45] The ATLAS Collaboration. Technical Design Report for the ATLAS Muon Spectrometer. Cern/lhcc/97-22, CERN, 1997.
- [46] J. Dubbert, S. Horvat, O. Kortner, H. Kroha S. Kotov, S. Mohr dieck-Möck, and R.Richter. Final Evaluation of the Mechanical Precision of the ATLAS Muon Drift Tube Chambers. In *Proceedings of the 2006 IEEE Nuclear Science Symposium, San Diego, USA, 29 October–4 November 2006*. MPP report MPP-2006-167, November 2006.
- [47] F. Bauer et al. Construction and Test of MDT Chambers for the ATLAS Muon Spectrometer. *Nucl. Instr. and Methods*, A(461), 2001.  
F. Bauer et al. Construction and Test of the Precision Drift Chambers for the ATLAS Muon Spectrometer. *IEEE Trans. Nucl. Sci.*, 48:302, 2001.  
F. Bauer et al. The First Precision Drift Tube Chambers for the ATLAS Muon Spectrometer. *Nucl. Instr. and Methods*, A(478):153, 2002.  
F. Bauer et al. The First Precision Drift Tube Chambers for the ATLAS Muon Spectrometer. *Nucl. Instr. and Methods*, A(518):69, 2004.
- [48] J. Dubbert et al. Integration, Commissioning, and Installation of Monitored Drift Tube Chambers for the ATLAS Barrel Muon Spectrometer. A(572):53, 2007. Proceedings of the 10<sup>th</sup> Pisa Meeting on Advanced Detectors, Isola d'Elba, Italy, 21.–27.5.2006, MPP report MPP-2006-164.  
J. Dubbert et al. Integration, Commissioning and Installation of Large Drift-Tube Chambers for the ATLAS Barrel Muon Spectrometer. In *Proceedings of the 2006 IEEE Nuclear Science Symposium, San Diego, USA, 29 October–4 November 2006*, volume 3, pages 1368–1372. MPP report MPP-2006-163.
- [49] J. v.Loeben. Test und Kalibrierung der Präzisionsdriftrohrkammern des ATLAS-Myonspektrometers. Technical report, Technische Universität München, December 2006. Diploma thesis, MPP Report MPP-2006-241.
- [50] J. Schmalzer. Test and Alignment of the ATLAS Precision Muon Chambers. Technical report, Technische Universität München, March 2007. Diploma thesis, MPP Report MPP-2007-30.

- [51] M. Groh. *Study of the Higgs Boson Discovery Potential in the Process  $pp \rightarrow Hq\bar{q}$ ,  $H \rightarrow \tau\tau$  with the ATLAS Detector*. PhD thesis, Technische Universität München, May 2009. MPP Report MPP-2009-56, CERN-THESIS-2009-039.
- [52] B. Bittner. Alignment of the ATLAS Muon Spectrometer Using Muon Tracks. Technical report, Technische Universität München, November 2008. Diploma thesis, MPP Report, MPP-2008-270.
- [53] J. Dubbert (on behalf of the ATLAS collaboration). First Experience with the ATLAS Muon Spectrometer. *Nucl. Instr. and Methods*, A(581):507, 2007. Proceedings of the 11<sup>th</sup> Vienna Conference on Instrumentation, Vienna, Austria, 19.–24.2.2007.
- [54] J. von Loeben (on behalf of the ATLAS collaboration). First Cosmic Ray Results of the ATLAS Muon Spectrometer with Magnetic Field. In *Proceedings of the 2007 IEEE Nuclear Science Symposium, Honolulu, Hawaii, USA, 28 October–2 November 2007*. MPP report MPP-2007-175.
- [55] J. von Loeben, M. Deile, N. Hessey, H. Kroha O. Kortner, and A. Staude. An Efficient Method to Determine the Space-to-Drift Time Relationship of the ATLAS Monitored Drift Tube Chambers. In *Proceedings of the 2007 IEEE Nuclear Science Symposium, Honolulu, Hawaii, USA, 28 October–2 November 2007*. MPP report MPP-2007-176.
- [56] S. Horvat, O. Kortner, and H. Kroha. Determination of the Spatial Drift-Tube Resolution Using Muon Tracks. ATLAS Note ATL-MUON-PUB-2006-008, CERN, 2006.
- [57] C. Adorisio et al. System Test of the ATLAS Muon Spectrometer at the H8 Beam at the CERN SPS. *Nucl. Instr. and Meth.*, A(593):232, 2008.
- [58] C. Adorisio et al. Study of the ATLAS MDT Spectrometer Using High Energy CERN Combined Test Beam Data. *Nucl. Instr. and Meth.*, A(598):400, 2009.
- [59] M. Deile et al. Performance of the ATLAS Precision Muon Chambers under LHC Operating Conditions. *Nucl. Instr. and Methods*, A(5518):65, 2004. Proceedings of the 10<sup>th</sup> Pisa Meeting on Advanced Detectors, Isola d’Elba, Italy, 21.–27.5.2006.
- M. Deile et al. Resolution and Efficiency of the ATLAS Muon Drift-Tube Chambers at High Background Rates. *Nucl. Instr. and Methods*, A(535):212, 2004. Proceedings of the 10<sup>th</sup> Vienna Conference on Instrumentation, Vienna, Austria, 19.–24.2.2007.
- S. Horvat et al. Operation of the ATLAS Muon Drift-Tube Chambers at High Background Rates and in Magnetic Fields. *IEEE Trans. Nucl. Sci.*, 53(2):562, 2006. MPP report MPP-2006-131.
- [60] J. Dubbert et al. Modelling of the Space-to-Drift-Time Relationship of the ATLAS Monitored Drift-Tube Chambers in the Presence of Magnetic Fields. *Nucl. Instr. and Methods*, A(572):50, 2007. MPP report MPP-2006-166.
- [61] P. Bagnaia, O. Biebel, C. Guyot, D. Orestano H. Kroha, and B. Zhou. A Proposal for the Calibration and Alignment of the ATLAS Muon Spectrometer. ATLAS Note ATL-MUON-INT-2006-006, CERN, 2008.
- P. Bagnaia et al. Calibration model for the MDT chambers of the ATLAS Muon Spectrometer. ATLAS Note ATL-MUON-PUB-2008-004, CERN, 2008.
- [62] Ch. Amelung et al. The ATLAS Muon Alignment System. In *Proceedings of the First LHC Alignment Workshop, CERN, Geneva, Switzerland, 4–6 September 2006*. CERN report CERN-2007-004.
- J.C. Barriere et al. The Alignment System of the Barrel Part of the ATLAS Muon Spectrometer. ATLAS Note ATL-MUON-PUB-2008-007, CERN, 2008.
- [63] O. Kortner, S. Kotov, H. Kroha, and I. Potrap. Alignment of the ATLAS Muon Spectrometer with Straight Tracks Using MILLEPEDE Method. ATLAS Note ATL-COM-MUON-2007-017, CERN, 2007.
- [64] O. Kortner, S. Kotov, H. Kroha, J. Schmalder, and Ch. Valderanis. Alignment of the ATLAS Muon Spectrometer with Tracks and Muon Identification at High Background Rates, journal = *Nucl. Instr. and Methods*. A(581):545, 2007.
- [65] O. Kortner, S. Kotov, H. Kroha, I. Potrap, and J. Schmalder. New Methods for the Alignment of the ATLAS Muon Spectrometer with Tracks. In *Proceedings of the 2007 IEEE Nuclear Science Symposium, Honolulu, Hawaii, USA, 28 October–2 November 2007*. MPP report MPP-2007-177.
- [66] St. Kaiser. *Search for the Higgs Boson in the Process  $pp \rightarrow Hq\bar{q}$ ,  $H \rightarrow WW$  with the ATLAS Detector*. PhD thesis, Technische Universität München, January 2010. MPP report MPP-2010-38, CERN-THESIS-2010-043.
- [67] N. Benekos, L. Chevalier, J.-F. Laporte, and M. Schott. Impacts of Misalignment on the Reconstructed Z-Boson Resonance at the ATLAS Muon Spectrometer. A(572):16, 2007. Proceedings of the 10<sup>th</sup> Pisa Meeting on Advanced Detectors, Isola d’Elba, Italy, 21.–27.5.2006.
- N. Benekos, L. Chevalier, J.-F. Laporte, and M. Schott. Final Evaluation of the Mechanical Precision of the ATLAS Muon Drift Tube Chambers. In *Proceedings of the 2006 IEEE Nuclear Science Symposium, San Diego, USA, 29 October–4 November 2006*. MPP report MPP-2006-173, November 2006.
- [68] N. Benekos and M. Schott. Study of Z-Boson Measurements at the ATLAS Experiment. In *Proceedings of the Physics at LHC conference, Cracow, Poland, 3–8 July 2006*. MPP report MPP-2006-174, July 2006.
- [69] O. Kortner, G. Mikenberg, H. Messer, and O. Primor. A Novel Approach to Track Finding in a Drift Tube Detector. *JINST* 2 P01009 (2007).
- [70] S. Baranov et al. Muon Detector Description as built and its Simulation for the ATLAS Experiment. A(572):14, 2007. Proceedings of the 10<sup>th</sup> Pisa Meeting on Advanced Detectors, Isola d’Elba, Italy, 21.–27.5.2006.
- D. Rebutti et al. Muon Detector Description as built and its Simulation for the ATLAS Experiment. In *Proceedings of the 2006 IEEE Nuclear Science Symposium, San Diego, USA, 29 October–4 November 2006*, volume 3. MPP report MPP-2006-170.

- [71] D. Reuzzi et al. GEANT4 Muon Digitization in the ATHENA Framework. In *Proceedings of the 2006 Computing in High Energy Physics Conference, Mumbai, India, 13–17 February 2006*, volume 3. MPP report MPP-2006-178.
- [72] J. v.Loeben. *Calibration of the ATLAS Muon Precision Chambers and Study of the Decay  $\tau \rightarrow \mu\mu\mu$  at the LHC*. PhD thesis, Technische Universität München, May 2010. MPP report MPP-2010-88.
- [73] M. Cirilli et al. Conditions Database and Calibration Software Framework for ATLAS Monitored Drift Tube Chambers. *Nucl. Instr. and Methods*, A(572):38, 2007.
- [74] O. Kortner (on behalf of the ATLAS collaboration). Commissioning of the Charged Lepton Identification with Cosmic Rays in ATLAS. *PoS (HCP2009) 009*, 2009.
- [75] The ATLAS collaboration. Expected Performance of the ATLAS Experiment: Detector, Trigger and Physics. *arXiv:1006.4384*. submitted to EPIC (18 June 2010).
- [76] The ATLAS collaboration. Expected Performance of the ATLAS Experiment: Detector, Trigger and Physics. *arXiv:0901.0512*, 2008. CERN-OPEN-2008-020.
- [77] M. Antonelli et al. In-situ determination of the performance of the ATLAS muon spectrometer. *Nucl. Phys. Proc. Suppl.*, (177-178):326, 2008. Proceedings of the 11<sup>th</sup> Vienna Conference on Instrumentation, Vienna, Austria, 19.–24.2.2007.
- [78] The ATLAS collaboration. Muon Performance in Minimum Bias pp Collision Data at  $\sqrt{s}=7$  TeV with ATLAS. ATLAS Conference Note ATL-CONF-2010-036, CERN, 2010.
- [79] The ATLAS collaboration. Muon Reconstruction Performance. ATLAS Note ATL-COM-PHYS-2010-430, CERN, 2010.
- [80] D. Adams et al., CERN-LHCC-2004-037 (2005).
- [81] G. Duckeck et al., CERN-LHCC-2005-022 (2005).
- [82] H. Hoffmann et al., CERN-LHCC-2001-004 (2001).
- [83] The WLCG Parties, CERN-C-RRB-2005-01 (2005).
- [84] J. Mejia, S. Kluth, S. Stojek, (2009), Poster contributed to International Conference on Computing in High Energy and Nuclear Physics (CHEP2009).
- [85] The MPP ATLAS group, *ATLAS Physics Analysis*, Annual Report 2006-2007 Part II, (2008), 107-116.
- [86] The ATLAS Collaboration,  
*Preliminary studies for the measurement of the inclusive muon spectrum in pp collisions at  $\sqrt{s} = 7$  TeV with the ATLAS detector*, ATLAS conference note, Contribution to PLHC 2010, ATL-COM-CONF-2010-035, MPP-2010-107.
- [87] The ATLAS Collaboration, *Extraction of the prompt muon component in inclusive muons produced at  $\sqrt{s} = 7$  TeV*, ATLAS conference note (under approval), Contribution to ICHEP 2010, ATL-COM-PHYS-2010-431.
- [88] The ATLAS Collaboration, *Observation of prompt inclusive electrons in the ATLAS experiment at  $\sqrt{s} = 7$  TeV*, ATLAS conference note (under approval), Contribution to ICHEP 2010, ATL-COM-PHYS-2010-422.
- [89] The ATLAS Collaboration, *Measurement of the  $W \rightarrow \ell\nu$  production cross-section and observation of  $Z \rightarrow \ell\ell$  production in proton-proton collisions at  $\sqrt{s}=7$  TeV with the ATLAS detector*, ATLAS conference note (under approval), Contribution to ICHEP 2010, ATL-COM-PHYS-2010-475.
- [90] The ATLAS Collaboration, *Measurement of the  $Z \rightarrow \ell\nu$  production cross-section in proton-proton collisions at  $\sqrt{s} = 7$  TeV with the ATLAS detector*, ATLAS conference note (under approval), Contribution to ICHEP 2010, ATL-COM-PHYS-2010-546.
- [91] G. Cortiana, T. Göttfert, P. Haefner, R. Nisius, P. Weigell, *Template Method for an early Top-Quark Mass Measurement in the  $t\bar{t} \rightarrow$  lepton+jets Channel with ATLAS Data*, ATLAS internal note, ATL-PHYS-INT-2010-007, December 2009.
- [92] G. Aad et al., The ATLAS Collaboration, *Expected Performance of the ATLAS Experiment - Detector, Trigger and Physics*, CERN-OPEN-2008-020, pp898 (2009), MPP-2009-1.
- [93] P. Weigell, *Constrained Kinematic Fitting for a Top Quark Mass Determination in the Electron + Jets Channel at ATLAS*, Diploma thesis, Technische Universität München, MPP-2009-177, Oct 2009.
- [94] The ATLAS Collaboration, *Prospects for the Measurement of the Top-Quark Mass using the Template Method with early ATLAS Data*, ATLAS public note, ATL-PHYS-PUB-2010-004, May 2010.
- [95] G. Cortiana, R. Nisius, *Measurement of the Top-Quark Mass using the stabilized Mass Variable via the Template Method in the  $t\bar{t} \rightarrow$  lepton+jets at ATLAS*, ATLAS internal note, ATL-PHYS-INT-2010-027, March 2010.
- [96] J. Schieck, *Early Top Physics with ATLAS*, ICPP Conference, Istanbul, Turkey, 27 - 31 Oct 2008, Balkan Phys. Lett. 17 (2009).
- [97] G. Cortiana, *Prospects for the measurement of the top-quark mass with early ATLAS data*, TOP 2010 Conference, Brügge, Belgium, May 31 - Jun 4 2010, to be published in Nuovo Cim. C., MPP-2010-74
- [98] G. Aad et al., The ATLAS Collaboration, *Higgs Boson in Expected performance of the ATLAS experiment - Detector, Trigger and Physics*, p. 1198-1511, CERN-OPEN-2008-020 (2009), arXiv:hep-ex/0901.0512, MPP-2009-1.
- [99] The ATLAS Collaboration, *Prospects for Higgs Boson Searches using the  $H \rightarrow WW^* \rightarrow \ell\nu\ell\nu$  decay mode with the ATLAS Detector for 10TeV*, ATLAS public note, ATL-PHYS-PUB-2010-005, CERN, Geneva, 2010.
- [100] The ATLAS Collaboration, *ATLAS Sensitivity Prospects for Higgs Boson Production at the LHC Running at 7 TeV*, ATLAS public note, ATL-PHYS-PUB-2010-009, CERN, Geneva, 2010, MPP-2010-108.

- [101] G. Aad *et al.*, The ATLAS Collaboration, *Search for the Standard Model  $H \rightarrow ZZ^{(*)} \rightarrow 4\ell$* , in *Expected performance of the ATLAS experiment - Detector, Trigger and Physics*, p. 1243-1270, CERN-OPEN-2008-020 (2009), arXiv:hep-ex/0901.0512, MPP-2009-1; ATL-PHYS-PUB-2009-054, MPP-2009-309.
- [102] Ch. Anastopoulos *et al.*, *ATLAS sensitivity prospects for the Standard Model Higgs boson in the decay channel  $H \rightarrow ZZ^{(*)} \rightarrow 4\ell$  at  $\sqrt{s}=10$  and 7TeV*, ATLAS internal note, ATL-PHYS-INT-2010-062, CERN, Geneva, 2010.
- [103] G. Aad *et al.*, The ATLAS Collaboration, *Higgs Boson Searches in Gluon Fusion and Vector Boson Fusion using the  $H \rightarrow WW$  Decay Mode, in Expected performance of the ATLAS experiment - Detector, Trigger and Physics*, p. 1306-1332, CERN-OPEN-2008-020 (2009), arXiv:hep-ex/0901.0512, MPP-2009-1; ATL-PHYS-PUB-2009-056, MPP-2009-310.
- [104] S. Kaiser, S. Horvat, O. Kortner, H. Kroha, *Impact of Pile-up on the Search for  $H \rightarrow WW$  in VBF Production and Study of Track Jets for the Central Jet Veto*, ATLAS internal note (under approval), ATL-COM-PHYS-2010-197, CERN, Geneva, 2010.
- [105] S. Kotov, S. Horvat, O. Kortner, H. Kroha, S. Mohrdieck-Möck; J. Yuan, *Search for the SM Higgs boson in the  $H \rightarrow b\bar{b}$  decay channel in associated production with  $t\bar{t}$  using neural network techniques*, ATLAS internal note, ATL-PHYS-INT-2008-027, CERN, Geneva, 2010.
- [106] S. Horvat, O. Kortner, H. Kroha, S. Kotov, J. Yuan, *Feasibility study of the observability of the  $H \rightarrow b\bar{b}$  in Vector Boson Fusion production with the ATLAS detector*, ATLAS internal note, ATL-PHYS-INT-2008-048, CERN, Geneva, 2010.
- [107] G. Aad *et al.*, The ATLAS Collaboration, *Search for the Standard Model Higgs Boson via Vector Boson Fusion Production Process in the Di-Tau Channels, in Expected performance of the ATLAS experiment - Detector, Trigger and Physics*, p. 1271-1305, CERN-OPEN-2008-020 (2009), arXiv:hep-ex/0901.0512, MPP-2009-1; ATL-PHYS-PUB-2009-055, MPP-2009-311.
- [108] Georgios Dedes, *Study of the Higgs Boson Discovery Potential in the Process  $pp \rightarrow H/A \rightarrow \mu^+\mu^-/\tau^+\tau^-$  with the ATLAS detector*, Dissertation, Technische Universität München, 2008, MPP-2008-32.
- [109] G. Aad *et al.*, The ATLAS Collaboration, *Search for the Neutral MSSM Higgs Bosons in the Decay Channel  $A/H/h \rightarrow \mu^+\mu^-$* , in *Expected performance of the ATLAS experiment - Detector, Trigger and Physics*, p. 1391-1418, CERN-OPEN-2008-020 (2009), arXiv:hep-ex/0901.0512, MPP-2009-1; ATL-PHYS-PUB-2009-060, MPP-2009-312.
- [110] S. Stern, *Measurement of the  $\mu^+\mu^-$  Background for Neutral MSSM Higgs Searches with the ATLAS Detector*, Diplomarbeit, Technische Universität München, 2009, CERN-THESIS-2009-135, MPP-2009-211.
- [111] S. Horvat, O. Kortner, H. Kroha, S. Stern, *Prospects for data-driven estimation of the  $\mu^+\mu^-$  background for neutral MSSM Higgs searches in the decay channel  $h/H/A \rightarrow \mu^+\mu^-$* , ATLAS internal note, ATL-PHYS-INT-2010-058, CERN, Geneva, 2010.
- [112] S. Horvat, O. Kortner, H. Kroha, S. Stern, *ATLAS sensitivity prospects for the neutral MSSM Higgs bosons in the  $H/A \rightarrow \mu^+\mu^-$  decay channel at  $\sqrt{s} = 7$  TeV*, ATLAS internal note, ATL-PHYS-INT-2010-057, CERN, Geneva, 2010.
- [113] G. Aad *et al.*, The ATLAS Collaboration, *Charged Higgs Boson Searches, in Expected performance of the ATLAS experiment - Detector, Trigger and Physics*, p. 1451-1479, CERN-OPEN-2008-020 (2009), arXiv:hep-ex/0901.0512, MPP-2009-1; ATL-PHYS-PUB-2009-062, MPP-2009-313.
- [114] Thies Ehrich, *Search for Light Charged Higgs Bosons in Hadronic Final States with the ATLAS Detector*, Dissertation, Technische Universität München, 2010.
- [115] T. Ehrich, S. Mohrdieck-Moeck, S. Horvat, O. Kortner, H. Kroha, *Data-driven measurement of the fake tau contribution from light jets and application for the  $t\bar{t}$  background estimation in charged Higgs Searches*, ATLAS internal note, ATL-COM-PHYS-2009-662 (under approval), CERN, Geneva, 2010.
- [116] T. Ehrich, *Searches for light charged Higgs bosons decaying to a hadronic tau and a neutrino in the one lepton mode with ATLAS*, Prospects for Charged Higgs Discovery at Colliders, Uppsala, Sweden, Sep 16 - 19, 2008, PoS CHARGED2008:037 (2008), ATL-PHYS-PROC-2008-066.
- [117] A. D’Orazio, *SM Higgs search in the 4-lepton final state with ATLAS*, Physics at the LHC Conference, Split, Croatia, Sep 29 - Oct 4, 2008, PoS 2008LHC:107 (2008), ATL-PHYS-PROC-2009-019.
- [118] S. Horvat, *Non-SM Higgs searches at the LHC*, DIS 2009 Conference, Madrid, Spain, Apr 26-30, 2009, doi:10.3360/dis.2009.53, ATL-PHYS-PROC-2009-063, MPP-2009-284.
- [119] G. Aad *et al.*, The ATLAS collaboration, *Data-driven determinations of W, Z and top background to supersymmetry searches at the LHC, in Expected Performance of the ATLAS Experiment - Detector, Trigger and Physics*, p. 1525, CERN-OPEN-2008-020 (2009), arXiv:hep-ex/0901.0512, MPP-2009-1; ATL-PHYS-PUB-2009-064, MPP-2009-314.
- [120] The ATLAS collaboration, *Data-Driven Determination of  $t\bar{t}$  Background to Supersymmetry Searches in ATLAS*, Atlas public note, ATL-PHYS-PUB-2009-083, CERN, Geneva, 2009.
- [121] The ATLAS collaboration, *Early supersymmetry searches without leptons with the ATLAS Detector*, ATLAS internal note, ATL-COM-PHYS-2010-411 (under approval), CERN, Geneva, 2010.

- [122] F. Legger, *Data-driven estimation of Standard Model backgrounds to SUSY searches in ATLAS*, SUSY08, Seoul, Korea, Jun 16-21, 2008, ATL-PHYS-PROC-2008-008, MPP-2008-184.
- [123] F. Legger, *New Developments in Data-driven Background Determinations for SUSY Searches in ATLAS*, SUSY09, Boston, Massachusetts, Jun 5 - 10, 2009, AIP Conf.Proc.1200:297-300 (2010), ATL-PHYS-PROC-2009-080.
- [124] V. Zhuravlov, *Extracting backgrounds to SUSY searches from LHC data*, Europhysics Conference on High Energy Physics, Krakow, Poland, Jul 16 - 22 2009, ATL-PHYS-PROC-2009-082, MPP-2009-233.
- [125] V. Zhuravlov, *Estimation of Top Background to SUSY Searches from Data*, 24th International Symposium on Lepton Photon Interactions at High Energies, DESY, Hamburg, Germany, Aug 17 - 22, 2009, ATL-PHYS-PROC-2010-012.
- [126] N. Hessey *et al.*, *Layout Requirements and Options for a new Inner Tracker for the ATLAS Upgrade*, ATLAS internal document, ATL-P-EP-0001, (2007).
- [127] R. Nisius *et al.*, *R&D on a novel interconnection technology for 3D integration of sensors and electronics and on thin pixel sensors*, ATL-P-MN-0019, ATLAS internal document, (2007).
- [128] L. Andriccek *et al.*, *Processing of ultra-thin silicon sensors for future linear collider experiments*, IEEE Transactions on Nuclear Science 51 (2004) 1117-1120.
- [129] E. Fretwurst *et al.*, *High energy proton damage effects in thin high resistivity FZ silicon detectors*, Nucl. Instr. and Meth. A552 (2005) 124-130.
- [130] A. Klumpp *et al.*, *Vertical System Integration by Using Inter-Chip Vias and Solid-Liquid InterDiffusion Bonding*, Japanese Journal of Applied Physics 43, No 7A.
- [131] Fraunhofer-Institut für Zuverlässigkeit und Mikrointegration IZM, Institutsteil München, Hansastraße 27d, 80686 München, Germany.
- [132] A. Macchiolo *et al.*, *Development of thin pixel sensors and a novel interconnection technology for the SLHC*, 9th International Workshop on Radiation Imaging Detectors, Erlangen, Germany 22-26 July 2007, Nucl. Instr. and Meth. A591 (2008) 229-232.
- [133] M. Beimforde, *Investigations towards a pixel detector for the Super LHC*, PhD thesis, MPP and Technical University München (2010) MPP-2010-??.
- [134] A. Macchiolo *et al.*, *Application of a new interconnection technology for the ATLAS pixel upgrade at SLHC*, TWEPP-09, Topical Workshop on Electronics for Particle Physics, Paris, France, 21-25 Sep 2009, CERN-2009-006 (2009) 216-219.
- [135] L. Andriccek *et al.*, *Development of thin sensors and a novel interconnection technology for the upgrade of the ATLAS pixel system*, 7th International Hiroshima Symposium on Development and Applications of Semiconductor Tracking Devices, Hiroshima, Japan, Aug. 29-Sep.1, 2009, Nucl. Instr. and Meth. A (2010) to be published.
- [136] M. Beimforde, *The ATLAS Planar Pixel Sensor R&D project*, 7th International Hiroshima Symposium on Development and Applications of Semiconductor Tracking Devices, Hiroshima, Japan, Aug. 29-Sep.1, 2009, Nucl. Instr. and Meth. A (2010) to be published.
- [137] Fraunhofer-Institut für Zuverlässigkeit und Mikrointegration IZM, Institutsteil Berlin, Gustav-Meyer-Allee 25, 13355 Berlin, Germany.
- [138] J. Ban *et al.*, *Cold Electronics for the Liquid Argon Hadronic End-cap Calorimeter of ATLAS*, Nucl. Instr.& Meth. **A556**, 158-168 (2006).
- [139] P. Schacht for the Hilum and HECPAS collaboration, ATLAS Liquid Argon Endcap Calorimeter R & D for sLHC, Proceedings of the 11th ICATPP Conference on Astroparticle, Particle, Space Physics, Detectors and Medical Physics Applications, Como, 5-9 October 2009.
- [140] Hilum Collaboration, *A proposal for R & D to establish the limitations on the operation of the ATLAS end-cap calorimeters at high LHC luminosities*, INTAS Project INTAS-CERN 05-103-7555, INTAS Progress Report 2008 (2008) and INTAS Final Report (2009).
- [141] Y. Arai *et al.*, *ATLAS Muon Drift Tube Electronics*, JINST **3** P09001 (2008)
- [142] O. Biebel, J. Dubbert, S. Horvat, O. Kortner, H. Kroha, R. Richter, D. Schaile, *Expression of Interest: R&D on Precision Drift Tube Detectors for Very High Background Rates at SLHC*, ATLAS document, ATL-M-MN-0006, March 2007.
- [143] O. Biebel, J. Dubbert, S. Horvat, O. Kortner, H. Kroha, R. Richter, D. Schaile, *Upgrade of the MDT Readout Chain for the SLHC*, ATLAS document, ATL-M-MN-0003, March 2007.
- [144] O. Biebel, J. Dubbert, S. Horvat, O. Kortner, H. Kroha, R. Richter, D. Schaile, *Upgrade of the MDT Electronics for the SLHC Using Selective Readout*, ATLAS document, ATL-M-MN-0005, March 2007.
- [145] J. Dubbert, S. Horvat, O. Kortner, H. Kroha, F. Legger, R. Richter, F. Rauscher, *Development of Precision Drift Tube Detectors for the Very High Background Rates at the Super-LHC*, proceedings of the 2007 IEEE Nuclear Science Symposium, Honolulu, Hawaii, USA, 28 October-2 November 2007, MPP report, MPP-2007-172, November 2007, to be published in the IEEE Transactions on Nuclear Science.

## Chapter 2

# Publications

- I. Abt, A. Caldwell, D. Gutknecht, K. Kröniger, M. Lampert, X. Liu, B. Majorovits, D. Quirion, F. Stelzer, and P. Wendling. *Characterization of the first true coaxial 18-fold segmented n-type prototype detector for the GERDA project.* Nucl.Instrum.Meth.A **577**, (2007), 574. MPP-2007-1, nucl-ex/0701004.
- I. Abt, A. Caldwell, K. Kröniger, J. Liu, X. Liu, and B. Majorovits. *Identification of photons in double beta-decay experiments using segmented germanium detectors - studies with a GERDA Phase II prototype detector.* Nucl.Instrum.Meth.A **583**, (2007), 332–340. MPP-2007-2, nucl-ex/0701005.
- I. Abt, M. Altmann, A. Caldwell, K. Kröniger, X. Liu, B. Majorovits, L. Pandola, and C. Tomei. *Background reduction in neutrinoless double beta decay experiments using segmented detectors - a Monte Carlo study for the GERDA setup.* Nucl.Instrum.Meth.A **570**, (2007), 479–486. MPP-2007-3.
- Béla Majorovits. *The GERDA Neutrinoless-Double-Beta decay experiment* 433–438. MPP-2007-4.
- Johanna Erdmenger, Rene Meyer, and Jeong-Hyuck Park. *Spacetime Emergence in the Robertson-Walker Universe from a Matrix model.* Phys.Rev.Lett. **98**, (2007), 261301. MPP-2007-5, arxiv:0705.1586.
- G. G. Raffelt and G. Sigl. *Self-induced decoherence in dense neutrino gases.* Phys.Rev.D **75**, (2007), 083002. MPP-2007-6, hep-ph/0701182.
- Gabriel Lopes Cardoso, Johannes M. Oberreuter, and Jan Perz. *Entropy function for rotating extremal black holes in very special geometry.* JHEP **0705**, (2007), 025. LMU-ASC 01/07, MPP-2007-7, hep-th/0701176.
- Helmut Rechenberg. *Kopenhagen 1941 und die Natur des deutschen Uranprojektes* (Saechsische Akademie der Wissenschaften, Leipzig). MPP-2007-8 (2005).
- Sean Fleming, Andre H. Hoang, Sonny Mantry, and Iain W. Stewart. *Jets from Massive Unstable Particles: Top-Mass Determination.* Phys.Rev.D **77**, (2008), 074010. MIT-CTP 3791, CALT-68-2624, MPP-2007-9, hep-ph/0703207.
- Georg G. Raffelt. *Supernova neutrino observations: What can we learn?* MPP-2007-10, astro-ph/0701677.
- Daniel Mazin and Martin Raue. *New limits on the density of the extragalactic background light in the optical to the far-infrared from the spectra of all known TeV blazars.* Astron.Astrophys. **439-452**. MPP-2007-11, astro-ph/0701694.
- Dimitrios Tsimpis. *Fivebrane instantons and Calabi-Yau fourfolds with flux.* JHEP **0703**, (2007), 099. MPP-2007-12, hep-th/0701287.
- N. Otte. *Constraints on the steady and pulsed VHE gamma-ray emission from observation of PSR B1951+32 / CTB 80 with the MAGIC Telescope.* Astrophys.J. **669**, (2007), 1143–1149. MPP-2007-13, astro-ph/0702077.
- J. Albert et al. (MAGIC). *Variable VHE gamma-ray emission from Markarian 501.* Astrophys.J. **669**, (2007), 862. SLAC-PUB-12334, MPP-2007-14, astro-ph/0702008.
- J. Barranco, O. G. Miranda, and T. I. Rashba. *Low energy neutrino experiments sensitivity to physics beyond the Standard Model.* Phys.Rev.D **76**, (2007), 073008. MPP-2007-15, hep-ph/0702175.
- Riccardo Apreda, Johanna Erdmenger, Dieter Lust, and Christoph Sieg. *Adding D7-branes to the Polchinski-Strassler gravity background.* Fortschr.Phys. **55**, (2007), 639–643. IFUM 887-FT, MPP-2007-16, hep-th/0701246.
- Monika Blanke, Andrzej J. Buras, Bjoern Duling, Anton Poschenrieder, and Cecilia Tarantino. *Charged Lepton Flavour Violation and  $(g-2)_{\mu}$  in the Littlest Higgs Model with T-Parity: a clear Distinction from Supersymmetry.* JHEP **0705**, (2007), 013. TUM-HEP-657/07, MPP-2007-17, hep-ph/0702136.
- Steen Hannestad and Yvonne Y. Y. Wong. *Neutrino mass from future high redshift galaxy surveys: sensitivity and detection threshold.* JCAP **0707**, (2007), 004. MPP-2007-19, astro-ph/0703031.
- Monika Blanke and Andrzej J. Buras. *A Guide to Flavour Changing Neutral Currents in the Littlest Higgs Model with T-Parity.* Acta Phys.Polon.B **38**, (2007), 2923. TUM-HEP-664/07, MPP-2007-20, hep-ph/0703117.
- Stefan Berge, Wolfgang Hollik, Wolf M. Mosle, and Doreen Wackerroth. *SUSY QCD one-loop effects*

- in (un)polarized top-pair production at hadron colliders. *Phys.Rev.D* **76**, (2007), 034016. MPP-2007-21, hep-ph/0703016.
- Florian Gmeiner, Dieter Lust, and Maren Stein. *Statistics of intersecting D-brane models on  $T^6/Z_6$* . *JHEP* **0705**, (2007), 018. NIKHEF/2007-006, LMU-ASC 14/07, MPP-2007-22, hep-th/0703011.
- S. Dittmaier, P. Uwer, and S. Weinzierl. *NLO QCD corrections to  $t$  bar + jet production at hadron colliders*. *Phys.Rev.Lett.* **98**, (2007), 262002. MPP-2007-23, hep-ph/0703120.
- Kathrin A. Hochmuth, Manfred Lindner, and Georg G. Raffelt. *Exploiting the directional sensitivity of the Double Chooz near detector*. *Phys.Rev.D* **76**, (2007), 073001. MPP-2007-24, arxiv:0704.3000.
- R. Mirzoyan, B. Dolgoshein, P. Holl, et al. *SiPM and ADD as advanced detectors for astro-particle physics*. *Nucl.Instrum.Meth.A* **572**, (2007), 439–494. MPP-2007-25.
- I. Britovitch, E. Lorenz, et al. *Development of scintillation detectors based on avalanche microchannel photodiodes*. *Nucl.Instrum.Meth.A* **571**, (2007), 317–320. MPP-2007-26.
- K. A. Hochmuth, S. T. Petcov, and W. Rodejohann.  $U_{PMNS} = U_e I I^dagger U_{nu}$ . *Phys.Lett.B* **654**, (2007), 177–188. SISSA 44/2007/EP, MPP-2007-27, arxiv:0706.2975.
- C. Cattadori, O. Chkvorets, M. Junker, K. Kröniger, L. Pandola, A. Pullia, V. Re, C. Tomei, C. Ur, and F. Zocca. *The GERmanium Detector Array read-out: Status and developments*. *Nucl.Instrum.Meth.A* **572**, (2007), 479–480. MPP-2007-28.
- Oliver Kortner, Hubert Kroha, Jens Schmalzer, and Chrysosomos Valderanis. *Alignment of the ATLAS Muon Spectrometer with Tracks and Muon Identification at High Background Rates* MPP-2007-29.
- The collaboration (MAGIC). *Very high energy gamma-ray observations during moonlight and twilight with the MAGIC telescope* MPP-2007-31, astro-ph/0702475.
- E. Lorenz. *Gamma-ray astronomy with ground-based array detectors: status and perspectives*. *J.Phys.Conf.Ser.* **60**, (2007), 1–7. MPP-2007-32.
- Monika Blanke, Andrzej J. Buras, Stefan Recksiegel, Cecilia Tarantino, and Selma Uhlig. *Littlest Higgs Model with T-Parity Confronting the New Data on  $D^0 - \bar{D}^0$  Mixing*. *Phys.Lett.B* **657**, (2007), 81–86. TUM-HEP-666/07, MPP-2007-33, hep-ph/0703254.
- Max Niedermaier, Erhard Seiler, and Peter Weisz. *Perturbative and nonperturbative correspondences between compact and non-compact sigma-models*. *Nucl.Phys.B* **788**, (2008), 89–119. MPP-2007-34, hep-th/0703212.
- Johann H. Kuhn, A. Kulesza, S. Pozzorini, and M. Schulze. *Electroweak corrections to large transverse momentum production of W bosons at the LHC*. *Phys.Lett.B* **651**, (2007), 160–165. TTP07-07, SFB/PPP-07-12, DESY 07-041, MPP-2007-35, hep-ph/0703283.
- Ben C. Allanach, Kyle Cranmer, Christopher G. Lester, and Arne M. Weber. *Natural Priors, mSUGRA Fits and LHC Weather Forecasts*. *JHEP* **0708**, (2007), 023. DAMTP-2007-18, Cavendish-HEP-2007-03, MPP-2007-36, arxiv:0705.0487.
- M. Hayashida, J. Ninkovic, J. Hose, C. C. Hsu, R. Mirzoyan, and M. Teshima. *Development status of High-QE HPDs with 18-mm GaAsP photocathode for IACTs*. *Nucl.Instrum.Meth.A* **572**, (2007), 456–458. MPP-2007-38.
- R. Mirzoyan, M. Garczarczyk, J. Hose, and D. Paneque. *A method to measure the mirror reflectivity of a prime focus telescope*. *Astropart.Phys.* **26**, (2007), 509–511. MPP-2007-40.
- Johanna Erdmenger, Matthias Kaminski, and Felix Rust. *Isospin diffusion in thermal AdS/CFT with flavor*. *Phys.Rev.D* **76**, (2007), 046001. MPP-2007-42, arxiv:0704.1290.
- Monika Blanke, Andrzej J. Buras, Stefan Recksiegel, Cecilia Tarantino, and Selma Uhlig. *Correlations between epsilon'/epsilon and Rare K Decays in the Littlest Higgs Model with T-Parity*. *JHEP* **0706**, (2007), 082. TUM-HEP-667/07, MPP-2007-43, arxiv:0704.3329.
- Alessandro Mirizzi, Georg G. Raffelt, and Pasquale D. Serpico. *Signatures of axion-like particles in the spectra of TeV gamma-ray sources*. *Phys.Rev.D* **76**, (2007), 023001. FERMILAB-PUB-07-082-A, MPP-2007-44, arxiv:0704.3044.
- S. Andriamonje, S. Aune, D. Autiero, K. Barth, A. Belov, B. Beltran, H. Brauninger, J. M. Carmona, S. Cebrian, J. I. Collar, T. Dafni, M. Davenport, L. Di Lella, C. Eleftheriadis, J. Englhauser, G. Fanourakis, E. Ferrer Ribas, H. Fischer, J. Franz, P. Friedrich, T. Geralis, I. Giomataris, S. Gninenko, H. Gomez, M. Hasinoff, F. H. Heinsius, D. H. H. Hoffmann, I. G. Irastorza, J. Jacoby, K. Jakovcic, D. Kang, K. Konigsmann, R. Kotthaus, M. Krcmar, K. Kousouris, M. Kuster, B. Lakic, C. Lasseur, A. Liolios, A. Ljubicic, G. Lutz, G. Luzon, D. Miller, A. Morales, J. Morales, A. Ortiz, T. Papaevangelou, A. Placci, G. Raffelt, H. Riege, A. Rodriguez, J. Ruz, I. Savvidis, Y. Semertzidis, P. Serpico, L. Stewart, J. Vieira, J. Villar, J. Vogel, L. Walckiers, and K. Zioutas. *An Improved limit on the axion-photon coupling from the CAST experiment*. *JCAP* **04**, (2007), 010. MPP-2007-45, hep-ex/0702006.
- Pedro D. Ruiz-Femenia. *The soft-energy region in the radiative decay of bound states*. *Nucl.Phys.B* **788**, (2008), 21–46. MPP-2007-46, arxiv:0705.1330.
- I. Abt, A. Caldwell, K. Kröniger, J. Liu, X. Liu, and B. Majorovits. *Pulse shapes from electron and photon*

- induced events in segmented high-purity germanium detectors.* Eur.Phys.J.C **52**, (2007), 19–27. MPP-2007-47, arxiv:0704.3016.
- K. Kröniger, L. Pandola, and V. Tretyak. *Feasibility study of the observation of the neutrino accompanied double beta-decay of Ge-76 to the 0+(1) excited state of Se-76 using segmented germanium detectors.* Ukrainian Journal of Physics **52**, (2007), 1036–1044. MPP-2007-48, nucl-ex/0702030.
- Jan Hamann, Steen Hannestad, Georg G. Raffelt, and Yvonne Y. Y. Wong. *Observational bounds on the cosmic radiation density.* JCAP **0708**, (2007), 021. TUM-HEP-668/07, MPP-2007-50, arxiv:0705.0440.
- J. Aysto, A. Badertscher, L. Bezrukov, J. Bouchez, A. Bueno, J. Busto, J. E. Campagne, Ch. Cavata, A. de Bellefon, J. Dumarchez, J. Ebert, T. Enqvist, A. Ereditato, F. von Feilitzsch, P. Fileviez Perez, M. Goger-Neff, S. Gninenko, W. Gruber, C. Hagner, M. Hess, K. A. Hochmuth, J. Kisiel, L. Knecht, I. Kreslo, V. A. Kudryavtsev, P. Kuusiniemi, T. Lachenmaier, M. Laffranchi, B. Lefievre, P. K. Lightfoot, M. Lindner, J. Maalampi, M. Maltoni, A. Marchionni, T. Marrodan Undagoitia, A. Mereaglia, M. Messina, M. Mezzetto, A. Mirizzi, L. Mosca, U. Moser, A. Muller, G. Natterer, L. Oberauer, P. Otiougova, T. Patzak, J. Peltoniemi, W. Potzel, C. Pistillo, G. G. Raffelt, E. Rondio, M. Roos, B. Rossi, A. Rubbia, N. Savvinov, T. Schwetz, J. Sobczyk, N. J. C. Spooner, D. Stefan, A. Tonazzo, W. Trzaska, J. Ulbricht, C. Volpe, J. Winter, M. Wurm, A. Zalewska, and R. Zimmermann. *Large underground, liquid based detectors for astro-particle physics in Europe: scientific case and prospects.* JCAP **0711**, (2007), 011. MPP-2007-51, arxiv:0705.0116.
- S. Heinemeyer, W. Hollik, H. Rzehak, and G. Weiglein. *The Higgs sector of the complex MSSM at two-loop order: QCD contributions.* Phys.Lett.B **652**, (2007), 300–309. DCPT/07/34, IPPP/07/17, PSI-PR-07-02, MPP-2007-52, arxiv:0705.0746.
- Georg G. Raffelt and Alexei Yu. Smirnov. *Self-induced spectral splits in supernova neutrino fluxes.* Phys.Rev.D **76**, (2007), 081301. MPP-2007-53, arxiv:0705.1830.
- G. L. Fogli, E. Lisi, A. Marrone, and A. Mirizzi. *Collective neutrino flavor transitions in supernovae and the role of trajectory averaging.* JCAP **0712**, (2007), 010. MPP-2007-54, arxiv:0707.1998.
- Nikolas Akerblom, Ralph Blumenhagen, Dieter Lust, and Maximilian Schmidt-Sommerfeld. *Thresholds for Intersecting D-branes Revisited.* Phys.Lett.B **652**, (2007), 53–59. LMU-ASC 30/07, MPP-2007-55, arxiv:0705.2150.
- R. Mirzoyan, F. Goebel, et al. *Enhanced quantum efficiency bialkali photo multiplier tubes.* Nucl.Instrum.Meth.A **572**, (2007), 449–453. MPP-2007-56.
- Nikolas Akerblom, Ralph Blumenhagen, Dieter Lust, and Maximilian Schmidt-Sommerfeld. *Instantons and Holographic Couplings in Intersecting D-brane Models.* JHEP **0708**, (2007), 44. LMU-ASC 31/07, MPP-2007-57, arxiv:0705.2366.
- Oliver Brein and Wolfgang Hollik. *Distributions for MSSM Higgs boson + jet production at hadron colliders.* Phys.Rev.D **76**, (2007), 035002. IPPP/07/18, DCPT/07/36, MPP-2007-58, arxiv:0705.2744.
- J. Albert (MAGIC). *VHE Gamma-Ray Observation of the Crab Nebula and its Pulsar with the MAGIC Telescope.* Astrophys.J. **674**, (2008), 1037–1055. MPP-2007-59, arxiv:0705.3244.
- Andreu Esteban-Pretel, Sergio Pastor, Ricard Tomas, Georg G. Raffelt, and Gunter Sigl. *Decoherence in supernova neutrino transformations suppressed by deleptonization.* Phys.Rev.D **76**, (2007), 125018. IFIC/07-26, MPP-2007-60, arxiv:0706.2498.
- Jan De Rydt, Jan Rosseel, Torsten T. Schmidt, Antoine Van Proeyen, and Marco Zagermann. *Symplectic structure of N=1 supergravity with anomalies and Chern-Simons terms.* Class.Quant.Grav. **24**, (2007), 5201–5220. KUL-TF-07/11, MPP-2007-61, arxiv:0705.4216.
- The collaboration (MAGIC). *Discovery of VHE Gamma Radiation from IC443 with the MAGIC Telescope.* Astrophys.J.L. **664**, (2007), L87. MPP-2007-62, arxiv:0705.3119.
- A. Mirizzi, D. Montanino, and P. Serpico. *Revisiting cosmological bounds on radiative neutrino lifetime.* Phys.Rev.D **76**, (2007), 053007. FERMILAB-PUB-07-135-A, MPP-2007-63, arxiv:0705.4667.
- J. Ellis, S. Heinemeyer, K. A. Olive, A. M. Weber, and G. Weiglein. *The Supersymmetric Parameter Space in Light of B-physics Observables and Electroweak Precision Data.* JHEP **0708**, (2007), 083. CERN-PH-TH/2007-087, DCPT/07/50, IPPP/07/25, MN-TH-2606-07, FTPI-MINN-07-19, MPP-2007-64, arxiv:0706.0652.
- S. Heinemeyer, W. Hollik, A. M. Weber, and G. Weiglein. *Z Pole Observables in the MSSM.* JHEP **0804**, (2008), 039. DCPT/07/110, IPPP/07/55, MPP-2007-65, arxiv:0710.2972.
- Paul Koerber and Dimitrios Tsimpis. *Supersymmetric sources, integrability and generalized-structure compactifications.* JHEP **0708**, (2007), 82. LMU-ASC 37/07, MPP-2007-66, arxiv:0706.1244.
- The collaboration (H1). *Search for Lepton Flavour Violation in ep Collisions at HERA.* Eur.Phys.J.C **52**, (2007), 833–847. MPP-2007-67, hep-ex/0703004.
- The collaboration (H1). *Tests of QCD Factorisation in the Diffractive Production of Dijets in Deep-Inelastic Scattering and Photoproduction at HERA.* Eur.Phys.J.C

- 51**, (2007), 549–568. DESY 07-018, MPP-2007-68, hep-ex/0703022.
- The collaboration (H1). *Search for Baryonic Resonances Decaying to Xi pi in Deep-Inelastic Scattering at HERA*. Eur.Phys.J.C **52**, (2007), 507–514. DESY 07-045, MPP-2007-69, arxiv:0704.3594.
- Sven Menke. *Determination of the Jet Energy Scale*. Nucl.Phys.B (Proc.Suppl.) **177-178**, (2008), 195–199. MPP-2007-70, arxiv:0706.1474.
- Gabriel Lopes Cardoso, Anna Ceresole, Gianguido Dall’Agata, Johannes M. Oberreuter, and Jan Perz. *First-order flow equations for extremal black holes in very special geometry*. JHEP **0710**, (2007), 063. DFPD-07TH10, LMU-ASC 38/07, MPP-2007-73, arxiv:0706.3373.
- Johanna Erdmenger, Kazuo Ghoroku, and Ingo Kirsch. *Holographic heavy-light mesons from non-Abelian DBI*. JHEP **0709**, (2007), 111. FIT HE-07-01, MPP-2007-74, arxiv:0706.3978.
- A. Duncan, M. Niedermaier, and P. Weisz. *Non-compact sigma-models: Large N expansion and thermodynamic limit*. Nucl.Phys.B **791**, (2007), 193–230. MPP-2007-75, arxiv:0706.2929.
- Sebastian Franco, Amihay Hanany, Daniel Krefl, Jaemo Park, Angel M. Uranga, and David Vegh. *Dimers and orientifolds*. JHEP **0709**, (2007), 075. CERN-PH-TH/2007-099, IFT-UAM/CSIC-07-34, LMU-ASC 41/07, MIT-CTP, MPP-2007-76, arxiv:0707.0298.
- Christian Kiesling. *Physics Results from HERA* MPP-2007-77.
- S. Stieberger and T. Taylor. *Supersymmetry Relations and MHV Amplitudes in Superstring Theory*. Nucl.Phys.B **793**, (2008), 83–113. MPP-2007-79, arxiv:0708.0574.
- Steen Hannestad, Alessandro Mirizzi, Georg G. Raffelt, and Yvonne Y. Wong. *Cosmological constraints on neutrino plus axion hot dark matter*. JCAP **0708**, (2007), 015. MPP-2007-81, arxiv:0706.4198.
- M. Ciccolini, A. Denner, and S. Dittmaier. *Strong and electroweak corrections to the production of Higgs+2jets via weak interactions at the LHC*. Phys.Rev.Lett. **99**, (2007), 99. PSI-PR-07-03, MPP-2007-82, arxiv:0707.0381.
- Robert Wagner. *AGN Observations in the GeV/TeV Energy Range with the MAGIC Telescope*. Publications of the Astronomical Society of the Pacific Conference Series **386**, (2008), 295–301. MPP-2007-83, arxiv:0706.4439.
- Robert Wagner. *A First Synoptic Blazar Study Comprising Eleven Blazars Visible in  $E > 100$  GeV Gamma Rays* 527–532. MPP-2007-84.
- Robert Wagner. *A First Synoptic Blazar Study Comprising Thirteen Blazars Visible in  $E > 100$  GeV Gamma Rays*. Proc. 30th Int. Cosm. Ray Conf., R. Caballero et al. (eds.), UNAM, Vol. 3 (OG part 2) 881–884. MPP-2007-85, arxiv:0706.4442.
- Robert Wagner and Markus Meyer. *Detection of very high energy gamma-rays from the BL Lac object IES 2344+514 in a low emission state with the MAGIC telescope* MPP-2007-86.
- Robert Wagner, Daniela Dorner, Masaaki Hayashida, Thomas Hengstebeck, Daniel Kranich, Daniel Mazin, Nina Nowak, and Diego Tescaro. *Detection of very high energy gamma-rays from the BL Lac object PG 1553+113 with the MAGIC telescope*. Proc. 30th Int. Cosm. Ray Conf., R. Caballero et al. (eds.), UNAM, Vol. 3 (OG part 2) 889–892. MPP-2007-87, arxiv:0711.1586.
- J. Albert et al. *Discovery of Very High Energy gamma-rays from IES1011+496 at  $z=0.212$* . Astrophys.J. **667**, (2007), L21–L24. MPP-2007-88, arxiv:0706.4435.
- Robert Wagner. *Blazar Observations in the TeV energy range with the MAGIC Telescope* MPP-2007-89.
- Robert Wagner. *Fifteen Blazars in Very-High Energy Gamma Rays: A Comparative Study* MPP-2007-90.
- I. Bavykina, P. Christ, P. Huff, J. Ninkovic, F. Proebst, W. Seidel, and L. Stodolsky. *Interpretation of Light-Quenching Factor Measurements*. Astropart.Phys. **28**, (2007), 489. MPP-2007-91, arxiv:0707.0766.
- Paul Koerber and Luca Martucci. *From ten to four and back again: how to generalize the geometry*. JHEP **0708**, (2007), 059. KUL-TF-07/12, MPP-2007-92, arxiv:0707.1038.
- Ralph Blumenhagen, Mirjam Cvetič, Dieter Lust, Robert Richter, and Timo Weigand. *Non-perturbative Yukawa Couplings from String Instantons*. Phys.Rev.Lett. **100**, (2008), 061602. MPP-2007-93, arxiv:0707.1871.
- Dieter Lust. *String Landscape and the Standard Model of Particle Physics* LMU-ASC 49/07, MPP-2007-94, arxiv:0707.2305.
- J. Albert et al. *Unfolding of differential energy spectra in the MAGIC experiment*. Nucl.Instrum.Meth.A **583**, (2007), 494. MPP-2007-95, arxiv:0707.2453.
- W. Hollik, T. Kasprzik, and B. A. Kniehl. *Electroweak corrections to W-boson hadroproduction at finite transverse momentum*. Nucl.Phys.B **790**, (2007), 138–159. DESY 07-103, MPP-2007-96, arxiv:0707.2553.
- C. Kounnas, D. Lust, P. M. Petropoulos, and D. Tsimpis. *AdS4 flux vacua in type II superstrings and their domain-wall solutions*. JHEP **0709**, (2007), 051. LPTENS/07/32, LMU-ASC 50/07, CPTH-RR060.0707, MPP-2007-98, arxiv:0707.4270.
- J. Barranco, O. G. Miranda, and T. I. Rashba. *Improved limit on electron neutrino charge radius through a new evaluation of the weak mixing angle*. Phys.Lett.B **662**, (2008), 431–435. MPP-2007-99, arxiv:0707.4319.

- Ralph Blumenhagen, Mirjam Cvetič, Robert Richter, and Timo Weigand. *Lifting D-Instanton Zero Modes by Recombination and Background Fluxes*. JHEP **0710**, (2007), 98. MPP-2007-100, arxiv:0708.0403.
- Johann H. Kuhn, A. Kulesza, S. Pozzorini, and M. Schulze. *Electroweak corrections to hadronic production of W bosons at large transverse momenta*. Nucl.Phys.B **797**, (2008), 27–77. TTP07-19, SFB/CPP-07-43, DESY 07-112, MPP-2007-102, arxiv:0708.0476.
- Sean Fleming, Andre H. Hoang, Sonny Mantry, and Iain W. Stewart. *Top Jets in the Peak Region: Factorization Analysis with NLL Resummation*. Phys.Rev.D **77**, (2008), 114003. MIT-CTP 3868, CALT-68-2625, MPP-2007-103, arxiv:0711.2079.
- Maxim Dvornikov, Timur Rashba, and Victor Semikoz. *Coriolis force corrections to g-mode spectrum in 1D MHD model*. Astron.Rep. **52**, (2008), 335–342. MPP-2007-104, arxiv:0705.2923.
- M. Fairbairn, S. N. Gninenko, N. V. Krasnikov, V. A. Matveev, T. I. Rashba, A. Rubbia, and Sergey Troitsky. *Searching for energetic cosmic axions in a laboratory experiment: testing the PVLAS anomaly*. Eur.Phys.J.C **52**, (2007), 899–904. MPP-2007-105, arxiv:0706.0108.
- Wolfgang Hollik and Monika Kollar. *NLO QED contributions to top-pair production at hadron collider*. Phys.Rev.D **77**, (2008), 014008. MPP-2007-106, arxiv:0708.1697.
- Steen Hannestad, Georg Raffelt, and Yvonne Y. Y. Wong. *Unparticle constraints from SN1987A*. Phys.Rev.D **76**, (2007), 121701. MPP-2007-108, arxiv:0708.1404.
- Robert Wagner. *Measurement of Very High Energy Gamma-Ray Emission from Four Blazars Using the MAGIC Telescope and a Comparative Blazar Study*. Publications of the Astronomical Society of the Pacific **119**, (2007), 1201–1203. MPP-2007-109.
- Stephan Stieberger and Tomasz R. Taylor. *Complete Six-Gluon Disk Amplitude in Superstring Theory*. Nucl.Phys.B **801**, (2008), 128–152. MPP-2007-110, arxiv:0711.4354.
- Masahiro Teshima, Elisa Prandini, Rudolf Bock, Manel Errando, Daniel Kranich, Elina Lindfors, Eckart Lorenz, Daniel Mazin, Pratik Majumdar, Mose Mariotti, Villi Scalzotto, and Robert Wagner. *Discovery of Very High Energy Gamma-Rays from the Distant Flat Spectrum Radio Quasar 3C 279 with the MAGIC Telescope* MPP-2007-111.
- J. Albert, John Ellis, N. E. Mavromatos, D. V. Nanopoulos, A. S. Sakharov, E. K. G. Sarkisyan, et al. *Probing Quantum Gravity using Photons from a Mkn 501 Flare Observed by MAGIC*. Phys.Rev.Lett. **668**, (2008), 253–257. CERN-PH-TH/2007-137, MPP-2007-112, arxiv:0708.2889.
- Frank D. Steffen and Markus H. Thoma. *Erratum to "Hard Thermal Photon Production in Relativistic Heavy Ion Collisions" [Phys.Lett.B510 (2001) 98]*. Phys.Lett.B **660**, (2008), 604–606. CERN-TH/2001-080, HD-THEP-01-13, MPP-2007-113, hep-ph/0103044.
- H. Bartko (. *Observation of Galactic Sources of Very High Energy Gamma-Rays with the MAGIC Telescope*. Mod.Phys.Lett.A **22**, (2007), 2167–2174. MPP-2007-114, arxiv:0708.2934.
- Josef Pradler and Frank Daniel Steffen. *Implications of Catalyzed BBN in the CMSSM with Gravitino Dark Matter*. Phys.Lett.B **666**, (2008), 181–184. MPP-2007-115, arxiv:0710.2213.
- T. Hahn and J. I. Illana. *Extensions in FormCalc 5.3*. PoSACAT **2007**, (2007), 074. MPP-2007-116, arxiv:0708.3652.
- J. Ellis, T. Hahn, S. Heinemeyer, K. A. Olive, and G. Weiglein. *WMAP-Compliant Benchmark Surfaces for MSSM Higgs Bosons*. JHEP **0710**, (2007), 092. CERN-PH-TH/2007-138, DCPT/07/102, IPPP/07/51, UMN-TH-2615-07, FTPI-MINN-07-25, MPP-2007-117, arxiv:0709.0098.
- A. Bredenstein, A. Denner, S. Dittmaier, and M. M. Weber. *Precision calculations for  $H \rightarrow WW/ZZ \rightarrow 4\text{fermions}$  with PROPHECY4f* MPP-2007-118, arxiv:0708.4123.
- Georg G. Raffelt and Alexei Yu. Smirnov. *Adiabaticity and spectral splittings in collective neutrino transformations*. Phys.Rev.D **76**, (2007), 125008. MPP-2007-120, arxiv:0709.4641.
- Stefan Antusch and Steve F. King. *Lepton Flavour Violation in the Constrained MSSM with Constrained Sequential Dominance*. Phys.Lett.B **659**, (2008), 640–650. SHEP-07-30, MPP-2007-121, arxiv:0709.0666.
- Johanna Erdmenger, Rene Meyer, and Jonathan P. Shock. *AdS/CFT with Flavour in Electric and Magnetic Kalb-Ramond Fields*. JHEP **0712**, (2007), 091. MPP-2007-122, arxiv:0709.1551.
- F. Goebel, M. Backes, T. Bretz, M. Hayashida, C. Hsu, K. Mannheim, A. Moralejo, W. Rhode, K. Satalecka, M. Shayduk, M. Teshima, and R. M. Wagner. *Long term monitoring of bright TeV Blazars with the MAGIC telescope*. Proc. 30th Int. Cosm. Ray Conf., R. Caballero et al. (eds.), UNAM, Vol. 3 (OG part 2) 1025–1028. MPP-2007-124, arxiv:0709.2032.
- G. Hermann, W. Hofmann, T. Schweizer, and M. Teshima. *Cherenkov Telescope Array: The next-generation ground-based gamma-ray observatory*. Proc. 30th Int. Cosm. Ray Conf., R. Caballero et al. (eds.), UNAM, Vol. 3 (OG part 2) 1313–1316. MPP-2007-125, arxiv:0709.2048.
- Hendrik Bartko. *Observations of VHE gamma-Ray Sources with the MAGIC Telescope* MPP-2007-126, arxiv:0709.2807.
- Florian Goebel, Hendrik Bartko, Emiliano Carmona, Nicola Galante, Tobias Jogler, Razmik Mirzoyan, Jose Antonio Coarasa, and Masahiro Teshima (MAGIC). *Upgrade*

- of the *MAGIC Telescope with a Multiplexed Fiber-Optic 2 GSamples/s FADC Data Acquisition system*. Proc. 30th Int. Cosmic Ray Conf. Vol. 3 (OG part 2) 1481–1484. MPP-2007-128, arxiv:0709.2363.
- R. Wagner. *Synoptic studies of seventeen blazars detected in very high energy gamma-rays*. Mon.Not.R.Astron.Soc. **385**, (2008), 119. MPP-2007-129, arxiv:0711.3025.
- M. Ackermann, E. Bernardini, N. Galante, F. Goebel, M. Hayashida, K. Satalecka, M. Tluczykont, and R. M. Wagner. *Test run of Neutrino triggered Target of Opportunity (NTO) gamma ray observations using AMANDA and MAGIC* MPP-2007-130, arxiv:0709.2640.
- Florian Goebel. *Status of the second phase of the MAGIC telescope*. Proc. 30th Int. Cosm. Ray Conf., R. Caballero et al. (eds.), UNAM, Vol. 3 (OG part 2) 1485–1488. MPP-2007-131, arxiv:0709.2605.
- Silja Brensing, Stefan Dittmaier, Michael Krämer, and Alexander Mück. *Radiative corrections to W-boson hadroproduction: higher-order electroweak and supersymmetric effects*. Phys.Rev.D **77**, (2008), 073006. PITHA 07/08, UWThPh-2007-24, PSI-PR-07-08, MPP-2007-132, arxiv:0710.3309.
- Jan Hamann and Yvonne Y. Y. Wong. *Effects of CMB temperature uncertainties on cosmological parameter estimation*. JCAP **0803**, (2008), 025. TUM-HEP-674/07, MPP-2007-134, arxiv:0709.4423.
- Andre H. Hoang and Iain W. Stewart. *Designing Gapped Soft Functions for Jet Production*. Phys.Lett.B **660**, (2008), 483–493. MIT-CTP 3792, MPP-2007-135, arxiv:0709.3519.
- Johanna Erdmenger, Matthias Kaminski, and Felix Rust. *Holographic vector mesons from spectral functions at finite baryon or isospin density*. Phys.Rev.D **77**, (2008), 046005. MPP-2007-136, arxiv:0710.0334.
- D. F. Torres and J. Cortina (MAGIC). *Highlights of MAGIC Observations of galactic sources* MPP-2007-137.
- D. Mazin (MAGIC). *Observations of AGNs with the MAGIC Telescope* MPP-2007-138.
- D. Paneque (MAGIC). *Study of the Flux and Spectral Variations in the VHE Emission from the Blazar Markarian 501, with the MAGIC telescope* MPP-2007-139.
- M. Lopez, N. Otte, E. Aliu, et al. (MAGIC). *Pulsar observations with the MAGIC Telescope* MPP-2007-140.
- H. Bartko (MAGIC). *Observations of VHE Gamma-Ray Sources with the MAGIC Telescope*. Chin.J.Astron.Astrophys MPP-2007-141.
- O. Buchmueller, R. Cavanaugh, A. De Roeck, S. Heinemeyer, G. Isidori, P. Paradisi, F. J. Ronga, A. M. Weber, and G. Weiglein. *Prediction for the Lightest Higgs Boson Mass in the CMSSM using Indirect Experimental Constraints*. Phys.Lett.B **657**, (2007), 87–94. IPPP/07/43, DCPT/07/86, MPP-2007-142, arxiv:0707.3447.
- M. Doro (MAGIC). *Technical Solutions for the MAGIC Telescope* MPP-2007-143.
- S. Dittmaier, S. Kallweit, and P. Uwer. *NLO QCD corrections to WW+jet production at hadron colliders*. Phys.Rev.Lett. **100**, (2008), 062003. SFB/CPP-07-64, MPP-2007-144, arxiv:0710.1577.
- Dietmar Ebert, Jan Plefka, and Andreas Rodigast. *Absence of gravitational contributions to the running Yang-Mills coupling*. Phys.Lett.B **660**, (2008), 579–582. HU-EP-07/49, MPP-2007-145, arxiv:0710.1002.
- Roberto De Pietri, Alessandra Feo, Erhard Seiler, and Ion-Olimpiu Stamatescu. *A Model for QCD at high density and large quark mass*. Phys.Rev.D **76**, (2007), 114501–114522. MPP-2007-147, arxiv:0705.3420.
- S. Heinemeyer, W. Hollik, A. M. Weber, and G. Weiglein. *MSSM precision physics at the Z resonance* IPPP/07/58, DCPT/07/116, MPP-2007-148, arxiv:0710.2982.
- Wolfgang Hollik, Monika Kollar, and Maike K. Trenkel. *Hadronic production of top-squark pairs with electroweak NLO contributions*. JHEP **02**, (2008), 018. MPP-2007-149, arxiv:0712.0287.
- Alessandra Feo, Roberto De Pietri, Erhard Seiler, and Ion-Olimpiu Stamatescu. *The High Density Region of QCD from an Effective Model*. PoSLAT **2007**, (2007), 184. DFTT 24/2007, MPP-2007-150, arxiv:0710.3102.
- Sean Fleming, Andre H. Hoang, Sonny Mantry, and Iain W. Stewart. *Factorization Approach for Top Mass Reconstruction at High Energies*. eConf C **0705302**, (2007), TOP06. MIT-CTP 3866, MPP-2007-151, arxiv:0710.4205.
- Mariano Ciccolini, Ansgar Denner, and Stefan Dittmaier. *Electroweak and QCD corrections to Higgs production via vector-boson fusion at the LHC*. Phys.Rev.D **77**, (2008), 013002. PSI-PR-07-06, UWThPh-2007-26, MPP-2007-152, arxiv:0710.4749.
- Luzi Bergamin, Daniel Grumiller, Robert McNees, and Rene Meyer. *Black Hole Thermodynamics and Hamilton-Jacobi Counterterm*. J.Phys.A **41**, (2008), 164068. MIT-CTP-3887, MPP-2007-153, arxiv:0710.4140.
- Josef Pradler and Frank D. Steffen. *CBBN in the CMSSM*. Eur.Phys.J.C **56**, (2008), 287–291. MPP-2007-154, arxiv:0710.4548.
- T. Hahn, S. Heinemeyer, W. Hollik, H. Rzehak, and G. Weiglein. *Higgs Masses and More in the Complex MSSM with FeynHiggs* IPPP/07/74, DCPT/07/148, PSI-PR-07-09, MPP-2007-155, arxiv:0710.4891.
- S. Ruijsenaars and L. Stodolsky. *On the Euclidean Version of the Photon Number Integral*. J.Math.Phys. **49**, (2008), 023502. MPP-2007-156, arxiv:0710.4276.

- The collaboration (H1). *Charged Particle Production in High  $Q_2$  Deep-Inelastic Scattering at HERA*. Phys.Lett.B **654**, (2007), 148–159. DESY 07-065, MPP-2007-157, arxiv:0706.2456.
- The collaboration (H1). *Measurement of Isolated Photon Production in Deep-Inelastic Scattering at HERA*. Eur.Phys.J.C **54**, (2008), 371–387. DESY 07-147, MPP-2007-158, arxiv:0711.4578.
- The collaboration (H1). *Dijet Cross Sections and Parton Densities in Diffractive DIS at HERA*. JHEP **0710**, (2007), 042. DESY-07-115, MPP-2007-159, arxiv:0708.3217.
- The collaboration (H1). *Measurement of Deeply Virtual Compton Scattering and its  $t$ -dependence at HERA*. Phys.Lett.B **659**, (2008), 796–806. DESY-07-142, MPP-2007-160, arxiv:0709.4114.
- Yvonne Y. Y. Wong. *Neutrinos in cosmology*. AIP Conf.Proc. **972**, (2008), 427–435. MPP-2007-161.
- Paul Koerber and Luca Martucci. *D-branes on AdS flux compactifications*. JHEP **01**, (2008), 047. LMU-ASC 69/07, MPP-2007-162, arxiv:0710.5530.
- Ralph Blumenhagen and Maximilian Schmidt-Sommerfeld. *Gauge Thresholds and Kaehler Metrics for Rigid Intersecting D-brane Models*. JHEP **0712**, (2007), 072. MPP-2007-163, arxiv:0711.0866.
- J. Astrom, P. C. F. Di Stefano, F. Probst, L. Stodolsky, and J. Timonen. *Brittle fracture down to femto-Joules - and below* MPP-2007-164, arxiv:0708.4315.
- Frank Daniel Steffen. *Supersymmetric Dark Matter Candidates - The Lightest Neutralino, the Gravitino, and the Axino* 184–196. MPP-2007-165, arxiv:0711.1240.
- T. Hahn and P. Lang. *FeynEdit - a tool for drawing Feynman diagrams*. Comput.Phys.Commun. **179**, (2008), 931–935. MPP-2007-166, arxiv:0711.1345.
- W. Bednarek and R. M. Wagner. *A Model for Delayed Emission in a Very-High Energy Gamma-Ray Flare in Markarian 501*. Astron.Astrophys. **486**, (2008), 679–682. MPP-2007-167, arxiv:0804.0619.
- Johanna Erdmenger, Nick Evans, Ingo Kirsch, and Ed Threlfall. *Mesons in Gauge/Gravity Duals - A Review*. Eur.Phys.J.A **35**, (2008), 81–133. SHEP-07-45, NI-07-071, MPP-2007-168, arxiv:0711.4467.
- Ralph Blumenhagen, Sebastian Moster, and Erik Plauschinn. *Moduli Stabilisation versus Chirality for MSSM like Type IIB Orientifolds*. JHEP **0801**, (2008), 58. MPP-2007-169, arxiv:0711.3389.
- Max Niedermaier and Erhard Seiler. *On the large  $N$  expansion in hyperbolic sigma-models*. J.Math.Phys. **49**, (2008), 073301. ESI preprint 1979, MPP-2007-170, arxiv:0711.3756.
- Luzi Bergamin and Rene Meyer. *Two-Dimensional Quantum Gravity with Boundary* MPP-2007-171, arxiv:0711.3595.
- J. Dubbert, S. Horvat, H. Kroha, F. Legger, O. Kortner, R. Richter, and F. Rauscher. *Development of Precision Drift Tube Detectors for Very High Background Rates at the Super-LHC* MPP-2007-172.
- Wolfgang Ochs. *The glueball among the light scalar mesons* MPP-2007-173, arxiv:0711.3902.
- Pilar Coloma, Andrea Donini, Enrique Fernandez-Martinez, and Jacobo Lopez-Pavon.  $\theta_{13}$ ,  $\delta$  and the neutrino mass hierarchy at a  $\gamma = 350$  double baseline Li/B  $\beta$ -Beam. JHEP **0805**, (2008), 050. MPP-2007-174, arxiv:0712.0796.
- J. v. Loeben et al. (ATLAS Muon). *First Cosmic Ray Results of the ATLAS Muon Spectrometer with Magnetic Field*. IEEE Nuclear Science Symposium Conference Record **3**, (2007), 1891–1894. MPP-2007-175.
- J. v. Loeben, M. Deile, N. Hessey, O. Kortner, H. Kroha, and A. Staude. *An Efficient Method to Determine the Space-to-Drift-Time Relationship of the ATLAS Monitored Drift Tube Chambers*. IEEE Nuclear Science Symposium Conference Record **1**, (2007), 685–688. MPP-2007-176.
- Oliver Kortner, Sergey Kotov, Hubert Kroha, Igor Potrap, and Jens Schmaler. *New Methods for the Alignment of the ATLAS Muon Spectrometer with Tracks* MPP-2007-177.
- Andreu Esteban-Pretel, Sergio Pastor, Ricard Tomas, Georg G. Raffelt, and Gunter Sigl. *Mu-tau neutrino re-fraction and collective three-flavor transformations in supernovae*. Phys.Rev.D **77**, (2008), 065024. IFIC/07-69, MPP-2007-178, arxiv:0712.1137.
- The collaboration (H1). *Three- and Four-jet Production at Low  $x$  at HERA*. Eur.Phys.J.C **54**, (2008), 389–409. DESY 07-200, MPP-2007-179, arxiv:0711.2606.
- Stefan Antusch, Stephen F. King, and Michal Malinsky. *Third Family Corrections to Tri-bimaximal Lepton Mixing and a New Sum Rule*. Phys.Lett.B **671**, (2009), 263–266. MPP-2007-180, arxiv:0711.4727.
- Jörg Dubbert. *First experience with the ATLAS Muon Spectrometer*. Nucl.Instrum.Meth.A **581**, (2007), 507–510. MPP-2007-181.
- L. Anchordoqui, H. Goldberg, S. Nawata, and T. R. Taylor. *Jet signals for low mass Jet signals for low mass strings at the LHC*. Phys.Rev.Lett. MPP-2007-182.
- K. R. Ito and E. Seiler. *On the recent paper on quark confinement by Tomboulis* MPP-2007-183, arxiv:0711.4930.
- Timur Rashba. *Low energy neutrino experiments sensitivity to physics beyond the Standard Model* MPP-2007-184.
- A. Nepomuk Otte. *Observation of the Crab Nebula with the MAGIC telescope* MPP-2007-185, arxiv:0712.1386.

- A. N. Otte, I. Britvitch, A. Biland, F. Goebel, E. Lorenz, F. Pauss, D. Renker, U. Roeser, and T. Schweizer. *Detection of Cherenkov light from air showers with Geiger-APDs*. Nucl.Instrum.Meth.A **610**, (2009), 415–418. MPP-2007-186, arxiv:0712.1592.
- Nikolas Akerblom, Ralph Blumenhagen, Dieter Lust, and Maximilian Schmidt-Sommerfeld. *D-brane Instantons in 4D Supersymmetric String Vacua*. Fortschr.Phys. **56**, (2008), 313–323. LMU-ASC 74/07, MPP-2007-187, arxiv:0712.1793.
- Andreu Esteban-Pretel, Sergio Pastor, Ricard Tomas, Georg Raffelt, and Gunter Sigl. *Multi-angle effects in collective supernova neutrino oscillations*. J.Phys.Conf.Ser. **120**, (2008), 052021. MPP-2007-188, arxiv:0712.2176.
- Wolfgang Hollik, Monika Kollar, and Maike K. Trenkel. *EW NLO corrections to pair production of top-squarks at the LHC* MPP-2007-189, arxiv:0710.2472.
- Mariano Ciccolini, Ansgar Denner, and Stefan Dittmaier. *Electroweak and QCD corrections to Higgs-boson production in vector-boson fusion at the LHC*. PoSRADCOR **2007**, (2007), 014. PSI-PR-07-12, UWThPh-2007-29, MPP-2007-190, arxiv:0712.2895.
- H. Bartko and W. Bednarek. *Gamma-Ray Emission from PWNe Interacting with Molecular Clouds* MPP-2007-192, arxiv:0712.2964.
- Stefan Dittmaier, Stefan Kallweit, and Peter Uwer. *NLO QCD corrections to  $pp \rightarrow WW + jet + X$* . PoSRADCOR **2007**, (2007), 009. SFB/CP-07-87, UWThPh-2007-30, MPP-2007-193, arxiv:0712.3163.
- I. Bavykina, G. Angloher, D. Hauff, E. Pantic, F. Petricca, F. Proebst, W. Seidel, and L. Stodolsky. *Investigation of ZnWO<sub>4</sub> crystals as scintillating absorbers for direct Dark Matter search experiments* MPP-2007-195.
- Hans-Günther Moser. *Development of backside illuminated silicon photomultipliers at the MPI semiconductor laboratory*. PoS MPP-2007-196.
- J. Albert et al. (MAGIC). *Systematic search for VHE gamma-ray emission from X-ray bright high-frequency BL Lac objects*. Astrophys.J. **667**, (2007), L21–L23. MPP-2007-197, arxiv:0706.4453.
- V. Scapin (MAGIC). *Resent results from the MAGIC Telescope*. Nucl.Phys.B(Proc.Suppl.)**595**, issue **1**, (2008), 77–79. MPP-2007-198.
- J. K. Becker, M. Gaug, Ch. Ch. Hsu, and W. Rhode (MAGIC). *GRB neutrino search with MAGIC*. AIP Conf.Proc. **1000**, (2008), 245–248. MPP-2007-199.
- J. Albert et al. (MAGIC). *Upper limit for gamma-ray emission above 140 GeV from the dwarf spheroidal galaxy Draco*. Astrophys.J. **679**, (2008), 428–431. MPP-2007-200, arxiv:0711.2574.
- J. Albert. *Observation of VHE gamma-rays from Cassiopeia A with the MAGIC telescope*. Astron.Astrophys. **474**, (2007), 937–940. MPP-2007-201, arxiv:0706.4065.
- J. Albert (MAGIC). *Discovery of very high energy gamma-ray emission from the low-frequency peaked BL Lacertae object BL Lacertae*. Astrophys.J.L. **666**, (2007), L17. MPP-2007-202, astro-ph/0703084.
- J. Albert (MAGIC). *Very High Energy Gamma-ray Radiation from the Stellar-mass Black Hole Cygnus X-1*. Astrophys.J.L. **665**, (2007), L51. MPP-2007-203, arxiv:0706.1505.
- Erhard Seiler and Ion-Olimpiu Stamatescu. *The many-fold way of contemporary high energy theoretical physics*, 3–18 (Springer-Verlag, Lect. Notes Phys. 721, Heidelberg, New York). MPP-2007-204 (2007).
- A. Abdesselam et al. *The ATLAS semiconductor tracker end-cap module*. Nucl.Instrum.Meth.A **575**, (2007), 353–389. MPP-2007-205.
- A. Ahmad et al. *The Silicon microstrip sensors of the ATLAS semiconductor tracker*. Nucl.Instrum.Meth.A **578**, (2007), 98–118. MPP-2007-206.
- P. Weisz. *News from lattice QCD* MPP-2007-207.
- B. Majorovits. *The GERDA Neutrinoless Double Beta Decay Experiment*. AIP Conf.Proc. **942**, (2007), 57–61. MPP-2007-208.
- I. Bavykina, A. Bento, D. Hauff, P. Huff, R. Lang, B. Majorovits, E. Pantic, F. Petricca, F. Proebst, W. Seidel, L. Stodolsky, C. Ciemniak, C. Coppi, F. von Feilitzsch, C. Isaila, J. Lanfranchi, S. Pfister, W. Potzel, W. Westphal, S. Henry, J. Imber, S. Ingleby, H. Kraus, M. Malek, R. McGowan, V. Mikhailik, B. Tolhurst, M. Bauer, J. Jochum, M. Kimmerle, K. Rottler, S. Scholl, and C. Bucci. *The CRESST Dark Matter Search* MPP-2007-209.
- S. Blusk, O. Buchmuller, A. Jacholkowski, T. Ruf, J. Schieck, and S. Viret. *Proceedings of the first LHC Detector Alignment Workshop* MPP-2007-210.
- H. Kraus, G. Angloher, M. Bauer, I. Bavykina, C. Bucci, P. Christ, C. Ciemniak, C. Cozzini, C. Coppi, F. von Feilitzsch, D. Hauff, S. Henry, J. Imber, C. Isaila, Th. Jagemann, J. Jochum, J. C. Lanfranchi, R. Lang, B. Majorovits, M. Malek, R. McGowan, V. Mikhailik, J. Ninkovic, E. Pantic, F. Petricca, S. Pfister, W. Potzel, F. Pröbst, Y. Ramachers, W. Rau, M. Razeti, K. Rottler, S. Scholl, W. Seidel, M. Stark, L. Stodolsky, A. J. B. Tolhurst, W. Westphal, and H. Wulandari. *CRESST - status and future*. Nucl.Phys.B (Proc.Suppl.) **173**, (2007), 104–107. MPP-2007-211.
- G. Mennessier, P. Minkowski, S. Narison, and W. Ochs. *Can the gamma-gamma processes reveal the nature of the sigma ?* HEP-MAD-2007-217.1, MPP-2007-212, arxiv:0707.4511.

- The collaboration (H1). *Measurement of Inclusive Jet Production in Deep-Inelastic Scattering at High  $Q^2$  and Determination of the Strong Coupling*. Phys.Lett.B **653**, (2007), 134–144. DESY 07-073, MPP-2007-213, arxiv:0706.3722.
- S. Chekanov (ZEUS). *Exclusive  $\rho^0$  production in deep inelastic scattering at HERA*. PMC Phys.A **1**, (2007), 6. DESY-07-118, MPP-2007-214, arxiv:0708.1478.
- Allen Caldwell and Guenter Grindhammer. *In the heart of matter. (In German)*. Physik Journal **11**, (2007), 39–45. MPP-2007-215.
- S. Chekanov et al. (ZEUS). *Dijet production in diffractive deep inelastic scattering at HERA*. Eur.Phys.J.C **52**, (2007), 813–832. DESY-07-126, MPP-2007-217, arxiv:0708.1415.
- S. Chekanov (ZEUS). *Three- and four-jet final states in photoproduction at HERA*. Nucl.Phys.B **792**, (2008), 1–47. MPP-2007-218, arxiv:0707.3749.
- S. Chekanov (ZEUS). *Forward-jet production in deep inelastic ep scattering at HERA*. Eur.Phys.J.C **52**, (2007), 515–530. MPP-2007-219, arxiv:0707.3093.
- S. Chekanov (ZEUS). *High- $E_T$  dijet photoproduction at HERA*. Phys.Rev.D **76**, (2007), 072011. DESY 07-092, MPP-2007-220, arxiv:0706.3809.
- The collaboration (ZEUS). *Bose-Einstein Correlations of Charged and Neutral Kaons in Deep Inelastic Scattering at HERA*. Phys.Lett.B **652**, (2007), 1–12. DESY-07-069, MPP-2007-221, arxiv:0706.2538.
- The collaboration (ZEUS). *Measurement of (anti)deuteron and (anti)proton production in DIS at HERA*. Nucl.Phys.B DESY 07-070, MPP-2007-222, arxiv:0705.3770.
- The collaboration (ZEUS). *Multijet production at low  $x_Bj$  in deep inelastic scattering at HERA*. Nucl.Phys.B **786**, (2007), 152–180. DESY-07-062, MPP-2007-223, arxiv:0705.1931.
- The collaboration (ZEUS). *Measurement of  $D$  mesons Production in Deep Inelastic Scattering at HERA*. JHEP **0707**, (2007), 074. DESY-07-052, MPP-2007-224, arxiv:0704.3562.
- S. Chekanov (ZEUS). *Diffractive Photoproduction of  $D^{*+/-}(2010)$  at HERA*. Eur.Phys.J.C **51**, (2007), 301–315. DESY-07-039, MPP-2007-225, hep-ex/0703046.
- The collaboration (ZEUS). *Measurement of  $D^{*+/-}$  meson production in ep scattering at low  $Q^2$* . Phys.Lett.B **649**, (2007), 111–121. DESY-07-012, MPP-2007-226, hep-ex/0702034.
- The collaboration (ZEUS). *Leading neutron energy and  $p_T$  distributions in deep inelastic scattering and photoproduction at HERA*. Nucl.Phys.B **776**, (2007), 1–37. DESY-07-011, MPP-2007-227, hep-ex/0702028.
- J. Albert and E. Aliu (MAGIC). *Implementation of the Random Forest method for the Imaging Atmospheric Cherenkov Telescope MAGIC*. Nucl.Instrum.Meth.A MPP-2007-228.
- P. Fischer, L. Andricek, S. Herrmann, M. Karagounis, R. Kohrs, C. Kreidl, H. Krüger, G. Lutz, G. G. Moser, I. Peric, M. Porro, L. Reuen, R. H. Richter, S. Rummel, C. Sandow, L. Strüder, E. Torne, J. Treis, M. Trimpl, J. Velthuis, and N. Wermes. *Progress towards a large area, thin DEPFET detector module*. Nucl.Instrum.Meth.A **3**, (2007), 843–848. MPP-2007-229.
- J. Ninkovic, R. Eckhardt, R. Hartmann, P. Holl, C. Koitsch, G. Lutz, C. Merck, R. Mirzoyan, H. G. Moser, N. Otte, R. Richter, G. Schaller, F. Schopper, H. Soltau, M. Teshima, and G. Valceanu. *The avalanche drift diode - a black illumination drift silicon photomultiplier*. Nucl.Instrum.Meth.A **2**, (2007), 1013–1015. MPP-2007-230.
- G. Lutz, R. Andritschke, L. Andricek, R. Eckhardt, J. Englhäuser, G. Fuchs, O. Hälker, R. Hartmann, K. Heinzinger, S. Herrmann, P. Holl, N. Kimmel, P. Lechner, N. Meidinger, M. Porro, R. H. Richter, G. Schaller, M. Schnecke, F. Schopper, H. Soltau, L. Strüder, J. Treis, U. Weichert, and S. Wöfl. *Spectroscopic silicon imaging detectors: past achievements and new developments*. Nucl.Instrum.Meth.A **2**, (2007), 960–967. MPP-2007-231.
- J. Velthuis, R. Kohrs, M. Mathes, A. Raspereza, L. Reuen, L. Andricek, M. Koch, Z. Dolezal, P. Fischer, A. Frey, F. Giesen, P. Kodys, C. Kreidl, H. Krüger, P. Lodomez, G. Lutz, H. G. Moser, R. H. Richter, C. Sandow, D. Scheirich, E. Torne, M. Trimpl, Q. Wei, and N. Wermes. *DEPFET, a monolithic active pixel sensor for the ILC*. Nucl.Instrum.Meth.A **2**, (2007), 685–689. MPP-2007-232.
- S. Wöfl, S. Herrmann, P. Lechner, G. Lutz, M. Porro, R. H. Richter, L. Strüder, and J. Treis. *A novel way of single optical photon detection: beating the  $1/f$  noise limit with ultra high resolution DEPFET-RNDR devices*. IEEE Transactions on Nuclear Science **4**, (2007), 1311–1318. MPP-2007-233.
- P. Lechner, L. Andricek, K. Heinzinger, S. Herrmann, N. Kimmel, T. Lauf, G. Lutz, R. H. Richter, M. Porro, G. Schaller, M. Schnecke, F. Schopper, H. Soltau, L. Strüder, J. Treis, S. Wöfl, and Zhang Chen. *The wide field imager of the European X-ray observatory*. IEEE Nuclear Science Symposium Conference Record **3**, (2006), 1595–1604. MPP-2007-234.
- P. Holl, R. Andritschke, R. Eckhardt, R. Hartmann, C. Koitsch, G. Lutz, N. Meidinger, R. H. Richter, G. Schaller, H. Soltau, L. Strüder, and G. Valceanu. *A new high-speed, single photon imaging CCD for the optical*. IEEE Nuclear Science Symposium Conference Record **3**, (2006), 1589–1594. MPP-2007-235.
- C. Alt, V. Eckardt, N. Schmitz, P. Seyboth, et al. (NA49). *Inclusive production of charged pions in  $p+C$  collisions at*

- 158 GeV/c beam momentum. *Eur.Phys.J.C* **49**, (2007), 897–917. MPP-2007-236, hep-ex/0606028.
- D. M. Gingrich et al. (The ATLAS Hadronic End-Cap Calorimeter Group). *Construction, assembly and testing of the ATLAS hadronic end-cap calorimeter*. *J.Inst.* **2**, (2007), P05005. ATL-LARG-PUB-2007-009, ATL-COM-LARG-2007-006, MPP-2007-237.
- C. Alt, V. Eckardt, N. Schmitz, P. Seyboth, et al. (NA49). *Elliptic flow of Lambda hyperons in Pb+Pb collisions at 158A GeV*. *Phys.Rev.C* **75**, (2007), 044901. AS-IP-06-001, MPP-2007-238, nucl-ex/0606026.
- C. Alt, V. Eckardt, N. Schmitz, P. Seyboth, et al. (NA49). *Centrality and system size dependence of multiplicity fluctuations in nuclear collisions at 158 AGeV*. *Phys.Rev.C* **75**, (2007), 064904. MPP-2007-239, nucl-ex/0612010.
- C. Alt, V. Eckardt, N. Schmitz, P. Seyboth, et al. (NA49). *Rapidity and energy dependence of the electric charge correlations in A+A collisions at the SPS energies*. *Phys.Rev.C* **76**, (2007), 024914. MPP-2007-240, arxiv:0705.1122.
- J. Adams, V. Eckardt, N. Schmitz, P. Seyboth, et al. (STAR). *The energy dependence of  $p_t$  angular correlations inferred from mean- $p_t$  fluctuation scale dependence in heavy ion collisions at the SPS and RHIC*. *J.Phys.G* **33**, (2007), 451–466. MPP-2007-242, nucl-ex/0605021.
- B. Abelev, V. Eckardt, N. Schmitz, P. Seyboth, et al. (STAR). *Energy dependence of charged pion, proton and anti-proton transverse momentum spectra for Au+Au collisions at  $\sqrt{s_{NN}} = 62.4$  and 200 GeV*. *Phys.Lett.B* **655**, (2007), 104–113. MPP-2007-243, nucl-ex/0703040.
- J. Adams, V. Eckardt, N. Schmitz, P. Seyboth, et al. (STAR). *Delta- phi Delta- eta Correlations in Central Au+Au Collisions at  $\sqrt{s_{NN}} = 200$  GeV*. *Phys.Rev.C* **75**, (2007), 034901. MPP-2007-244, nucl-ex/0607003.
- B. Abelev, V. Eckardt, N. Schmitz, P. Seyboth, et al. (STAR). *Mass, quark-number, and  $\sqrt{s_{NN}}$  dependence of the second and fourth flow harmonics in ultra-relativistic nucleus-nucleus collisions*. *Phys.Rev.C* **75**, (2007), 054906. MPP-2007-245, nucl-ex/0701010.
- B. Abelev, V. Eckardt, N. Schmitz, P. Seyboth, et al. (STAR). *Measurements of Strange Particle Production in  $p + p$  Collisions at  $\sqrt{s} = 200$  GeV*. *Phys.Rev.C* **75**, (2007), 064901. MPP-2007-246, nucl-ex/0607033.
- B. Abelev, V. Eckardt, N. Schmitz, P. Seyboth, et al. (STAR). *Strangelet Search in AuAu Collisions at 200 GeV*. *Phys.Rev.C* **76**, (2007), 011901. MPP-2007-247, nucl-ex/0511047.
- B. I. Abelev, V. Eckardt, N. Schmitz, P. Seyboth, et al. (STAR). *Global polarization measurement in Au+Au collisions*. *Phys.Rev.C* **76**, (2007), 024915. Star-05-11-2007, MPP-2007-248, arxiv:0705.1691.
- B. Abelev, V. Eckardt, N. Schmitz, P. Seyboth, et al. (STAR). *Rapidity and species dependence of particle production at large transverse momentum for d+Au collisions at  $\sqrt{s_{NN}} = 200$  GeV*. *Phys.Rev.C* **76**, (2007), 054903. MPP-2007-249, nucl-ex/0609021.
- B. Abelev, V. Eckardt, N. Schmitz, P. Seyboth, et al. (STAR). *Forward Lambda Production and Nuclear Stopping Power in d + Au Collisions at  $\sqrt{s_{NN}} = 200$  GeV*. *Phys.Rev.C* **76**, (2007), 064904. MPP-2007-250, arxiv:0706.0472.
- J. Adams, V. Eckardt, N. Schmitz, P. Seyboth, et al. (STAR). *Scaling Properties of Hyperon Production in Au+Au Collisions at  $\sqrt{s_{NN}} = 200$  GeV*. *Phys.Rev.Lett.* **98**, (2007), 062301. MPP-2007-251, nucl-ex/0606014.
- B. Abelev, V. Eckardt, N. Schmitz, P. Seyboth, et al. (STAR). *Partonic flow and  $\phi$ -meson production in Au+Au collisions at  $\sqrt{s_{NN}} = 200$  GeV*. *Phys.Rev.Lett.* **99**, (2007), 112301. MPP-2007-252, nucl-ex/0703033.
- B. I. Abelev, V. Eckardt, N. Schmitz, P. Seyboth, et al. (STAR). *Transverse momentum and centrality dependence of high- $p_t$  non-photonic electron suppression in Au+Au collisions at  $\sqrt{s_{NN}} = 200$  GeV*. *Phys.Rev.Lett.* **98**, (2007), 192301. MPP-2007-253, nucl-ex/0607012.
- B. I. Abelev, V. Eckardt, N. Schmitz, P. Seyboth, et al. (STAR). *Measurement of Transverse Single-Spin Asymmetries for Di-Jet Production in Proton-Proton Collisions at  $\sqrt{s} = 200$  GeV*. *Phys.Rev.Lett.* **99**, (2007), 142003. MPP-2007-254, arxiv:0705.4629.
- Roland Härtel. *Alignment of the ATLAS Inner Detector*. PoS MPP-2007-255.
- The collaboration (LEP Collaborations, ALEPH , DELPHI , L3 , OPAL , the LEP Electroweak Working Group). *Precision Electroweak Measurements and Constraints on the Standard Model* CERN-PH-EP/2007-039, MPP-2007-256, arxiv:0712.0929.
- The collaboration (OPAL). *Measurement of the  $e+e^- \rightarrow W+W^-$  cross section and W decay branching fractions at LEP*. *Eur.Phys.J.C* **52**, (2007), 767–785. CERN-PH-EP/2007-027, MPP-2007-257, arxiv:0708.1311.
- The collaboration (OPAL). *Bose-Einstein study of position-momentum correlations of charged pions in hadronic Z0 decays*. *Eur.Phys.J.C* **52**, (2007), 787–803. CERN-PH-EP/2007-025, MPP-2007-258, arxiv:0708.1122.
- The collaboration (OPAL). *Search for Direc Magnetic Monopoles in  $e+e^-$  Collisions with the OPAL Detector at LEP2*. *Phys.Lett.B* **663**, (2008), 37–42. CERN-PH-EP/2007-019, MPP-2007-259, arxiv:0707.0404.
- The collaboration (OPAL). *Search for invisibly decaying Higgs bosons in  $e+e^- \rightarrow Z$  production at  $\sqrt{s} = 183 - 209$  GeV*. *Phys.Lett.B* **682**, (2010), 381–390. CERN-PH-EP/2007-018, MPP-2007-260, arxiv:0707.0373.

- The collaboration (OPAL). *Inclusive Jet Production in Photon-Photon Collisions at  $\sqrt{s_{e,e}}$  from 189 to 209 GeV*. Phys.Lett.B **658**, (2008), 185–192. CERN-PH-EP/2007-016, MPP-2007-261, arxiv:0706.4382.
- Redamy Perez Ramos, Francois Arleo, and Bruno Machet. *Next-to-MLLA corrections to single inclusive  $kt$ -distributions and 2-particle correlations in a jet*. Phys.Rev.D **78**, (2008), 014019. MPP-2007-262, arxiv:0712.2212.
- Franić,  $\frac{1}{2}$ ois Arleo, Redamy Perez Ramos, and Bruno Machet. *hadronic single inclusive  $k_{p,erp}$  distributions inside one jet beyond MLLA*. Phys.Rev.Lett. **100**, (2008), 052002. MPP-2007-263, arxiv:0707.3391.
- W Seidel, G Angloher, M Bauer, I Bavykina, A Bento, A Brown, C Bucci, C Ciemiak, C Coppi, G Deuter, Fv Feilitzsch, D Hauff, S Henry, P Huff, J Imber, S Ingleby, C Isaila, J Jochum, M Kiefer, M Kimmerle, H Kraus, J-C Lanfranchi, R Lang, M Malek, R McGowan, V Mikhailik, E Pantic, F Petricca, S Pfister, W Potzel, F Pröbst, S Roth, K Rottler, C Sailer, K Schäffner, J Schmalzer, S Scholl, L Stodolsky, B Tolhurst, I Usherow-Marshak, and W Westphal. *The CRESST Dark Matter Search*. J.Phys.Conf.Ser. MPP-2007-264.
- J. Adams, V. Eckardt, N. Schmitz, P. Seyboth, et al. (STAR). *Two-particle correlations on transverse momentum and momentum dissipation in Au-Au collisions at  $\sqrt{s_{NN}} = 130$  GeV*. J.Phys.G **34**, (2007), 799–816. MPP-2007-265.
- C. Alt, V. Eckardt, N. Schmitz, P. Seyboth, et al. (NA 49). *Anisotropic Flow of Strange Particles at SPS*. PoS MPP-2007-266, nucl-ex/0611003.
- C. Alt, V. Eckardt, N. Schmitz, P. Seyboth, et al. (NA49). *Energy Dependence of Multiplicity Fluctuations in Heavy Ion Collisions* MPP-2007-267, nucl-ex/0610046.
- Klaus Gottstein. *Erinnerungen an Pugwash und an die Rolle der VDW als deutsche Pugwash-Gruppe*, 35–47 (MPI für Wissenschaftsgeschichte, Berlin). MPP-2007-268 (2007).
- Klaus Gottstein. *The State of Science Advising in Europe*. Atti dei Convegni Lincei **230**, (2007), 27–32. MPP-2007-269.
- Klaus Gottstein and Nele Matz. *Political Problems Facing Governments in Using Scientific Advice, and Legal and Other Problems Facing Scientists when Trying to Give Independent Advice to Governments*. Atti Dei Convegni Lincei **230**, (2007), 33–45. MPP-2007-270.
- Klaus Gottstein. *Why do governments need independent scientific advice? Discussion remark following presentation of paper MPP-2007-270* 66–68. MPP-2007-271.
- W. Lampl, S. Laplace, H. Ma, S. Menke, and G. Unal (Atlas). *Digitization of LAr calorimeter for CSC simulations* ATL-LARG-PUB-2007-011, MPP-2007-272.
- D. Costanzo, I. Hinchliffe, and S. Menke (Atlas). *Analysis Model Forum Report ATL-GEN-INT-2008-001*, MPP-2007-273.
- A. Anisimov, S. Blanchet, and P. Di Bari. *Viability of Dirac phase leptogenesis*. JCAP **0804**, (2008), 033. MPP-2007-274, arxiv:0707.3024.
- S. Blanchet. *Dirac phase leptogenesis*. J.Phys.Conf.Ser. **120**, (2008), 022007. MPP-2007-275, arxiv:0710.0570.
- S. Blanchet and P. Di Bari. *Flavor effects in thermal leptogenesis*. Nucl.Phys.B (Proc.Suppl.) **168**, (2007), 372–374. MPP-2007-276, hep-ph/0702089.
- Christian Kiesling. *Low  $x$  Final States at HERA*. MPP-2007-277.
- S. Chekanov (ZEUS). *Diffraction photoproduction of dijets in ep collisions at HERA*. Eur.Phys.J.C **55**, (2008), 177–191. DESY-07-161, MPP-2007-278, arxiv:0710.1498.
- A. E. Kiryunin and D. Salihagic. *Hadronic Shower Validation Experience for the ATLAS End-Cap Calorimeter*. AIP Conf.Proc. **896**. MPP-2007-279.
- E. rhard Seiler and Ion-Olimpiu Stamatescu. *Approaches to Fundamental Physics: An Assessment of Current Theoretical Ideas*. MPP-2007-280 (2007).
- Klaus Fredenhagen, Karl-Henning Rehren, and Erhard Seiler. *Quantum Field Theory: Where We Are*, vol. 721, 61–87 (Springer-Verlag, New York, Heidelberg ...). MPP-2007-281 (2007).
- Vladimir Chekelian. *Review of Results of the Electron-Proton Collider HERA* MPP-2007-284.
- G. Lutz, R. Andritschke, L. Andricek, R. Eckhardt, J. Englhauer, G. Fuchs, O. Hälker, R. Hartmann, K. Heinzinger, S. Herrmann, P. Holl, N. Kimmel, P. Lechner, N. Meidinger, M. Porro, R. H. Richter, G. Schaller, M. Schnecke, F. Schopper, and H. Soltau et al. *Spectroscopic silicon imaging detectors: Past achievements and new developments*. Nucl.Instrum.Meth.A **580**, (2007), 960–967. MPP-2007-285.
- G. Lutz, L. Andricek, R. Eckardt, O. Hälker, S. Herrmann, P. Lechner, R. Richter, G. Schaller, F. Schopper, H. Soltau, L. Strüder, J. Treis, S. WÄ¶llfl, and C. Zhang. *DEPFET-detectors: New developments*. Nucl.Instrum.Meth.A **572**, (2007), 311–315. MPP-2007-287.
- P. Fischer et al. *Progress towards a large area, thin DEPFET detector module*. Nucl.Instrum.Meth.A **582**, (2007), 843–848. MPP-2007-289.
- S. Woelfel, S. Herrmann, P. Lechner, G. Lutz, M. Porro, R. H. Richter, L. Strüder, and J. Treis. *A novel way of single optical photon detection: beating the  $1/f$  noise limit with ultra high resolution DEPFET-RNDR devices*. IEEE Transactions on Nuclear Science **54**, (2007), 1311–1318. MPP-2007-291.

- G. Lutz et al. *Spectroscopic silicon imaging detectors: Past achievements and new developments*. Nucl.Instrum.Meth.A **580**, (2007), 960–967. MPP-2007-293.
- Stephan Stieberger. *Open & Closed vs. Pure Open String Disk Amplitudes* MPP-2008-1, arxiv:0907.2211.
- B. Dasgupta, A. Dighe, A. Mirizzi, and G. G. Raffelt. *Spectral split in prompt supernova neutrino burst: Analytic three-flavor treatment*. Phys.Rev.D **77**, (2008), 113007. MPP-2008-3, arxiv:0801.1660.
- Stefan Dittmaier, Alois Kabelschacht, and Tobias Kasprzik. *Polarized QED splittings of massive fermions and dipole subtraction for non-collinear-safe observables*. Nucl.Phys.B **800**, (2008), 146–189. MPP-2008-4, arxiv:0802.1405.
- Dieter Lust, Stephan Stieberger, and Tomasz R. Taylor. *The LHC String Hunter's Companion*. Nucl.Phys.B **808**, (2009), 1–52. MPP-2008-5, arxiv:0807.3333.
- Gia Dvali and Dieter Lust. *Power of Black Hole Physics: Seeing through the Vacuum Landscape*. JHEP CERN-PH-TH/2008-003, LMU-ASC 01/08, MPP-2008-6, arxiv:0801.1287.
- Marco Zagermann. *Generalized Chern-Simons Terms and Chiral Anomalies in  $N=1$  Supersymmetry* MPP-2008-7, arxiv:0801.1666.
- A. Denner, B. Jantzen, and S. Pozzorini. *Two-loop electroweak Sudakov logarithms for massive fermion scattering*. PoS **002**. PSI-PR-08-01, MPP-2008-8, arxiv:0801.2647.
- J. Albert. *MAGIC observations of the unidentified TeV gamma-ray source J2032+4130*. Astrophys.J.L. **675**, (2008), L25. MPP-2008-9, arxiv:0801.2391.
- F. Hahn-Woernle and M. Plumacher. *Effects of reheating on leptogenesis*. Nucl.Phys.B **806**, (2009), 68–83. MPP-2008-10, arxiv:0801.3972.
- A. Abada, C. Biggio, F. Bonnet, M. B. Gavela, and T. Hambye.  *$\mu \rightarrow e\gamma$  and  $\tau \rightarrow l\gamma$  decays in the fermion triplet seesaw model*. Phys.Rev.D **78**, (2008), 033007. FTUAM-08-02, IFT-UAM/CSIC-08-12, LPT-Orsay 08-05, ULB-TH/08-04, MPP-2008-11, arxiv:0803.0481.
- The collaboration (H1). *A Search for Excited Neutrinos in  $e$ - $p$  Collisions at HERA*. Phys.Lett.B **663**, (2008), 382–389. DESY 08-009, MPP-2008-12, arxiv:0802.1858.
- Santi Bejar, Jaume Guasch, David Lopez-Val, and Joan Sola. *FCNC-induced heavy-quark events at the LHC from Supersymmetry*. Phys.Lett.B **668**, (2008), 364–372. UB-ECM-PF 08/06, MPP-2008-15, arxiv:0805.0973.
- Allen Caldwell. *Behavior of  $\sigma^{**}(\gamma P)$  at Large Coherence Lengths*. MPP-2008-16, arxiv:0802.0769.
- G. L. Cardoso and V. Grass. *On five-dimensional non-extremal charged black holes and FRW cosmology*. Nucl.Phys.B **803**, (2008), 209–233. LMU-ASC 11/08, MPP-2008-17, 0803.2819.
- H. G. Moser, L. Andricek, X. Chen, A. Frey, G. Lutz, R. H. Richter, M. Schneck, A. Raspereza, S. Rummel, L. Feld, R. Jussen, W. Karpinski, P. Hettkamp, R. Kohrs, M. Karagounis, M. Koch, H. Krueger, P. Lodomez, M. Mathes, L. Reuen, C. Sandow, J. Schneider, E. von Torne, M. Trimpl, J. Velthuis, N. Wermes, W. de Boer, J. Bol, A. Sabellek, P. Fischer, G. Giesen, C. Kreidel, I. Peric, J. Treis, F. Schopper, L. Strueder, Z. Dolezal, Z. Drasal, P. Kodys, P. Kvasnicka, D. Scheirich, I. Carbonell, J. Fuster, C. Lacasta, C. Marinas, and M. Vos. *DEPFET Active Pixel Detectors*. PoS MPP-2008-18.
- Ralph Blumenhagen and Maximilian Schmidt-Sommerfeld. *Power Towers of String Instantons for  $N=1$  Vacua*. JHEP **0807**, (2008), 027. MPP-2008-19, arxiv:0803.1562.
- Steen Hannestad, Alessandro Mirizzi, Georg G. Raffelt, and Yvonne Y. Y. Wong. *Cosmological constraints on neutrino plus axion hot dark matter: Update after WMAP-5*. JCAP **0804**, (2008), 019. MPP-2008-20, arxiv:0803.1585.
- Paul Koerber and Luca Martucci. *Warped generalized geometry compactifications, effective theories and non-perturbative effects*. Fortschr.Phys. **56**, (2008), 862–868. LMU-ASC 15/08, MPP-2008-21, arxiv:0803.3149.
- K. R. Ito and E. Seiler. *Further discussion of Tomboulis' approach to the confinement problem* MPP-2008-22, arxiv:0803.3019.
- Mattias Blennow. *Prospects for cosmic neutrino detection in tritium experiments in the case of hierarchical neutrino masses*. Phys.Rev.D **77**, (2008), 113014. MPP-2008-23, arxiv:0803.3762.
- Andre H. Hoang, Ambar Jain, Ignazio Scimemi, and Iain W. Stewart. *Infrared Renormalization Group Flow for Heavy Quark Masses*. Phys.Rev.Lett. **101**, (2008), 151602. MIT-CTP 3940, MPP-2008-24, arxiv:0803.4214.
- Andre H. Hoang and Stefan Kluth. *Hemisphere Soft Function at  $O(\alpha_s^2)$  for Dijet Production in  $e+e-$  Annihilation* MPP-2008-25, arxiv:0806.3852.
- Michael Haack, Renata Kallosh, Axel Krause, Andrei Linde, Dieter Lust, and Marco Zagermann. *Update of D3/D7-Brane Inflation on  $K3 \times T^2/Z_2$* . Nucl.Phys.B **806**, (2009), 103–177. LMU-ASC 18/08, SU-ITP-2008-08, YITP-2008-25, MPP-2008-26, arxiv:0804.3961.
- T. Jogler, V. Bosch-Ramon, et al. *MAGIC Observations of the HMXB LS I+61 303 in VHE gamma rays*. Nucl.Instrum.Meth.A **588**, (2008), 33–36. MPP-2008-27.
- D. Bastiere (MAGIC). *Highlights of MAGIC results*. Nucl.Instrum.Meth.A **588**, (2008), 1–6. MPP-2008-28.
- Paul Koerber, Dieter Lust, and Dimitrios Tsimpis. *Type IIA AdS4 compactifications on cosets, interpolations and domain walls*. JHEP **0807**, (2008), 017. LMU-ASC 19/08, MPP-2008-29, arxiv:0804.0614.

- F. Lucarelli, F. Goebel, E. Lorenz, N. Otte, et al. *The central pixel of the MAGIC telescope for optical observations*. Nucl.Instrum.Meth.A MPP-2008-30.
- S. Antusch and M. Spinrath. *Quark and lepton masses at the GUT scale including SUSY threshold corrections*. Phys.Rev.D **78**, (2008), 075020. MPP-2008-31, arxiv:0804.0717.
- Jan Hamann, Steen Hannestad, Alessandro Melchiorri, and Yvonne Y. Y. Wong. *Nonlinear corrections to the cosmological matter power spectrum and scale-dependent galaxy bias: implications for parameter estimation*. JCAP **0807**, (2008), 017. LAPTH-1242/08, MPP-2008-33, arxiv:0804.1789.
- S. Antusch, S. F. King, M. Malinsky, L. Velasco-Sevilla, and I. Zavala. *Flavon Inflation*. Phys.Lett.B **666**, (2008), 176–180. DCPT-08-54, IPPP-08-27, SHEP-08-19, MPP-2008-34, arxiv:0805.0325.
- Mattias Blennow, Davide Meloni, Tommy Ohlsson, Francesco Terranova, and Mattias Westerberg. *Non-standard interactions using the OPERA experiment*. Eur.Phys.J.C **56**, (2008), 529–536. RM3-TH/08-7, MPP-2008-35, arxiv:0804.2744.
- W. Hollik, T. Plehn, M. Rauch, and H. Rzehak. *Supersymmetric Higgs Bosons in Weak Boson Fusion*. Phys.Rev.Lett. **102**, (2009), 091802. Edinburgh 2008/16, PSI-PR-08-05, MPP-2008-36, arxiv:0804.2676.
- S. Antusch and E. Fernandez-Martinez. *Signals of CPT Violation and Non-Locality in Future Neutrino Oscillation Experiments*. Phys.Lett.B **665**, (2008), 190–196. MPP-2008-37, arxiv:0804.2820.
- S. Aoki, J. Balog, and P. Weisz. *Bethe–Salpeter wave functions in integrable models*. Prog.Theor.Phys. **121**, (2009), 1003–1034. UTHEP 562, MPP-2008-38, arxiv:0805.3098.
- Martin Ammon, Johanna Erdmenger, Stephan Hühne, Dieter Lust, and Rene Meyer. *Fayet-Iliopoulos Terms in AdS/CFT with Flavour*. JHEP **0807**, (2008), 068. LMU-ASC 27/08, MPP-2008-40, arxiv:0805.1917.
- Johanna Knapp and Emanuel Scheidegger. *Towards Open String Mirror Symmetry for One-parameter Calabi-Yau Hypersurfaces* MPP-2008-42, arxiv:0805.1013.
- Wolfgang Ochs. *Searching for the Scalar Glueball*. AIP Conf.Proc. **1030**, (2008), 207–212. MPP-2008-43, arxiv:0805.0997.
- G. Mennessier, S. Narison, and W. Ochs. *Glueball nature of the  $\sigma/f_0(600)$  from  $\pi\text{-}\pi$  and  $\gamma\text{-}\gamma$  scatterings*. Phys.Lett.B **665**, (2008), 205–211. MPP-2008-44, arxiv:0804.4452.
- Mattias Blennow and Tommy Ohlsson. *Approximative two-flavor framework for neutrino oscillations with non-standard interactions*. Phys.Rev.D **78**, (2008), 093002. MPP-2008-45, arxiv:0805.2301.
- Kevin Dusling, Johanna Erdmenger, Matthias Kaminski, Felix Rust, Derek Teaney, and Clint Young. *Quarkonium transport in thermal AdS/CFT*. JHEP **0810**, (2008), 098. MPP-2008-46, arxiv:0808.0957.
- B. Dasgupta, A. Dighe, A. Mirizzi, and G. G. Raffelt. *Collective neutrino oscillations in non-spherical geometry*. Phys.Rev.D **78**, (2008), 033014. TIFR/TH/08-19, MPP-2008-47, arxiv:0805.3300.
- Thomas Schweizer, Robert Wagner, and Eckart Lorenz. *A Statistical Study of Sub-Hour Flares of the VHE Gamma-Ray Emission of Markarian 421 During A High-Flux State in 2001*. Astrophys.J. MPP-2008-48.
- Monika Blanke, Andrzej J. Buras, Stefan Recksiegel, and Cecilia Tarantino. *The Littlest Higgs Model with T-Parity Facing CP-Violation in  $B_s$  - anti- $B_s$  Mixing* TUM-HEP-689/08, RM3-TH/08-1, MPP-2008-50, arxiv:0805.4393.
- A. Abdesselam. *Engineering for the ATLAS SemiConductor Tracker (SCT) End-cap*. J.Inst. **3**. MPP-2008-51.
- J. Albert et al. *MAGIC Observations of a 13-Day Flare Complex in M87 in February 2008*. Astrophys.J.L. **23**. MPP-2008-52, arxiv:0806.0988.
- Wolfgang Hollik and Edoardo Mirabella. *Squark anti-squark pair production at the LHC: the electroweak contribution*. JHEP **12**, (2008), 087. MPP-2008-53, arxiv:0806.1433.
- Wolfgang Hollik, Edoardo Mirabella, and Maike K. Trenkel. *Electroweak contributions to squark–gluino production at the LHC*. JHEP **0902**, (2009), 002. MPP-2008-54, arxiv:0810.1044.
- Anders Basboll, Ole Eggers Bjælde, Steen Hannestad, and Georg G. Raffelt. *Are cosmological neutrinos free-streaming?* Phys.Rev.D **79**, (2009), 043512. MPP-2008-55, arxiv:0806.1735.
- Enrique Fernandez-Martinez and Licia Verde. *Prospects in Constraining the Dark Energy Potential*. JCAP **08**, (2008), 023. MPP-2008-56, arxiv:0806.1871.
- Frank Daniel Steffen. *Probing the Reheating Temperature at Colliders and with Primordial Nucleosynthesis*. Phys.Lett.B **669**, (2008), 74–80. MPP-2008-58, arxiv:0806.3266.
- C. Biggio. *The contribution of fermionic seesaws to the anomalous magnetic moment of leptons*. Phys.Lett.B **668**, (2008), 378–384. MPP-2008-59, arxiv:0806.2558.
- Ralph Blumenhagen, Sebastian Moster, and Erik Plauschinn. *String GUT Scenarios with Stabilised Moduli*. Phys.Rev.D **78**, (2008), 066008. MPP-2008-60, arxiv:0806.2667.
- Claudio Caviezel, Paul Koerber, Simon Kors, Dieter Lust, Dimitrios Tsimpis, and Marco Zagermann. *The effective theory of type IIA AdS4 compactifications on nilmanifolds*

- and cosets. *Class.Quant.Grav.* **26**, (2009), 025014. LMU-ASC 37/08, MPP-2008-62, arxiv:0806.3458.
- Maxim Pospelov, Josef Pradler, and Frank Daniel Steffen. *Constraints on Supersymmetric Models from Catalytic Primordial Nucleosynthesis of Beryllium*. *JCAP* **0811**, (2008), 020. UVIC-TH-08/13, MPP-2008-63, arxiv:0807.4287.
- Johanna Erdmenger, Matthias Kaminski, Patrick Kerner, and Felix Rust. *Finite baryon and isospin chemical potential in AdS/CFT with flavor*. *JHEP* **11**, (2008), 031. MPP-2008-65, arxiv:0807.2663.
- A. Esteban-Pretel, A. Mirizzi, S. Pastor, R. Tomas, G. G. Raffelt, P. D. Serpico, and G. Sigl. *Role of dense matter in collective supernova neutrino transformations*. *Phys.Rev.D* **78**, (2008), 085012. FERMILAB-PUB-08-207-A, IFIC/08-34, MPP-2008-66, arxiv:0807.0659.
- Robert Wagner. *Correlated Variability in Blazars* MPP-2008-68, arxiv:0808.2843.
- Paolo Gondolo and Georg Raffelt. *Solar neutrino limit on the axion-like interpretation of the DAMA signal* MPP-2008-69, arxiv:0807.2926.
- The collaboration (H1). *Search for Excited Electrons in ep Collisions at HERA*. *Phys.Lett.B* **666**, (2008), 131–139. DESY 08-052, MPP-2008-70, arxiv:0805.4530.
- The collaboration (H1). *Measurement of the Proton Structure Function  $F_L$  at Low  $x$* . *Phys.Lett.B* **665**, (2008), 139–146. DESY 08-053, MPP-2008-71, arxiv:0805.2809.
- The collaboration (H1). *Multi-Lepton Production at High Transverse Momenta in ep Collisions at HERA*. *Phys.Lett.B* **668**, (2008), 268–276. DESY 08-065, MPP-2008-72, arxiv:0806.3987.
- Stefan Dittmaier, Stefan Kallweit, and Peter Uwer. *NLO QCD corrections to  $pp \rightarrow WW + \text{jet} + X$* . *Nucl.Phys.B (Proc.Suppl.)* **183**, (2008), 279–284. MPP-2008-73, arxiv:0807.0708.
- Stefan Antusch, Jochen P. Baumann, and Enrique Fernandez-Martinez. *Non-Standard Neutrino Interactions with Matter from Physics Beyond the Standard Model*. *Nucl.Phys.B* **810**, (2009), 369–388. MPP-2008-74, arxiv:0807.1003.
- Steve Blanchet and Pasquale Di Bari. *New aspects of leptogenesis bounds*. *Nucl.Phys.B* **807**, (2009), 155–187. MPP-2008-76, arxiv:0807.0743.
- Axel Bredenstein, Ansgar Denner, Stefan Dittmaier, and Stefano Pozzorini. *NLO QCD corrections to  $pp \rightarrow t\bar{b}b + X$  via quark anti-quark annihilation*. *Nucl.Phys.B (Proc.Suppl.)* **183**, (2008), 226–231. PSI-PR-08-10, MPP-2008-78, arxiv:0807.1453.
- Karsten Berger, Daniel Mazin, Diego Tescaro, and Robert Wagner. *Monitoring of the Radio Galaxy M87 with the MAGIC Telescope* MPP-2008-79.
- Thomas Schweizer, Robert Wagner, and Eckart Lorenz. *A Statistical Study Of Sub-Hour Flares of the VHE Gamma-Ray Emission of Markarian 421 During a High Flux State in 2001*. *AIP Conf.Proc.* MPP-2008-80.
- Wlodek Bednarek and Robert Wagner. *Modeling the Delayed Emission in the 2005 Mkn 501 Very-High-Energy Gamma-Ray Flare* MPP-2008-81.
- Andre H. Hoang, Vicent Mateu, and S. Mohammad Zebarjad. *Heavy Quark Vacuum Polarization Function at  $O(\alpha_s^2)$  and  $O(\alpha_s^3)$* . *Nucl.Phys.B* **813**, (2009), 349–369. MPP-2008-83, arxiv:0807.4173.
- The collaboration (MAGIC Collaboration: J. Albert et al.). *Very-High-Energy Gamma Rays from a Distant Quasar: How Transparent is the Universe?*. *Science* **320**, (2008), 1752–1754. MPP-2008-84, arxiv:0807.2822.
- Luis A Anchordoqui, Haim Goldberg, Dieter Lust, Satoshi Nawata, Stephan Stieberger, and Tomasz R. Taylor. *Di-jet signals for low mass strings at the LHC*. *Phys.Rev.Lett.* **101**, (2008), 241803. LMU-ASC 42/08, NUB-3262-TH-08, MPP-2008-86, arxiv:0808.0497.
- Dieter Lust, Fernando Marchesano, Luca Martucci, and Dimitrios Tsimpis. *Generalized non-supersymmetric flux vacua* LMU-ASC 41/08, CERN-PH-TH/2008-162, MPP-2008-87, arxiv:0807.4540.
- Jan Hamann, Steen Hannestad, Martin S. Sloth, and Yvonne Y. Y. Wong. *Observing trans-Planckian ripples in the primordial power spectrum with future large scale structure probes*. *JCAP* **0809**, (2008), 015. LAPTH-1263/08, MPP-2008-88, arxiv:0807.4528.
- Ansgar Denner, Bernd Jantzen, and Stefano Pozzorini. *Two-loop electroweak next-to-leading logarithms for processes involving heavy quarks*. *JHEP* **0811**, (2008), 062. PSI-PR-08-11, MPP-2008-89, arxiv:0809.0800.
- Stefan Antusch, Subinoy Das, and Koushik Dutta. *Phenomenology of Hybrid Scenarios of Neutrino Dark Energy*. *JCAP* **0810**, (2008), 016. MPP-2008-90, arxiv:0807.4930.
- H. K. Dreiner, S. Grab, and M. K. Trenkel. *Stau-LSP Phenomenology: Two- versus Four-Body Decay Modes. Example: Resonant Single Slepton Production at the LHC*. *Phys.Rev.D* **79**, (2009), 016002. BONN-TH-2008-08, MPP-2008-92, arxiv:0808.3079.
- Andre H. Hoang and Iain W. Stewart. *Top Mass Measurements from Jets and the Tevatron Top-Quark Mass*. *Nucl.Phys.B (Proc.Suppl.)* **185**, (2008), 220–226. MIT-CTP 3966, MPP-2008-93, arxiv:0808.0222.
- Stefan Antusch, Stephen F. King, Michal Malinsky, and Graham G. Ross. *Solving the SUSY Flavour and CP Problems with Non-Abelian Family Symmetry and Supergravity*. *Phys.Lett.B* **670**, (2009), 383–389. MPP-2008-95, arxiv:0807.5047.

- Jan De Rydt, Torsten T. Schmidt, Mario Trigiante, Antoine Van Proeyen, and Marco Zagermann. *Electric/magnetic duality for chiral gauge theories with anomaly cancellation*. JHEP **0812**, (2008), 105. CERN-PH-TH/2008-172, KUL-TF-08/15, MPP-2008-97, arxiv:0808.2130.
- G. Raffelt, S. Hannestad, A. Mirizzi, and Y. Y. Y. Wong. *Axion hot dark matter bounds* MPP-2008-99, arxiv:0808.0814.
- T. Bretz, D. Dorner, R. M. Wagner, and P. Sawallisch. *The Drive System of the Major Atmospheric Gamma-ray Cherenkov Imaging Telescope*. Astropart.Phys. MPP-2008-101, arxiv:0810.4593.
- E. Lindfors, D. Mazin, K. Nilsson, and L. Takalo (MAGIC). *Optically triggered target of opportunity observations with the MAGIC Telescope*. PoS MPP-2008-102.
- E. Carmona, P. Majumdar, A. Moralejo, V. Vitale, D. Sobczynska, M. Haffke, C. Bigongiari, N. Otte, G. Cabras, M. De Maria, and F. De Sabata. *Monte Carlo Simulation for the MAGIC-II System*. Proc. 30th Int. Cosmic Ray Conf. Vol. 3 (OG part 2) 1373–1376. MPP-2008-103, arxiv:0709.2959.
- J. Rico, E de Ona-Wilhelmi, J. Cortina, and E. Lorenz. *Observations of Very High Energy Gamma-Rays during Moonlight and Twilight with the MAGIC Telescope*. Proc. 30th Int. Cosmic Ray Conf. Vol. 3 (OG part 2) 1365–1368. MPP-2008-104, arxiv:0709.2283.
- Sergio Pastor, Teguayco Pinto, and Georg Raffelt. *Relic density of neutrinos with primordial asymmetries*. Phys.Rev.Lett. **102**, (2009), 241302. IFIC/07-59, MPP-2008-105, arxiv:0808.3137.
- Fernando Cornet and Wolfgang Hollik. *Pair Production of Two-Higgs-Doublet Model Higgs Bosons in  $\gamma\gamma$  Collisions*. Phys.Lett.B **669**, (2008), 59–61. MPP-2008-106, arxiv:0808.0719.
- Josef Pradler and Frank Daniel Steffen. *Thermal relic abundances of long-lived staus*. Nucl.Phys.B **809**, (2009), 318–346. MPP-2008-107, arxiv:0808.2462.
- Stefan Antusch, Mar Bastero-Gil, Koushik Dutta, Steve F. King, and Philipp M. Kostka. *Solving the  $\eta$ -Problem in Hybrid Inflation with Heisenberg Symmetry and Stabilized Modulus*. JCAP **0901**, (2009), 040. CAFPE-103/08, UGFT-233/08, MPP-2008-108, arxiv:0808.2425.
- Christian Kiesling. *Implication of the HERA Measurements on Astroparticle Data Interpretation* MPP-2008-110.
- Yvonne Y. Y. Wong. *Higher order corrections to the large scale matter power spectrum in the presence of massive neutrinos*. JCAP **0810**, (2008), 035. MPP-2008-111, arxiv:0809.0693.
- The collaboration (H1). *Study of Charm Fragmentation into  $D^{*\pm}$  Mesons in Deep-Inelastic Scattering at HERA*. Eur.Phys.J.C **2009**, (2009), 1–18. DESY-08-080, MPP-2008-112, arxiv:0808.1003.
- Georg G. Raffelt. *Self-induced parametric resonance in collective neutrino oscillations*. Phys.Rev.D **78**, (2008), 125015. MPP-2008-113, arxiv:0810.1407.
- Y. Y. Y. Wong, S. Hannestad, A. Mirizzi, and G. Raffelt. *Cosmological limits on axions* MPP-2008-114.
- Monika Blanke, Andrzej J. Buras, Bjoern Duling, Stefania Gori, and Andreas Weiler. *Delta F=2 Observables and Fine-Tuning in a Warped Extra Dimension with Custodial Protection*. JHEP **03**, (2009), 001. TUM-HEP-698/08, MPP-2008-115, arxiv:0809.1073.
- Robert Wagner. *Scientific Highlights from Observations of Active Galactic Nuclei with the MAGIC Telescope*. AIP Conf. Ser. **1085**, (2008), 399. MPP-2008-117, arxiv:0810.1068.
- W. Bednarek and R. M. Wagner. *Modeling the Delayed Emission in the 2005 Mkn 501 Very-High-Energy Gamma-Ray Flare* MPP-2008-118.
- K. Berger, R. M. Wagner, M. Hayashida, D. Kranich, E. Lindfors, and E. Lorenz (V. Vitale on behalf of the MAGIC). *Observations of BL Lacertae with the MAGIC Telescope* MPP-2008-119.
- Robert Wagner and Wlodek Bednarek. *Modeling the Delayed Emission in the 2005 July Flare of Mkn 501* MPP-2008-120.
- W. Hollik, M. Kollar, E. Mirabella, and M. K. Trenkel. *Hadronic Production of Colored SUSY Particles with Electroweak NLO Contributions*. AIP Conf.Proc. **1078**, (2009), 250–252. MPP-2008-121, arxiv:0810.1138.
- Luzi Bergamin and Rene Meyer. *Wolfgang Kummer and the Vienna School of Dilaton (Super-)Gravity* (World Scientific). MPP-2008-123. arxiv:0809.2245.
- C. Biggio. *Low energy processes to distinguish among seesaw models*. NuovoCim.B **123**, (2008), 880–882. MPP-2008-125, arxiv:0809.3922.
- G. Angloher, M. Bauer, I. Bavykina, A. Bento, A. Brown, C. Bucci, C. Ciemiak, C. Coppi, G. Deuter, F. von Feilitzsch, D. Hauff, S. Henry, P. Huff, J. Imber, S. Ingleby, C. Isaila, J. Jochum, M. Kiefer, M. Kimmerle, H. Kraus, J. C. Lanfranchi, R. F. Lang, B. Majorovits, M. Malek, R. McGowan, V. B. Mikhailik, E. Pantic, F. Petricca, S. Pfister, W. Potzel, F. Proebst, W. Rau, S. Roth, K. Rottler, C. Sailer, K. Schaeffner, J. Schmalzer, S. Scholl, W. Seidel, L. Stodolsky, A. J. B. Tolhurst, I. Usherov, and W. Westphal (CRESST). *Commissioning Run of the CRESST-II Dark Matter Search*. Astropart.Phys. **31**, (2009), 270–276. MPP-2008-126, arxiv:0809.1829.
- Carla Biggio, Mattias Blennow, and Enrique Fernandez-Martinez. *Loop bounds on non-standard neutrino interactions*. JHEP **0903**, (2009), 139. GEF-TH-2-09, MPP-2008-127, 0902.0607.

- S. Aoki, J. Balog, T. Hatsuda, N. Ishii, K. Murano, H. Nemura, and P. Weisz. *Energy dependence of nucleon-nucleon potentials*. PoS LATTICE **2008**, (2008), 152. MPP-2008-128, arxiv:0812.0673.
- Malcolm Fairbairn, Timur Rashba, and Sergey Troitsky. *Gamma-ray halo around 3C 279: looking through the Sun on October 8* MPP-2008-129, arxiv:0809.4886.
- Frank Daniel Steffen. *Dark Matter Candidates*. Eur.Phys.J.C **59**, (2009), 557–588. MPP-2008-130, arxiv:0811.3347.
- S. Bethke, S. Kluth, C. Pahl, and J. Schieck (JADE). *Determination of the Strong Coupling  $\alpha_s$  from hadronic Event Shapes and NNLO QCD predictions using JADE Data*. Eur.Phys.J.C **64**, (2009), 351–360. MPP-2008-131, arxiv:0810.1389.
- M. Beneke, P. Ruiz-Femenia, and M. Spinrath. *Higgs couplings in the MSSM at large  $\tan(\beta)$* . JHEP **01**, (2009), 031. PITHA 08-27, MPP-2008-132, arxiv:0810.3768.
- Martin Ammon, Johanna Erdmenger, Matthias Kaminski, and Patrick Kerner. *Superconductivity from gauge/gravity duality with flavor*. Phys.Lett.B **680**, (2009), 516–520. IFT-UAM/CSIC-08-65, MPP-2008-133, arxiv:0810.2316.
- Mattias Blennow, Alessandro Mirizzi, and Pasquale D. Serpico. *Nonstandard neutrino-neutrino refractive effects in dense neutrino gases*. Phys.Rev.D **78**, (2008), 113004. CERN-PH-TH/2008-223, FERMILAB-PUB-08-532-A, MPP-2008-134, arxiv:0810.2297.
- Christoph Pahl, Siegfried Bethke, Stefan Kluth, and Jochen Schieck. *Study of moments of event shapes and a determination of  $\alpha_s$  using  $e^+e^-$  annihilation data from JADE*. Eur.Phys.J.C **60**, (2009), 181–196. MPP-2008-135, arxiv:0810.2933.
- Andre H. Hoang, Christoph J. Reisser, and Pedro Ruiz-Femenia. *Implementing invariant mass cuts and finite lifetime effects in top production at threshold*. Nucl.Phys.B (Proc.Suppl.) **186**, (2009), 403–406. SFB/CPP-08-84, PITHA 08/28, MPP-2008-137, arxiv:0810.2934.
- E. Arik, S. Aune, D. Autiero, K. Barth, A. Belov, B. Beltrán, S. Borghi, G. Bourlis, F. S. Boydag, H. Bräuninger, J. M. Carmona, S. Cebrián, S. A. Cetin, J. I. Collar, T. Dafni, M. Davenport, L. Di Lella, O. B. Dogan, C. Eleftheriadis, N. Elias, G. Fanourakis, E. Ferrer-Ribas, H. Fischer, P. Friedrich, J. Franz, J. Galán, T. Geralis, I. Giomataris, S. Gninenko, H. Gómez, R. Hartmann, M. Hasinoff, F. H. Heinsius, I. Hikmet, D. H. H. Hoffmann, I. G. Irastorza, J. Jacoby, K. Jakovčić, D. Kang, K. Königsmann, R. Kotthaus, M. Krčmar, K. Kousouris, M. Kuster, B. Lakić, C. Lasseur, A. Liolios, A. Ljubičić, G. Lutz, G. Luzón, D. Miller, J. Morales, T. Niinikoski, A. Nordt, A. Ortiz, T. Papaevangelou, M. J. Pivovarov, A. Placci, G. Raffelt, H. Riege, A. Rodríguez, J. Ruz, I. Savvidis, Y. Semertzidis, P. Serpico, R. Soufli, L. Stewart, K. van Bibber, J. Villar, J. Vogel, L. Walckiers, and K. Zioutas (CAST). *Probing  $eV$ -scale axions with CAST*. JCAP **0902**, (2009), 008. MPP-2008-138, arxiv:0810.4482.
- J. Barranco, O. G. Miranda, and T. I. Rashba. *Probing non-standard interactions with reactor neutrinos*. Nucl.Phys.B (Proc.Suppl.) **188**, (2009), 214–216. MPP-2008-140, arxiv:0810.5361.
- Andy O’Bannon. *Toward a Holographic Model of Superconducting Fermions*. JHEP **0901**, (2009), 074. MPP-2008-141, arxiv:0811.0198.
- L. Stodolsky. *Some Practical Applications of Dark Matter Research*. J.Phys.Conf.Ser. **173**, (2009), 012001. MPP-2008-142, arxiv:0810.4446.
- Ralph Blumenhagen, Volker Braun, Thomas W. Grimm, and Timo Weigand. *GUTs in Type IIB Orientifold Compactifications*. Nucl.Phys.B **815**, (2009), 1–94. MPP-2008-144, arxiv:0811.2936.
- Erik Plauschinn. *The Generalized Green-Schwarz Mechanism for Type IIB Orientifolds with D3- and D7-Branes*. JHEP **0905**, (2009), 062. MPP-2008-145, arxiv:0811.2804.
- G. Aad et al. (ATLAS). *The ATLAS Experiment at the CERN Large Hadron Collider*. J.Inst. **3**, (2008), S08003. MPP-2008-146.
- Ralph Blumenhagen. *Gauge Coupling Unification in F-theory GUT Models*. Phys.Rev.Lett. **102**, (2009), 071601. MPP-2008-147, arxiv:0812.0248.
- Timur Rashba. *Constraining neutrino properties with low energy experiments*. J.Phys.Conf.Ser. **136**. MPP-2008-149.
- I. Donnarumma et al. *The June 2008 flare of Markarian 421 from optical to TeV energies*. Astrophys.J.L. MPP-2008-150.
- Stefan Antusch, Stephen F. King, and Michal Malinsky. *Perturbative Estimates of Lepton Mixing Angles in Unified Models*. Nucl.Phys.B **820**, (2009), 32–46. MPP-2008-151, arxiv:0810.3863.
- Monika Blanke, Andrzej J. Buras, Bjoern Duling, Katrin Gemmler, and Stefania Gori. *Rare K and B Decays in a Warped Extra Dimension with Custodial Protection*. JHEP **0903**, (2009), 108. TUM-HEP-704/08, MPP-2008-152, arxiv:0812.3803.
- H. Anderhub et al. (MAGIC). *MAGIC upper limits to the VHE gamma-ray flux of 3C454.3 in high emission state*. Astron.Astrophys. MPP-2008-153, arxiv:0811.1680.
- E. Aliu (MAGIC). *Discovery of a very high energy gamma-ray signal from the 3C 66A/B region*. Astrophys.J.L. **692**, (2009), 29–33. MPP-2008-154, arxiv:0810.4712.
- The collaboration (MAGIC). *Improving the performance of the single-dish Cherenkov telescope MAGIC through the use of signal timing*. Astropart.Phys. **30**, (2009), 293–305. MPP-2008-156, arxiv:0810.3568.

- E. Aliu (MAGIC). *MAGIC upper limits on the VHE gamma-ray emission from the satellite galaxy Willman 1*. *Astrophys.J.* MPP-2008-157, arxiv:0810.3561.
- Carla Biggio, Eduard Masso, and Javier Redondo. *Mixing of photons with massive spin-two particles in a magnetic field*. *Phys.Rev.D* **79**, (2009), 015012. UAB-FT-598, FTUAM-06-02, IFT-UAM/CSIC-06-10, DESY-08-167, MPP-2008-158, hep-ph/0604062.
- Johanna Knapp and Emanuel Scheidegger. *Matrix Factorizations, Massey Products and F-Terms for Two-Parameter Calabi-Yau Hypersurfaces* MPP-2008-160, arxiv:0812.2429.
- Claudio Caviezel, Paul Koerber, Simon Kors, Dieter Lust, Timm Wrase, and Marco Zagermann. *On the Cosmology of Type IIA Compactifications on  $SU(3)$ -structure Manifolds*. *JHEP* **0904**, (2009), 010. LMU-ASC 64/08, ESI-2105, MPP-2008-165, arxiv:0812.3551.
- Andreas Karch, Andy O'Bannon, and Ethan Thompson. *The Stress-Energy Tensor of Flavor Fields from AdS/CFT*. *JHEP* MPP-2008-166.
- Keiichi R. Ito and Erhard Seiler. *Critical discussion of Tomboulis' approach to the confinement problem*. *PoS(Confinement8)* **034**. MPP-2008-168, arxiv:0901.4246.
- Raphael Flauger, Sonia Paban, Daniel Robbins, and Timm Wrase. *On Slow-roll Moduli Inflation in Massive IIA Supergravity with Metric Fluxes*. *Phys.Rev.D* **79**, (2009), 086011. UTTG-09-08, MPI-2008-170, MPP-2008-170, arxiv:0812.3886.
- Javier Rico and Robert Wagner. *Status and recent results of MAGIC*. *AIP Conf.Proc.* MPP-2008-171.
- Robert Wagner. *Exploring Quantum Gravity with Very-High-Energy Gamma-Ray Instruments - Prospects and Limitations*. *AIP Conf.Proc.* **1112**, (2009), 187. MPP-2008-172, arxiv:0901.2932.
- Konstancja Satalecka, Ching-Cheng Hsu, Elisa Bernardini, Giacomo Bonnoli, Nicola Galante, Florian Goebel, Elina Lindfors, Pratik Majumdar, Antonio Stamerra, and Robert Wagner. *Monitoring of Bright Blazars with MAGIC in the 2007/8 Season*. *AIP Conf.Proc.* **1112**, (2009), 223. MPP-2008-173, arxiv:0902.4594.
- D. Mazin (MAGIC). *Constraints on Extragalactic Background Light from Cherenkov Telescopes: status and perspectives for the next 5 years* MPP-2008-174.
- Konstancja Satalecka, Ching-Cheng Hsu, Elisa Bernardini, et al. (MAGIC). *Monitoring of Bright Blazars with MAGIC in the 2007/2008 Season* MPP-2008-175.
- R. De los Reyes (MAGIC). *Recent results on galactic sources with the MAGIC telescope*. *Nucl.Phys.B (Proc.Suppl.)* **190**, (2009), 313–316. MPP-2008-176.
- V. Scalzotto (MAGIC). *Recent results from the observation of extragalactic gamma sources with the MAGIC telescope*. *Nucl.Phys.B (Proc.Suppl.)* **190**, (2009), 308–312. MPP-2008-177.
- E. Lindfors, D. Mazin, M. Hayashida, and P. Majumdar (MAGIC). *Target of Opportunity Observations of Blazars with the MAGIC Telescope* MPP-2008-178.
- Iris Abt, Allen Caldwell, Kevin Kroeninger, Jing Liu, Xiang Liu, and Bela Majorovits. *Neutron interactions as seen by a segmented germanium detector*. Other MPP-2008-179.
- Michael Kiefer, Franz Pröbst, Godehard Angloher, Irina Bavykina, Dieter Hauff, and Wolfgang Seidel. *Glued CaWO4 detectors for the CRESST-II experiment*. *Optical Materials* MPP-2008-180, arxiv:0809.4975.
- A. Abdesselam et. al. (ATLAS). *The integration and engineering of the ATLAS SemiConductor Tracker Barrel*. *J.Inst.* **3**, (2008), P10006. MPP-2008-181.
- Iris Abt, Allen Caldwell, Kevin Kroeninger, Jing Liu, Xiang Liu, and Bela Majorovits. *Test of pulse shape analysis using simple Compton scattering*. *Eur.Phys.J.C* **54**, (2008), 425–433. MPP-2008-182.
- Bela Majorovits. *The GERDA Neutrinoless-Double-Beta decay experiment*. *PoS* MPP-2008-183.
- F. Legger (on behalf of the ATLAS). *Data-driven estimation of Standard Model backgrounds to SUSY searches in ATLAS* MPP-2008-184.
- A. Engl, R. Hertenberger, O. Kortner, H. Kroha, F. Legger, R. Richter, and F. Rauscher. *Precision Drift-Tube Chambers for the ATLAS Muon Spectrometer at Super-LHC* MPP-2008-185.
- T. Lari, L. Pape, W. Porod, J. A. Aguilar-Saavedra, F. del Aguila, B. C. Allanach, J. Alwall, Yu. Andreev, D. Ariztizabal Sierra, A. Bartl, M. Beccaria, S. Bejar, L. Benucci, S. Bitjukov, I. Borjanovic, G. Bozzi, G. Burdman, J. Carvalho, N. Castro, B. Clerbaux, F. de Campos, A. de Gouvea, C. Dennis, A. Djouadi, O. J. P. Eboli, U. Ellwanger, D. Fassouliotis, P. M. Ferreira, R. Frederix, B. Fuks, J. M. Gerard, A. Giammanco, S. Gopalakrishna, T. Goto, B. Grzadkowski, J. Guasch, T. Hahn, S. Heinemeyer, A. Hektor, M. Herquet, B. Herrmann, K. Hidaka, M. K. Hirsch, K. Hohenwarter-Sodek, W. Hollik, G. W. S. Hou, T. Hurth, A. Ibarra, J. Illana, M. Kadastik, S. Kalinin, C. Karafasoulis, M. Karagoz Unel, T. Kernreiter, M. M. Kirsanov, M. Klasen, E. Kou, C. Kourkoumelis, S. Kraml, N. Krasnikov, and F. Krauss. *Collider aspects of flavour physics at high  $Q$* . *Eur.Phys.J.C* **57**, (2008), 183–308. MPP-2008-186, arxiv:0801.1800.
- The collaboration (H1). *Strangeness Production at low  $Q^2$  in Deep-Inelastic ep Scattering at HERA*. *Eur.Phys.J.C* **61**, (2009), 185–205. DESY-08-095, MPP-2008-187, arxiv:0810.4036.
- The collaboration (H1). *Events with Isolated Leptons and Missing Transverse Momentum and Measurement of*

- W Production at HERA*. Eur.Phys.J.C **64**, (2009), 251–271. DESY-08-170, MPP-2008-188, arxiv:0901.0488.
- The collaboration (H1). *Inclusive Photoproduction of  $\rho^0$ ,  $K^{*0}$  and  $\phi$  Mesons at HERA*. Phys.Lett.B **673**, (2009), 119–126. DESY-08-172, MPP-2008-189, arxiv:0901.0477.
- The collaboration (H1). *A General Search for New Phenomena at HERA*. Phys.Lett.B **674**, (2009), 257–268. DESY-08-173, MPP-2008-190, arxiv:0901.0507.
- Jörg Dubbert, Oliver Kortner, Hubert Kroha, Federica Legger, Robert Richter, Albert Engl, Ralf Hertenberger, and Felix Rauscher. *Precision Drift-Tube Chambers for the ATLAS Muon Spectrometer at Super-LHC* MPP-2008-191.
- Bernhard Bittner, Steffen Kaiser, Oliver Kortner, Sergey Kotov, Hubert Kroha, Igor Potrap, Robert Harrington, Jeremy Love, and Nigel Nation. *Alignment of the ATLAS Muon Spectrometer with Muon Tracks* MPP-2008-192.
- Klaus Gottstein. *Carl Friedrich von Weizsäcker und die Pugwash Conferences on Science and World Affairs* (LIT Verlag Dr. W. Hopf, Berlin). MPP-2008-193 (2008).
- P. Majumdar and The MAGIC Collaboratin. *A MAGIC view of the Very High Energy  $\gamma$ -ray Sky*. Nucl.Phys.B (Proc.Suppl.) **196**, (2009), 221–226. MPP-2008-195.
- S. C. Commichau, A. Biland, et al. (MAGIC). *Monte Carlo Studies of Geomagnetic Field Effects on the Imaging Air Cherenkov Technique for the MAGIC Telescope Site*. Nucl.Instrum.Meth.A **595**, (2008), 572–586. MPP-2008-196, arxiv:0802.2551.
- E. Aliu (MAGIC). *First bounds on the high-energy emission from isolated Wolf-Rayet binary systems*. Astrophys.J.L. **685**, (2008), L71. MPP-2008-197, arxiv:0808.1832.
- J. Albert et al. (MAGIC). *MAGIC Observations of PG 1553+113 during a Multi-Wavelength Campaign in July 2006*. Astron.Astrophys. **493**, (2009), 467–469. MPP-2008-199.
- E. Aliu (MAGIC). *Observation of Pulsed Gamma-Rays above 25 GeV From the Crab Pulsar with MAGIC*. Science **322**, (2008), 1221–1224. MPP-2008-200.
- J. Albert (MAGIC). *Multi-wavelength (radio, X-ray and gamma-ray) observations of the gamma-ray binary LS I +61 303*. Astrophys.J. **684**, (2008), 1351–1358. MPP-2008-201, arxiv:0801.3150.
- J. Rico (MAGIC). *Observations Of Microquasar Candidates With The MAGIC Telescope* MPP-2008-202.
- J. Rico (MAGIC). *Results of MAGIC on Galactic sources* 183–186. MPP-2008-203.
- N. Galante, D. Bastieri, G. Gaug, M. Garczarezyk, et al. *MAGIC Observation of the Prompt and Afterglow Emission from GRBs*. AIP Conf.Proc. **1000**, (2008), 125–128. MPP-2008-204.
- T. Jogler et al. (MAGIC). *A MAGIC study of the gamma-ray binary LS I+61i;  $\frac{1}{2}$ 303*. AIP Conf.Proc. **1085**, (2008), 211–214. MPP-2008-205.
- N. Galante (MAGIC). *Observation and Upper Limits of GRBs with the MAGIC Telescope*. AIP Conf.Proc. **1085**, (2008), 411–414. MPP-2008-206.
- D. Mazin (MAGIC). *Very-High-Energy Gamma-Ray Observations of a Strong Flaring Activity in M 87 in 2008 February*. AIP Conf.Proc. **1085**, (2008), 541–544. MPP-2008-208.
- D. Hadasch, T. Bretz, and D. Mazin (MAGIC). *High zenith angle observations of PKS 2155-304 with the MAGIC telescope*. AIP Conf.Proc. **1085**, (2008), 557–560. MPP-2008-209.
- Elina J. Lindfors (Daniel Mazin. The MAGIC). *Optically Triggered Target of Opportunity VHE -Gamma ray Observations with the MAGIC Telescope*. AIP Conf.Proc. **1085**, (2008), 715–718. MPP-2008-210.
- G. Mennessier, S. Narison, and W. Ochs. *Two-photon width and gluonic component of  $\sigma/f_0(600)$* . Nucl.Phys.B (Proc.Suppl.) **238–242**. MPP-2008-211, arxiv:0806.4092.
- Wolfgang Ochs and Redamy Perez Ramos. *Particle Multiplicity in Jets and Sub-jets with Jet Axis from Color Current*. Phys.Rev.D **78**, (2008), 034010. MPP-2008-212, arxiv:0807.1082.
- M. Errando, R. Böck, D. Kranich, E. Lorenz, et al. (MAGIC). *Discovery of very high energy gamma-rays from the flat spectrum radio quasar 3C 279 with the MAGIC telescope*. AIP Conf.Proc. **1085**, (2008), 423–426. MPP-2008-213.
- J. J. Velthuis, Z. Drasal, G. Hanninger, R. Kohrs, M. Mathes, L. Reuen, D. Scheireich, L. Andricek, I. C. Pascual, X. Chen, Z. Dolezal, P. Fischer, A. Frey, J. A. Fuster, M. Koch, P. Kodys, P. Kvasnicka, H. Krueger, C. L. Llacer, P. Lodomez, H. G. Moser, I. Peric, A. Raspereza, R. Richter, S. Rummel, E. von Toerne, and N. Wermes. *A DEPFET Based Beam Telescope with Submicron Precision Capability*. IEEE Transactions on Nuclear Science **55**, (2008), 662–666. MPP-2008-214.
- Tobias Göttfert. *ATLAS inner detector alignment*. J.Phys.Conf.Ser. **110**. MPP-2008-216.
- B. I. Abelev, N. Schmitz, P. Seyboth, F. Simon, et al. (STAR). *System-size independence of directed flow at the BNL Relativistic Heavy-Ion Collider*. Phys.Rev.Lett. **101**, (2008), 252301. MPP-2008-217, arxiv:0807.1518.
- B. I. Abelev, N. Schmitz, P. Seyboth, F. Simon, et al. (STAR). *Forward Neutral Pion Transverse Single Spin Asymmetries in p+p Collisions at  $\sqrt{s}=200$  GeV*. Phys.Rev.Lett. **101**, (2008), 222001. MPP-2008-218, arxiv:0801.2990.

- C. Alt, V. Eckardt, N. Schmitz, P. Seyboth, et al. *Energy dependence of phi meson production in central Pb+Pb collisions at  $\sqrt{s_{NN}} = 6$  to 17 GeV*. Phys.Rev.C **78**, (2008), 044907. IGC-08/6-1, MPP-2008-219, arxiv:0806.1937.
- B. I. Abelev, N. Schmitz, P. Seyboth, F. Simon, et al. (STAR). *Hadronic resonance production in d+Au collisions at  $\sqrt{s_{NN}} = 200$  GeV measured at the BNL Relativistic Heavy Ion Collider*. Phys.Rev.C **78**, (2008), 044906. MPP-2008-220, arxiv:0801.0450.
- C. Alt, V. Eckardt, N. Schmitz, P. Seyboth, et al. (NA49). *Energy dependence of Lambda and Xi production in central Pb+Pb collisions at 20A, 30A, 40A, 80A, and 158A GeV measured at the CERN Super Proton Synchrotron*. Phys.Rev.C **78**, (2008), 034918. MPP-2008-221, arxiv:0804.3770.
- C. Alt, V. Eckardt, N. Schmitz, P. Seyboth, et al. (NA49). *Energy Dependence of Multiplicity Fluctuations in Heavy Ion Collisions at 20 A to 158 A GeV*. Phys.Rev.C **78**, (2008), 034914. MPP-2008-222, arxiv:0712.3216.
- C. Alt, V. Eckardt, N. Schmitz, P. Seyboth, et al. (NA49). *Bose-Einstein correlations of pion pairs in central Pb+Pb collisions at 20A, 30A, 40A, 80A, and 158A GeV*. Phys.Rev.C **77**, (2008), 064908. MPP-2008-223, arxiv:0709.4507.
- B. I. Abelev, N. Schmitz, P. Seyboth, et al. (STAR). *Longitudinal double-spin asymmetry for inclusive jet production in p+p collisions at  $\sqrt{s}=200$  GeV*. Phys.Rev.Lett. **100**, (2008), 232003. MPP-2008-224, arxiv:0710.2048.
- B. I. Abelev, N. Schmitz, P. Seyboth, F. Simon, et al. (STAR). *Spin alignment measurements of the  $K^{*0}(892)$  and  $\phi(1020)$  vector mesons in heavy ion collisions at  $\sqrt{s_{NN}} = 200$  GeV*. Phys.Rev.C **77**, (2008), 061902. MPP-2008-225, arxiv:0801.1729.
- B. I. Abelev, N. Schmitz, P. Seyboth, F. Simon, et al. (STAR). *Centrality dependence of charged hadron and strange hadron elliptic flow from  $\sqrt{s_{NN}} = 200$  GeV Au+Au collisions*. Phys.Rev.C **77**, (2008), 054901. MPP-2008-226, arxiv:0801.3466.
- B. I. Abelev, N. Schmitz, P. Seyboth, F. Simon, et al. (STAR). *Enhanced strange baryon production in Au+Au collisions compared to p+p at  $\sqrt{s_{NN}} = 200$  GeV*. Phys.Rev.C **77**, (2008), 044908. MPP-2008-227, arxiv:0705.2511.
- B. I. Abelev, N. Schmitz, P. Seyboth, F. Simon, et al. (STAR).  *$\rho^0$  Photoproduction in Ultra-Peripheral Relativistic Heavy Ion Collisions at  $\sqrt{s_{NN}} = 200$  GeV*. Phys.Rev.C **77**, (2008), 034910. MPP-2008-228, arxiv:0712.3320.
- C. Alt, V. Eckardt, N. Schmitz, P. Seyboth, et al. (NA49). *High Transverse Momentum Hadron Spectra at  $\sqrt{s_{NN}} = 17.3$  GeV in Pb+Pb and p+p Collisions*. Phys.Rev.C **77**, (2008), 034906. MPP-2008-229, arxiv:0711.0547.
- C. Alt et al, V. Eckardt, N. Schmitz, and P. Seyboth (NA49). *Pion and kaon production in central Pb+Pb collisions at 20A and 30A GeV: Evidence for the onset of deconfinement*. Phys.Rev.C **77**, (2008), 024903. MPP-2008-230, arxiv:0710.0118.
- Anna Macchiolo, Ladislav Andricek, Michael Beimforde, Joerg Dubbert, Nabil Ghodbane, Oliver Kortner, Hubert Kroha, Hans-Gunther Moser, R. Nisius, and Rainer H. Richter. *Development of thin pixel sensors and a novel interconnection technology for the SLHC*. Nucl.Instrum.Meth.A **591**, (2008), 229–232. MPP-2008-231.
- The collaboration (H1). *Measurement of Diffractive Scattering of Photons with Large Momentum Transfer at HERA*. Phys.Lett.B **672**, (2009), 219–226. DESY-08-077, MPP-2008-232, arxiv:0810.3096.
- S. C. Commichau, A. Biland, D. Kranich, R. de los Reyes, A. Moralejo, and D. Sobczynska. *Geomagnetic Field effects on the Imaging Air Shower Cherenkov Technique*. Proc. 30th Int. Cosmic Ray Conf.Vol.3 (OG part 2) 1357–1360. MPP-2008-233, arxiv:0709.1251.
- T. Jogler et. al. (MAGIC). *Observations of the gamma-ray binary LS I +61 303 with MAGIC*. J.Phys.Conf.Ser. **120**, (2008), 1–3. MPP-2008-234.
- D. Tescaro, H. Bartko, N. Galante, F. Goebel, T. Jogler, R. Mirzoyan, A. Moralejo, T. Schweizer, M. Shayduk, and M. Teshima. *Study of the performance and capability of the new ultra-fast 2 GSample/s FADC data acquisition system of the MAGIC telescope*. Proc. 30th Int. Cosmic Ray Conf.Vol 3 (OG part 2) 1393–1396. MPP-2008-235, arxiv:0709.1410.
- A. Biland, M. Garczarczyk, H. Anderhub, V. Danielyan, D. Hakobyan, E. Lorenz, and R. Mirzoyan. *The Active Mirror Control of the MAGIC Telescope*. Proc. 30th Int. Cosmic Ray Conf.Vol. 3 (OG part 2) 1353–1356. MPP-2008-236, arxiv:0709.1574.
- T. Y. Saito, M. Shayduk, M. V. Fonseca, M. Hayashida, E. Lorenz, K. Mannheim, R. Mirzoyan, T. Schweizer, and M. Teshima. *Recent progress of GaAsP HPD development for the MAGIC telescope project*. Proc. 30th Int. Cosmic Ray ConfVol. 3 (OG part 2) 1461–1464. MPP-2008-238, arxiv:0709.2052.
- S. Chekanov (ZEUS). *Deep inelastic inclusive and diffractive scattering at  $Q^2$  values from 25 to 320 GeV<sup>2</sup> with the ZEUS forward plug calorimeter* DESY-08-011, MPP-2008-241, arxiv:0802.3017.
- S. Chekanov (ZEUS). *Multi-jet cross sections in charged current e+p scattering at HERA*. Phys.Rev.D **78**, (2008), 032004. DESY-08-024, MPP-2008-242, arxiv:0802.3955.
- The collaboration (ZEUS). *Energy dependence of the charged multiplicity in deep inelastic scattering at HERA*.

- JHEP **0806**, (2008), 061. DESY-08-036, MPP-2008-243, arxiv:0803.3878.
- S. Chekanov (ZEUS). *Beauty photoproduction using decays into electrons at HERA*. Phys.Rev.D **78**, (2008), 072001. DESY-08-056, MPP-2008-244, arxiv:0805.4390.
- S. Chekanov (ZEUS). *Inclusive KOSKOS resonance production in ep collisions at HERA*. Phys.Rev.Lett. **101**, (2008), 112003. DESY-08-068, MPP-2008-245, arxiv:0806.0807.
- The collaboration (ZEUS). *Search for events with an isolated lepton and missing transverse momentum and a measurement of W production at HERA*. Phys.Lett.B **672**, (2009), 106–115. DESY-08-089, MPP-2008-246, arxiv:0807.0589.
- The collaboration (ZEUS). *Production of excited charm and charm-strange mesons at HERA*. Eur.Phys.J.C **60**, (2009), 25–45. DESY-08-093, MPP-2008-247, arxiv:0807.1290.
- S. Chekanov (ZEUS). *Angular correlations in three-jet events in ep collisions at HERA* DESY-08-100, MPP-2008-248, arxiv:0808.3783.
- S. Chekanov (ZEUS). *Measurement of beauty production from dimuon events at HERA*. JHEP **0902**, (2009), 032. DESY-08-129, MPP-2008-249, arxiv:0811.0894.
- The collaboration (ZEUS). *Deep inelastic scattering with leading protons or large rapidity gaps at HERA*. Nucl.Phys.B **816**, (2009), 1–61. DESY-08-175, MPP-2008-250, arxiv:0812.2003.
- The collaboration (ZEUS). *A measurement of the  $Q^2$ , W and t dependences of deeply virtual Compton scattering at HERA*. JHEP **0905**, (2009), 108. DESY-08-132, MPP-2008-251, arxiv:0812.2517.
- The collaboration (ZEUS). *Leading proton production in deep inelastic scattering at HERA*. JHEP **0906**, (2009), 074. DESY-08-176, MPP-2008-252, arxiv:0812.2416.
- S. Chekanov (ZEUS). *Subjet distributions in deep inelastic scattering at HERA* DESY-08-178, MPP-2008-253, arxiv:0812.2864.
- The collaboration (ZEUS). *Measurement of charged current deep inelastic scattering cross sections with a longitudinally polarised electron beam at HERA*. Eur.Phys.J.C **61**, (2009), 223–235. DESY-08-177, MPP-2008-254, arxiv:0812.4620.
- S. Chekanov (ZEUS). *Measurement of  $D^{+-}$  and  $D^0$  production in deep inelastic scattering using a lifetime tag at HERA*. Eur.Phys.J.C **63**, (2009), 171–188. MPP-2008-255, arxiv:0812.3775.
- A. E. Kiryunin, H. Oberlack, D. Salihagic, P. Schacht, and P. Strizenec. *GEANT4 physics evaluation with test-beam data of the ATLAS hadronic end-cap calorimeter*. J.Phys.Conf.Ser. **160**, (2009), 012075. MPP-2008-256.
- J. Pinfold et al. *Performance of the ATLAS liquid argon endcap calorimeter in the pseudorapidity region  $2.5 < |\eta| < 4.0$  in beam tests*. Nucl.Instrum.Meth.A **593**, (2008), 324–342. MPP-2008-257.
- The collaboration (OPAL). *Search for Charged Higgs Bosons in  $e+e-$  Collisions at  $\sqrt{s(s)} = 189-209$  GeV* CERN-PH-EP/2008-016, MPP-2008-258, arxiv:0812.0267.
- SLD electroweak heavy flavour groups (ALEPH , CDF , DO , DELPHI , L3 , OPAL , SLD , LEP Electroweak Working Group, Tevatron Electroweak Working Group). *Precision Electroweak Measurements and Constraints on the Standard Model* CERN-PH-EP/2008-020, MPP-2008-259, arxiv:0811.4682.
- Guennadi Pospelov et al. *The overview of the ATLAS local hadronic calibration*. J.Phys.Conf.Ser. **160**, (2009), 012079. MPP-2008-260.
- G. Abbiendi et al. *Measurement of  $\alpha_s$  with radiative hadronic events*. Eur.Phys.J.C **53**, (2007), 21–39. CERN-PH-EP-2007-032, MPP-2008-261.
- W. Lampl, S. Laplace, D. Lelas, P. Loch, H. Ma, S. Menke, S. Rajagopalan, D. Rousseau, S. Snyder, and G. Unal. *Calorimeter clustering algorithms: Description and performance* ATL-LARG-PUB-2008-002 ; ATL-COM-LARG-2008-003, MPP-2008-262.
- Vladimir Chekelian. *Longitudinal Structure Function Measurements from HERA* MPP-2008-263, arxiv:0810.5112.
- Y. Arai et al. *ATLAS Muon Drift Tube Electronics*. J.Inst. **3**, (2008), P09001. MPP-2008-264.
- C. Adorisio et al. *System test of the ATLAS muon spectrometer in the H8 beam at the CERN SPS*. Nucl.Instrum.Meth.A **593**, (2008), 232–254. MPP-2008-265.
- Robert Richter. *Upgrade of ATLAS for High Luminosity at the Super-LHC (sLHC)* MPP-2008-266.
- J. Albert (MAGIC). *Periodic very high energy gamma-ray emission from LS I +61 303 observed with the MAGIC telescope*. Astrophys.J. **693**, (2009), 303–310. MPP-2008-268, arxiv:0806.1865v1.
- G. Tagliaferri et al. (MAGIC). *Simultaneous multiwavelength observations of the blazar 1ES1959+650 at a low TeV flux*. Astrophys.J. **679**, (2008), 1029–1059. MPP-2008-269, arxiv:0801.4029.
- The collaboration (H1). *Measurement of the Inclusive ep Scattering Cross Section at Low  $Q^2$  and x at HERA*. Eur.Phys.J.C DESY08-171, MPP-2008-272, arxiv:0904.0929.
- Allen Caldwell, Daniel Kollar, and Kevin Kroeninger. *BAT - The Bayesian Analysis Toolkit* MPP-2008-273, arxiv:0808.2552.

- Dominik Dannheim, Tancredi Carli, Karl-Johan Grahn, Peter Speckmayer, and Alexander Voigt. *PDE-Foam - a probability-density estimation method using self-adapting phase-space binning*. Nucl.Instrum.Meth.A **606**, (2009), 717–727. MPP-2008-274, arxiv:0812.0922.
- N. J. Buchanan et al. *Radiation qualification of the front-end electronics for the readout of the ATLAS liquid argon calorimeters*. J.Inst. **3**, (2008), 10005. MPP-2008-275.
- E. Abat et al. (ATLAS). *Combined performance tests before installation of the ATLAS Semiconductor and Transition Radiation Tracking Detectors*. J.Inst. **3**, (2008), P08003. MPP-2008-276.
- A. Ahmad (ATLAS). *Alignment of the Pixel and SCT Modules for the 2004 ATLAS Combined Test Beam*. J.Inst. **3**, (2008), P09004. MPP-2008-277.
- Erhard Seiler and Klaus Sibold. *Quantum Field Theory and Beyond*. MPP-2008-278.
- V. Chekelian. *Longitudinal Structure Function Measurements from HERA* MPP-2008-279, arxiv:0810.5112.
- John Paul Archambault, Joseph Boudreau, Tancredi Carli, Davide Costanzo, Andrea Dell’Acqua, Andrea Di Simone, Fares Djama, Manuel Gallas, Margaret Fincke-Keeler, Mohsen Khakzad, Andrei Kiryunin, Peter Krieger, Mikhail Leltchouk, Peter Loch, Hong Ma, Sven Menke, Emmanuel Monnier, Armin Nairz, Valentin Niess, Gerald Oakham, Chris Oram, Guennadi Pospelov, Srinivasen Rajagopalan, Adele Rimoldi, David Rousseau, John Rutherford, William Seligman, Andrei Soukharev, Pavol Strizenec, Moustapha Thioye, Jozsef Toth, Ilya Tsukerman, Vakhtang Tsulaia, Guillaume Unal, and Karl-Johan Grahn. *The Simulation of the ATLAS Liquid Argon Calorimetry* MPP-2008-280.
- T. Barillari, Elin Bergeaas Kuutmann, T. Carli, J. Erdmann, P. Giovannini, K. J. Grahn, C. Issever, A. Jantsch, A. Kiryunin, K. Lohwasser, A. Maslennikov, S. Menke, H. Oberlack, G. Pospelov, E. Rauter, P. Schacht, F. Spano, P. Speckmayer, P. Stavina, and P. Strizenec. *Local Hadronic Calibration* MPP-2008-281.
- Thomas Gehrmann, Guenter Grindhammer, Vivian O’Dell, and Roman Walczak. *Hadronic Final States and QCD: Summary* ZU-TH 14/08, MPP-2008-282, arxiv:0808.2616.
- Hannes Jung, Albert De Roeck, Jochen Bartels, Olaf Behnke, Johannes Blumlein, Stanley Brodsky, Amanda Cooper-Sarkar, Michal Deak, Robin Devenish, Markus Diehl, Thomas Gehrmann, Guenter Grindhammer, Gosta Gustafson, Valery Khoze, Albert Knutsson, Max Klein, Frank Krauss, Krzysztof Kutak, Eric Laenen, Leif Lonnblad, Leszek Motyka, Paul R. Newman, Fred Olness, Daniel Pitzl, Marta Ruspa, Agustin Sabio Vera, Gavin P. Salam, Thomas Schorner-Sadenius, and Mark Strikman. *What HERA may provide ?* MPP-2008-283, arxiv:0809.0549.
- Vladimir Chekelian. *Direct  $F_L$  measurement at high  $Q^2$  at HERA* MPP-2008-284.
- G. Aad, E. Abat, B. Abbott, J. Abdallah, A. A. Abdellalim, A. Abdesselam, O. Abidinov, B. Abi, M. Abolins, H. Abramowicz, B. S. Acharya, D. L. Adams, T. N. Addy, C. Adorisio, P. Adragna, T. Adye, J. A. Aguilar-Saavedra, M. Aharrouche, S. P. Ahlen, F. Ahles, A. Ahmad, H. Ahmed, G. Aielli, T. Akdogan, T. P. A. Akesson, G. Akimoto, M. A. Alam, S. M. Alam, J. Albert, S. Albrand, M. Aleksa, I. N. Aleksandrov, F. Alessandria, C. Alexa, G. Alexander, G. Alexandre, T. Alexopoulos, M. Alhroob, G. Alimonti, J. Alison, M. Aliyev, P. P. Allport, S. E. Allwood-Spiers, A. Aloisio, R. Alon, A. Alonso, J. Alonso, M. G. Alviggi, K. Amako, P. Amaral, C. Amelung, V. V. Ammosov, A. Amorim, G. Amoros, N. Amram, C. Anastopoulos, C. F. Anders, K. J. Anderson, A. Andreazza, V. Andrei, M-L. Andrieux, X. S. Anduaga, et al. (ATLAS). *Expected Performance of the ATLAS Experiment - Detector, Trigger and Physics*. CERN-OPEN-2008-020, MPP-2009-1. arxiv:0901.0512.
- Guenter Sigl, Ricard Tomas, Andreu Esteban-Pretel, Sergio Pastor, Alessandro Mirizzi, Georg G. Raffelt, and Pasquale D. Serpico. *Collective flavor transitions of supernova neutrinos*. Nucl.Phys.B (Proc.Suppl.) **188**, (2009), 101–106. MPP-2009-2, arxiv:0901.0725.
- J. Barranco, A. Bolanos, O. G. Miranda, C. A. Moura, and T. I. Rashba. *Unparticle physics and neutrino phenomenology*. Phys.Rev.D **79**, (2009), 073011. MPP-2009-3, arxiv:0901.2099.
- Mattias Blennow and Davide Meloni. *Non-standard interaction effects on astrophysical neutrino fluxes*. Phys.Rev.D **80**, (2009), 065009. MPP-2009-4, arxiv:0901.2110.
- Bela Majorovits, Hashmed Kader, Hans Kraus, Adalbert Lossin, Emilia Pantic, Federica Petricca, Franz Proebst, and Wolfgang Seidel. *Production of low-background CuSn6-bronze for the CRESST dark-matter-search experiment*. Applied Radiation and Isotopes **67**, (2009), 197–200. MPP-2009-7.
- Jui yu Chiu, Andreas Fuhrer, Andre H. Hoang, Randall Kelley, and Aneesh V. Manohar. *Soft-Collinear Factorization and Zero-Bin Subtractions*. Phys.Rev.D **79**, (2009), 053007. MPP-2009-8, arxiv:0901.1332.
- Johanna Erdmenger, Matthias Kaminski, and Felix Rust. *QGP thermodynamics and meson spectroscopy with AdS/CFT*. PoS Confinement **8**, (2008), 131. MPP-2009-9, arxiv:0901.2456.
- J. Balog, F. Niedermayer, and P. Weisz. *Logarithmic corrections to  $O(a^2)$  lattice artifacts*. Phys.Lett.B **676**, (2009), 188–192. MPP-2009-10, arxiv:0901.4033.
- Hans-Günther Moser. *Silicon Detector Systems in High Energy Physics*. Progr.Part.Nucl.Phys. **63**, (2009), 186–237. Doi: 10.1016/j.pnpnp.2008.12.002, MPP-2009-11.

- Ayres Freitas, Frank Daniel Steffen, Nurhana Tajuddin, and Daniel Wyler. *Upper Limits on the Peccei-Quinn Scale and on the Reheating Temperature in Axino Dark Matter Scenarios*. Phys.Lett.B **679**, (2009), 270–277. ZU-TH 06/09, MPP-2009-12, arxiv:0904.3218.
- Malcolm Fairbairn, Timur Rashba, and Sergey Troitsky. *Photon-axion mixing in the Milky Way and ultra-high-energy cosmic rays from BL Lac type objects - Shining light through the Universe* MPP-2009-13, arxiv:0901.4085.
- Dieter Lust and Dimitrios Tsimpis. *Classes of AdS4 type IIA/IIB compactifications with SU(3) $\times$ SU(3) structure*. JHEP **0904**, (2009), 111. LMU-ASC 05/09, MPP-2009-14, arxiv:0901.4474.
- Ralph Blumenhagen, Mirjam Cvetič, Shamit Kachru, and Timo Weigand. *D-brane Instantons in Type II String Theory*. Ann.Rev.Nucl.Part.Sci. **59**, (2009), 269–296. MPP-2009-15, arxiv:0902.3251.
- Thi Nhung Dao and Duc Ninh Le. *DOC : A code to calculate scalar one-loop four-point integrals with complex masses* MPP-2009-16, arxiv:0902.0325.
- Michaela E. Albrecht, Monika Blanke, Andrzej J. Buras, Bjoern Duling, and Katrin Gemmler. *Electroweak and Flavour Structure of a Warped Extra Dimension with Custodial Protection*. JHEP **09**, (2009), 064. TUM-HEP-711/09, MPP-2009-17, arxiv:0903.2415.
- H. Anderhub, R. Sato, M. Ushio, J. Kataoka, G. Madejski, and T. Takahashi (MAGIC). *Simultaneous Multi-wavelength observation of Mkn 501 in a low state in 2006*. Astrophys.J. **705**, (2009), 1624–1649. MPP-2009-20, arxiv:0910.2093.
- Arnd Brandenburg and Frank Daniel Steffen. *Axino dark matter from thermal production*. JCAP **0408**, (2004), 008. DESY 04-082, MPP-2009-22, hep-ph/0405158.
- Wolfgang Ehrenfeld, Ayres Freitas, Ananda Landwehr, and Daniel Wyler. *Distinguishing spins in decay chains with photons at the Large Hadron Collider*. JHEP **0907**, (2009), 056. DESY 09-048, ZU-TH 01/09, MPP-2009-23, arxiv:0904.1293.
- Monika Blanke. *Insights from the Interplay of  $K \rightarrow \pi \nu$  anti- $\nu$  and  $\epsilon_{\pi K}$  on the New Physics Flavour Structure*. Acta Phys.Polon.B **41**, (2010), 127. TUM-HEP-714/09, MPP-2009-25, 0904.2528.
- Stefan Antusch and Martin Spinrath. *New GUT predictions for quark and lepton mass ratios confronted with phenomenology*. Phys.Rev.D **79**, (2009), 095004. MPP-2009-26, arxiv:0902.4644.
- Robert Wagner. *Physics Insights from Recent MAGIC AGN Observations*. International Journal of Modern Physics D MPP-2009-27.
- Georg Raffelt and Timur Rashba. *Mimicking diffuse supernova antineutrinos with the Sun as a source* MPP-2009-28, arxiv:0902.4832.
- Martin Ammon, Johanna Erdmenger, Matthias Kaminski, and Patrick Kerner. *Flavor Superconductivity from Gauge/Gravity Duality*. JHEP **0910**, (2009), 067. IFT-UAM/CSIC-09-12, MPP-2009-29, arxiv:0903.1864.
- Mattias Blennow and Enrique Fernandez-Martinez. *Neutrino oscillation parameter sampling with MonteCUBES*. Comput.Phys.Commun. **181**, (2010), 227. EURONU-WP6-09-03, MPP-2009-30, 0903.3985.
- Stefan Antusch, Mattias Blennow, Enrique Fernandez-Martinez, and Jacobo Lopez-Pavon. *Probing non-unitary mixing and CP-violation at a Neutrino Factory*. Phys.Rev.D **80**, (2009), 033002. IFT-UAM/CSIC-09-16, EURONU-WP6-09-04, MPP-2009-31, arxiv:0903.3986.
- Peter Breitenlohner and D. H. Tchrakian. *Gravitating BPS Monopoles in all  $d=4p$  Spacetime Dimensions* MPP-2009-32, arxiv:0903.3505.
- Basudeb Dasgupta, Amol Dighe, Georg G. Raffelt, and Alexei Yu. Smirnov. *Multiple Spectral Splits of Supernova Neutrinos*. Phys.Rev.Lett. **103**, (2009), 051105. MPP-2009-33, arxiv:0904.3542.
- Elena Caceres, Raphael Flauger, and Timm Wrase. *Hagedorn Systems from Backreacted Finite Temperature  $N_f = 2N_c$  Backgrounds* MPP-2009-34, arxiv:0908.4483.
- Paul Koerber. *A new family of non-homogeneous type IIA flux vacua from AdS4/CFT3*. JHEP **0909**, (2009), 008. MPP-2009-35, 0904.0012.
- Ikaros I. Bigi, Monika Blanke, Andrzej J. Buras, and Stefan Recksiegel. *CP Violation in  $D_0$  - anti- $D_0$  Oscillations: General Considerations and Applications to the Lightest Higgs Model with T-Parity*. JHEP **07**, (2009), 097. UND-HEP-08-BIG 05, TUM-HEP-719/09, MPP-2009-36, 0904.1545.
- J. Hamann, S. Hannestad, G. G. Raffelt, and Y. Y. Y. Wong. *Isocurvature forecast in the anthropic axion window*. JCAP **0906**, (2009), 022. CERN-PH-TH/2009-044, LAPTH-1323/09, MPP-2009-37, arxiv:0904.0647.
- Christoph Pahl, Sigi Bethke, Otmar Biebel, Stefan Kluth, and Jochen Schieck. *Tests of analytical hadronisation models using event shape moments in  $e^+e^-$  annihilation*. Eur.Phys.J.C MPP-2009-38, arxiv:0904.0786.
- Wolfgang Hollik. *Electroweak precision physics from LEP to LHC and ILC*. Int.J.Mod.Phys.A **24**, (2009), 3382–3391. MPP-2009-39.
- Sven Menke. *On the determination of  $\alpha_s$  from hadronic tau decays with contour-improved, fixed order and renormalon-chain perturbation theory* MPP-2009-41, arxiv:0904.1796.
- Luis A. Anchordoqui, Haim Goldberg, Dieter Lust, Satoshi Nawata, Stephan Stieberger, and Tomasz R. Taylor. *LHC Phenomenology for String Hunters*. Nucl.Phys.B **821**, (2009), 181–196. LMU-ASC 18/09, MPP-2009-42, arxiv:0904.3547.

- Frank Simon. *Hadronic showers in the CALICE calorimeter prototypes* MPP-2009-43, arxiv:0904.2991.
- Dieter Lust. *Seeing through the string landscape - a string hunter's companion in particle physics and cosmology*. JHEP MPP-2009-44, arxiv0904.4601.
- Andrzej J. Buras, Bjoern Duling, and Stefania Gori. *The Impact of Kaluza-Klein Fermions on Standard Model Fermion Couplings in a RS Model with Custodial Protection*. JHEP **0909**, (2009), 076. MPP-2009-46, 0905.2318.
- D. Renker and E. Lorenz. *Advances in solid state photon detectors*. J.Inst. **4**, (2009), 4004–4052. MPP-2009-47.
- Barbara de Lotto (MAGIC). *The MAGIC Extragalactic Sky* MPP-2009-48.
- D. Mazin et al (MAGIC). *DISCOVERY OF A VERY HIGH ENERGY GAMMA-RAY SIGNAL FROM THE 3C66 A/B REGION* MPP-2009-49.
- D. Hadasch (MAGIC). *LOOKING AT OUR GALAXY WITH THE MAGIC EYE* MPP-2009-50.
- D. Borla Tridon, T. Schweizer, R. Mirzoyan, and M. Teshima. *The MAGIC-II gamma-ray stereoscopic telescope system* MPP-2009-51.
- Martin Ammon, Johanna Erdmenger, Rene Meyer, Andy O'Bannon, and Timm Wrase. *Adding Flavor to AdS/CFT3*. JHEP **0911**, (2009), 125. ITP-UH-17/09, MPP-2009-52, arxiv:0909.3845.
- Andre H. Hoang, Ambar Jain, Ignazio Scimemi, and Iain W. Stewart. *The R-evolution of QCD matrix elements* MIT CTP-4040, MPP-2009-59, arxiv:0905.3193.
- Jui yu Chiu, Andreas Fuhrer, Andre H. Hoang, Randall Kelley, and Aneesh V. Manohar. *Using SCET to calculate electroweak corrections in gauge boson production*. PoSEFT **09**, (2009), 009. MPP-2009-60, arxiv:0905.1141.
- Christian Kiesling, Ana Dubak, and Bob Olivier. *The Liquid Argon Jet Trigger of the H1 Experiment at HERA* MPP-2009-61.
- The collaboration (H1). *A Precision Measurement of the Inclusive ep Scattering Cross Section at HERA*. Eur.Phys.J.C **64**, (2009), 561–587. DESY09-005, MPP-2009-62, arxiv:0904.3513.
- The collaboration (H1). *Jet Production in ep Collisions at High Q<sup>2</sup> and Determination of  $\alpha_s$* . Eur.Phys.J.C **65**, (2010), 363–383. DESY09-032, MPP-2009-63, arxiv:0904.3870.
- The collaboration (H1). *Search for Excited Quarks in ep Collisions at HERA*. Phys.Lett.B **678**, (2009), 335–343. DESY09-040, MPP-2009-64, arxiv:0904.3392.
- The collaboration (H1). *Search for Single Top Quark Production at HERA*. Phys.Lett.B **678**, (2009), 450–458. DESY09-050, MPP-2009-65, arxiv:0904.3876.
- Ralph Blumenhagen, Thomas W. Grimm, Benjamin Jurke, and Timo Weigand. *F-theory uplifts and GUTs*. JHEP **0909**, (2009), 053. MPP-2009-66, arxiv:0906.0013.
- G. L. Cardoso, G. Dall'Agata, and V. Grass. *On Subextensive Corrections to Fluid Dynamics from Gravity*. JHEP **1004**, (2010), 064. DFPD-09TH09, LMU-ASC 25/09, MPP-2009-67, 0906.0587.
- Monika Blanke, Andrzej J. Buras, Bjoern Duling, Stefan Recksiegel, and Cecilia Tarantino. *FCNC Processes in the Littlest Higgs Model with T-Parity: a 2009 Look*. Acta Phys.Polon.B **41**, (2010), 657. TUM-HEP-726/09, RM3-TH/09-12, MPP-2009-68, 0906.5454.
- S. Kluth.  $\alpha_s(M_Z)$  from Jade Event Shapes MPP-2009-69, arxiv:0905.4891.
- Andreas Karch, Andy O'Bannon, and Laurence G. Yaffe. *Critical Exponents from AdS/CFT with Flavor*. JHEP **09**, (2009), 042. MPP-2009-70, 0906.4959.
- H. Seta et al. (MAGIC). *Suzaku and Multi-wavelength Observations of OJ 287 during the Periodic Optical Outburst in 2007*. Publ. Astro. Soc. Jap. **61**. MPP-2009-74, arxiv:0906.0234.
- The collaboration (MAGIC). *Search for VHE Gamma-ray emission from the globular cluster M13 with the MAGIC telescope*. Astrophys.J. **702**, (2009), 266–269. MPP-2009-75, arxiv:0905.2427.
- R. Blumenhagen, J. P. Conlon, S. Krippendorf, S. Moster, and F. Quevedo. *SUSY Breaking in Local String/F-Theory Models*. JHEP **0909**, (2009), 007. MPP-2009-76, arxiv:0906.3297.
- Dieter Lust, (Munich, Max Planck Inst. & ASC, Munich & Munich U. ), Dimitros Tsimpis, (ASC, and Munich & Munich U. ). *New supersymmetric AdS4 type II vacua* MPP-2009-77, arxiv0906.2561.
- Carla Biggio, Mattias Blennow, and Enrique Fernandez-Martinez. *General bounds on non-standard neutrino interactions*. JHEP **0908**, (2009), 090. EURONU-WP6-09-05, MPP-2009-83, arxiv:0907.0097.
- Eckart Lorenz, Razmick Mirzoyan, Hiroko Miyamoto, Nepomuk Otte, and Dieter Renker. *First tests and long-term prospects of Geigermode avalanche photodiodes as camera sensors for IACTs* MPP-2009-87, arxiv:0907.0853.
- M. Antonelli, D. M. Asner, D. Bauer, T. Becher, M. Beneke, A. J. Bevan, M. Blanke, C. Bloise, M. Bona, A. Bondar, C. Bozzi, J. Brod, N. Cabibbo, A. Carbone, G. Cavoto, V. Cirigliano, M. Ciuchini, J. P. Coleman, D. P. Cronin-Hennessy, J. P. Dalseno, C. H. Davies, F. Di Lodovico, J. Dingfelder, Z. Dolezal, S. Donati, W. Dungel, U. Egede, R. Faccini, T. Feldmann, F. Ferroni, J. M. Flynn, E. Franco, M. Fujikawa, I. K. Furic, P. Gambino, E. Gardi, T. J. Gershon, S. Giagu, E. Golowich, T. Goto, C. Greub, C. Grojean, D. Guadagnoli, U. A. Haisch, R. F. Harr, A. H. Hoang,

- G. Isidori, D. E. Jaffe, A. Jüttner, S. Jäger, A. Khodjamirian, P. Koppenburg, R. V. Kowalewski, P. Krokovny, A. S. Kronfeld, J. Laiho, G. Lanfranchi, T. E. Latham, J. Libby, A. Limosani, D. Lopes Pegna, C. D. Lu, E. Lunghi, V. G. Lüth, K. Maltman, W. J. Marciano, E. C. Martin, G. Martinelli, F. Martinez-Vidal, A. Masiero, V. Matheu, F. Mescia, G. Mohanty, M. Moulson, M. Neubert, H. Neufeld, S. Nishida, N. Offen, M. Palutan, P. Paradisi, Z. Parsa, E. Passemar, M. Patel, B. D. Pecjak, A. A. Petrov, A. Pich, M. Pierini, B. Plaster, A. Powell, S. Prell, J. Rademaker, M. Rescigno, S. Ricciardi, P. Robbe, E. Rodrigues, M. Rotondo, R. Sacco, C. J. Schilling, O. Schneider, E. E. Scholz, B. A. Schumm, C. Schwanda, A. J. Schwartz, B. Sciascia, J. Serrano, J. Shigemitsu, I. J. Shipsey, A. Sibidanov, L. Silvestrini, F. Simonetto, S. Simula, C. Smith, A. Soni, L. Sonnenschein, V. Sordini, M. Sozzi, T. Spadaro, P. Spradlin, A. Stocchi, N. Tantalò, C. Tarantino, A. V. Telnov, D. Tonelli, I. S. Towner, K. Trabelsi, P. Urquijo, R. S. Van de Water, R. J. Van Kooten, J. Virto, G. Volpi, R. Wanke, S. Westhoff, G. Wilkinson, M. Wingate, Y. Xie, and J. Zupan. *Flavor Physics in the Quark Sector* BNL-90299-2009-BC, CERN-PH-TH-2009-112, FERMILAB-PUB-09-323-T, LAL, MPP-2009-88, arxiv:0907.5386.
- Karsten Berger, Pratik Majumdar, Elina Lindfors, Fabrizio Tavecchio, and Masahiro Teshima. *MAGIC observations of the distant quasar 3C279 during an optical outburst in 2007* MPP-2009-89, arxiv:0907.1046.
- P. Colin, D. Borla Tridon, D. Britzger, E. Lorenz, R. Mirzoyan, T. Schweizer, and M. Teshima. *Observation of shadowing of the cosmic electrons and positrons by the Moon with IACT* MPP-2009-90, arxiv:0907.1026.
- T. Y. Saito, R. Zanin, P. Bordas, V. Bosh-Ramon, T. Jogler, J. M. Paredes, M. Ribo, M. Rissi, J. Rico, and D. F. Torres. *Microquasar observations with the MAGIC telescope* MPP-2009-91, arxiv:0907.1017.
- E. Carmona, M. T. Costado, L. Font, and J. Zapatero. *Observation of selected SNRs with the MAGIC Cherenkov Telescope* MPP-2009-92, arxiv:0907.1009.
- E. Carmona, J. A. Coarasa, and M. Barcelo. *A Flexible High Demand Storage System for MAGIC-I and MAGIC-II using GFS* MPP-2009-93, arxiv:0907.1003.
- Markus Garczarczyk, Markus Gaug, Angelo Antonelli, Denis Bastieri, Josefa Becerra-Gonzalez, Stefano Covino, Antonio La Barbera, Alessandro Carosi, Nicola Galante, Francesco Longo, Valeria Scapin, and Susanna Spiro. *GRB Observations with the MAGIC Telescopes* MPP-2009-94, arxiv:0907.1001.
- R. Zanin and J. Cortina. *The Central Control of the MAGIC telescopes* MPP-2009-95, arxiv:0907.0946.
- D. Borla Tridon, F. Goebel, D. Fink, W. Haberer, J. Hose, C. C. Hsu, T. Jogler, R. Mirzoyan, R. Orito, O. Reimann, P. Sawallisch, J. Schlammer, T. Schweizer, B. Steinke, and M. Teshima. *Performance of the Camera of the MAGIC II Telescope* MPP-2009-96, arxiv:0906.5448.
- B. Steinke, T. Jogler, and D. Borla Tridon. *MAGIC-II Camera Slow Control Software* MPP-2009-97, arxiv:0906.5259.
- D. Tescaro, J. Aleksic, M. Barcelo, M. Bitossi, J. Cortina, M. Fras, D. Hadasch, J. M. Illa, M. Martinez, D. Mazin, R. Paoletti, and R. Pegna. *The readout system of the MAGIC-II Cherenkov Telescope* MPP-2009-98, arxiv:0907.0466.
- Ignasi Reichardt, Javier Rico, Emiliano Carmona, Jose Luis Contreras, Juan Cortina, Roger Firpo, Lluís Font, Abelardo Moralejo, Daniel Nieto, Igor Oya, and Raquel de los Reyes. *The MAGIC Data Center* MPP-2009-99, arxiv:0907.0968.
- A. Moralejo, M. Gaug, E. Carmona, P. Colin, C. Delgado, S. Lombardi, D. Mazin, V. Scalzotto, J. Sitarek, and D. Tescaro. *MARS, the MAGIC Analysis and Reconstruction Software* MPP-2009-100, arxiv:0907.0943.
- Daniel Britzger, Emiliano Carmona, Pratik Majumdar, Oscar Blanch, Javier Rico, Julian Sitarek, and Robert Wagner. *Studies of the Influence of Moonlight on Observations with the MAGIC Telescope* MPP-2009-101, arxiv:0907.0973.
- P. Colin, D. Borla Tridon, E. Carmona, F. De Sabata, M. Gaug, S. Lombardi, P. Majumdar, A. Moralejo, V. Scalzotto, and J. Sitarek. *Performance of the MAGIC telescopes in stereoscopic mode* MPP-2009-102, arxiv:0907.0960.
- R. Orito, E. Bernardini, D. Bose, A. Dettlaff, D. Fink, V. Fonseca, M. Hayashida, J. Hose, E. Lorenz, K. Mannheim, R. Mirzoyan, O. Reimann, T. Y. Saito, T. Schweizer, M. Shayduk, and M. Teshima. *Development of HPD Clusters for MAGIC-II* MPP-2009-103, arxiv:0907.0865.
- M. Lopez, N. Otte, M. Rissi, T. Schweizer, M. Shayduk, and S. Klepser. *Detection of the crab pulsar with MAGIC* MPP-2009-105, arxiv:0907.0832.
- T. Jogler, N. Puchades, O. Blanch Bigas, V. Bosch-Ramon, J. Cortina, J. Moldón, J. M. Paredes, M. A. Perez-Torres, M. Ribó, J. Rico, D. F. Torres, and V. Zabalza (MAGIC). *The MAGIC highlights of the gamma ray binary LS I +61 303* MPP-2009-106, arxiv:0907.0992.
- Diego F. Torres, Javier Rico, and Vincenzo Vitale. *First bounds on the VHE gamma-ray emission from isolated Wolf-Rayet binary systems* MPP-2009-107, arxiv:0907.0399.
- T. Jogler, C. Delgado Mendez, M. T. Costado, W. Bednarek, and J. Sitarek. *MAGIC observation of Globular Cluster M13 and its millisecond pulsars* MPP-2009-108, arxiv:0907.0987.

- Manel Errando, Elina Lindfors, Daniel Mazin, Elisa Prandini, and Fabrizio Tavecchio. *A TeV source in the 3C 66A/B region* MPP-2009-109, arxiv:0907.0994.
- D. Mazin, E. Lindfors, K. Berger, N. Galante, E. Prandini, and T. Saito. *Discovery of Very High Energy gamma-rays from the blazar S5 0716+714* MPP-2009-110, arxiv:0907.0366.
- Elisa Prandini, Daniela Dorner, Nijil Mankuzhiyil, Mosé Mariotti, and Daniel Mazin. *A new upper limit on the redshift of PG 1553+113 from observations with the MAGIC Telescope* MPP-2009-112, arxiv:0907.0157.
- D. Tescaro, D. Mazin, R. M. Wagner, K. Berger, and N. Galante. *The strong flaring activity of M87 in early 2008 as observed by the MAGIC telescope* MPP-2009-113, arxiv:0907.0460.
- C. C. Hsu, K. Satalecka, M. Thom, M. Backes, E. Bernardini, G. Bonnoli, N. Galante, F. Goebel, E. Lindfors, P. Majumdar, A. Stamerra, and R. M. Wagner. *Monitoring of bright blazars with MAGIC telescope* MPP-2009-114, arxiv:0907.0893.
- D. Hadasch, T. Bretz, and D. Mazin. *High zenith angle observations of PKS 2155-304 with the MAGIC telescope* MPP-2009-115, arxiv:0907.0370.
- Julian Sitarek and Razmik Mirzoyan. *Search for an extended emission around blazars with the MAGIC telescope* MPP-2009-116, arxiv:0906.5503.
- Elina J. Lindfors, Riho Reinthal, Daniel Mazin, Kari Nilsson, Leo Takalo, Aimo Sillanpaa, and Andrei Berduygin. *The connection between optical and VHE gamma-ray high states in the blazar jets* MPP-2009-117, arxiv:0907.0550.
- Sandhya Choubey, Pilar Coloma, Andrea Donini, and Enrique Fernandez-Martinez. *Optimized Two-Baseline Beta-Beam Experiment*. JHEP **0912**, (2009), 020. IFT-UAM/CSIC-09-33, EUROnu-WP6-09-07, CUP-TH-09-01, MPP-2009-118, arxiv:0907.2379.
- S. Rügamer, I. Oya, M. Hayashida, D. Mazin, R. M. Wagner, J. L. Contreras, and T. Bretz. *MWL observations of VHE blazars in 2006* MPP-2009-119, arxiv:0907.0551.
- Giacomo Bonnoli, Ching-Cheng Hsu, Florian Goebel, Elina Lindfors, Pratik Majumdar, Konstancja Satalecka, Antonio Stamerra, Fabrizio Tavecchio, and Robert Wagner. *MAGIC observations of Mkn 421 in 2008, and related optical/X-ray/TeV MWL study* MPP-2009-120, arxiv:0907.0831.
- Nijil Mankuzhiyil, Daniela Dorner, Elisa Prandini, Massimo Persic, Elena Pian, and Stefano Vercellone. *Simultaneous multi-frequency observations of PG 1553+113* MPP-2009-121, arxiv:0907.0740.
- E. Leonardo, D. Bose, N. Mankuzhiyil, I. Oya, S. Rügamer, A. Stamerra, F. Tavecchio, L. Foschini, and G. Tagliaferri. *Multiwavelength observation of the blazar 1ES1426+428 in May-June 2008* MPP-2009-122, arxiv:0907.0959.
- Stefano Covino, Markus Garzarczyk, Markus Gaug, Angelo Antonelli, Denis Bastieri, Josefa Becerra-Gonzalez, Antonio La Barbera, Alessandro Carosi, Nicola Galante, Francesco Longo, Valeria Scapin, Susanna Spiro, Antonio de Ugarte-Postigo, Alessandra Galli, and R. Salvaterra. *MAGIC observation of GRB080430* MPP-2009-123, arxiv:0907.0993.
- S. Lombardi, J. Aleksic, J. A. Barrio, A. Biland, M. Doro, D. Elsaesser, M. Gaug, K. Mannheim, M. Mariotti, M. Martinez, D. Nieto, M. Persic, F. Prada, J. Rico, M. Rissi, M. A. Sanchez-Conde, L. S. Stark, and F. Zandanel. *Search for Dark Matter signatures with MAGIC-I and prospects for MAGIC Phase-II* MPP-2009-125, arxiv:0907.0738.
- M. Hayashida, G. Bonnoli, A. Stamerra, E. Lindfors, K. Nilsson, M. Teshima, H. Seta, N. Isobe, M. S. Tashiro, K. Nakanishi, M. Sasada, Y. Shimajiri, and M. Uemura. *Multiwavelength observation from radio through very-high-energy Gamma-ray of OJ 287 during the 12-year cycle flare in 2007* MPP-2009-126, arxiv:0907.1343.
- D. Kranich, D. Paneque, A. Cesarini, A. Falcone, M. Giroletti, E. Hoversten, T. Hovatta, Y. Y. Kovalev, A. Lahteenmaki, E. Nieppola, C. Pagani, A. Pichel, K. Satalecka, J. Scargle, D. Steele, F. Tavecchio, D. Tescaro, M. Tornikoski, and M. Villata. *Multiwavelength Observations of Mrk 501 in 2008* MPP-2009-127, arxiv:0907.1098.
- R. De los Reyes, W. Bednarek, M. Camara, and M. Lopez. *Upper limits for pulsars with MAGIC (2005/2006 observations)* MPP-2009-128, arxiv:0907.1168.
- Juan Cortina, Florian Goebel, and Thomas Schweizer. *Technical Performance of the MAGIC Telescopes* MPP-2009-129, arxiv:0907.1211.
- Richard Nisius. *Experimental Review of Photon Structure Function Data* 163–171. MPP-2009-131, arxiv:0907.2782.
- W. Altmannshofer, A. J. Buras, S. Gori, P. Paradisi, and D. Straub. *Anatomy and Phenomenology of FCNC and CPV Effects in SUSY Theories* TUM-HEP-727/09, MPP-2009-133, 0909.1333.
- I. de la Calle Perez, A. Ibarra, and P. Rodriguez (VERTAS, MAGIC). *Simultaneous Multiwavelength Observations of Markarian 421 During Outburst* MPP-2009-135, arxiv:0907.3923.
- The collaboration (H1). *Observation of the Hadronic Final State Charge Asymmetry in High  $Q^2$  Deep-Inelastic Scattering at HERA*. Phys.Lett.B **681**, (2009), 125–133. DESY09-084, MPP-2009-136, arxiv:0907.2666.
- The collaboration (H1). *Measurement of the Charm and Beauty Structure Functions using the H1 Vertex Detector*

- at HERA. Eur.Phys.J.C **65**, (2010), 89–109. DESY09-096, MPP-2009-137, 0907.2643.
- The collaboration (H1, ZEUS). *Multi-Leptons with High Transverse Momentum at HERA*. JHEP **0910**, (2009), 013. DESY-09-108, MPP-2009-138, 0907.3627.
- D. Lust, O. Schlotterer, S. Stieberger, and T. R. Taylor. *The LHC String Hunter's Companion (II): Five-Particle Amplitudes and Universal Properties*. Nucl.Phys.B **828**, (2010), 139–200. MPP-2009-139, arxiv:0908.0409.
- D. Haertl, O. Schlotterer, and S. Stieberger. *Higher Point Spin Field Correlators in D=4 Superstring Theory* MPP-2009-140, arxiv:0911.5168.
- Christian Kiesling. *CP Violation and the Future of Flavor Physics* MPP-2009-146.
- H. Anderhub (MAGIC). *Discovery of Very High Energy gamma-rays from the blazar S5 0716+714*. Astrophys.J.L. **704**, (2009), L129–L133. 0907.2386, MPP-2009-147, arxiv:0907.2386.
- Ralph Blumenhagen, Thomas W. Grimm, Benjamin Jurke, and Timo Weigand. *Global F-theory GUTs*. Nucl.Phys.B **829**, (2010), 325–369. MPP-2009-148, arxiv:0908.1784.
- Stefan Antusch and Martin Spinrath. *GUT predictions for quark and lepton mass ratios*. AIP Conf.Proc. **1200**, (2010), 928–931. MPP-2009-150, arxiv:0908.1520.
- Stefan Antusch, Koushik Dutta, and Philipp M. Kostka. *Tribrid Inflation in Supergravity*. AIP Conf.Proc. **1200**, (2010), 1007–1010. MPP-2009-151, arxiv:0908.1694.
- Francis Halzen and Georg G. Raffelt. *Reconstructing the supernova bounce time with neutrinos in Ice-Cube*. Phys.Rev.D **80**, (2009), 087301. MPP-2009-152, arxiv:0908.2317.
- Martin Ammon, Thanh Hai Ngo, and Andy O'Bannon. *Holographic Flavor Transport in Arbitrary Constant Background Fields*. JHEP **0910**, (2009), 027. MPP-2009-154, arxiv:0908.2625.
- Ayres Freitas, Frank Daniel Steffen, Nurhana Tajuddin, and Daniel Wyler. *Late Energy Injection and Cosmological Constraints in Axino Dark Matter Scenarios*. Phys.Lett.B **682**, (2009), 193–199. ZU-TH 13/09, MPP-2009-155, arxiv:0909.3293.
- Andre H. Hoang, Ambar Jain, Ignazio Scimemi, and Iain W. Stewart. *R-evolution: Improving perturbative QCD*. Phys.Rev.Lett. **1182**, (2009), 503–507. MIT-CTP 4062, MPP-2009-156, arxiv:0908.3189.
- S. Stieberger. *On tree-level higher order gravitational couplings in superstring theory* MPP-2009-158, 0910.0180.
- Luis A. Anchordoqui, Haim Goldberg, Dieter Lust, Stephan Stieberger, and Tomasz R. Taylor. *String Phenomenology at the LHC*. Mod.Phys.Lett.A **9**, (2009), 2481–2490. LMU-ASC 39/09, CERN-PH-TH/2009-167, MPP-2009-159, arxiv0909.2216.
- Johanna Erdmenger, Constantin Greubel, Matthias Kaminski, Patrick Kerner, Karl Landsteiner, and Francisco Pena-Benitez. *Quasinormal modes of massive charged flavor branes*. JHEP **1003**, (2010), 117. IFT-UAM/CSIC-09-43, PUPT-2315, MPP-2009-162, 0911.3544.
- Stefan Dittmaier and Max Huber. *Radiative corrections to the neutral-current Drell-Yan process in the Standard Model and its minimal supersymmetric extension*. JHEP **01**, (2010), 1–65. MPP-2009-164, arxiv:0911.2329.
- The VERITAS Collaboration and the VLBA 43 GHz M87 Monitoring Team (H. E. S. S., MAGIC). *Radio Imaging of the Very-High-Energy gamma-Ray Emission Region in the Central Engine of a Radio Galaxy*. Science **325**, (2009), 444–448. MPP-2009-166.
- Alan Bross, Malcolm Ellis, Enrique Fernandez-Martinez, Steve Geer, Tracey Li, Olga Mena, and Silvia Pascoli. *The multi-channel low energy neutrino factory* IPPP/09/84, DCPT/09/168, FERMILAB-PUB-09-574-APC, MPP-2009-167, arxiv:0911.3776.
- G. Barenboim, E. Fernandez-Martinez, O. Mena, and L. Verde. *The dark side of curvature* MPP-2009-168, arxiv:0910.0252.
- J. Aleksic, C. Frommer, A. Pinzke, T. A. Ensslin, S. Inoue, and G. Ghisellini (MAGIC). *MAGIC Gamma-Ray Observation of the Perseus Galaxy Cluster*. Astrophys.J. **710**, (2010), 634–647. MPP-2009-169, arxiv:0909.3267.
- Mattias Blennow, Henrik Melbeus, and Tommy Ohlsson. *Neutrinos from Kaluza-Klein dark matter in the Sun*. JCAP **1001**, (2010), 018. MPP-2009-170, arxiv:0910.1588.
- Robert Wagner. *Cherenkov Telescope Array - The Future of Ground-Based Gamma-Ray Astronomy*. J.Phys.Conf.Ser. MPP-2009-171.
- I. Donnarumma, J. Grube, C. M. Raiteri, S. Vercellone, M. Villata, R. M. Wagner, GASP-WEBT teams, and the MAGIC (VERITAS collaborations). *The June 2008 flare of Markarian 421 from optical to TeV energies* MPP-2009-172.
- Clemens P. Kiessig and Michael Plumacher. *Thermal masses in leptogenesis* MPP-2009-173, arxiv:0910.4872.
- Stefan Antusch, Stephen F. King, Michal Malinsky, and Martin Spinrath. *Quark mixing sum rules and the right unitarity triangle*. Phys.Rev.D **81**, (2010), 033008. NORDITA-2009-68, MPP-2009-174, arxiv:0910.5127.
- Stefan Antusch, Steve Blanchet, Mattias Blennow, and Enrique Fernandez-Martinez. *Non-unitary Leptonic Mixing and Leptogenesis*. JHEP **1001**, (2010), 017. UMD-PP-09-056, MPP-2009-175, arxiv:0910.5957.

- S. Aoki, J. Balog, and P. Weisz. *The repulsive core of the NN potential and the operator product expansion* MPP-2009-176, arxiv:0910.4255.
- Enrique Fernandez-Martinez. *The gamma = 100 Beta-Beam revisited* MPP-2009-178, arxiv:0912.3804.
- Ioannis Bakas, Francois Bourliot, Dieter Lust, and Marios Petropoulos. *Geometric flows in Horava-Lifshitz gravity*. JHEP MPP-2009-179, arxiv1002.0062.
- Ioannis Bakas, Francois Bourliot, Dieter Lust, and Marios Petropoulos. *Mixmaster universe in Horava-Lifshitz gravity* CPHT-RR111.1109, LMU-ASC 48/09, MPP-2009-180, arxiv:0911.2665.
- The collaboration (H1). *Deeply Virtual Compton Scattering and its Beam Charge Asymmetry in  $e^\pm p$  Collisions at HERA*. Phys.Lett.B **681**, (2009), 391–399. DESY09-109, MPP-2009-182, arxiv:0907.5289.
- The collaboration (H1). *Prompt Photons in Photoproduction at HERA*. Eur.Phys.J.C DESY09-135, MPP-2009-183, arxiv:0910.5631.
- The H1 (ZEUS Collaborations). *Events with an Isolated Lepton and Missing Transverse Momentum and Measurement of W Production at HERA*. Mon.Not.R.Astron.Soc. DESY-09-140, MPP-2009-184, arxiv:0911.0858.
- The H1 (ZEUS Collaborations). *Combined Measurement and QCD Analysis of the Inclusive ep Scattering Cross Section at HERA*. JHEP **1001**, (2010), 109. DESY09-158, MPP-2009-185, arxiv:0911.0884.
- The collaboration (H1). *Diffraction Electroproduction of rho and phi Mesons at HERA*. JHEP DESY 09-093, MPP-2009-186, arxiv:0910.5831.
- Jens Schmalzer (CRESST). *Status of the CRESST Dark Matter Search*. AIP Conf.Proc. **1185**, (2009), 631–634. MPP-2009-187, arxiv:0912.3689.
- Rafael F. Lang and Wolfgang Seidel. *Search for Dark Matter with CRESST*. New Journal of Physics **11**, (2009), 105017. MPP-2009-188, arxiv:0906.3290.
- R. F. Lang, G. Angloher, M. Bauer, I. Bavykina, A. Bento, A. Brown, C. Bucci, C. Ciemniak, C. Coppi, G. Deuter, F. von Feilitzsch, D. Hauff, S. Henry, P. Huff, J. Imber, S. Ingleby, C. Isaila, J. Jochum, M. Kiefer, M. Kimmerle, H. Kraus, J. C. Lanfranchi, B. Majorovits, M. Malek, R. McGowan, V. B. Mikhailik, E. Pantic, F. Petricca, S. Pfister, W. Potzel, F. Pröbst, S. Roth, K. Rottler, C. Sailer, K. Schäffner, J. Schmalzer, S. Scholl, W. Seidel, L. Stodolsky, A. J. B. Tolhurst, I. Usherov, and W. Westphal. *Electron and Gamma Background in CRESST Detectors*. Astropart.Phys. **32**, (2010), 318–324. MPP-2009-189, arxiv:0905.4282.
- R. F. Lang, G. Angloher, M. Bauer, I. Bavykina, A. Bento, A. Brown, C. Bucci, C. Ciemniak, C. Coppi, G. Deuter, F. von Feilitzsch, D. Hauff, S. Henry, P. Huff, J. Imber, S. Ingleby, C. Isaila, J. Jochum, M. Kiefer, M. Kimmerle, H. Kraus, J. C. Lanfranchi, M. Malek, R. McGowan, V. B. Mikhailik, E. Pantic, F. Petricca, S. Pfister, W. Potzel, F. Pröbst, S. Roth, K. Rottler, C. Sailer, K. Schäffner, J. Schmalzer, S. Scholl, W. Seidel, L. Stodolsky, A. J. B. Tolhurst, I. Usherov, and W. Westphal. *Discrimination of Recoil Backgrounds in Scintillating Calorimeters*. Astropart.Phys. **33**, (2010), 60–64. MPP-2009-190, arxiv:0903.4687.
- R. F. Lang, G. Angloher, M. Bauer, I. Bavykina, A. Bento, A. Brown, C. Bucci, C. Ciemniak, C. Coppi, G. Deuter, F. von Feilitzsch, D. Hauff, S. Henry, P. Huff, J. Imber, S. Ingleby, C. Isaila, J. Jochum, M. Kiefer, M. Kimmerle, H. Kraus, J. C. Lanfranchi, M. Malek, R. McGowan, V. B. Mikhailik, E. Pantic, F. Petricca, S. Pfister, W. Potzel, F. Pröbst, S. Roth, K. Rottler, C. Sailer, K. Schäffner, J. Schmalzer, S. Scholl, W. Seidel, L. Stodolsky, A. J. B. Tolhurst, I. Usherov, and W. Westphal. *Scintillator Non-Proportionality and Gamma Quenching in CaWO4* MPP-2009-191, arxiv:0910.4414.
- Frederik Beaujean and Nicolas Moeller. *Delays in Open String Field Theory* LMU-ASC 50/09, MPP-2009-194, arxiv:0912.1232.
- Frank Simon. *Energy Reconstruction of Hadron Showers in the CALICE Calorimeters* MPP-2009-195, 0911.4575.
- L. Stodolsky, P. Korcyl, and J. Wosiek. *Studies in a Random Noise Model of Decoherence* MPP-2009-196, arxiv:0911.4368.
- The collaboration (H1). *Jet Production in ep Collisions at Low  $Q^2$  and Determination of  $\alpha_s$* . Eur.Phys.J.C DESY09-162, MPP-2009-198, arxiv:0911.5678.
- The collaboration (H1). *Measurement of the  $D^*$  Meson Production Cross Section and  $F_2^{cbar}$ , at High  $Q^2$ , in ep Scattering at HERA*. Phys.Lett.B DESY09-165, MPP-2009-199, arxiv:0911.3989.
- S. Halter, B. v. Harling, and A. Hebecker. *Tachyons in Throat Cosmology*. JHEP **063**, (2010), 063. HD-THEP-09-26, MPP-2009-200, 0912.2111.
- L. Huedepohl, B. Mueller, H. Th. Janka, A. Marek, and G. G Raffelt. *Neutrino Signal of Electron-Capture Supernovae from Core Collapse to Cooling* MPP-2009-201, arxiv:0912.0260.
- Basudeb Dasgupta, Tobias Fischer, Shunsaku Horiuchi, Matthias Liebendoerfer, Alessandro Mirizzi, Irina Sagert, and Jurgen Schaffner-Bielich. *Detecting the QCD phase transition in the next Galactic supernova neutrino burst* MPP-2009-203, arxiv:0912.2568.
- Gia Dvali and Dieter Lust. *Evaporation of Microscopic Black Holes in String Theory and the Bound on Species* CERN-PH-TH/2009-243, LMU-ASC 56/09, MPP-2009-205, arxiv:0912.3167.

- H. Anderhub, L. A. Antonelli, P. Antoranz, M. Backes, C. Baixeras, S. Balestra, J. A. Barrio, D. Bastieri, J. Becerra González, J. K. Becker, W. Bednarek, K. Berger, E. Bernardini, A. Biland, O. Blanch Bigas, R. K. Bock, G. Bonnoli, P. Bordas, D. Borla Tridon, V. Bosch-Ramon, D. Bose, I. Braun, T. Bretz, D. Britzger, M. Camara, E. Carmona, A. Carosi, P. Colin, S. Commichau, J. L. Contreras, J. Cortina, M. T. Costado, S. Covino, F. Dazzi, A. De Angelis, E. de Cea del Pozo, R. De los Reyes, B. De Lotto, M. De Maria, F. De Sabata, C. Delgado Mendez, A. Domínguez, D. Dorner, M. Doro, D. Elsaesser, M. Errando, D. Ferenc, E. Fernández, R. Firpo, M. V. Fonseca, L. Font, N. Galante, R. J. García López, M. Garczarczyk, M. Gaug, N. Godinovic, F. Goebel, D. Hadasch, A. Herrero, D. Hildebrand, D. Höhne-Mönch, J. Hose, D. Hrupec, C. C. Hsu, T. Jogler, S. Klepser, D. Kranich, A. La Barbera, A. Laille, E. Leonardo, E. Lindfors, S. Lombardi, F. Longo, M. López, E. Lorenz, P. Majumdar, G. Maneva, N. Mankuzhiyil, K. Mannheim, L. Maraschi, M. Mariotti, M. Martínez, D. Mazin, M. Meucci, J. M. Miranda, R. Mirzoyan, H. Miyamoto, J. Moldón, M. Moles, A. Moralejo, D. Nieto, K. Nilsson, J. Ninkovic, R. Orito, I. Oya, R. Paoletti, J. M. Paredes, M. Pasanen, D. Pascoli, F. Pauss, R. G. Pegna, M. A. Perez-Torres, M. Persic, L. Peruzzo, F. Prada, E. Prandini, N. Puchades, I. Puljak, I. Reichardt, W. Rhode, M. Ribó, J. Rico, M. Rissi, S. Rügamer, A. Saggion, T. Y. Saito, M. Salvati, M. Sánchez-Conde, K. Satalecka, V. Scalzotto, V. Scapin, T. Schweizer, M. Shayduk, S. N. Shore, A. Sierpowska-Bartosik, A. Sillanpää, J. Sitarek, D. Sobczynska, F. Spanier, S. Spiro, A. Stamerra, B. Steinke, N. Strah, J. C. Struebig, T. Suric, L. Takalo, F. Tavecchio, P. Temnikov, D. Tescaro, M. Teshima, D. F. Torres, N. Turini, H. Vankov, R. M. Wagner, V. Zabalza, F. Zandanel, R. Zanin, J. Zapatero, E. Pian, V. Bianchin, F. D'Ammando, G. Di Cocco, D. Fugazza, G. Ghisellini, O. M. Kurtanidze, C. M. Raiteri, G. Tosti, A. Treves, S. Vercellone, and M. Villata (MAGIC). *Simultaneous multi-frequency observation of the unknown redshift blazar PG 1553+113 in March-April 2008* MPP-2009-207, arxiv:0911.1088.
- Andrzej J. Buras, Lorenzo Calibbi, and Paride Paradisi. *Slepton mass-splittings as a signal of LFV at the LHC*. JHEP TUM-HEP-742-09, MPP-2009-208, arxiv:0912.1309.
- He Zhang and Shun Zhou. *The minimal seesaw model at the TeV scale*. Phys.Lett.B MPP-2009-210, arxiv:0912.2661.
- Claudio Caviezel, Timm Wrase, and Marco Zagermann. *Moduli Stabilization and Cosmology of Type IIB on SU(2)-Structure Orientifolds* MPP-2009-212, arxiv:0912.3287.
- Fawzi Boudjema, Le Duc Ninh, Sun Hao, and Marcus M. Weber. *NLO corrections to  $ee \rightarrow WWZ$  and  $ee \rightarrow ZZZ$* . Phys.Rev.D **81**, (2010), 073007. LAPTH-1372/09, MPP-2009-214, arxiv:0912.4234.
- Martin Ammon, Johanna Erdmenger, Viviane Grass, Patrick Kerner, and Andy O'Bannon. *On Holographic p-wave Superfluids with Back-reaction*. Phys.Lett.B **686**, (2010), 192–198. MPP-2009-215, 0912.3515.
- M. Kiefer, G. Angloher, M. Bauer, I. Bavykina, A. Bento, A. Brown, C. Bucci, C. Ciemiak, C. Coppi, G. Deuter, F. von Feilitzsch, D. Hauff, S. Henry, P. Huff, J. Imber, S. Ingleby, C. Isaila, J. Jochum, M. Kimmerle, H. Kraus, J. C. Lanfranchi, R. F. Lang, M. Malek, R. McGowan, V. B. Mikhailik, E. Pantic, F. Petricca, S. Pfister, W. Potzel, F. Pröbst, S. Roth, K. Rottler, C. Sailer, K. Schäffner, J. Schmalzer, S. Scholl, W. Seidel, L. Stodolsky, A. J. B. Tolhurst, I. Usherov, and W. Westphal. *Composite CaWO<sub>4</sub> Detectors for the CRESST-II Experiment*. AIP Conf.Proc. **1185**. MPP-2009-216, arxiv:0912.0170.
- G. Aarts, E. Seiler, and I. O. Stamatescu. *The Complex Langevin method: When can it be trusted?* MPP-2009-220, arxiv:0912.3360.
- J. Aleksić, H. Anderhub, L. A. Antonelli, P. Antoranz, M. Backes, C. Baixeras, S. Balestra, J. A. Barrio, D. Bastieri, J. Becerra González, J. K. Becker, W. Bednarek, A. Berdyugin, K. Berger, E. Bernardini, A. Biland, R. K. Bock, G. Bonnoli, P. Bordas, D. Borla Tridon, V. Bosch-Ramon, D. Bose, I. Braun, T. Bretz, D. Britzger, M. Camara, E. Carmona, A. Carosi, P. Colin, S. Commichau, J. L. Contreras, J. Cortina, M. T. Costado, S. Covino, F. Dazzi, A. De Angelis, E. de Cea del Pozo, R. De los Reyes, B. De Lotto, M. De Maria, F. De Sabata, C. Delgado Mendez, D. Dominis Prester, D. Dorner, M. Doro, D. Elsaesser, M. Errando, D. Ferenc, E. Fernández, R. Firpo, M. V. Fonseca, L. Font, N. Galante, R. J. García López, M. Garczarczyk, M. Gaug, N. Godinovic, F. Goebel, D. Hadasch, A. Herrero, D. Hildebrand, D. Höhne-Mönch, J. Hose, D. Hrupec, C. C. Hsu, T. Jogler, S. Klepser, T. Krähenbühl, D. Kranich, A. La Barbera, A. Laille, E. Leonardo, E. Lindfors, S. Lombardi, F. Longo, M. López, E. Lorenz, P. Majumdar, G. Maneva, N. Mankuzhiyil, K. Mannheim, L. Maraschi, M. Mariotti, M. Martínez, D. Mazin, M. Meucci, J. M. Miranda, R. Mirzoyan, H. Miyamoto, J. Moldón, M. Moles, A. Moralejo, D. Nieto, K. Nilsson, J. Ninkovic, R. Orito, I. Oya, R. Paoletti, J. M. Paredes, M. Pasanen, D. Pascoli, F. Pauss, R. G. Pegna, M. A. Perez-Torres, M. Persic, L. Peruzzo, F. Prada, E. Prandini, N. Puchades, I. Puljak, I. Reichardt, W. Rhode, M. Ribó, J. Rico, M. Rissi, A. Robert, S. Rügamer, A. Saggion, T. Y. Saito, M. Salvati, M. Sánchez-Conde, K. Satalecka, V. Scalzotto, V. Scapin, T. Schweizer, M. Shayduk, S. N. Shore, N. Sidro, A. Sierpowska-Bartosik, A. Sillanpää, J. Sitarek, D. Sobczynska, F. Spanier, S. Spiro, A. Stamerra, L. S. Stark, T. Suric, L. Takalo, F. Tavecchio, P. Temnikov, D. Tescaro, M. Teshima, D. F. Torres, N. Turini, H. Vankov, R. M. Wagner, V. Zabalza, F. Zandanel, R. Zanin, J. Zapatero, A. Falcone, L. Vetere, N. Gehrels, S. Trushkin, V. Dhawan, and P. Reig (MAGIC). *Correlated X-ray and Very High Energy emission in the gamma-ray binary LS I +61 303*. Astrophys.J. **706**, (2009), L27–L32. MPP-2009-206, arxiv:0910.4381.

- G. Aarts, E. Seiler, and I. O. Stamatescu. *Adaptive stepsize and instabilities in complex Langevin dynamics* MPP-2009-221, arxiv:0912.0617.
- J. Aleksic et al. (MAGIC). *MAGIC TeV Gamma-Ray Observations of Markarian 421 during Multiwavelength Campaigns in 2006*. Astron.Astrophys. MPP-2009-224.
- Klaus Gottstein and Goetz Neunck. *Proceedings* 1–298. MPP-2009-225.
- Klaus Gottstein. *Preface*, 9–12 (DESY, Hamburg). MPP-2009-226 (2009).
- Klaus Gottstein. *Die VDW und die Pugwash Conferences on Science and World Affairs*, 359–376 (Berliner Wissenschafts-Verlag BWV, Berlin). MPP-2009-227 (2009).
- Klaus Gottstein. *Erlebnisse im Kalten Krieg. Beiträge der Wissenschaft zur Entspannung*. AFK-RundbriefDezember **2009**, (2009), 38–45. MPP-2009-228.
- Oliver Kortner. *Commissioning of the Charged Lepton Identification with Cosmic Rays in ATLAS*. PoS MPP-2009-229.
- I. Abt, A. Caldwell, D. Gutknecht, J. Janicsko-Csáthy, M. Lampert, D. Lenz, X. Liu, J. Liu, B. Majorovits, D. Quirion, J. Schubert, F. Stelzer, and P. Wendling. *Operation of an 18-fold segmented n-type HPGe detector in liquid nitrogen*. J.Inst. **4**, (2009), P11008. MPP-2009-230.
- The collaboration (ATLAS). *Data-Driven Determination of  $t\bar{t}$  Background to Supersymmetry Searches in ATLAS*. MPP-2009-231.
- Andreas Wassatsch, Sven Herrmann, Rainer H. Richter, and Ladislav Andricek. *A clustering engine for data rate reduction in the Belle II pixel detector*. Conference records of NSS **2009**, (2009), N13–35. MPP-2009-232.
- V. Zhuravlov. *Extracting backgrounds to SUSY searches from LHC data*. PoS MPP-2009-233.
- T. Hahn, S. Heinemeyer, W. Hollik, H. Rzehak, and G. Weiglein. *FeynHiggs: A program for the calculation of MSSM Higgs-boson observables - Version 2.6.5*. Comput.Phys.Commun. **180**, (2009), 1426–1427. MPP-2009-234.
- A. De Roeck, J. Ellis, C. Grojean, S. Heinemeyer, K. Jakobs, G. Weiglein, J. Wells, G. Azuelos, S. Dawson, B. Gripaios, T. Han, J. Hewett, M. Lancaster, C. Mariotti, F. Moortgat, G. Moortgat-Pick, G. Polesello, S. Riemann, M. Schumacher, K. Assamagan, P. Bechtle, M. Carena, G. Chachamis, K. F. Chen, S. De Curtis, K. Desch, M. Dittmar, H. Dreiner, M. Dührssen, B. Foster, M. T. Frandsen, A. Giammanco, R. Godbole, P. Govoni, J. Gunion, W. Hollik, W. S. Hou, G. Isidori, A. Juste, J. Kalinowski, A. Korytov, E. Kou, S. Kraml, M. Krawczyk, A. Martin, D. Milstead, V. Morton-Thurtle, K. Moenig, B. Mele, E. Ozcan, M. Pieri, T. Plehn, L. Reina, E. Richter-Was, T. Rizzo, K. Rolbiecki, F. Sannino, M. Schram, J. Smillie, S. Sultansoy, J. Tattersall, P. Uwer, B. Webber, and P. Wienemann. *From the LHC to Future Colliders* CERN-PH-TH/2009-166, DCPT/09/136, IPPP/09/068, SLAC-PUB-13782, MPP-2009-235, arxiv:0909.3240.
- Jan Germer, Wolfgang Hollik, Edoardo Mirabella, and Maike K. Trenkel. *NLO electroweak contributions to squark pair production at the LHC* MPP-2009-236, arxiv:0909.3046.
- Janicsko Csathy Jozsef. *Status of the GERDA experiment*. Nucl.Phys.B (Proc.Suppl.) **188**, (2009), 68–70. MPP-2009-237.
- The collaboration (H1). *Measurement of Leading Neutron Production in Deep-Inelastic Scattering at HERA*. Eur.Phys.J.C DESY09-185, MPP-2009-239, arxiv:1001.0532.
- The collaboration (H1). *Inelastic Production of  $J/\psi$  Mesons in Photoproduction and Deep Inelastic Scattering at HERA*. Eur.Phys.J.C DESY09-225, MPP-2009-240, arxiv:1002.0234.
- A. N. Otte, F. Goebel, E. Lorenz, T. Schweizer, et al. *Detection of Cherenkov light from air showers with Geigermode-APDs*. Nucl.Instrum.Meth.A **610**, (2009), 415–418. MPP-2009-241.
- T. Y. Saito, E. Lorenz, R. Mirzoyan, R. Orito, T. Schweizer, M. Shayduk, M. Teshima, et al. *Very high QE HPDs with a GaAsP photocathode for the MAGIC telescope project*. Nucl.Instrum.Meth.A **610**, (2009), 258–261. MPP-2009-242.
- I. Braun, S. Commichau, E. Lorenz, et al. *First Avalanche photodiode camera test (FACT): A novel camera using G-APDs for the observation of very high-energy  $\gamma$ -rays with Cherenkov telescopes*. Nucl.Instrum.Meth.A **610**, (2009), 400–403. MPP-2009-243.
- P. Buzhan, B. Dolgoshein, R. Mirzoyan, M. Teshima, et al. *The cross-talk problem in SiPMs and their use as light sensors for imaging atmospheric Cherenkov telescopes*. Nucl.Instrum.Meth.A **610**, (2009), 131–134. MPP-2009-244.
- M. Shayduk, R. Mirzoyan, V. Zimmer, E. Lorenz, T. Schweizer, and M. Teshima. *Selection of photomultipliers for the Cherenkov Telescope Array facility*. Nucl.Instrum.Meth.A MPP-2009-245.
- E. Lorenz, D. Ferenc, M. V. Fonseca, and R. Wagner. *A conceptual design of an advanced 23 m diameter IACT of 50 ton for ground-based gamma-ray astronomy*. Nucl.Instrum.Meth.A MPP-2009-246.
- A. Chilingarian, R. Mirzoyan, and M. Zazyan. *Cosmic Ray research in Armenia*. Advances in Space Research **44**, (2009), 1183–1193. MPP-2009-247.
- B. I. Abelev, N. Schmitz, P. Seyboth, F. Simon, et al. *Energy and system size dependence of phi meson production in*

- Cu + Cu and Au + Au collisions*. Phys.Lett.B **673**, (2009), 183. MPP-2009-248, arxiv:0810.4979.
- B. I. Abelev, N. Schmitz, P. Seyboth, F. Simon, et al. *Indications of Conical Emission of Charged Hadrons at the BNL Relativistic Heavy Ion Collider*. Phys.Rev.Lett. **102**, (2009), 052302. MPP-2009-249, arxiv:0805.0622.
- B. I. Abelev, N. Schmitz, P. Seyboth, F. Simon, et al. *Observation of Two-source Interference in the Photoproduction Reaction Au Au to Au Au  $\rho^0$* . Phys.Rev.Lett. **102**, (2009), 112301. MPP-2009-250, arxiv:0812.1063.
- B. I. Abelev, N. Schmitz, P. Seyboth, F. Simon, et al. *Beam-Energy and System-Size Dependence of Dynamical Net Charge Fluctuations*. Phys.Rev.C **79**, (2009), 024906. MPP-2009-251, arxiv:0807.3269.
- B. I. Abelev, N. Schmitz, P. Seyboth, F. Simon, et al. *Systematic Measurements of Identified Particle Spectra in pp, d+Au, and Au+Au Collisions at the STAR Detector*. Phys.Rev.C **79**, (2009), 034909. MPP-2009-252, arxiv:0808.2041.
- T. Anticic, V. Eckardt, N. Schmitz, P. Seyboth, et al. *Energy dependence of transverse momentum fluctuations in Pb+Pb collisions at the CERN Super Proton Synchrotron (SPS) at 20A to 158A GeV*. Phys.Rev.C **79**, (2009), 044904. MPP-2009-253, arxiv:0810.5580.
- C. Alt, V. Eckardt, N. Schmitz, P. Seyboth, et al. *Energy dependence of particle ratio fluctuations in central Pb+Pb collisions from  $\sqrt{s_{NN}} = 6.3$  to  $17.3$  GeV*. Phys.Rev.C **79**, (2009), 044910. MPP-2009-254, arxiv:0808.1237.
- B. I. Abelev, N. Schmitz, P. Seyboth, F. Simon, et al. *Measurements of phi meson production in relativistic heavy-ion collisions at the BNL Relativistic Heavy Ion Collider (RHIC)*. Phys.Rev.C **79**, (2009), 064903. MPP-2009-255, arxiv:0809.4737.
- B. I. Abelev, N. Schmitz, P. Seyboth, F. Simon, et al. *Measurement of  $D^*$  Mesons in Jets from p+p Collisions at  $\sqrt{s} = 200$  GeV*. Phys.Rev.D **79**, (2009), 112006. MPP-2009-256, arxiv:0901.0740.
- B. I. Abelev, N. Schmitz, P. Seyboth, F. Simon, et al. *K/pi Fluctuations at Relativistic Energies*. Phys.Rev.Lett. **103**, (2009), 092301. MPP-2009-257, arxiv:0901.1795.
- Growth of Long Range Forward-Backward Multiplicity Correlations with Centrality in Au+Au Collisions at  $\sqrt{s_{NN}} = 200$  GeV, author = B. I. Abelev and N. Schmitz and P. Seyboth and F. Simon and others, journal = Phys.Rev.Lett., volume = 103, pages = 172301, year = 2009, eprint = arxiv:0905.0237, note = MPP-2009-258*.
- B. I. Abelev, N. Schmitz, P. Seyboth, F. Simon, et al. *Azimuthal Charged-Particle Correlations and Possible Local Strong Parity Violation*. Phys.Rev.Lett. **103**, (2009), 251601. MPP-2009-259, arxiv:0909.1739.
- B. I. Abelev, N. Schmitz, P. Seyboth, F. Simon, et al. *Pion Interferometry in Au+Au and Cu+Cu Collisions at  $\sqrt{s_{NN}} = 62.4$  and  $200$  GeV*. Phys.Rev.C **80**, (2009), 024905. MPP-2009-260, arxiv:0903.1296.
- T. Anticic, V. Eckardt, N. Schmitz, P. Seyboth, et al. *System-size dependence of Lambda and Xi production in nucleus-nucleus collisions at 40A and 158A GeV measured at the CERN Super Proton Synchrotron*. Phys.Rev.C **80**, (2009), 034906. MPP-2009-261, arxiv:0906.0469.
- B. I. Abelev, N. Schmitz, P. Seyboth, F. Simon, et al. *J/psi production at high transverse momenta in p+p and Cu+Cu collisions at  $\sqrt{s_{NN}} = 200$  GeV*. Phys.Rev.C **80**, (2009), 041902. MPP-2009-262, arxiv:0904.0439.
- B. I. Abelev, N. Schmitz, P. Seyboth, F. Simon, et al. *Neutral Pion Production in Au+Au Collisions at  $\sqrt{s_{NN}} = 200$  GeV*. Phys.Rev.C **80**, (2009), 044905. MPP-2009-263, arxiv:0907.2721.
- B. I. Abelev, N. Schmitz, P. Seyboth, F. Simon, et al. *Long range rapidity correlations and jet production in high energy nuclear collisions*. Phys.Rev.C **80**, (2009), 064912. MPP-2009-264, arxiv:0909.0191.
- B. I. Abelev, N. Schmitz, P. Seyboth, F. Simon, et al. *Longitudinal Spin Transfer to Lambda and barLambda Hyperons in Polarized Proton-Proton Collisions at  $\sqrt{s} = 200$  GeV*. Phys.Rev.D **80**, (2009), 111102. MPP-2009-265, arxiv:0910.1428.
- B. I. Abelev, N. Schmitz, P. Seyboth, F. Simon, et al. *Longitudinal double-spin asymmetry and cross section for inclusive neutral pion production at midrapidity in polarized proton collisions at  $\sqrt{s} = 200$  GeV*. Phys.Rev.D **80**, (2009), 111108. MPP-2009-266, arxiv:0911.2773.
- R. Mirzoyan and M. I. Andersen. *A  $15\bar{\nu}_e \frac{1}{2}$  wide field of view imaging air Cherenkov telescope*. Astropart.Phys. **31**, (2009), 1–5. MPP-2009-267.
- S. Chekanov et al. (ZEUS). *Measurement of the charm fragmentation function in  $D^*$  photoproduction at HERA*. JHEP **0904**, (2009), 082. MPP-2009-268, arxiv:0901.1210.
- The collaboration (ZEUS). *Measurement of beauty photoproduction using decays into muons in dijet events at HERA*. JHEP **0904**, (2009), 133. DESY-08-210, MPP-2009-269, arxiv:0901.2226.
- The collaboration (ZEUS). *Exclusive photoproduction of Y mesons at HERA*. Phys.Lett.B **680**, (2009), 4–12. DESY-09-036, MPP-2009-270, arxiv:0903.4205.
- The collaboration (ZEUS). *Measurement of the Longitudinal Proton Structure Function at HERA*. Phys.Lett.B **682**, (2009), 8–22. DESY-09-046, MPP-2009-271, arxiv:0904.1092.
- S. Chekanov (ZEUS). *Measurement of charm and beauty production in deep inelastic ep scattering from decays into muons at HERA*. Eur.Phys.J.C **65**, (2010), 65–79. DESY-09-056, MPP-2009-272, arxiv:0904.3487.

- The collaboration (ZEUS). *Scaled momentum distributions of charged particles in dijet photoproduction at HERA*. JHEP **0908**, (2009), 077. DESY-09-059, MPP-2009-273, arxiv:0904.3466.
- The collaboration (ZEUS). *Multi-lepton production at high transverse momentum at HERA*. Phys.Lett.B **680**, (2009), 13–23. DESY-09-072, MPP-2009-274, arxiv:0906.1504.
- The collaboration (ZEUS). *Measurement of  $J/\psi$  helicity distributions in inelastic photoproduction at HERA*. JHEP **0912**, (2009), 007. DESY-09-077, MPP-2009-275, arxiv:0906.1424.
- The collaboration (ZEUS). *Measurement of dijet photoproduction for events with a leading neutron at HERA*. Nucl.Phys.B **827**, (2010), 1–33. DESY-09-139, MPP-2009-276, arxiv:0909.3032.
- The collaboration (ZEUS). *Measurement of  $J/\psi$  photoproduction at large momentum transfer at HERA*. DESY-09-137, MPP-2009-277, arxiv:0910.1235.
- The collaboration (ZEUS). *A QCD analysis of ZEUS diffractive data*. Nucl.Phys.B **831**, (2010), 1–25. MPP-2009-278, arxiv:0911.4119.
- The collaboration (ZEUS). *Measurement of isolated photon production in deep inelastic ep scattering*. DESY-09-142.rev, MPP-2009-279, arxiv:0909.4223.
- The collaboration (ZEUS). *Measurement of high- $Q^2$  neutral current deep inelastic  $e^- p$  scattering cross sections with a longitudinally polarised electron beam at HERA*. Eur.Phys.J.C **62**, (2009), 625–658. DESY-08-202, MPP-2009-280, arxiv:0901.2385.
- Allen Caldwell, Konstantin Lotov, Alexander Pukhov, and Frank Simon. *Proton Driven Plasma Wakefield Acceleration*. MPP-2009-281, arxiv:0807.4599.
- A. Caldwell and H. Kowalski. *The  $J/\psi$  Way to Nuclear Structure*. MPP-2009-282, arxiv:0909.1254.
- Allen Caldwell. *Small- $x$  and diffractive physics*. Nucl.Phys.A **827**, (2009), 171C–178C. MPP-2009-283.
- Sandra Horvat. *Non-SM Higgs Searches at the LHC*. Progress in High Energy Physics MPP-2009-284.
- C. Adloff, A. Frey, S. Lu, K. Prothmann, F. Simon, et al. *Response of the CALICE Si-W Electromagnetic Calorimeter Physics Prototype to Electrons*. Nucl.Instrum.Meth.A **608**, (2009), 372. MPP-2009-287, arxiv:0811.2354.
- Frank Simon, James Kelsey, Michael Kohl, Richard Majka, Miro Plesko, Tai Sakuma, Nikolai Smirnov, Harold Spinka, Bernd Surrow, and David Underwood. *Beam Performance of Tracking Detectors with Industrially Produced GEM Foils*. Nucl.Instrum.Meth.A **598**, (2009), 432. MPP-2009-288, arxiv:0808.3477.
- G. Pakhlova, J. Dalseno, et al. (Belle). *Measurement of the  $e+e- \rightarrow D^0 D^{*+} \pi^+$  cross section using initial-state radiation*. Phys.Rev.D **80**, (2009), 091101. MPP-2009-289, arxiv:0908.0231.
- P. Chen, J. Dalseno, B. Reisert, F. Simon, et al. *Observation of  $B^+$  to  $p$   $\Lambda$   $\bar{d}$   $\bar{b}$   $\pi^+$   $\pi^-$  at Belle*. Phys.Rev.D **80**, (2009), 111103. MPP-2009-290, arxiv:0910.5817.
- E. Won, J. Dalseno, C. Kiesling, et al. *Measurement of  $D^+ \rightarrow K_S^0 K^+$  and  $D_s^+ \rightarrow K_S^0 \pi^+$  branching ratios*. Phys.Rev.D **80**, (2009), 111101. MPP-2009-291, arxiv:0910.3052.
- G. Cortiana (ATLAS). *Alignment of the ATLAS Inner Detector Tracking System*. ATL-INDET-PROC-2009-020, MPP-2009-292.
- Jelena Ninković, Ladislav Andriček, Gerhard Liemann, Gerhard Lutz, Hans-Günther Moser, Rainer Richter, and Florian Schopper. *SiMPI-An avalanche diode array with bulk integrated quench resistors for single photon detection*. Nucl.Instrum.Meth.A MPP-2009-293.
- Jelena Ninković, Ladislav Andriček, Gerhard Liemann, Gerhard Lutz, Hans-Günther Moser, Rainer Richter, and Florian Schopper. *SiMPI-Novel high QE photosensor*. Nucl.Instrum.Meth.A MPP-2009-294.
- E. Abat et al. *Study of the response of the ATLAS central calorimeter to pions of energies from 3 to 9 GeV*. Nucl.Instrum.Meth.A **607**, (2009), 372–386. MPP-2009-295.
- Karoline Schäffner, Godehard Angloher, Dieter Hauff, Franz Pröbst, and Wolfgang Seidel. *Inductive Method for Measuring the Local Transition Temperature of Thin Tungsten Films*. AIP Conf.Proc. **1185**, (2009), 187–190. MPP-2009-296.
- T. Bergauer, M. Dragicevic, M. Frey, P. Grabiec, M. Grodner, S. Hänsel, F. Hartmann, K. H. Hoffmann, J. Hrubec, M. Krammer, K. Kucharski, A. Macchiolo, and J. Marchewski. *Results from a first production of enhanced Silicon Test Structures produced by ITE Warsaw*. Nucl.Instrum.Meth.A **598**, (2009), 86–88. MPP-2009-297.
- A. Macchiolo, L. Andricek, M. Beimforde, H. G. Moser, R. Nisius, and R. Richter. *Application of a new interconnection technology for the ATLAS pixel upgrade at SLHC*. MPP-2009-298.
- The collaboration (OPAL). *Sigma-antihyperon correlations in  $Z^0$  decay and investigation of the baryon production mechanism*. Eur.Phys.J.C **64**, (2009), 609–625. CERN-PH-EP/2007-013, MPP-2009-299, arxiv:0910.2174.
- S. Andriamonje, S. Aune, D. Autiero, K. Barth, A. Belov, B. Beltrán, H. Bräuninger, J. M. Carmona, S. Cebrián, J. I. Collar, T. Dafni, M. Davenport, L. Di Lella, C. Eleftheriadis, J. Englhauser, G. Fanourakis, E. Ferrer-Ribas, H. Fischer, J. Franz, P. Friedrich, T. Geralis, I. Giomataris, S. Gninenko, H. Gómez, M. Hasinoff, F. H. Heinsius, D. H. H.

- Hoffmann, I. G. Irastorza, J. Jacoby, K. Jakovčić, D. Kang, K. Königsmann, R. Kotthaus, M. Krčmar, K. Kousouris, M. Kuster, B. Lakić, C. Lasseur, A. Liolios, A. Ljubičić, G. Lutz, G. Luzón, D. Miller, J. Morales, A. Ortiz, T. Papaevangelou, A. Placci, G. Raffelt, H. Riege, A. Rodríguez, J. Ruz, I. Savvidis, Y. Semertzidis, P. Serpico, L. Stewart, J. Villar, J. Vogel, L. Walckiers, and K. Zioutas. *Search for 14.4 keV solar axions emitted in the M1-transition of  $^{57}\text{Fe}$  nuclei with CAST*. JCAP **0912**, (2009), 002. MPP-2009-300, arxiv:0906.4488.
- S. Andriamonje, S. Aune, D. Autiero, K. Barth, A. Belov, B. Beltran, H. Brauninger, J. M. Carmona, S. Cebrian, J. I. Collar, T. Dafni, M. Davenport, L. Di. Lella, C. Eleftheriadis, J. Englhauser, G. Fanourakis, E. Ferrer. Ribas, H. Fischer, J. Franz, P. Friedrich, T. Gerasis, I. Giomataris, S. Gninenko, H. Gomez, M. Hasinoff, F. H. Heinsius, D. H. H. Hoffmann, I. G. Irastorza, J. Jacoby, K. Jakovcic, D. Kang, K. Königsmann, R. Kotthaus, M. Krčmar, K. Kousouris, M. Kuster, B. Lakić, C. Lasseur, A. Liolios, A. Ljubičić, G. Lutz, G. Luzon, D. W. Miller, J. Morales, A. Ortiz, T. Papaevangelou, A. Placci, G. Raffelt, H. Riege, A. Rodríguez, J. Ruz, I. Savvidis, Y. Semertzidis, P. Serpico, L. Stewart, J. D. Vieira, J. Villar, J. Vogel, L. Walckiers, and K. Zioutas. *Search for solar axion emission from  $^7\text{Li}$  and  $D(p,\gamma)^3\text{He}$  nuclear decays with the CAST gamma-ray calorimeter*. JCAP **1003**, (2010), 032. MPP-2009-301, arxiv:0904.2103.
- The collaboration (ATLAS). *Readiness of the ATLAS Liquid Argon Calorimeter for LHC Collisions* MPP-2009-302, arxiv:0912.2642.
- G. Grindhammer, B. A. Kniehl, G. Kramer, and W. Ochs. *HERA 2008, Proc. Ringberg Workshop New Trends in HERA Physics 2008*. HERA 2008. MPP-2009-303 (2009).
- The collaboration (ATLAS). *Jet reconstruction performance* MPP-2009-304.
- The collaboration (ATLAS). *Detector Level Jet Corrections* MPP-2009-305.
- The collaboration (ATLAS). *Measurement of Missing Transverse Energy* MPP-2009-306.
- Vladimir Chekelian. *Proton Structure Function Measurements at HERA* MPP-2009-307.
- The collaboration (ATLAS). *Search for the Standard Model  $H$  to  $ZZ^*$  to  $4l$*  MPP-2009-309.
- The collaboration (ATLAS). *Higgs Boson Searches in Gluon Fusion and Vector Boson Fusion using the  $H$  to  $WW$  Decay Mode* MPP-2009-310.
- The collaboration (ATLAS). *Search for the Standard Model Higgs Boson via Vector Boson Fusion Production Process in the Di-Tau Channels* MPP-2009-311.
- The collaboration (ATLAS). *Search for the Neutral MSSM Higgs Bosons in the Decay Channel  $A/H/h$  to  $\mu^+ \mu^-$*  MPP-2009-312.
- The collaboration (ATLAS). *Charged Higgs Boson Searches* MPP-2009-313.
- The collaboration (ATLAS). *Data-Driven Determinations of  $W, Z$  and Top Backgrounds to Supersymmetry* MPP-2009-314.
- Uli Baur, Doreen Wackerroth, and Marcus M. Weber. *Radiative corrections to  $W$  gamma gamma production at the LHC* MPP-2010-3, arxiv:1001.2688.
- Riccardo Abbate, Michael Fickinger, Andre H. Hoang, Vicent Mateu, and Iain W. Stewart. *Thrust at NNNLL with Power Corrections and a Precision Global Fit for  $\alpha_s(m_Z)$*  MIT-CTP 4101, MPP-2010-7, arxiv:1006.3080.
- Riccardo Abbate, Michael Fickinger, Andre Hoang, Vicent Mateu, and Iain W. Stewart. *Thrust at NNNLL with power corrections and precision global fit for  $\alpha_s(m_Z)$*  MIT-CTP 4118, MPP-2010-8, arxiv:1004.4894.
- Wolfgang Ochs. *No indication of  $f_0(1370)$  in  $\pi\pi$  phase shift analyses* MPP-2010-9, arxiv:1001.4486.
- Ralph Blumenhagen, Andres Collinucci, and Benjamin Jurke. *On Instanton Effects in  $F$ -theory* LMU-ASC 05/10, MPP-2010-11, arxiv:1002.1894.
- Basudeb Dasgupta, Georg G. Raffelt, and Irene Tamborra. *Triggering collective oscillations by three-flavor effects* MPP-2010-12, arxiv:1001.5396.
- B. Majorovits. *Segmented HPGe Detectors for the Search of Neutrinoless Double Beta-Decay*. Progr.Part.Nucl.Phys. MPP-2010-13.
- S. Aoki, J. Balog, and P. Weisz. *Application of the operator product expansion to the short distance behavior of nuclear potentials* UTHER-603, MPP-2010-14, arxiv:1002.0977.
- Fawzi Boudjema, Le Duc Ninh, Sun Hao, and Marcus M. Weber. *Electroweak corrections to  $WWZ$  and  $ZZZ$  production at the linear collider* LAPTH-004/10, MPP-2010-15, arxiv:1002.0816.
- Javier Redondo. *Photon-Axion conversions in transversely inhomogeneous magnetic fields* MPP-2010-16.
- Javier Redondo. *A hidden microwave background? - signatures of photon-WISP oscillations in the CMB-* MPP-2010-17.
- F. Simon, K. Ackermann, L. Andricek, C. Heller, C. Kiesling, A. Moll, H-G. Moser, J. Ninkovic, K. Prothmann, B. Reiser, R. Richter, M. Ritter, S. Rummel, and A. Wassatsch. *The Belle-II Pixel Vertex Detector at the SuperKEKB Flavor Factory* MPP-2010-18, arxiv:1002.1007.
- Frank Simon. *Beam Test Results with Highly Granular Hadron Calorimeters for the ILC* MPP-2010-19, arxiv:1002.1012.
- Andre Hoang, Christoph Reisser, and Pedro Ruiz-Femenia. *Phase Space Matching and Finite Lifetime Effects for*

- Top-Pair Production Close to Threshold.* Phys.Rev.D TTK-10-14, TPP10-15, SFB/PPP-10-18, MPP-2010-22, arxiv:1002.3223.
- The collaboration (ZEUS). *Scaled momentum spectra in deep inelastic scattering at HERA* DESY-09-229, MPP-2010-24, arxiv:1001.4026.
- Yu Bao, Allen Caldwell, Daniel Greenwald, and Guoxing Xia. *Low-energy muons via frictional cooling* MPP-2010-26, arxiv:1001.3064.
- Martin Ammon, Johanna Erdmenger, Matthias Kaminski, and Andy O'Bannon. *Fermionic Operator Mixing in Holographic p-wave Superfluids.* JHEP **1005**, (2010), 053. PUPT-2331, MPP-2010-28, arxiv:1003.1134.
- Wolfgang Ochs, Valery A. Khoze, and M. G. Ryskin. *Limiting soft particle emission in  $e^+e^-$ , hadronic and nuclear collisions.* Eur.Phys.J.C IPPP/10/20, DCPT/10/40, MPP-2010-29, arxiv:1003.2127.
- Stefan Antusch, Mar Bastero-Gil, Jochen P. Baumann, Koushik Dutta, Steve F. King, and Philipp M. Kostka. *Gauge Non-Singlet Inflation in SUSY GUTs* MPP-2010-30, arxiv:1003.3233.
- Clemens P. Kiessig, Markus H. Thoma, and Michael Pluemacher. *Decay of a Yukawa fermion at finite temperature and applications to leptogenesis* MPP-2010-31, arxiv:1003.3016.
- Gia Dvali and Cesar Gomez. *Species and Strings* CERN-PH-TH/2010-069, IFT-UAM/CSIC-10-25, MPP-2010-33, arxiv:1004.3744.
- Stefan Antusch, Pasquale Di Bari, David A. Jones, and Steve F. King. *A fuller flavour treatment of  $N_2$ -dominated leptogenesis* MPP-2010-34, arxiv:1003.5132.
- S. Antusch, S. Boudjemaa, and S. F. King. *Neutrino Mixing Angles in Sequential Dominance to NLO and NNLO* MPP-2010-35, arxiv:1003.5498.
- Steen Hannestad, Alessandro Mirizzi, Georg G. Raffelt, and Yvonne Y. Y. Wong. *Neutrino and axion hot dark matter bounds after WMAP-7* TTK-10-28, MPP-2010-36, arxiv:1004.0695.
- Martin Ammon, Carlos Hoyos, Andy O'Bannon, and Jackson M. S. Wu. *Holographic Flavor Transport in Schroedinger Spacetime.* JHEP **1006**, (2010), 012. MPP-2010-37, arxiv:1003.5913.
- Johannes Held, Dieter Lust, Fernando Marchesano, and Luca Martucci. *DWSB in heterotic flux compactifications* LMU-ASC 21/10, CERN-PH-TH/2010-075, MPP-2010-39, arxiv:1004.0867.
- Weisz and P. *Renormalization and lattice artifacts* MPP-2010-42, arxiv:1004.3462.
- J. Aleksić, L. A. Antonelli, P. Antoranz, M. Backes, C. Baixeras, J. A. Barrio, D. Bastieri, J. Becerra González, W. Bednarek, A. Berdyugin, K. Berger, E. Bernardini, A. Biland, O. Blanch, R. K. Bock, G. Bonnoli, P. Bordas, D. Borla Tridon, V. Bosch-Ramon, D. Bose, I. Braun, T. Bretz, D. Britzger, M. Camara, E. Carmona, A. Carosi, P. Colin, S. Commichau, J. L. Contreras, J. Cortina, M. T. Costado, S. Covino, F. Dazzi, A. De Angelis, E. De Cea del Pozo, R. De los Reyes, B. De Lotto, M. De Maria, F. De Sabata, C. Delgado Mendez, M. Doert, A. Domínguez, D. Dominis Prester, D. Dorner, M. Doro, D. Elsaesser, M. Errando, D. Ferenc, M. V. Fonseca, L. Font, R. J. García López, M. Garzarczyk, M. Gaug, N. Godinovic, D. Hadasch, A. Herrero, D. Hildebrand, J. Hose, D. Hrupec, C. C. Hsu, T. Jogler, S. Klepser, T. Krähenbühl, D. Kranich, A. La Barbera, A. Laille, E. Leonardo, E. Lindfors, S. Lombardi, F. Longo, M. López, E. Lorenz, P. Majumdar, G. Maneva, N. Mankuzhiyil, K. Mannheim, L. Maraschi, M. Mariotti, M. Martínez, D. Mazin, M. Meucci, J. M. Miranda, R. Mirzoyan, H. Miyamoto, J. Moldón, M. Moles, A. Moralejo, D. Nieto, K. Nilsson, J. Ninkovic, R. Orito, J. Sitarek, D. Sobczynska, F. Spanier, S. Spiro, A. Stamerra, B. Steinke, J. C. Struebig, T. Suric, L. Takalo, F. Tavecchio, P. Temnikov, T. Terzic, D. Tescaro, M. Teshima, D. F. Torres, H. Vankov, R. M. Wagner, Q. Weitzel, V. Zabalza, F. Zandanel, R. Zanin, A. Neronov, and D. V. Semikoz. *Search for an extended VHE gamma-ray emission from Mrk 421 and Mrk 501 with the MAGIC Telescope.* Astron.Astrophys. MPP-2010-44, arxiv:1004.1093.
- J. Aleksić, L. A. Antonelli, P. Antoranz, M. Backes, C. Baixeras, J. A. Barrio, D. Bastieri, J. Becerra González, W. Bednarek, A. Berdyugin, K. Berger, E. Bernardini, A. Biland, O. Blanch, R. K. Bock, G. Bonnoli, P. Bordas, D. Borla Tridon, V. Bosch-Ramon, D. Bose, I. Braun, T. Bretz, D. Britzger, M. Camara, E. Carmona, A. Carosi, P. Colin, S. Commichau, J. L. Contreras, J. Cortina, M. T. Costado, S. Covino, F. Dazzi, A. De Angelis, E. De Cea del Pozo, R. De los Reyes, B. De Lotto, M. De Maria, F. De Sabata, C. Delgado Mendez, M. Doert, A. Domínguez, D. Dorner, M. Doro, D. Elsaesser, M. Errando, D. Ferenc, M. V. Fonseca, L. Font, R. J. García López, M. Garzarczyk, M. Gaug, N. Godinovic, D. Hadasch, A. Herrero, D. Hildebrand, D. Höhne-Mönch, J. Hose, D. Hrupec, C. C. Hsu, T. Jogler, S. Klepser, T. Krähenbühl, D. Kranich, A. La Barbera, A. Laille, E. Leonardo, E. Lindfors, S. Lombardi, F. Longo, M. López, E. Lorenz, P. Majumdar, G. Maneva, N. Mankuzhiyil, K. Mannheim, L. Maraschi, M. Mariotti, M. Martínez, D. Mazin, M. Meucci, J. M. Miranda, R. Mirzoyan, H. Miyamoto, J. Moldón, M. Moles, A. Moralejo, D. Nieto, K. Nilsson, J. Ninkovic, R. Orito,

- I. Oya, S. Paiano, R. Paoletti, J. M. Paredes, S. Partini, M. Pasanen, D. Pascoli, F. Pauss, R. G. Pegna, M. A. Perez-Torres, M. Persic, L. Peruzzo, F. Prada, E. Prandini, N. Puchades, I. Puljak, I. Reichardt, W. Rhode, M. Ribó, J. Rico, M. Rissi, S. Rügamer, A. Saggion, T. Y. Saito, M. Salvati, M. Sánchez-Conde, K. Satalecka, V. Scalzotto, V. Scapin, C. Schultz, T. Schweizer, M. Shayduk, S. N. Shore, A. Sierpowska-Bartosik, A. Sillanpää, J. Sitarek, D. Sobczynska, F. Spanier, S. Spiro, A. Stamerra, B. Steinke, J. C. Struebig, T. Suric, L. Takalo, F. Tavecchio, P. Temnikov, T. Terzic, D. Tescaro, M. Teshima, D. F. Torres, H. Vankov, R. M. Wagner, Q. Weitzel, V. Zabalza, F. Zandanel, and R. Zanin (MAGIC). *Gamma-ray excess from a stacked sample of high-frequency peaked blazars observed with the MAGIC telescope*. *Astrophys.J.* MPP-2010-45, arxiv:1002.2951.
- H. Anderhub, L. A. Antonelli, and P. Antoranz (MAGIC). *SEARCH FOR VERY HIGH ENERGY GAMMA-RAY EMISSION FROM PULSAR-PULSAR WIND NEBULA SYSTEMS WITH THE MAGIC TELESCOPE*. *Astrophys.J.* MPP-2010-46.
- Tina Lund, Andreas Marek, Cecilia Lunardini, Hans-Thomas Janka, and Georg Raffelt. *Fast time variations of supernova neutrino fluxes and their detectability* MPP-2010-47, arxiv:1006.1889.
- Gia Dvali and Cesar Gomez. *Self-Completeness of Einstein Gravity* MPP-2010-49, arxiv:1005.3497.
- Clemens P. Kiessig, Markus H. Thoma, and Michael Plumacher. *Neutrino decay into fermionic quasiparticles in leptogenesis* MPP-2010-50, arxiv:1004.3999.
- Stefan Antusch, Stephen F. King, and Martin Spinrath. *Measurable Neutrino Mass Scale in  $A4 \times SU(5)$*  MPP-2010-52, arxiv:1005.0708.
- Michael Haack, Dieter Lust, Luca Martucci, and Alessandro Tomasiello. *Domain walls from ten dimensions*. *JHEP* **0910**, (2009), 089. MPP-2009-54, LMU-ASC 19/09, MPP-2010-54, arxiv:0905.1582.
- Georg G. Raffelt and Irene Tamborra. *Synchronization vs. decoherence of neutrino oscillations at intermediate densities* MPP-2010-55, arxiv:1006.0002.
- Lorenzo Calibbi, Eung Jin Chun, and Liliana Velasco-Sevilla. *Bridging flavour violation and leptogenesis in  $SU(3)$  family models* KIAS-P10014, IC/2010/021, MPP-2010-58, arxiv:1005.5563.
- G. Aad et al (ATLAS). *Charged-particle multiplicities in  $pp$  interactions at  $\sqrt{s} = 900$  GeV measured with the ATLAS detector at the LHC*. *Phys.Lett.B* **688**, (2010), 21–42. CERN-PH-EP/2010-004, MPP-2010-60, arxiv:1003.3124.
- G. Aad et al. (ATLAS). *The ATLAS Inner Detector commissioning and calibration*. *Eur.Phys.J.C* MPP-2010-61, arxiv:1004.5293.
- Basudeb Dasgupta and Georg G. Raffelt. *Adiabatic Faraday effect in analogy to resonant neutrino oscillations* MPP-2010-62, arxiv:1006.4158.
- J. Aleksic (MAGIC). *Magic constraints on Gamma-ray emission from Cygnus X-3* MPP-2010-63, arxiv:1005.0740.
- L. Andricek, M. Beimforde, A. Macchiolo, H. G. Moser, R. Nisius, and R. H. Richter. *Development of thin sensors and a novel interconnection technology for the upgrade of the ATLAS pixel system*. *Nucl.Instrum.Meth.A* MPP-2010-66.
- M. Beimforde. *The ATLAS Planar Pixel Sensor R&D project*. *Nucl.Instrum.Meth.A* MPP-2010-67.
- Guennadi Pospelov. *Validation of the hadronic calibration of the ATLAS calorimeter with testbeam data corresponding to the pseudorapidity range  $2.5 < |\eta| < 4.0$* . *Astroparticle, Particle, Space Physics, Radiation Interaction, Detectors and Medical Physics Applications* **5**. MPP-2010-69.
- Sebastian Stern, Sandra Horvat, Oliver Kortner, and Hubert Kroha. *Prospects for data-driven estimation of the  $\mu^+\mu^-$  background for neutral MSSM Higgs searches in the decay channel  $H/A \rightarrow \mu^+\mu^-$* . *ATL-PHYS-INT-2010-058*, MPP-2010-70 (2010).
- K. Seidel. *AHCAL Energy Resolution* MPP-2010-71, arxiv:1006.3712v1.
- Lars Weuste. *Track Segments within Hadronic Showers using the CALICE AHCAL* MPP-2010-72, arxiv:1006.3734v1.
- Jan Hamann, Steen Hannestad, Georg G. Raffelt, Irene Tamborra, and Yvonne Y. Wong. *Cosmology seeking friendship with sterile neutrinos* TTK-10-36, MPP-2010-73, arxiv:1006.5276.
- G. Cortiana (on behalf of the ATLAS). *Prospects for the measurement of the top-quark mass with early ATLAS data*. *NuovoCim.Cto* to be published MPP-2010-74.
- Zhi zhong Xing, Deshan Yang, and Shun Zhou. *Broken  $S3$  Flavor Symmetry of Leptons and Quarks: Mass Spectra and Flavor Mixing Patterns*. *Phys.Lett.B* **690**, (2010), 304–310. MPP-2010-75, arxiv:1004.4234.
- Frank Simon. *DEPFET Vertex Detectors: Status and Plans* MPP-2010-77, arxiv:1007.0428.
- Jan-Philip Gehrcke, Stefan Kluth, and Stefan Stonjek. *ATLAS@AWS*. *J.Phys.Conf.Ser.* **219**, (2010), 052020. MPP-2010-80.
- H. Abramowicz (ZEUS). *Inclusive-jet cross sections in NC DIS at HERA and a comparison of the  $kT$ , anti- $kT$  and SIScone jet algorithms* DESY-10-034, MPP-2010-81, arxiv:1003.2923.
- I. Abt, A. Caldwell, D. Lenz, J. Liu, X. Liu, and B. Majorovits. *Pulse shape simulation for*

segmented true-coaxial HPGe detectors MPP-2010-82, arxiv:1004.0862.

J. Mejia, S. Stonjek and S. Kluth. *ATLAS grid compute cluster with virtualized service nodes.* J.Phys.Conf.Ser. **219**, MPP-2010-83.

C. Adloff, A. Frey, C. Kiesling, S. Lu, K. Prothmann, K. Seidel, F. Simon, C. Soldner, L. Weuste, et al. *Construction and Commissioning of the CALICE Analog Hadron Calorimeter Prototype.* J.Inst. **5**, (2010), P05004. DESY 10-032, MPP-2010-84, arxiv:1003.2662.

C. Adloff, A. Frey, S. Lu, K. Seidel, F. Simon, C. Soldner, L. Weuste, et al. *Study of the interactions of pions in the CALICE silicon-tungsten calorimeter prototype.* J.Inst. **5**, (2010), P05007. MPP-2010-85, arxiv:1004.4996.

G. Aad et al. (ATLAS). *Prospects for the Measurement of the Top-Quark Mass using the Template Method with early ATLAS Data* MPP-2010-86.

The collaboration (H1). *Diffraction Dijet Photoproduction in ep Collisions at HERA.* Eur.Phys.J.C DESY10-043, MPP-2010-89, arxiv:1006.0946.

Jan Germer, Wolfgang Hollik, Edoardo Mirabella, and Maik K. Trenkel. *Hadronic production of squark-squark pairs: The electroweak contributions* MPP-2010-1, IPHT-10/007, MPP-2010-90, arxiv:1004.2621.

Bernhard Bittner, Jörg Dubbert, Sandra Horvat, Oliver Körtner, Hubert Kroha, Federica Legger, Robert Richter, Stefanie Adomeit, Otmar Biebel, Albert Engl, Ralf Hertzenberger, Felix Rauscher, and Andre Zibell. *Development of fast high-resolution muon drift-tube detectors for high counting rates.* Nucl.Instrum.Meth.A MPP-2010-91.

A. Afonin, A. V. Akimov, T. Barillari, V. Bezzubov, M. Blagov, H. M. Braun, D. Bruncko, S. V. Chekulaev, A. Cheplakov, R. Degele, S. P. Denisov, V. Drobin, P. Eckstein, V. Ershov, V. N. Evdokimov, J. Ferencei, V. Fimushkin, A. Fischer, H. Fatterschneider, V. Garkusha, A. Glatte, C. Handel, J. Huber, N. Javadov, M. Kazarinov, A. Khoroshilov, A. E. Kiryunin, E. Kladiva, M. Kobel, A. A. Komar, M. Komogorov, A. Kozelov, G. Krupny, V. Kukhtin, S. Kulikov, L. L. Kurchaninov, E. Ladygin, A. B. Lazarev, A. Levin, W. F. Mader, A. L. Maslennikov, S. Menke, L. Merkulov, A. Neganov, H. Oberlack, C. J. Oram, R. Othegraven, S. V. Peleganchuk, V. Petrov, S. Pivovarov, G. E. Pospelov, N. Prokopenko, J. Rascvetalov, N. Rusakovich, J. P. Rutherford, D. Salihagic, A. Y. Savine, P. Schacht, H. Secker, F. Seifert, L. Shaver, S. Shilov, A. A. Snesev, M. Soldatov, J. Spalek, M. Speransky, D. Stoyanova, A. Straessner, P. Strizenec, V. V. Sulin, A. Talyshev, S. Tapprogge, Yu. A. Tikhonov, Y. Usov, V. Vadeev, I. Vasiliev, R. Walker, and C. Zeitnitz. *Relative luminosity measurement of the LHC with the ATLAS forward calorimeter.* J.Inst. **5**, (2010), P05005. MPP-2010-92, arxiv:1005.1784.

Vladimir Chekelian. *Neutral current interactions in ep scattering with longitudinally polarised leptons at H1* MPP-2010-95.

Shushkevich Stanislav. *Charged current interactions in  $e^\pm p$  scattering at H1 with longitudinally polarized lepton beams* MPP-2010-96.

Shushkevich Stanislav. *Electroweak Measurements at High  $Q^2$  at HERA* MPP-2010-97.

The collaboration (ATLAS). *Preliminary studies for the measurement of the inclusive muon spectrum in pp collisions at  $\sqrt{s}=7$  TeV with the ATLAS detector* MPP-2010-107.

The collaboration (ATLAS). *ATLAS Sensitivity Prospects for Higgs Boson Production at the LHC Running at 7 TeV.* MPP-2010-108.

Juli 2010

Alle Rechte vorbehalten

Max-Planck-Institut für Physik (Werner-Heisenberg-Institut), München  
(edited by S. Stonjek)